UNIVERSITÀ DI PARMA

UNIVERSITA' DEGLI STUDI DI PARMA

DOTTORATO DI RICERCA IN

INGEGNERIA INDUSTRIALE

CICLO XXXVII

Scambiatoti Microscambiatori per l'industria farmaceutica e alimentare / Heat Exchangers and Micro Heat Exchangers for the Pharmaceutical and Food Industries

Coordinatore:

Chiar.mo Prof. Gianni ROYER CARFAGNI

Tutore:

Chiar.mo Prof. Ing. Fabio BOZZOLI

Dottorando: Dr. Muhammad Waheed AZAM

Anni Accademici 2022 /2023 – 2023/2024

Index

List of Figures

List of Tables

Nomenclature

a	Thermal diffusivity	$\frac{m^2}{s}$
A_c	Cross sectional area	m^2
C_p	Fluid-specific heat at constant pressure	$j.kg^{-1}K^{-1}$
D_o	Tube outer diameter	m
D_i	Tube internal diameter	m
e	Corrugation depth	m
f	Darcy friction factor	$-$
Gr	Grashof number	$-$
h	Convective heat transfer coefficient	$W.m^{-2}K^{-1}$
l	Corrugation pitch	m
$\boldsymbol{J}$	Sensitivity matrix	
L	Length of pipe	m
$\dot{m}$	Mass flowrate	$\frac{Kg}{s}$
Nu	Nusselt number	$-$
N	Set of unknown parameters	$-$
p	Pressure	Pa
p	Pitch size	m
P	Vector of unknown parameters	$-$
Pr	Prandtl number, Pr $= \frac{cp \cdot \mu}{\lambda}$	$-$
Δp	Pressure drops	Pa
Q	Heat power	W
q	Heat flux exchanged per unit surface	$W.m^{-2}$

$\mathbf{q}$	Heat flux vector	$W.m^{-2}$
q_g	Internal heat generation per unit volume	$W.m^{-3}$
r	Radial coordinate	m
Re	Reynolds number	$-$
R_{env}	Overall heat-transfer resistance between the external wall tube and surrounding environment	$-$
r, α	Cylindrical coordinates on tube section	$-$
r_{ext}	External radius	m
r_{int}	Internal radius	m
S	Surface	$-$
t	Wall thickness	m
T	Temperature	K
T_b	Bulk temperature	K
T_{env}	Environment temperature	K
T_s	Surface temperature	K
T_w	Wall temperature	K
μ_c	Cutoff frequency	m^{-1}
μ_f, υ_f	Frequency components	m^{-1}
x	Axial coordinate	m
ω	Mean fluid axial velocity	$\frac{m}{s}$
Y	Estimated temperature	K
z	Axial coordinate	m

Greek Symbols

α	Angular coordinate	rad
ε	Uncertainty	–
ε_f	Friction factor enhancement	–
ε_h	Heat transfer enhancement	–
η	Enhancement efficiency	–
λ	Thermal conductivity	$W.m^{-1}K^{-1}$
μ	Dynamic viscosity	$Pa.s$
μ^k	damping parameter	
ν	Kinematic viscosity	$m^{-2}s^{-1}$
ρ	Density	$kg.m^{-3}$
σ	Standard deviation	–
σ^2	Variance	–
Ω	Diagonal matrix in Levenberg-Marquardt method	

Subscripts and superscripts

b	Bulk
e	Enhanced geometry
env	Environment
ext	External wall
int	Internal wall
i	Inlet section
S	Surface
T	Transpose of the matrix
w	Wall

x	Local value along the curvilinear coordinate x
0	Reference geometry
$\bar{}$	Averaged

Acronyms

HX	Heat Exchanger
MCHE	Micro channel heat exchanger
AI	Artificial intelligence
IHTP	Inverse Heat Transfer Problems
IHCP	Inverse Heat Conduction Problems

Preface

The thesis aims to discuss the application and optimization of conventional and micro heat exchangers within the pharmaceutical and food industries, focusing on their critical roles in enhancing process efficiency and product quality. By examining traditional heat exchangers, which are integral to large-scale operations for maintaining consistent temperature control, and comparing them with advanced micro heat exchangers, which offer precision and compactness for smaller-scale or specialized processes. The research investigates how these technologies contribute to enhancing energy efficiency, regulatory compliance, and overall process optimization, providing insights into their design, operational performance, and potential for innovation in high-demand environments. Moreover, this thesis also offers valuable recommendations for the effective implementation of heat exchange systems to the specific needs of the pharmaceutical and food sectors.

Heat transfer enhancement is crucial in the food and pharmaceutical industries to enhance process efficiency, product quality, and energy savings. To improve the local convective heat transfer coefficient, this research introduces an inverse study approach using an experimental infrared camera to measure temperature data obtained within a corrugated pipe. Specifically, six pipes with different corrugation profiles were studied to investigate the effects of various designs, including helical, transversal, and cross-helical types, with pitch sizes of 16 mm and 32 mm. To evaluate their effect on heat transfer performance, the findings were examined and presented from both local and average viewpoints. The results indicate that pitch size and corrugation type/design play a significant role in enhancing the performance of the tested pipe. The result of this research in turbulent regime has shown that transversal corrugation generates the highest improvement in heat transfer performance. Consequently, the single helix solution is the preferred one in heat exchangers adopted in the food and pharmaceutical industries, and these helical corrugations are the easiest to manufacture. A merger solution between them is represented by the cross-helix profile. The cross-helix profile with the bigger pitch size performs better than all other corrugated pipes, especially in the low/intermediate Reynolds number range (i.e., 100-1000). The estimation process (for local heat transfer) proposed in this study employs the external surface temperature of the tube, acquired with an infrared thermal camera, as starting data for the inverse heat conduction problem inside the pipe wall region. The calculation of its Laplacian was finally achieved by a filtering technique applied to the infrared temperature acquisitions.

The dissertation consists of seven chapters. An overview of all chapters is discussed here.

Chapter 01 Highlights the aims and motivation of the current research. It describes the brief introduction of heat exchangers including conventional, compact, and micro heat exchangers. Furthermore, it also discussed the main passive techniques for heat transfer enhancement.

Chapter 02 Describe the basic concept of inverse heat transfer problems are introduced to estimate unknown values that occur during the research of physical difficulties. Furthermore, it explains the various filtering techniques and inverse heat conduction problems in pipes.

Chapter 03 reports the relevant literature about the research and development of corrugated pipes. Moreover, it also provides detailed information relating to the pipe geometries tested in this thesis.

Chapter 04 A detailed explanation of both local and global (average) experimental setup is presented. Moreover, it also reports the estimation procedure to determine the local convective heat transfer coefficient.

Chapter 05 The initial phase of the investigation focused on evaluating the average heat transfer and pressure drops in six corrugated pipes in a turbulent regime. The Nusselt number distribution for a smooth tube was presented experimentally and compared with the Dittus–Boelter correlation for a smooth pipe under a turbulent regime. In the second phase, the convective heat transfer coefficient on the pipe's inner wall was determined through IR camera analysis.

Chapter 06 Explain the results in the laminar regime of the corrugated pipe in global (average) analysis and compare it with smooth pipe.

Chapter 07 Provides a summary of key conclusions and some recommendations for extending the current research.

Introduction

1.1 Aim and scope of the work

The current work aims to discuss various types of heat exchangers with particular attention to the pharmaceutical and food industries to ensure enhanced efficiency and energy-saving potential. Heat transfer also plays a vital role in both industries including maintaining product quality, safety, and sterility through numerous processes such as heating, cooling, sterilization, drying, and packaging.

In this research work, experimental techniques are used to estimate the average and local heat transfer coefficient in pipes with different corrugation profiles including helical, transversal, and cross helix. Initially, the global performance and pressure drop of all corrugated pipes were evaluated along their heated length. After that, local heat transfer was measured, and an estimation method was applied to solve the inverse heat conduction problem (IHCP) within the pipe wall domain. This is achieved by using the temperature distribution on the outer surface as initial data and considering the convection coefficient distribution between the internal wall and the fluid. The distribution of wall temperature varies significantly along the pipe due to the complex effects of surface corrugation on the flow pattern. To measure these temperature variations accurately and precisely, a high-resolution infrared camera was used. It is noteworthy that the use of infrared (IR) cameras for high-temperature measurement applications relies mainly on cryogenic cooling systems/techniques making it an excellent choice for precise measurements. The coefficient of convection in corrugated pipes can be determined by employing a filtering technique with the temperature distribution through infrared acquisition to address the IHCP of an ill-conditioned nature. Moreover, the results obtained provide significant implementation for the design and optimization of heat exchangers that utilize corrugated tubes in the food and pharmaceutical sectors. It was also observed during the study that corrugated tubes performed better than conventional smooth tubes to enhance heat transfer efficiency. This can lead to more efficient thermal management in different processes of the food and pharmaceutical industry including heating, cooling, crystallization, fermentation, pasteurization, and sterilization.

1.2 Heat Exchangers

A heat exchanger is a device designed to transfer heat between two or more fluids at different temperatures without allowing them to mix and provide maximum transfer rate. They are used in various cooling and heating processes, where the fluids may come into contact directly or remain separated from one another through a solid wall. In heat exchangers, heat is transferred from a hot fluid to a cold fluid, typically without the fluids going through a phase change. The process becomes more complex when thermal convection, radiation, and heat conduction are considered. Heat exchangers have a significant role in the transportation of about 90% of the heat energy used in energy production and management. They are used in various engineering applications, such as food processing systems, pharmaceutical industries, power plants, chemical processing systems, waste heat recovery units, heating, ventilation and air conditioning and automobile radiators and so forth [1].

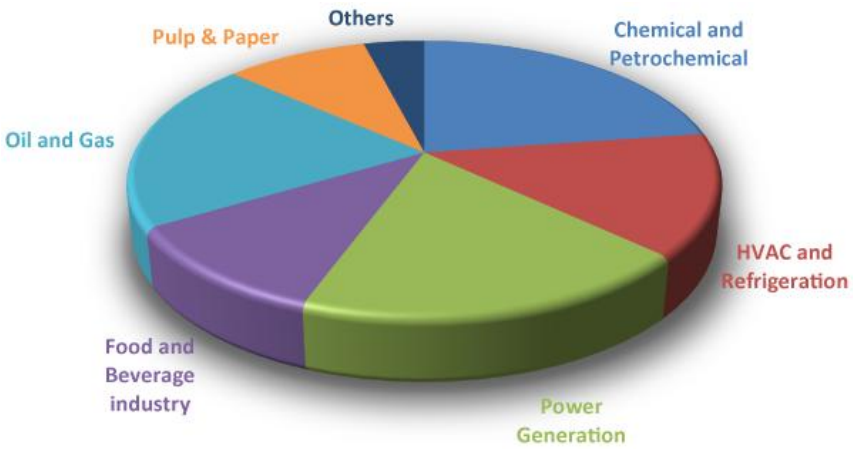

Figure 1. 1 Global heat exchangers market [2]

The increasing demand for heat exchangers for thermal management in different sectors is shown in Figure 1.1. The development and optimization of heat exchanger technology is continually growing and focusing not only enhancing efficiency but also on sustainability and reliability [3]. The role of heat exchangers in industries to reduce emissions and energy consumption becomes more significant, highlighting their importance in achieving both economic and environmental goals. They not only reduce overall energy consumption but also decrease maintenance costs, enhance industrial sustainability, and improve economic feasibility. Furthermore, the utilization of renewable energy sources and the recovery of waste heat further contribute to the transition to cleaner energy systems. Their design and operation must be optimal as energy prices increase with the decreasing supply of fossil fuel resources. Moreover, in response to the varying demands of a continuous process, the design of the

exchanger is improving day by day. Modern heat exchangers are now designed with advanced features such as enhanced surface areas, compact design, and advanced materials which help to minimize the size, weight, and cost of the equipment [4]. Their lifespan can be increased by using corrosion-resistant materials and fouling-resistant surfaces such as stainless steel, copper, aluminum, ceramic and silicon-based coatings. Additionally fouling, scaling and corrosion in heat exchangers can be eliminated with routine cleaning, inspection and degradation can be avoided by employing paints and protective coatings.

Heat exchangers can be classified into different categories by flow arrangement, construction, size, heat transfer mechanism, surface compactness, and phase of the process of the fluids [5]. In this research work, we focused on the heat exchangers utilized in the food and pharmaceutical industries, emphasizing their critical role in various processes and their classification based on size as illustrated in Figure 1.2.

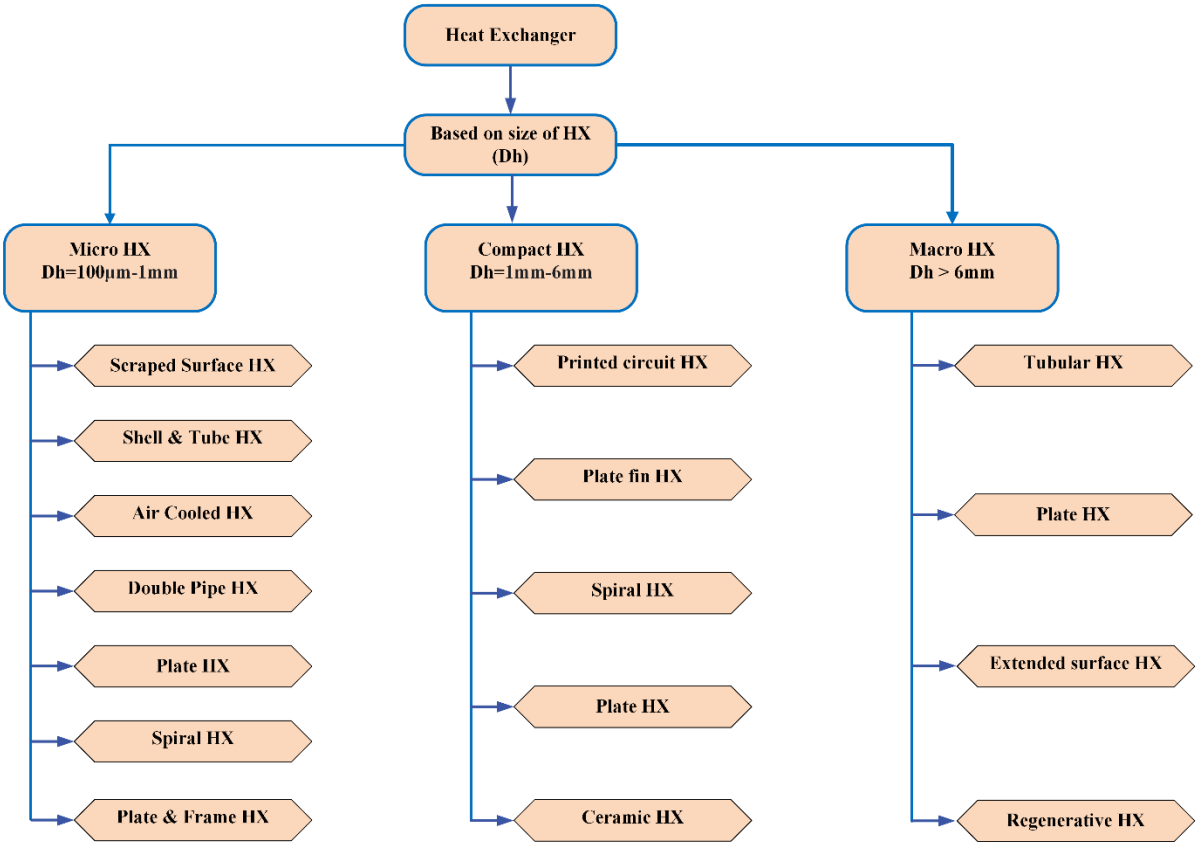

Figure 1. 2 Classification of HX

1.3 Heat exchangers for food and pharmaceuticals industry

Heat exchangers are essential to the food and pharmaceutical industries because they provide a variety of operations, including process efficiency, product quality, and safety. In the food industry, heat exchangers are used mainly for two purposes: in the industrial process (heating and cooling) themselves or in situations where cleanliness and sanitization are required. Similarly, in the pharmaceutical industry, heat exchangers are crucial in maintaining the precise thermal conditions and where extreme cleanliness and sanitization for producing medicines and vaccines. Table 1.1 displays numerous applications of micro heat exchangers in the food and pharmaceutical industries. A brief description of heat exchangers utilized in both industries is discussed below.

Food industry: In food industries heat transfer and thermal processes are crucial to ensure food preservation and prolonging shelf life, both of which are important to the safety of consumers. The methods for preserving food vary significantly depending on the procedure. Conventional thermal processing involves several types of steps including heating, cooling, and holding to reach the required temperature changes. Systems for alternative preservation procedures involve connecting the food product with a treatment for the period required to decrease the product's degradation reactions. Every processing system has a different design depending on the food product being processed [6]. Thermal processes in the food industry with energy consumption involve understanding how various heating and cooling operations impact overall energy use.

The food industry consumes about 30% of the energy used worldwide, that accounts for 20% of greenhouse emissions. By 2050, with the world's population expected to exceed 9 billion, there will be a significant increase in the demand for food. The food industry consumes a lot of energy for a variety of operations that are necessary for the production, preservation, and safety of food, including cooking, HVAC, heating, and cooling. Figure 1.3 shows energy consumption in the food industry for different sectors. The major proportion of energy consumption is utilized in the process heat.

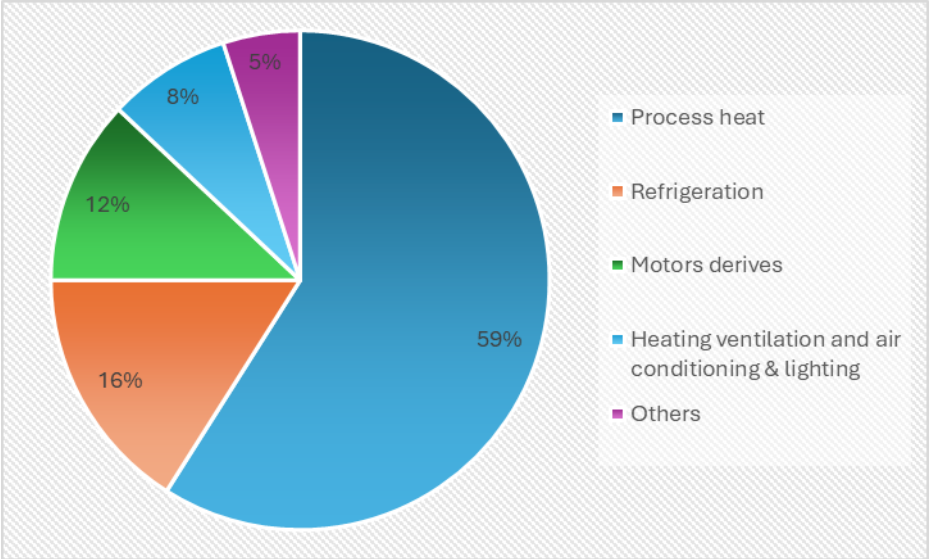

Figure 1. 3 Typical energy consumption in the food industry *[7]*

The following are the important applications of HX in the food industry.

***Pasteurization*:** Pasteurization is a physical technique that involves applying heat to minimize the microorganisms present in both liquid and solid foods by controlling the temperature and time period. This technique can be used to eliminate, microorganisms that affect food safety or cause food spoilage. Moreover, food is heated to less than 100ºC for a few minutes or seconds and then rapidly cool it [8]. Heat exchangers are crucial to the pasteurization process because they allow food products to be heated and cool down quickly and uniformly, removing harmful pathogens while maintaining quality. The advantages of heat exchangers over in-container processing are uniform heat treatment, low space requirements, better control over pasteurization conditions, higher energy efficiency, and flexibility for different products. Most commonly, tube or plate heat exchangers are used on a larger scale, when pasteurizing low-viscosity liquids such as fruit juices, milk, milk products, beers, and wines [9].

***Sterilization*:** Sterilization is the process in which all viable organisms are destroyed or eliminated by using chemicals, radiation, heat, or physical cell elimination. Typically, the product is sterilized by quickly heating it to 130–145°C, holding it there for the necessary amount of time, and then cooling it down. Heat exchangers help to achieve the necessary high temperatures to ensure sterility, preventing bacterial contamination and extending shelf life. Dairy and canned foods are typically sterilized using heat exchangers to ensure their long-term preservation. Moreover, their capacity to retain consistent sterilizing temperatures and energy-efficient performance contributes to reduced operational costs and enhanced food safety. The

sterilization procedure is often carried out with advanced-designed heat exchangers including plate, tube, or scraped surface [10].

Heating and cooling: Heating and cooling are two of the largest expenses associated with processing heat in the food industry. For this purpose, heat exchangers play a crucial role by providing effective temperature control that is necessary for food safety and quality. Perishable food products need specific parameters such as temperature, humidity, and ventilation both before and after preparation. Moreover, they are used in cooling applications to reduce the temperature of hot food products such as cooked foods, soups, and sauces. This prevents microbial development and spoiling while maintaining the flavor, food texture, and nutrients. They are used in heating applications to increase the temperature of fats and oils to the required levels for different processing stages, including blending or emulsification. Furthermore, heat exchangers improve their energy efficiency by recovering heat from hot products and utilizing it for preheating incoming cold products. This significantly reduces operating expenses and energy usage [11].

***Fermentation*:** Food fermentation is a food processing method that uses microorganisms' growth and metabolic activities to stabilize and transform perishable food products. It has been used to preserve a variety of meals made from plants, fish, and animals including cheese, cultured milk, and fermentation-based milk products. Heat exchangers are essential for maintaining regular fermentation conditions in beer, yogurt, and other fermented foods. Precise temperature control is important in fermentation operations for multiple reasons. The growth and metabolic processes of microorganisms, such as yeast and bacteria, are extremely temperature-sensitive, each type of microorganism has a range of temperatures where it grows and ferments most effectively. The most common heat exchangers used in the fermentation process are double pipe, shell and tube, and plate [12].

***Drying*:** Drying is another fascinating food preservation technique that is used in the food industry. Heat exchangers are used in drying procedures to heat food products to reduce moisture content, helping to preserve them and make them lighter for transportation. Precise control of temperatures is essential for preventing overheating, which may damage food quality, and to make sure drying is a reliable and energy-saving procedure. Heat exchangers are useful in the drying process of vegetables, dried fruits, and instant coffee [13].

***Meat Processing*:** It is widely acknowledged that temperature monitoring and control are crucial for processing meats products. For example, high cooking temperatures may

decrease cooking times but can result in increased cooking loss and worse texture quality. Heat exchangers help with the cooking and cooling operations, which improves the safety and quality of meat processing. They are employed in processing ready-to-eat foods, such as hams and sausages because they ensure consistent cooking and rapid cooling, thus preventing the growth of bacteria. [14].

***Bakery Products*:** Heat exchangers used in the baking and bread industries by precise control on the temperature of ingredients and proofing environments. They help to ensure that ingredients are prevented from becoming too heated or cold during the mixing process, which helps preserve the finished product's proper texture and structural integrity. Plate heat exchangers are commonly used for heating and cooling in bakery product [15].

Heat exchangers are utilized in other food-related processes, including the processing of dairy products, vegetables, sauces and dressings, oil and fat processing, seafood, beverages production, evaporation, and concentration of sugar, heat recovery and refining and freezing of sugar.

Table 1. 1 Application of MHE in food and pharmaceutical industries

Industry	Application	Purpose	Benefits	Examples
Food Industry	Pasteurization	Heating liquids to eliminate harmful microorganism	Precise temperature control, energy efficiency	Milk, juice, and liquid eggs
	Sterilization	Complete destruction of all microorganisms	High heat transfer rates, reduced processing time	Canned foods, sauces, baby food
	Cooling	Rapid cooling of processed food products	Consistent product quality, reduced energy consumption	Dairy products, beverages, ready-to-eat meals
	Concentration	Removing water from liquid food products	Enhanced evaporation rates, compact design	Fruit juices, sauces, purees
	Fermentation	Controlling temperature during fermentation processes	Precise temperature control, improved product consistency	Yogurt, beer, wine
	Crystallization	Formation of crystals in products like sugar or chocolate	Uniform crystal size, enhanced product quality	Sugar production, chocolate processing
Pharmaceutical Industry	Sterilization	Elimination of microorganisms in drug formulations	High heat transfer efficiency, precise temperature control	Injectable drugs, ophthalmic solutions
	Lyophilization (Freeze Drying)	Removal of moisture from products while preserving structure	Efficient heat transfer, energy savings	Vaccines, antibiotics, probiotics
	Reactor Temperature Control	Maintaining specific temperatures in chemical reactors	Accurate control, enhanced reaction consistency	API synthesis, biochemical processes

	Extraction and Purification	Temperature control during extraction and purification processes	Efficient heat transfer, reduced solvent usage	Herbal extracts, essential oils, protein purification
	Cooling	Rapid cooling of heat-sensitive pharmaceutical products	Preserved product stability, improved shelf life	Biopharmaceuticals, vaccines, heat-sensitive formulations

***Pharmaceutical industry*:** The pharmaceutical industry is a sensitive sector that provides the production of products that are critical for human health. Heat exchangers in the pharmaceutical industry are important for maintaining precise temperature control during various processes such as sterilization, crystallization, evaporation, heating and cooling, ensuring product quality, cost reduction, environmental impact, and optimizing energy efficiency. Pharmaceutical operations require a unique level of attention as compared to other industries, including strict hygienic guidelines, strict precautions to prevent contamination, and exact regulation of temperature and pressure in order to ensure the safety and effectiveness of the final product [16].

It is unacceptable to compromise on efficiency, quality, or safety in pharmaceutical production. Therefore, heat exchangers in hygienic sectors are carefully designed to be foolproof, ensuring protection against any such accidents. For many pharmaceutical firms, it can be difficult to reduce costs without compromising product quality. Research has demonstrated that efficient energy management can enhance product quality, efficiency, product and production rates. In the end, these enhancement results in higher profitability and productivity.

Therefore, in these sectors advanced energy management systems are required, which include on-site generating, demand response, dependability, and alternate fuel and energy supply alternatives. Pharmaceutical companies can find innovative strategies to reduce daily energy usage and waste, and this will improve productivity by thoroughly analyzing data on energy consumption. Figure 1.4 shows energy consumption in the pharmaceutical industry, with manufacturing lines accounting for just 18.2% of the total. In contrast, cold production units account for 29.5%, while air production and treatment units account for 20.7%. Pharma companies could achieve cost savings of up to 30% and enhance production rates, product

quality, and process efficiency by implementing changes in energy management. Furthermore, they should utilize renewable energy options to further reduce costs after reaching optimal energy efficiency. This is due to the fact that renewable energy sources such as solar thermal systems, wind turbines, and others provide sustainable energy choices to enhance the emissions balance of the pharmaceutical sector [17].

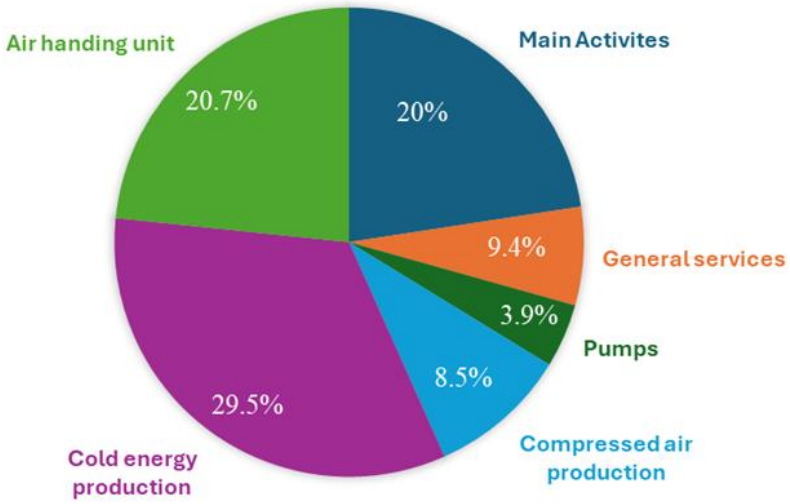

Figure 1. 4 Energy consumption in pharmaceutical industry [18]

The following are the important applications of HX in the pharmaceutical industry [19].

***Sterilization*:** Heat exchangers are essential to the sterilization process in the pharmaceutical industry because they provide consistent and efficient transfer of heat, which is necessary to remove all traces of microbiological life from products, equipment, and solutions. These devices provide a uniform distribution of heat and maintain a high temperature for effective sterilization. Precise temperature control is significant to ensure that every component of the object or fluid being sterilized is exposed to the appropriate level of heat. Furthermore, these devices improve energy efficiency by optimizing the heat transfer process, which is cost-effective and improves the environmental sustainability of sterilizing processes.

***Distillation*:** Heat exchangers are essential to the pharmaceutical industry production of high purity distilled water because they provide precise temperature control, effective heating and cooling, and increased energy efficiency. Distilled water is essential for use in the production of injectable pharmaceutical applications because of its high purity and absence of impurities, serving as a solvent to ensure that the medicines are pure and suitable for patient

use. Additionally, distilled water is utilized to sterilize and clean syringes and vials to avoid any contamination that would compromise the injections' safety. It is generally considered the purest water due to complete removal of organic impurities as well as ions and minerals.

***Air Conditioning and environmental control*:** In the pharmaceutical industry, heat exchangers are employed in air conditioning applications to maintain temperature and humidity at a controlled environment for manufacturing operations and storage facilities. These devices help in the prevention of microbiological development, the degradation of sensitive chemicals, and ensuring the compliance of regulatory standards for the stability and safety of products by controlling temperature and air quality.

***Crystallization*:** Crystallization plays a crucial role in the production and purification of 70-80% small-molecule active pharmaceutical ingredients for medical applications due to its high purity and lack of impurities. There are different factors that affect the crystallization process including, rate of cooling, temperature of crystallization, impurities and additives, and suspended particles. Therefore, heat exchangers play an important role in controlling these factors. Moreover, these devices are also used during the crystallization process to accurately control the solution or suspension temperature, developing the optimum conditions for the growth of crystals.

1.4 Macro heat exchangers

According to S.S. Mehendale macro heat exchangers are those having a hydraulic diameter larger than 6 mm. Figure 2 depicted the classification of macro heat exchangers. Shell and tube design are the most common among tubular heat exchangers because of their wide range of applications and flexibility. Figure 1.5 shows a visual representation of a shell and tube exchanger. As the name indicates, this specific type of heat exchanger consists of multiple tubes inside a shell, with one fluid passing through the tubes and another fluid passing through the shell. It is suitable for higher-pressure applications and is the most popular type of heat exchanger in the chemical process, power generation, heating ventilation and air conditioning, food and pharmaceutical industries and so on.

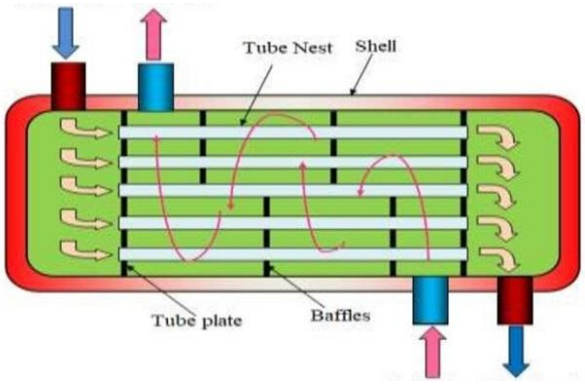

Figure 1. 5 Shell and tube heat exchanger [20]

This type of HX is especially preferred in both pharmaceutical and food industries due to the surface's easy sanitation and cleaning qualities. The exchanger's design considers the size and viscosity of the food ingredients and industrial requirements, providing low friction losses and high heat transfer. Eventually because of their outstanding safety in hygienic processes, high-temperature tolerance, and simple maintenance because of their flexible design. Moreover, these heat exchangers are the best option to meet hygiene requirements in the pharmaceutical industry [21].

Recently, many researchers are currently focusing on enhancing heat transfer, improving design, resistance to corrosion materials, reducing fouling effect and pressure drop in shells and tubes. There are important factors need to be considered to improve heat exchanger design, such as heat exchanger must be able to meet process requirements, withstand plant maintenance conditions, and be maintainable.

Moreover, it should have the lowest cost with a compact design regarding diameter, length, weight, and tube specifications. In terms of improved design [22], Asadbeigi et al. [23] conducted simulation-based study and designed a shell and tube heat exchanger for improvement in heat transfer during the pasteurization process of making tomato paste. The behavior of viscosity during the pasteurization of tomato paste was addressed by employing the Herschel-Bulkley model. It was demonstrated that the segmental baffle used in this heat exchanger was suitable provided that food is more heat-sensitive than other baffle types like helical baffles, which have less heat transfer. Furthermore, variation in the inlet mass flow rates did not affect the tomato paste output temperature. The performance of this type of heat exchanger has been significantly affected by the baffle. Regarding this, Mohammad and Reza [24] carried out an experimental study to investigate how a helical baffle affects the distribution

of shell side flow and the improvement of heat transfer. The mass flow rate, baffle pitch size, and helix angle were the performance-indicated parameters. At lower baffle pitches, the heat transfer coefficient is lower than at higher pitches; however, as the mass flow rate increases, it also increases. Moreover, when the helix angle increases, the pressure drops, and the heat transfer coefficient both decreases.

Similarly, Pranita et al. [25] also analyzed the effect of various types of baffles including helical, single, and double segmental on the performance of shell and tube heat exchanger. The problem of dead zones and poor heat transfer resulting from single-segmental baffles is resolved by double-segmental baffles. However, the result indicted that helical baffle was better performance than other two baffles. The thermal performance and pressure drop of a heat exchanger are affected by the fluid flow path and the types of baffles used, including their angles. Moreover, introducing more complexity to the baffles enhances heat transfer; however, this increased heat transfer also causes a higher pressure drop. Danish et al. [26] numerically carried out investigations to improve the design of shell and tube heat exchangers by staggered baffles to the enhance heat transfer rate. The baffles were oriented at a consistent angle, either clockwise or counterclockwise, between the next baffles. According to the results, the baffle cut, baffle spacing, baffle orientation angle, and the interior diameter of the shell all have a significant impact on the pressure drop and rate of heat transfer. Moreover, the optimal combination of variables leads to a pressure drop of 58.6 kPa, however, the maximum heat transfer produces 141kW. Ali and Reza [27] carried out a simulation-based investigation that combined a baffle and a longitudinally ribbed tube configuration to maximize fluid flow and heat transfer inside the segmental baffle shell and tube heat exchanger. The fluid moves axially along the tubes' axis, which lowers the pressure drop. The result indicated that a combination of baffles and longitudinal ribbed tubes improved the heat transfer than conventional baffles.

Another common type of macro heat exchangers are plate heat exchangers. This type of heat exchanger is fabricated with many parallel plates arranged one on above the other in order to form a series of channels which allow the fluids to flow between them. The schematic illustration of a plate heat exchanger is shown in Figure 1.6.

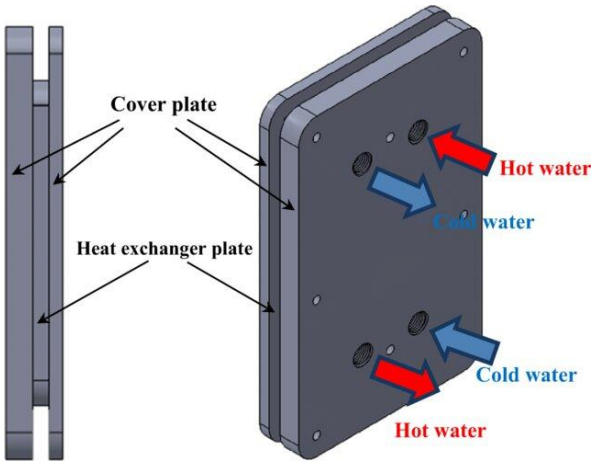

Figure 1. 6 Plate heat exchanger [28]

The most important features of modern PHE construction, which make them effective and energy-efficient heat exchangers in a variety of process scenarios are,

- Plates as thin as are possible due to the plate adjacent numerous contact points, which provide a strong structure that can withstand significant pressure differentials between streams in channels. Therefore, it is possible to utilize plates with smaller thicknesses, which lowers the weight and materials cost.
- PHEs have superior heat transfer coefficients, and they require a much smaller heat transfer area, making them much more compact and requiring less space for maintenance than conventional shell-and-tube heat exchangers.
- PHEs require significantly less material since the heat transfer surface is made up of thin metal plates. Due to this, even when more expensive materials are employed, costs can be reduced.
- PHEs have significantly lower heat losses to the environment since the plates only come into contact with the surrounding air on the outside surfaces.
- PHEs low weight results in reduced transportation expenses and foundation needs.
- Plate corrugation geometries can be modified to maximize PHE performance under particular process conditions.
- PHEs with small channels have a low hold-up volume, which makes them appropriate for handling costly and low weight provides easier process parameter control.

- The geometric shape of the PHE channels, which include contact sites for the corrugations inside, causes a change in the direction of flow as well as significant levels of swirl, vortex, and turbulence.

At present, the majority of PHEs produced for the market contain corrugations that are angled toward the plate axis, designing crossing flow channels between them. Plate heat exchangers are classified into three primary types including plates and frames, brazed, and brazed plate heat exchangers. It is noteworthy that certain aspects of the thermal and hydraulic design are significantly impacted by the kind of PHE construction. For all PHE designing techniques, the fundamental ideas of heat transfer intensification in these channels are still the same. The use of materials with optimum thermophysical and thermal characteristics, such as nanofluids, reduces costs and enhances the heat exchanger efficiency [29]. Plate heat exchangers are classified into three primary types such as, plate and frame, brazed, and welded heat exchangers. Jorge et al. [30] designed a new method for plate heat exchangers that takes into account the economic effects of chevron angles. The result revealed that, the corrugation angle affects the size of the component based on the plate dimensions (length and width). General correlations can be used to modify this angle, which acts as a variable. The optimal design for a two-stream heat exchanger was achieved with a corrugation angle of 46° and 166 thermal plates.

Behrozifard et al. [31] conducted an experimental investigation to improve the performance of plate heat exchanger by utilizing nanofluids including GO (Graphene oxide), Al_2O_3, and GO-Al_2O_3 with water. The primary objective was to achieve atomic stabilization, which involved adding surfactants applying ultrasonic vibrations to nanofluids at particular weight concentrations and increasing equilibrium, in order to improve the efficiency of the nanofluids. The results indicated that the maximum influence on heat exchanger performance was observed with GO nanoparticles, with an optimal heat exchanger performance as compared to other two nanofluids. Similarly, Calviño et al. [32] conducted researched to enhance the hydrodynamic efficiency and heat transfer of tubular and plate heat exchangers in both laminar and turbulent flows by using ZrO_2 nanofluids. The results revealed that in laminar flow within a plate heat exchanger, the nanofluids achieved convective heat transfer coefficient enhancements of up to 123%, while in turbulent flow within a tubular heat exchanger, the enhancements reached 8.8% compared to the base fluid. Moreover, for 0.75 weight percent ZrO_2, the Nusselt number rises approximately 65% under laminar flow conditions (Re = 400). On the other hand, with 0.25 weight percent ZrO_2, the Nusselt number rises by approximately

6.7% in turbulent flow (Re=22500). Therefore, weight percentage of nanofluid significantly impact on the performance of heat exchangers.

1.5 Compact heat exchangers

According to S.S. Mehendale, compact heat exchangers have a hydraulic diameter of 1 to 6 mm. These heat exchangers have reduced size and weight, higher heat transfer efficiency, lower fluid inventory, and enhanced design flexibility. They are designed by their high area density, which corresponds to a high ratio of heat transfer surface to volume. Typically, surface area density of a gaseous fluid is 700 m^2/m^3, whereas that of a liquid is 400 m^2/m^3 in these heat exchangers. Hence, a heat exchanger with a high surface area density should ideally have a large number of small heat transfer channels, resulting in a greater heat transfer capacity for a given volume. These heat exchangers can be used in a wide variety of industrial applications as the design temperature and pressure remain within the allowed range, (450°C and 40 bar gauge). Numerous industries utilize these heat exchangers significantly including HVAC, aerospace, chemical, food processing, and pharmaceutical industries. Figure 1.2 depicts the classification of compact heat exchangers. The most widely used varieties of these heat exchangers are plate, plate-fin, printed circuit, spiral, and ceramic heat exchangers [33]. Figure 1.7 depicts the schematic representation of a compact heat exchanger.

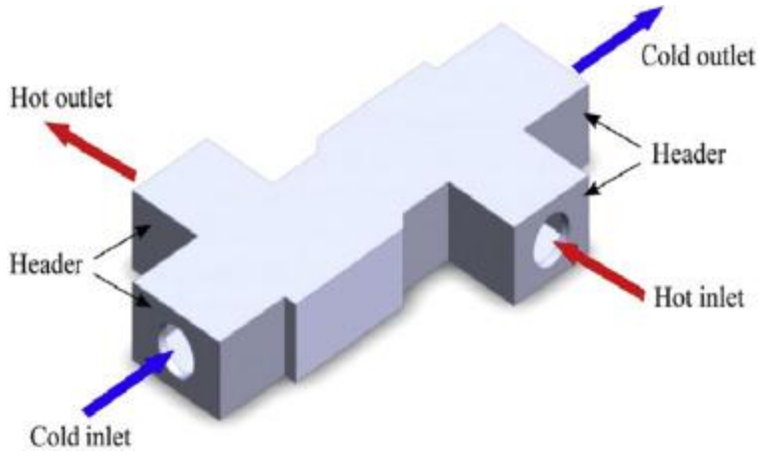

Figure 1. 7 Schematic representation of compact heat exchanger [34]

The raising demand for sustainable development, environmental conservation, and the current high cost of energy have contributed to a new interest in high-performance heat exchangers. In the design and development stage to enhance the performance of these heat exchangers, many researchers and scientist utilized a wide range of methods.

One of the methods adopted by Agarwal et al. [35] to enhance the performance of compact heat exchangers by computational fluid dynamics to apply ZnO/water nanofluid for enhancement in heat transfer. Compact heat exchanger design and optimization are investigated by computational fluid dynamics (CFD), which eliminates the need of physical prototypes. Moreover, computational fluid dynamics (CFD) simulations improve the development of more efficient flow channels by the evaluation of fluid flow patterns, pressure drops, and velocity distributions. According to the results, ZnO/water obtained the highest Nusselt number, whereas water obtained the lowest Nusselt number when used as the base fluid. However, when the rate of heat transfer increases, the pressure drop also rises, requiring an increase in pumping power. Chamil [36] optimized the design of compact heat exchangers by employing advanced Computational Fluid Dynamics (CFD) techniques. The Kern method was used to determine the pressure drop and energy consumption. Subsequently, ANSYS was used to create a computational model of the same heat exchanger, which was modified to six different models by changing its important design parameters for optimization. These parameters are mass flow rates, pressure drops, flow velocities, and vortices of shell and tube flows. The result indicated that there was only a 1.05% disagreement in the hot fluid's cooling performance between the theoretical and CFD values. Moreover, positive relationships were seen between the pumping power requirement the total heat transfer coefficient, and the axial pressure drops.

Experimental and theoretical research was conducted by Xiaojun et al. [37] analyzed the performance of a finned tube compact heat exchanger made up of steel for a heat recovery steam generator to recover both sensible and latent heat. According to the results, humid air has a higher friction factor and Colburn factor than dry air, with the difference in the friction factor decreasing as the air-side Reynolds number increases. On the other hand, for humid air, the friction factor and j factors increase as the concentration of water vapor rises. To recover waste heat from the flue gas, a fin-and-tube heat exchanger's heat transfer correlation was developed and has a maximum variation of ±7.3%. Wang et al. [38] did research on the performance of fin and tube compact heat exchangers in the air side of two louvered surfaces under dehumidifying conditions. According to the test results, fin pitch has a slight impact on heat transfer efficiency, while in completely wet conditions, fin pitch significantly increases friction factors. The relative humidity at the inlet has a negligible impact on the sensible heat transfer performance. Moreover, changes in fin pitch and tube row number did not have much impact on heat transfer performance. In order to correlate the current datasets, a correlation of

heat, momentum, and mass transfer was presented, with mean deviations of 5.94%, 6.1%, and 7.89%, respectively.

Printed circuit heat exchangers (PCHEs) are the most popular type of compact heat exchanger. The objective of printed circuit heat exchangers is to maximize the transfer of thermal energy between two fluids with minimal footprint. A printed circuit heat exchanger's have surface area density greater than 2500 m^2/m^3. Moreover, PCHEs obtained increased interest due to recent advancements in production techniques. These devices utilize the processes of chemical etching and diffusion bonding, in which metal plates are etched with flow channels. Due to its wide surface areas that facilitate efficient heat transfer between fluids. PCHEs channels' precise geometry and thermophysical properties of working fluid on flow also improves thermo-hydraulic performance. Engineers can design compact designs with printed circuit heat exchangers, which provide great thermal performance and effective heat transfer due to complex flow patterns. Furthermore, the reliability and performance of heat transfer are improved by their minimized fluid supply when compared to macro exchangers. Diffusion bonded in these heat exchangers are useful for heating and cooling processes in the industrial sector, among other uses, because of their high efficiency. Figure 1.8 depicts schematic representation of printed circuit heat exchangers.

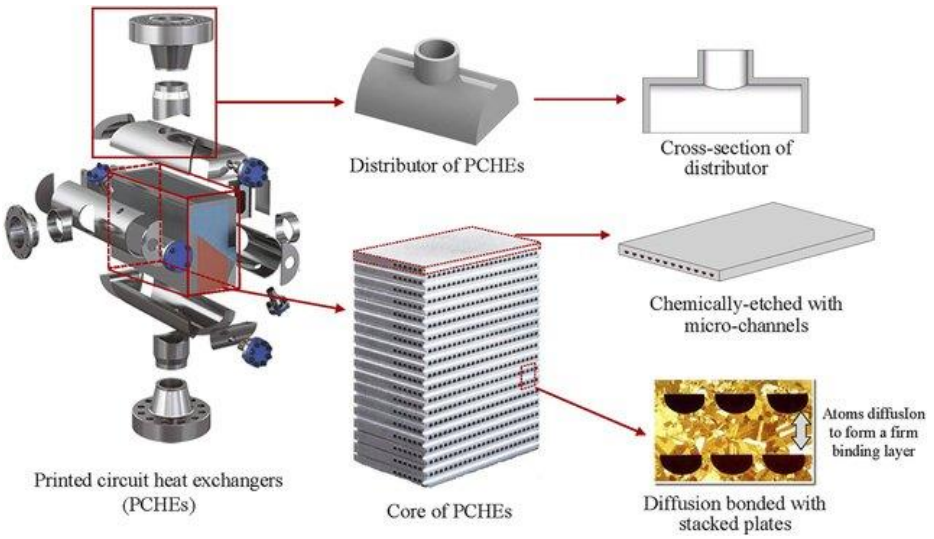

Figure 1. 8 Printed circuit heat exchangers [39]

These heat exchangers are usually made of metals with high thermal conductivity and corrosion resistance because of their application requirements. Grades 304 and 316 of stainless steel are the most popular choices for materials because of their affordability, corrosion resistance and durability. Numerous studies based on experimental and numerical simulations

of PCHEs applications have been conducted. However, more investigation is needed, particularly into the structural design and material choice for PCHEs. Konstantin et al. [40] studied the experimental supercritical CO_2 loop as well as the heat transfer and pressure drop characteristics of the PCHEs. The PCHE was made of flat metal plates with chemically machined fluid flow passages; this technique is similar to that of producing electronic printed circuit boards. According to the results, the compactness in relation to the heat exchanger core was roughly 1050 m^{-1}, while the overall heat transfer coefficient ranged from 300 to 650 W/m^2K.

Minghui et al. [41] conducted researched by computational fluid dynamics was used to simulate zigzag-channel PCHEs with high pressure and temperature helium on both the hot and cold sides and their thermal-hydraulic performance. It was noticed that a channel cross section's wall temperatures varied along its azimuthal direction. Moreover, it was determined that the zigzag channels with sharp bends had greater mean pressure losses and mean Nusselt numbers than the channels with rounded bends. The friction factor and Nusselt number decreased when the channel pitch lengths increased when the zigzag angle was fixed. Moreover, it was noted that at zigzag pitch angles larger than thirty, there was minimal increase in the Nusselt values. Mylavarapu et al. [42] researched to investigate the heat transfer and pressure drop in printed circuit heat exchangers at high temperatures for extremely high-temperature reactors. The experimental lab was built to be able to operate at pressures and temperatures as high as 3 MPa and 900–950°C, respectively. After the laboratory was built, two PCHEs with ten hot and cold plates and twelve channels in each plate were fabricated from alloy 617 plates. A modified PCHE model was successfully evaluated using simultaneous computational fluid dynamics simulations, and the outcomes for three flow rate scenarios including 15, 40, and 80 kg/h at a system pressure of 3 MPa. The result revealed that, the Nusselt number in a fully developed laminar flow was constant and unaffected by the Reynolds number. However, the local heat transfer coefficient was determined only by the fluid's thermal conductivity.

1.6 Micro heat exchangers

Tuckerman and Pease [44] introduced and used the micro-channel heat exchanger technology for the first time in 1981. S.S. Mehendale [45] defines a micro-channel heat exchanger as if the hydraulic diameter of the heat exchanger is less than 1mm. These are a unique and specialized category of heat exchangers, then macro-ones due to their smaller hydraulic diameters (D_h).

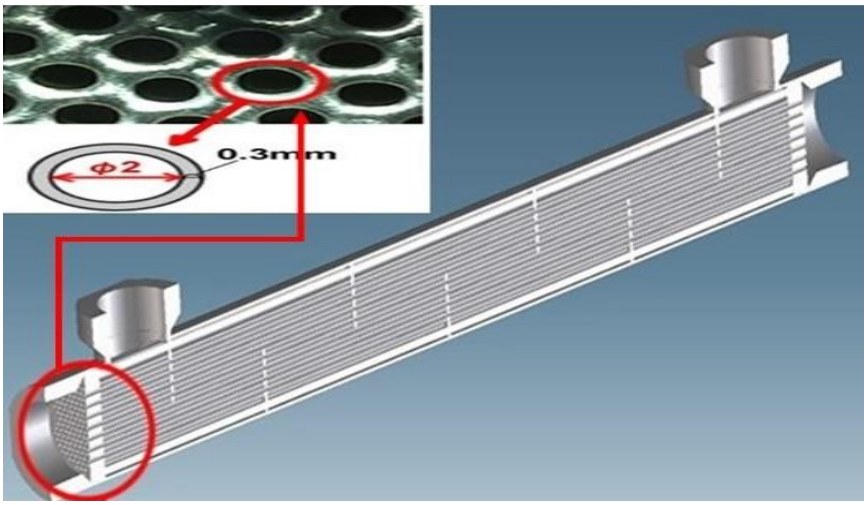

Figure 1. 9 Schematic representation of Micro heat exchanger [43]

The trend of miniaturization contributes to innovation across various sectors. Specifically lithographic and other microfabrication techniques which are conventionally employed in the integrated circuit (IC) industry, are being modified to fabricate ultra-compact heat exchangers. Micro heat exchangers are crucial for precise thermal management in areas such as microelectronics cooling, pharmaceutical industry, food industry, automotive industry, HVAC, chemical processes and so forth.

The advancements achieved in these areas highlight how crucial micro heat exchangers are in meeting the dynamic demands of modern technology and industry. In recent times, developments in industry and technology have made significant interest in micro heat exchangers, leading to numerous improvements focused on their design, efficiency, and applications. Schematic representation of micro heat exchangers as depicted in figure 1.9 developed by Tokyo titanium with high efficiency technology by processing 0.2 mm extremely thin internal diameter.

The most common type of micro heat exchanger is the micro-plate heat exchanger. A microplate heat exchanger is a highly efficient device that transfers heat between fluids using a series of very thin wavy or corrugated plates of metal. These plates provide a lot of surface area for heat exchange in a small amount of space, which makes the device extremely effective in transferring heat, and ensuring material compatibility with their compact design. The role of material is very important in the design of heat exchangers because it improves durability and potential of energy saving. Examples of the most common such materials are titanium, aluminum, copper, nickel, or stainless steel. The properties of the above-mentioned materials have high thermal conductivity and corrosion resistance, provide longer lifespans and high efficiency contribute to waste reduction. These materials have also the ability to lower carbon emissions and provide high energy savings potential. Moreover, they have the ability to work at higher and lower pressures and temperatures and also operate different fluids such as both gases and liquids. The application of microchannel heat exchangers is attracting more interest with the innovation and design of microchannel fabrication techniques, including lithography, electroplating, and molding, chemical milling, and femtosecond laser fabrication. As a result, micro-plate heat exchangers are significant in modern industries, offering reliable and efficient heat transfer solutions for a variety of applications in various industrial sectors such as the food industry, HVAC systems, chemical processing, pharmaceuticals, and food and beverage industries.

1.6.1 Factor affecting the performance of MHE

Channel geometry

In recent years, many researchers investigated the performance of micro heat exchangers in terms of efficiency by different methods. Microchannel heat exchangers can be manufactured with channels of different geometries and are depicted in Figure 1.10. Researchers are frequently searching for the ideal geometry, which could result in a small pressure drop and an increase in heat transfer. The channel size, types and various shapes in MCHE significantly impacts the heat exchanger's thermal and hydraulic performance.

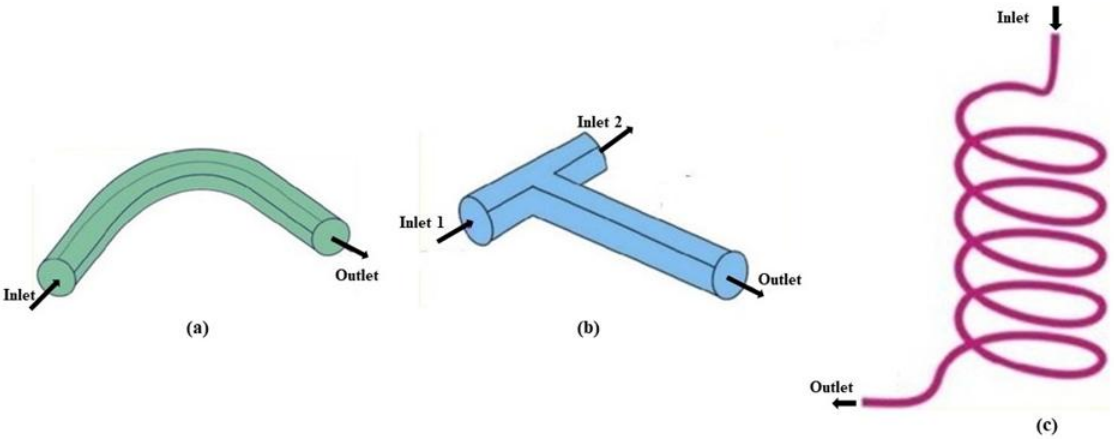

Figure 1. 10 Diagram of various microchannel (a) curved circular (b) T-shaped circular (c) curved spiral [46]

Application of channels with diameters in various fields are depicted in Figure 1.11. Different shapes/types of channels enhance heat transfer efficiency by increasing the surface area, reducing the boundary layer, and creating turbulence flow to improve convective heat transfer. Generally, velocity flow in the microchannel is low due to the smaller passage in microchannels as a result of a very low Reynolds number. Microchannel flows have relatively high friction factors and pressure gradients because there is a large amount of surface area available for a given flow volume. Similarly, the heat transfer coefficient is significantly high under laminar flow conditions and decreases as the channel hydraulic diameter increases, while maintaining a constant Nusselt number. The influence of channel size on heat transfer efficiency is highlighted by this inverse relation. Different types of microchannel are used to enhance the efficiency of micro heat exchangers such as circle, semicircle, triangle, rectangle, trapezoid, sinusoid, ellipse, annular sections and so forth. In this regard, Yaghoubi et al. [47] conducted research to investigate the impact of the size and shapes of channels on the performance of counter-flow micro heat exchangers. Investigations were also conducted on several channel configurations, such as square, wavy, ribs, V-shaped ribs, dimple, convergent, divergent, rectangular, circular, and iso-triangle. The result indicated that the influence of different channel shapes on pressure drops and heat transfer reveals that circular shape offers the best overall performance in terms of both hydrodynamic and thermal aspects and square channels offer the second-best overall performance. Moreover, heat transfer, pressure drop, and pumping increase by decreasing the volume of each channel or increasing the number of channels. Therefore, the application determines whether to increase or decrease the number of channels in micro heat exchangers.

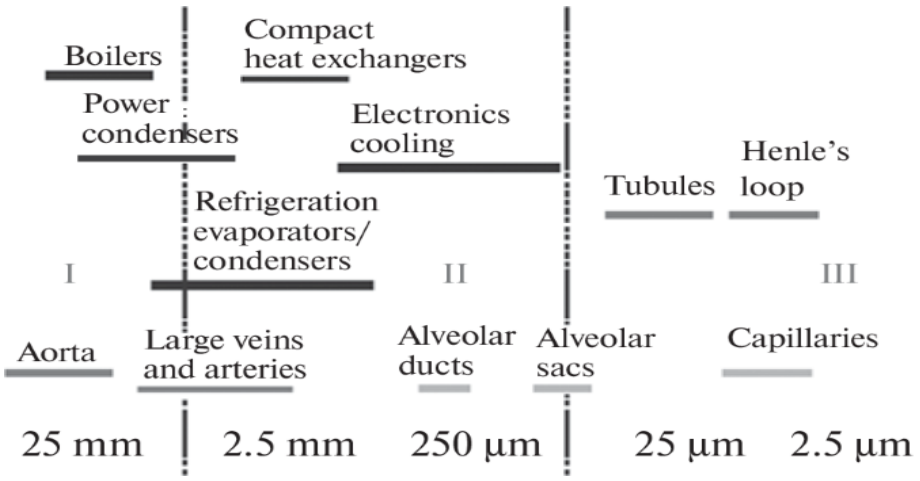

Figure 1. 11 Channel diameter ranges applied for various applications [48]

Similarly, Yang et al.[49] conducted an experimental study on three different shapes of channels in micro heat exchangers, those were designed with macro heat transfer enhancement concept, including chevron channels, long offset strips, and short-off strips for high heat flux. For comparison, a straight-channel heat exchanger was also designed. The result indicated that three micro heat exchangers have higher heat transfer enhancements and lower thermal resistance as compared to straight channel heat exchangers. Moreover, the performance of the short-strip micro heat exchanger was better than the long-strip micro heat exchanger. The third micro heat exchanger designed with a chevron channel provides lower thermal resistance, however five times higher pressure drops. Furthermore, it is important to note that traditional heat transfer enhancement techniques were successfully used to design a micro heat exchanger for high heat flux.

Tiantong et al. [50] increase the heat transfer and decrease the pressure drop in microchannel heat exchangers by introducing two different shapes of cavities and lengths of expansion and contraction sections. Microchannels were created using dry etching-based microfabrication techniques, and they were then used in fabricating single-crystal silicon for micro-electro-mechanical systems. Deionized water was used in that study as a working fluid because it has good thermal characteristics and low electrical conductivity. The result indicated that, due to adding cavity into the microchannels the heat transfer can be improved and minimize the pressure drop as compared to the straight microchannel. Conversly, for devices sensitive to increased pressure drop and pumping power consumption, cavities could be used instead of ribs, resulting in a greater pressure drop. Therefore, the conclusion obtained is that the channel's geometry significantly impacts the exchanger's thermal performance.

Nanofluids

Nanofluid is a powerful technique that plays a significant role in enhancing the performance of heat exchangers. An increase in temperature in nanofluids will cause the nanoparticles to move energetically, which will increase the amount of energy transferred. Debendra et al. [51] conducted an experimental and numerical study to analyze the performance of three different nanofluids including copper oxide, silicon dioxide, and aluminum oxide in microplate heat exchangers. They also reduce the size and pumping power and increase the higher heat flux of heat exchanger with the use of nanofluids as compared to macro heat exchanger. For comparison, three crucial parameters mass flow rate, heat transfer rate, and pumping power were used for comparison in the plate heat exchanger. There is a good agreement between experimental and predicted data in the rate of heat transfer and overall heat transfer coefficient. The result indicated that aluminum oxide nanofluid has better results than the others. The improvement in the overall and convective heat transfer coefficient was 4.85% and 11%, respectively. Moreover, it also reduced the pumping power by 6.65%, demonstrating the energy-saving potential of nanofluids.

Mehdi and Ali [52] researched to check the effect of different shapes of nanofluids on the performance of microplate heat. The shape of nanoparticles with various forms such as brick, blade, platelet, brick, oblate spheroid, blade, and cylinder with 1% of their concentration. The heat exchanger was designed with copper material having high thermal conductivity. The finding indicated that platelet-shaped nanoparticles had maximum heat flux and convective heat transfer coefficient as compared to others. The highest effectiveness was shown by the nanofluid having oblate spheroid and after which came the solutions containing nanoparticles shaped like bricks, blades, cylinders, and platelets. Finally, the microplate heat exchanger experiences the lowest pressure loss when the oblate spheroid-shaped nanofluid and pressure loss increases with the increase of Reynolds number. Chandrakant et al. [53] investigated the performance of microplate heat exchangers with hybrid nanofluids at various temperatures and flow rates. The nanofluids analyzed were ZnO/ethylene glycol nanofluids, TiO_2/ethylene glycol, and hybrid nanofluids with varied nanoparticle volume fractions. The effect on the thermal conductivity of hybrid nanofluids was determined from the measured conductivity values by using the temperature and volume fraction of nanocomposite powder. The study demonstrates that the thermal conductivity of composite nanofluids is significantly improved by both an increase in the volume percentage of solid particles and an increase in fluid temperature. Additionally, the thermal conductivity of nanofluids was shown

to increase with an increase in particle velocity and particle collisions with one another in the base fluid. Furthermore, the result demonstrated that the enhancement in the Nusselt number and convective heat transfer coefficient in hybrid nanofluids were higher than in nanofluids. Chaitanya et al. [54] conducted an experimental study to improve heat transfer by introducing the multiples twisted tapes inside the circular microchannels. The experiments performed at different twist ratios for single, twin, and times twisted tape inserts were 2.5,3 and 3.5. The result revealed, there was an increase in pressure drop but greater heat transfer was calculated by the 2.5 twist ratio compared to the smooth channel. They also developed a corelation for Nusselt number and friction factor as a function of Reynolds number with respect to twist ratio. Furthermore, as the number of twisted tape inserts increases, the Reynolds number has greater influence on the Nusselt number and friction factor values.

Yang et al. [55] conducted research to optimize the microchannel structure in order to improve plate heat exchanger performance based on three evaluation parameters such as heat transfer coefficient, pumping power consumption, and effectiveness. Thay designed optimized microchannel structure of plate heat exchanger based on minimum pressure drop and maximum heat transfer coefficient. A comparative study between the optimized structure and the contrast structures was conducted, using the area of a single microchannel element and the fluid volume fraction as limitations. The result revealed the optimized plate heat exchanger was 2.81-times higher effectiveness than comparison structure. Moreover, the pumping power and heat transfer coefficient was better than three contrast structure. The performance of a micro plate heat exchanger with a trapezoid-shaped cavity was examined by Yufeng et al. [56] in terms of heat transfer, pressure and flow characteristics. The flow characteristic is a major parameter that affects the heat transfer characteristics and pressure drop characteristics of heat exchangers. The geometry such as height, width, coincidence degree, number and distribution of cavity also influence on the performance of MPHX. The heat transfer capacity of the microplate heat exchanger, with and without the trapezoid-shaped cavity, decreases initially with an increase in flow rate before increasing once the flow rate reaches its optimal level. At higher flow rate MPHX with trapezoid shaped cavity experiences a lower pressure drop than conventional micro heat exchanger. Therefore, cavities could be useful instead of using ribs to improve the performance of heat exchangers.

The technique of simulating flow and heat transfer in heat exchangers with computational fluid dynamics (CFD) as well as other commercial software is very popular among research and scientists. Therefore, Lee et al. [57] used a CFD approach with different-

shaped nanofluids to investigate the microplate heat exchanger utilizing hybrid nanofluids Al_2O_3/Cu and single particles Al_2O_3. The obtained results obtained by using different shaped of nanofluids were compared by first and second law of thermodynamics. Different shapes of hybrid nanofluids and single particles were platelet, blade, cylinder, oblate spheroid, brick and prolate spheroid. According to first and second law characterizations, the results showed that for single particle and hybrid nanofluid, an oblate spheroid shape represents better performance index and a prolate spheroid shape demonstrates lower performance index at different temperature and mass flow rates for both hot and cold fluids. The OS-shaped nanoparticles demonstrate maximum values of 0.913 for the Bejan number and 4.07 for the performance index. Furthermore, as the volume fraction has increased, the characteristics of first and second law have become better. A research conducted by Shooshtari et al. [58] developed a computational fluid dynamics (CFD) model to calculate the heat transfer rate in microchannel plate heat exchanger (MPHE). Thay also used a hybrid technique to develop an MPHE, which has the advantage of requiring less computation time than a fully computational fluid dynamic model. There was good agreement found in the hybrid method results with experimental and computational fluid dynamic work. Moreover, approximation-based optimization technique applied and found that the optimized microchannel plate heat exchanger was superior to chevron plate heat exchanger designs in terms of heat transfer performance.

Dimension less number

There are three effective dimensionless parameters such as Nusselt, Rynolds and Knudsen numbers that effect on the performance of micro heat exchangers. In these aspects, Sheikholeslami et al. [59] investigated the effect of nanofluid on the performance of micro heat exchanger in the presence of magnetic fluid. According to the researchers, the particle size of the nanoparticles in the nanofluid correlates to the Nusselt number. The decrease in the size of the nanoparticles led to a reduction in the temperature differential between the wall and coolant, resulting in increased Nusselt. They also reported that Al_2O_3 have better Nusselt number copper oxide CuO. Moreover, the percentage of nanoparticles by volume that enhances particle movement, which has a significant impact on heat transfer. Sidik and Abubakar [60] numerically researched on heat transfer enhancement by utilizing nanofluid in rectangle microchannel heat sink. Their average diameter was 13 nm, and they employed Fe_2O_3-water nanofluid with varying volume percentages of 0.4%, 0.6%, and 0.8%, respectively. Figure 1.12 depicted the Nusselt number is increase with the increase of Reynolds number and volume

fraction of Fe_2O_3 nanofluid. Therefore, Nusselt number improve with the increase of volume percentage in the nanofluids.

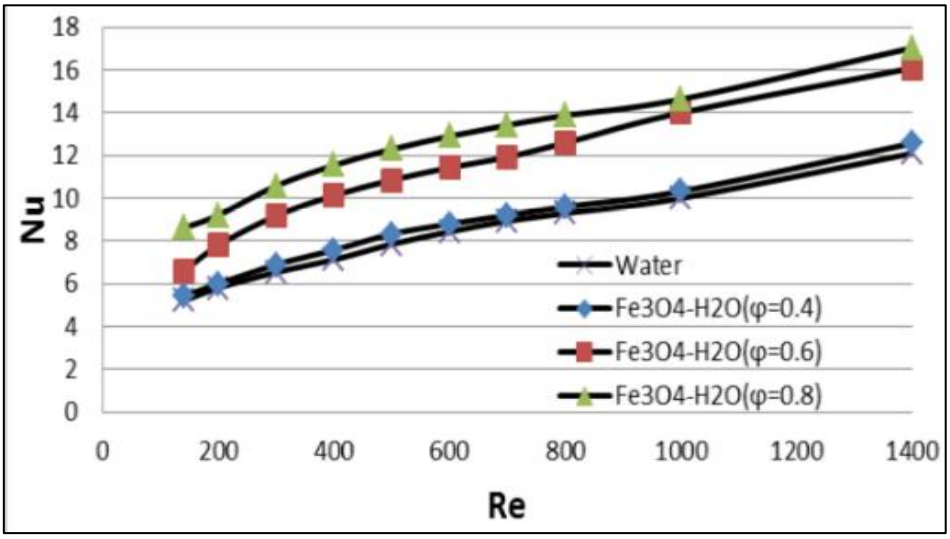

Figure 1. 12 Nusselt number with respect to Reynolds number [60]

Seungwhan et al. [61] a new measurement method was developed and implemented in order to investigate the properties of heat transfer on the wall of the microchannel with a particular focus on the conduction phenomenon across the channel walls. This model predicts the wall temperature varies across a location at the end of the heater to a certain distance from it. The size of the microchannel is very small, therefore it is difficult to measure the temperature inside the microchannel. Moreover, they also developed a numerical model to validate the experimental measurements of temperature changes and found a good agreement between them. The outcome showed that, for Reynolds numbers below 300, the Nusselt number was independent of the Reynolds number during the laminar flow regime. Mohammed et al. [62] researched to investigate the performance of microchannel heat exchangers with various factors including shapes of the microchannel, Reynolds number, and types of nanofluids. They utilized four different nanofluids such as silver, titanium dioxide, aluminium oxide, and silicon dioxide with volume percentages of 2%, 5%, and 10%, respectively. According to the results, an increased Reynolds number causes a decrease in effectiveness and an increase in pumping power due to higher shear stress along the channel walls. When the Reynolds number increased, the average temperature of the hot fluid increased, but the average temperature of the cold fluid decreased. Moreover, aluminium oxide showed a higher heat transfer coefficient, while silicon oxide indicated that higher pumping power was required at different Reynolds numbers (100-800). Furthermore, the silver nanofluids found a higher performance index than others followed

by titanium dioxide, aluminium oxide, and silicon dioxide, respectively. Shahabeddin et al. [63] compared the hydraulic and thermal performance of counter flow micro heat exchanger with and without nanofluids to investigate the effect of various parameters such as Reynolds number, volume fraction, efficiency, pressure drops, Brownian motion and consumption of pumping power on micro heat exchanger. There are two types of nanofluids used, both with three different volume fractions: water-Al_2O_3, with mean diameter of 47 nm, and water-CuO, with mean diameter of 29 nm. According to the results, pumping power, efficiency, and performance index significantly drop as the volume percentage of nanoparticles rise. The efficiency and performance index rise while pressure drops and pumping power declines as the Reynolds number drops. Moreover, the performance index for Al_2O_3 higher than the CuO with the increase of Renyolds number. Wang et al. [64] experimentally and numerically investigated the performance of microchannel heat sink with various shapes of pin fins including ellipsoidal, diamond, rectangular, backward and forward triangular. They concluded that various pin fins significantly improve the heat transfer enhancement by disrupting the boundary layer. The performance of microchannel heat sink improves in term of Nusselt number with the increase of Reynolds number; however, friction factor also increases which drawbacks of improvement. Moreover, below 300 Reynolds number rectangle pin fin while above 300 Reynolds number backward pin fin found maximum friction factor.

In microchannel, Kn number is inversely proportional with the length (L), and directly proportional with mean free path length (λ) therefore smaller length of microchannel leading to increase the Kn number. This number greatly effect on different parameters such as pressure drop, velocity profile and heat transfer [65]. Maqableh et al. [66] reported numerically the effect of Knudsen number on the performance of parallel and counter flow micro heat exchanger with heat conduction on the wall of microchannel. The result indicated that with the increase of Kn number and thermal resistance, temperature on the microchannel wall increases. On the other hand, number of unit (NTU) rise with decline of Kn number and thermal resistance. Furthermore, because of heat conduction in the separation wall and the entrance region, a thermally fully developed flow for counterflow may not occur throughout a significant part of the heat exchanger. Sinkovits et al. [67] reported the effect of three different Kn numbers at high speed with the variation of channel heights on microchannel flows. The aspect ratio was constant between the length and height of microchannels. The result indicated that with the increase of Kn number the angle and thickness increase at the entrance of

microchannels. Moreover, temperature jumps, and velocity slips were also observed and found at the entry point of microchannels.

Brownian motion

Another factor that effects the performance of microchannel heat exchangers is Brownian motion. The random movement of particles suspended in a liquid or gas as a result of collision with the fast-moving molecules of fluids is known as Brownian motion. Seyf and Nikaaein [68] numerically examined the effect of Brownian motion by utilizing various nanofluids on the thermal and cooling performance of microchannel heat sinks. Brownian motion plays a significant role in the enhancement of thermal conductivity of nanofluids. They found that in the thermal enhancement depends on various factors such as, nanofluid diameter, nanoparticle shape as well as Brownian motion. Wang et al. [69] a comprehensive study on the enhancement of thermal conductivity of nanofluids. The size of nanoparticle is subjected to several forces, such as the Van der Waals force, the electrostatic force produced by the electric double layer at the particle surface, the hydrodynamic force, and the stochastic force that cause the Brownian motion of particles. They found that, when the distance between the particles is smaller than dominating Van der forces. There are two factors that improvement the thermal conductivity as well as heat transfer of nanofluids including structure of nanoparticles and Brownian. Similarly, another study conducted by Shahabeddin et al. [63] to analyzed the effect of Brownian motion on the enhancement of thermal conductivity of nanofluids in counter flow micro heat exchanger. They found that, Brownian motion of nanofluids strongly influence on the enhancement of thermal conductivity as well as increase the efficiency of counter flow micro heat exchangers. Moreover, as the volume fraction and Reynolds number increase, the impact of Brownian motion on efficiency increases.

Mohammad et al. [70] reported the impact of viscous dissipation , trapezoidal structure of channel and Brownian motion on heat transfer enhancements for microchannel heat sink. The findings obtained demonstrate that the diffusion coefficient of Brownian particles decreases with an increase in nanoparticle diameter. Moreover, it increases as the temperature and volume percentage of nanoparticles rise. Moreover, the other parameters such as the volume percentage of nanoparticles and viscous dissipation increase as a result of heat transfer decreases.

It is concluded that various parameters including nanofluids, channel geometry, dimensionless number (*Nu, Re* and *Kn*) significantly effect on the performance of micro heat exchanger.

1.6.2 Manufacturing Techniques

Currently, it is challenging to manufacture microchannels for heat exchangers utilizing a variety of materials; therefore, more research is needed to find more effective manufacturing techniques as well as precise microchannel shapes. Typically, different types of materials are utilized to manufacture the microchannels such as metallic, polymeric, ceramic, glass, semiconductors and composite. These materials are preferred due to their unique properties such as excellent thermal conductivity, high strength, hardness, light weight, resistant to corrosion, high melting point, thermal stability, and so forth. Therefore, further research is needed to select the efficient materials, precise geometry as well as more efficient fabrication techniques. Regarding fabrication techniques are classified into two different types such as conventional and modern technologies are depicted in Figure 1.13 to manufacture the microchannels. The fabrication methods developed a microchannel with precisely measured geometries and dimensions, significantly enhancing the microchannel's performance.

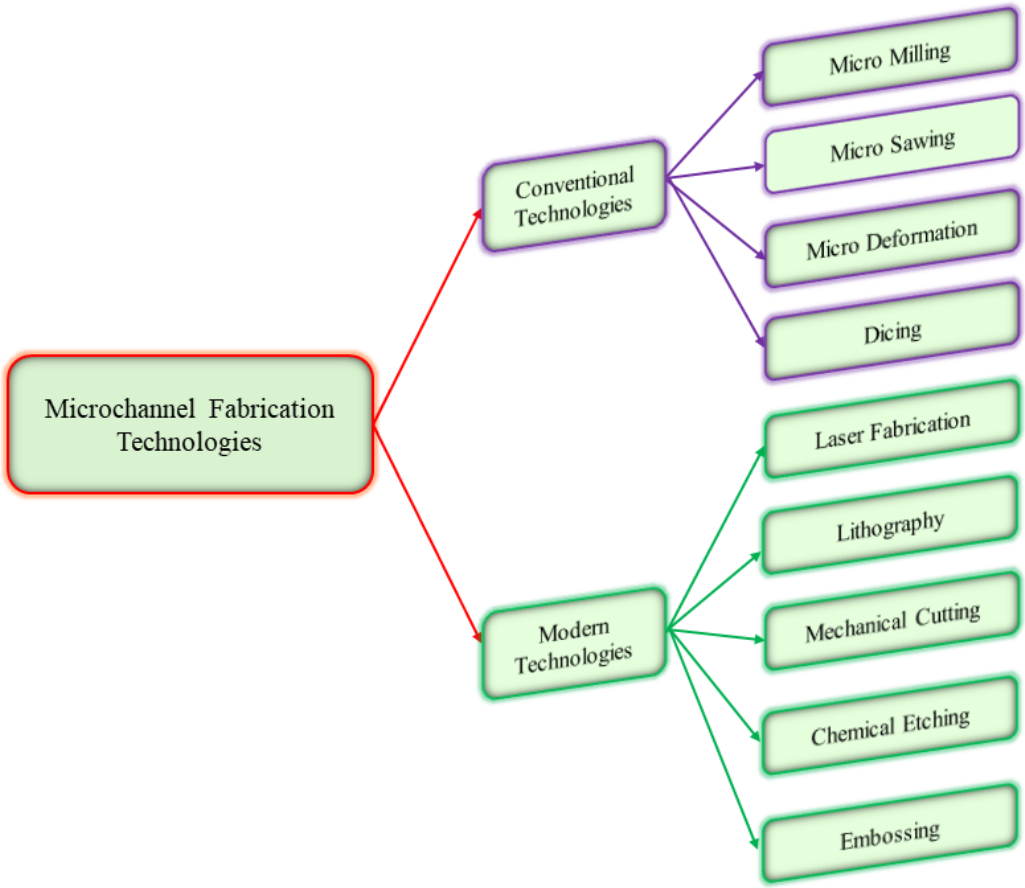

Figure 1. 13 Classification of microchannel fabrication techniques

Laser Fabrication

Laser fabrication is a innovative technique in which a high-powered laser is used to perform various operations with quickly and high precision and accuracy. Almost every type of substrate material can be processed with laser technology, which also has the advantage of being very flexible and requiring short processing times. This technology utilizes powerful laser beams to a variety of materials, including metals, polymers, ceramics, glass, semiconductors and composites, to perform a range of operations including cutting, engraving, welding, and surface modification. The advantages of laser techniques over other techniques because it is easy to use, scrapless, environmental friendly. Various laser fabrication methods for manufacturing microchannels are shown in Figure 1.14.

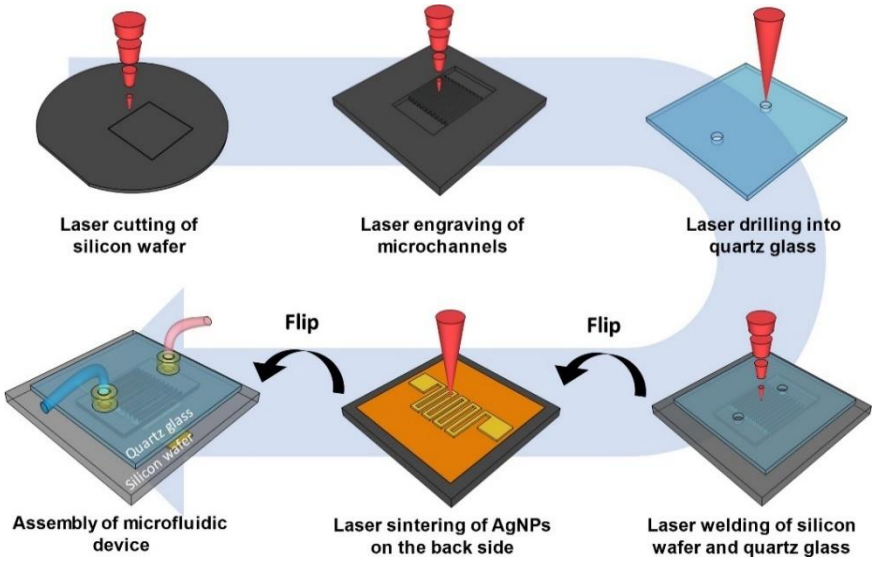

Figure 1. 14 Laser fabrication of microchannels [71]

In recent years, laser processing of microchannels have been developed and researched by various scientists. Chen et al. [72] did a simulation-based study to investigate the surface roughness and improvement in the microchannels with the excimer laser fabrication method. It was found that the excimer laser's fluence has a significant impact in determining the microchannel surface roughness because both the surface roughness and the depth of the microfluidic channel increase as it increases concentration. It is possible to significantly reduce the surface roughness of microfluidic channels by excimer laser polishing. The surface roughness decreases as the irradiation time frame increases, however, if the irradiation time is too long, some flimsy stripes will form on the corner of the edges, worsening the surface roughness. Similarly, another study Hong et al. [73] utilized novel techniques CO_2 laser beam for scribing microchannels. The results demonstrate that by using an CO_2 laser beam during

the scribing process, a smooth channel wall can be achieved without the requirement for a post-machining annealing operation. Moreover, this laser fabrication is a cost-effective and adaptable way to prototype polymethylmethacrylate-based microfluidic devices quickly. Recently, Jianlei et al. [74] used a UV nanosecond laser processing machine to conduct an experimental investigation by fabricating a microchannel composed of diamond material having high thermal conductivity. However, it is a big challenge to manufacture the straight microchannel by utilizing diamond material. They manufactured a 1600μm deep collecting groove with a smooth bottom geometry by combining an improved multi-feed technique with a grid path spaced 1 μm.

Micro-mechanical cutting

One of the key techniques for creating microchannels is micro-mechanical cutting, which enhances heat transfer in microchannels by providing better surface finish and channel accuracy using high-precision machine tools. The advantages of micromechanical cutting as compared to laser as it doesn't need a piece of particularly expensive equipment, in comparison with laser fabrication techniques, therefore microchannels are easily manufactured at a low cost. Furthermore, a wide range of materials can be fabricated, including steel, aluminium, brass, plastics, and polymers. Commonly, there are two types of micro-mechanical cutting are micro milling and micro cutting [74]. Recently, using micro-milling techniques, Zhou et al. [75] fabricated rectangular copper microchannels and investigated their burr formation and surface roughness characteristics at various feed rates, spindle speeds, and depth of cut. They also investigated how burr form within the microchannels by simulation based and experimentally. The finding indicated that by changing the micro-milling parameters, surface roughness variations of the microchannel bottom and sidewalls generally correlated with the top burr size on the down-milling side. It was observed that, in the micro-milling of microchannels, top burr formation and its size on the down-milling side were significantly larger than those on the up-milling side. Moreover, various micro-milling processes such as thin depth of cut, high spindle speed, and medium feed rate enhance the surface quality of the microchannel, emphasizing the selection of an optimum cutting-edge radius. Similarly, Vázquez et al. [76] analyzed experimentally the effect of various micro milling process such as spindle speed, feed per tooth, depth of cut, and coolant applications during fabrication of metallic microchannel (aluminium and copper). These parameters significantly influence on quality of finishing surface and precise dimensions of microchannels. It's important to determine which process factors have the greatest influence on the final product quality and

how much altering them would impact it. The outcome showed that, at high feed rates, aluminium microchannel width was more controllable during manufacturing than copper. Moreover, by utilizing coolant provides higher quality in terms of average micro-channel width and bottom surface roughness in both aluminium and copper materials. A mechanical cutting force model was proposed by Lee et al. [77], to estimate the cutting force accurately in micro-end milling under particular conditions. Based on measured cutting forces, these cutting force coefficients represent the effects of most cutting mechanisms utilized in micro-end milling, including the influence of the minimum chip-thickness.

The size and surface quality of the micro-structures depend on precision cutting tools and machine tools, which are essential to micro-mechanical cutting operations. Various mechanical cutting tool are shown in Figure 1.15. Hyuk et al. [78] carried out research to confirm precise accuracy and economic efficiency by fabricating the aluminium mould using two different techniques, micro cutting and microelectromechanical systems (MEMS). They found that micro cutting was fifteen time cheaper than MEMS techniques during manufacturing of aluminium microchips. Therefore, micro mechanical cutting is simple, fast, and cheaper for manufacturing the microchip. Jingwei et al. [79] developed a copper microchannel micro rolling process. They performed annealing operation at different temperature (400°C, 500°C, 600°C, 700°C, 800°C) on copper foil having thickness of 0.1mm. The result revealed that optimum annealing temperature (500°C) was made possible by refined microstructure and texture, which also improves the accuracy of microchannel formation during micro rolling.

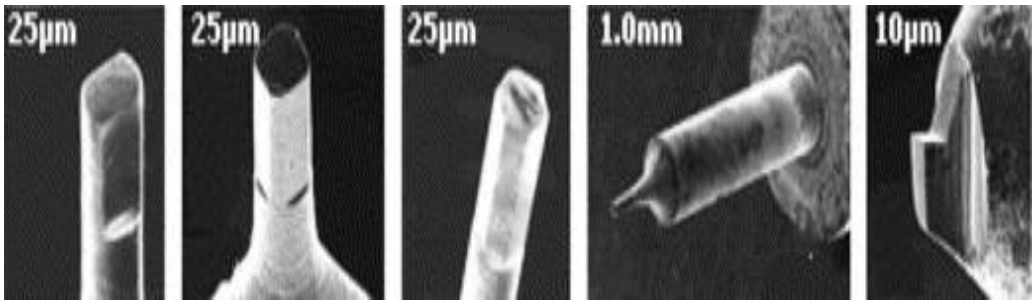

Figure 1. 15 Various micro cutting tools [80]

Lithography

One of the main methods for designing the microchannels is lithography. It is difficult to generate a wide variety of topography using other fabrication techniques, but lithography makes it possible. High resolution and precision are two major benefits of lithography-based microfabrication, but the complex structure of the fabrication process requires a clean-room

environment and costly equipment [81]. Photolithography is the most common technique of lithography, in this aspect Sungyoung and Je-Kyun [82] researched two-step photolithography that demonstrates the usage of the method for creating multilayer microchannels in microfluidic applications. They investigated how the thickness of printed microchannel features varied in the photoresist, using two-step photolithography. The thickness and width of the specified photoresist pattern in the first step and the spin-coated photoresist film's thickness in the second step determine the final photoresist thickness. Chihchen et al. [83] demonstrate the grayscale lithography in photoresist creating a photomask with fluids. The produced photoresist pattern for a specific microfluidic photomask can be predicted based on the photomask and dye concentration dimensions.

According to Kandlikar et al. [84], lithography, electroplating, and molding (LIGA) offers all the benefits of X-ray lithography. By projecting highly directed X-rays through a unique X-ray mask, LIGA is able to expose a thick photoresist that is almost diffraction-free. This method can produce structures with aspect ratios more than 100:1 and maintain submicron requirements. Recently, Haruki et al. [85] used ultraviolet nanoimprint lithography to manufacture the complex polymer microchannels. The findings demonstrate that the nanoimprint UV lithography approach quickly creates hybrid microchannels on a single resistance layer. Furthermore, collected cells within the channel can be imaged using the UV-curable polymer since the refractive index of it was nearly equal to that of water. Similarly, Azrena et al. [86] manufactured multiple size microchannels (1,3,5μm diameter) based micro sorting devices by utilizing ultraviolet lithography technique. The finding demonstrated that direct laser writing is an appropriate technique for fabricating the IP-L porous micro-channel and Polydimethylsiloxane PDMS micro-channel adhesion of the IP-L allows it to be suitable as a photoresist.

Chemical etching

Etching is typically used as a type of subtractive technique in various micro-machining processes. Usually, the materials used to make microchannel devices are typically metallic, polymer, semiconductors, and ceramic; however, these materials cannot withstand temperatures higher than 300°C. Therefore, constructing such devices using materials that can withstand higher temperatures is crucial because many chemical reactions function at temperatures above 300°C. Rao and Deepak [87]manufactured the microchannel having depths of nearly 200 μm with stainless steel by applying wet chemical etching. Etchant is made of various concentrations of HCl, $FeCl_3$, and HNO_3 mixed with water utilized to etch

microchannels on substrates made of stainless steel. The result revealed that the etch rate and etch factor increase as the concentration of HCl in the etchant increases, but the roughness was affected more adversely. Additionally, the channel depth and etch factor were highly influenced by the operating temperature and etchant composition. Rodrigo et al. [88] performed a chemical etching process by using a femtosecond laser to create microchannels with a rectangular shape in order to develop three-dimensional structures. During the engraving process, the femtosecond laser energy and sample were etched in acid to determine the final microchannel width. The control procedure involves increasing the laser power and concentration, developing the recording program, and etching the material to allow for different structural shapes for diverse purposes in order to maximize line-by-line imprinting.

Embossing or imprinting

In the 1990s, the Institute for Microstructure Technology at Forschungszentrum Karlsruhe used the embossing technique for the first time to recreate or replicate the microstructures. Hot embossing is the term for an embossing technique that is especially helpful in the replication process and typically requires a high degree of temperature that is comparable to the temperature of polymer molding. Additionally, wires are utilized for imprinting on plastic surfaces. It has been discovered in recent research that silicon stamps are superior imprinting tools for manufacturing microchannels.

Ming-Chung et al. [89] investigations were conducted on how the molding condition affected the precision of microfeature replication. The finding indicated that embossing load, temperature, and embossing time all have a substantial influence on the accuracy of the microchannel depth and width. Moreover, positions have an impact on the quality of imprint replication; higher replication accuracy is produced when one is closer to the center of moulded components. Similarly, Deshmukh et al. [90] did research on the improvement of accuracy of hot embossing an embossed micro-channel with a laser-patterned copper mold to replicate their design. A fibre laser machine was used to manufacture a positive-feature micro-patterned mold for hot embossing. They also investigated the impact of three different parameters including embossing temperature, embossing pressure, and embossing time. At the optimal condition, the depth of the embossed micro-channel increased from 28.6 μm to 46.5 μm, and the replication accuracy improved from 59.34% to 96.33% compared to the initial parameter levels. Moreover, the embossing temperature plays a significant role in replication accuracy, accounting for 70.52% of the process overall.

1.6.3 Advancements in micro heat exchangers: food and pharmaceutical industries

Micro heat exchangers play a crucial role in both food and pharmaceutical industries. Currently researchers are focused on several key areas to improve efficiency, cost-effectiveness, reliability, and applicability. Some of these key areas are as follows,

- Advanced materials
- New fabrication techniques
- Performance optimization
- Integration with other technologies
- Energy efficiency and sustainability
- CFD (Computational Fluid Dynamics) modeling
- Smart sensors
- Artificial Intelligence (AI)

Advanced materials: The researcher focuses on biocompatible, food grade and nanomaterial materials to enhance heat transfer and minimize thermal resistance for micro heat exchangers in industries such as pharmaceuticals and food processing. Regarding direct-contact applications, where material compatibility and hygiene are critical, these materials not only provide thermal efficiency but also provide safety. Biocompatible and food-grade materials such as advanced stainless steels, polymers, and ceramics possess remarkable resistance to corrosion and fouling. These materials contribute to better equipment lifetimes and lower maintenance costs in addition to maintaining the safety and hygienic standards required in both industries.

Another effective material is phase change material, which is suitable for applications with varying heat loads because it can absorb and release significant amounts of thermal energy during phase transitions, generally between solid and liquid or vice versa. They are widely used in thermal energy storage applications, especially for systems their utilization for cooling and heating. They are used in the food processing to control temperature during refrigeration, transportation, and preservation. This helps to maintain perishable product safety, flavor, and nutritional content while reducing waste and spoilage. On the other hand, these are effectively control thermal conditions by absorbing and releasing heat during phase transitions to maintain certain temperature ranges for drugs and vaccines in the pharmaceutical industry. The efficiency of a PCM-based thermal energy storage system, which is dependent on the properties of the PCM, including thermal conductivity, melting point, operating temperature range, energy

storage capacity, and heat of fusion, has a significant impact on energy savings and a more comfortable indoor environment [91]. The two main classifications of phase change materials are solid–solid and solid–liquid PCMs, which are differentiated by their specific phase transition behaviors. Solid–liquid PCMs move from a solid to a liquid state, whereas solid–solid PCMs oscillate between distinct solid states [92]. Ho et al. [93] enhanced a 70% improvement in heat transfer and a 45% in the performance index through introducing nano-encapsulated phase change materials into a mini-channel heat sink. Zhou et al. [94] used composite phase change materials (CPCM) to enhance the efficiency mini-channel plate heat exchanger. Their findings demonstrate the feasibility of using a mini-channel plate heat exchanger with composite phase change materials for efficient domestic hot water production.

Nanofluids improve heat transfer characteristics and reduce thermal resistance, therefore they significantly enhance the efficiency of micro heat exchangers. Various nanomaterials like graphene, nanostructured coatings and carbon-based nanomaterials are being used in micro heat exchangers. These materials have high thermal conductivity, enabling more efficient heat transfer across the exchangers as well as improving overall performance and reducing energy consumption. In heat exchangers, nanofluids can also minimize fouling and corrosion, prolonging the lifespan and lowering maintenance costs. Introducing nanofluids into micro heat exchanger designs can improve thermal performance and offer an economical solution for a range of applications, such as electronic cooling, HVAC systems, and manufacturing [95]. Painuly et al. [96] conducted an experimental investigation of the heat transfer and flow characteristics of hybrid nanofluids (SiC-MWCNT and Al_2O_3-MWCNT) in a heat exchanger using helically corrugated tubes. In comparison to smooth tubes, the results demonstrate that the addition of nanofluids improves the Nusselt number by 61.3%. The effect of nanofluids is briefly explained in the above section 1.6.1 (factor affecting the performance of MHE). Table 1.2 provides the material properties for micro heat exchangers.

Table 1. 2 Suitable material properties for MCHE.

Parameters	Properties
Thermal	High thermal stability, high heat transfer efficiency, high thermal conductivity
Mechanical	High fracture toughness, low thermal expansion coefficient, and mechanical stability
Economic and environmental	High resistance to corrosion, reduced energy consumption, lower manufacturing costs, and carbon footprints, lifecycle cost

New fabrication techniques: Complex microchannel structures are constructed with high accuracy and precision by employing cutting-edge design and production methods including additive manufacturing, 3D printing, advanced surface treatments and microfabrication. There are different 3D printing methods such as fused filament fabrication, binder jetting [97], material jetting [98], multijet fusion [99], stereolithography [100], selective laser melting [101], and electron beam melting [102]. These techniques allow for the manufacturing of these heat exchangers with improved heat transfer efficiency, with better surface area to volume ratios and compact designs that are perfect for integration into existing processing systems. 3D printing makes it possible to create micro heat exchangers with complex channel patterns that were previously impossible to do using conventional manufacturing techniques. Moreover, development of advanced microfabrication methods to produce highly accurate and effective microchannel structures by different methods such as 3D printing, laser fabrication and micro-machining [103]. Various heat exchangers manufactured through 3D printing techniques are shown in Figure 1.16.

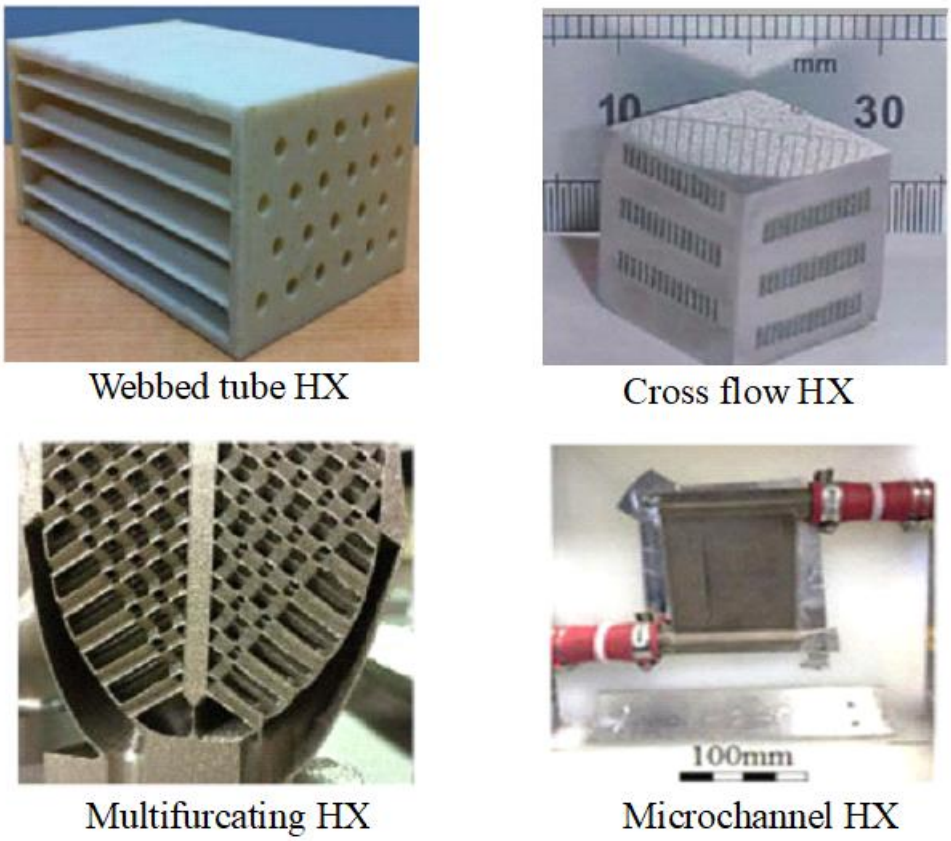

Figure 1. 16 Heat exchangers manufactured through 3D printing techniques [104]

Performance optimization: To enhance heat transfer, researchers investigated various flow patterns, surface treatments, and microchannel designs to maximize heat transfer efficiency. The different sizes, forms, and patterns of the channels that fluids pass through in micro heat exchangers are referred to as microchannel configurations. The most common configurations are including zigzag, straight, serpentine, and pin-fin channels. The objective is to find the ideal balance between fluid resistance and heat transfer efficiency, as each configuration has a different impact on fluid flow and heat transfer characteristics.

Heat transfer performance can be improved by using surface treatment methods such as adding micro- or nanostructures to facilitate fluid mixing, roughening the surface to produce turbulence, or coating the channels with thin coatings of highly thermally conductive materials. Furthermore, fouling or scaling is becoming a major barrier behind achieving high heat transfer exchange between two fluids and mostly found on tubes because it combines a number of contaminants, it is challenging to determine the type of scale production. Therefore, fouling has a major impact on the performance of heat exchangers and product quality in both food and pharmaceutical industries. Figure 1.17 illustrates possible deposition and removal

procedures for a typical system. Deposition rates are dependent on modifications that are caused by deposits, such as increased flow velocity and surface roughness, but they are not affected by the amount of deposits. On the other hand, removal rates often rise as deposit amounts do. Moreover, the fluid passing through most heat exchangers contains some dirt, oil, grease, and organic or chemical deposits, which lowers the heat transfer coefficient. Therefore, the deposition issue has to be the focus of future advancements in micro heat exchangers.

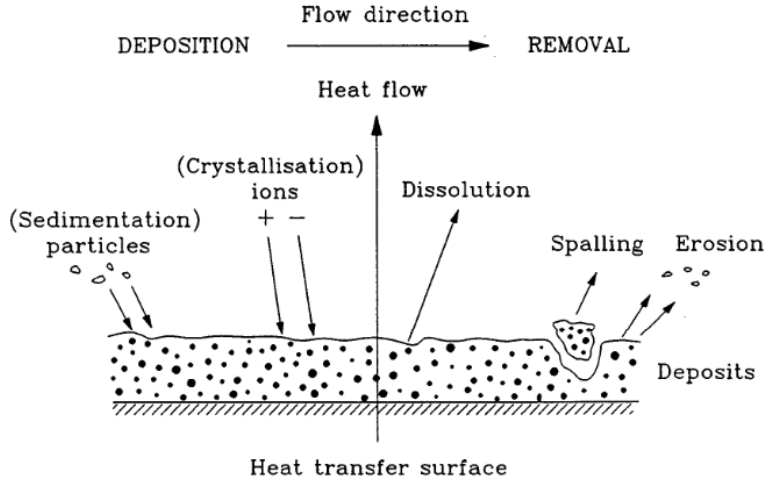

Figure 1. 17 Different deposition and removal processes during fouling [105]

CFD modeling: CFD has been used to heat exchangers during design and optimization stages to address problems including fouling, pressure loss, thermal analysis, and fluid flow maldistribution. In microchannel systems, flow maldistribution is a common issue that can result in poor performance due to unequal fluid distribution. In order to obtain a more uniform flow distribution, researchers improve the microchannel geometry by using CFD simulations to predict and identify areas of maldistribution. These models enable engineers to virtually explore different configurations, microchannel geometry, flow arrangements, predicting heat transfer efficiency, pressure drop, and other crucial parameters with precision. In micro heat exchangers, advanced computational fluid dynamics (CFD) models are utilized to simulate various designs and operating conditions, serving to optimize performance before physical prototypes are constructed. Moreover, machine learning algorithms play a vital role in analyzing operational data generated from micro heat exchangers. It can forecast performance trends, identify anomalies, and provide design changes by analyzing patterns and correlations from there data [106].

***Smart Sensors*:** A smart sensor is an advanced device that measures physical properties such as motion, flowrate, temperature, pressure, and significantly improves the precision, efficiency, and reliability in various applications such as HVAC, robotics, heat exchangers, industrial automation, food safety monitoring and so on [107]. It can be used in micro heat exchangers to monitor critical parameters including temperature, flow rates and pressure in real-time to improve thermal efficiency, sustainability, predictive maintenance, and fault detection and Diagnostics. As an example, if an extremely small temperature differential is observed, it may indicate that the heat exchanger is not transporting heat as it should be, either because of scale deposition or a fluid imbalance.

The use of IoT (Internet of Things) along with smart sensor integration for remote monitoring and predictive maintenance to detect temperature, flow rates, and pressure drops improves their efficiency and reliability. They enable precise control overheat management procedures and are a source of real-time data. Real-time data is very useful to keep the heat exchanger performing at its maximum effectiveness and to avoid overcooling or overheating. Micro heat exchangers are maintained at the proper temperatures for processing and storage by smart sensors, which are essential in the food and pharmaceutical industries where accurate temperature control is essential. They aid in the efficient management of heat dissipation in electronics cooling, protecting expensive components from thermal harm. With developments in sensor innovation and the incorporation of AI and IoT, smart sensors are now being utilized in micro heat exchangers. These developments will allow them to become more efficient, and diverse in their applications [108]. Chu et al. [109] studied integrated graded SMA vortex generator smart microchannel heat exchangers, which improve cooling performance by adapting at random hotspots. According to the findings, channels incorporating integrated graded SMA vortex generators perform better than conventional coil vortex generators in terms of heat transfer while requiring less pumping power.

Artificial intelligence (AI): Artificial Intelligence *(AI)* offer significant potential for the design, optimization, cost reduction, and performance analysis of micro heat exchangers [110]. Various artificial intelligence techniques including neural networks (ANN), machine learning, deep learning, data analytics and expert systems provide significant improvements in diagnostics, predictive maintenance, and performance optimization [111]. These technologies can be used to improve several types of micro heat exchanger applications, especially where precise heating and cooling is crucial, such as food processing and pharmaceuticals sectors. In this scenario, artificial intelligence (AI) has become significant for design optimization,

performance prediction, real-time monitoring and control, material innovation and selection, as well as enhanced simulation and modelling [112].

Heat exchanger data, both real-time and historical pattern data, can be analyzed by AI-driven machine learning algorithms to predict future breakdowns and maintenance needs. Due to this proactive strategy minimizes unscheduled downtime, lowers maintenance costs, and increases the equipment's lifespan. It can identify intricate correlations between variables such as variations in pressure and temperature that may not be evident through manual analysis or conventional statistical tools. Moreover, to identify degradation or fouling in the beginning, operators can correct possible problems before they cause noticeable drops in performance [113].

Artificial intelligence can optimize heat exchanger designs by identifying the most effective configurations and materials by evaluating vast amounts of data. To investigate a wide range of potential designs and suggest innovations that improve performance through the use of techniques such as reinforcement learning and genetic algorithms. Genetic algorithms are able to determine the best heat exchanger designs that compromise cost and performance by analyzing and refining design options through multiple iterations [114]. Moreover, heat transfer surfaces and flow patterns are two examples of parameters that reinforcement learning continuously learns from simulation results and real-world performance data to optimize in heat exchanger design.

Modern AI algorithms can monitor the heat exchangers performance in real-time, providing important details regarding possible problems and how well they are performing. These devices use sensors and data analytics to monitor temperature, pressure, and flow rates, which allows immediate improvements and corrections [115]. An important development in engineering has been made with the integration of AI into heat exchanger technology, which has allowed various industries to increase production, minimize costs, and improve operational reliability. Heat exchanger design, optimization, and maintenance could be completely changed by the field's ongoing research and development, which promises to unlock additional potential [112].

1.6.3.1 Case Study and real-world implementations of AI in the food industry

To analyze a case study that focuses on the food industry, especially the application of AI to predictive maintenance in a food processing plant. In food processing plants, heat exchangers play a significant role in controlling temperatures for operations such as

pasteurization and sterilizing. Predictive maintenance is an active approach used to ensure product quality and improve operational efficiency. This approach lowers maintenance costs and decreases downtime by utilizing cutting-edge AI technologies.

Implementation: The organization should analyze the previous operational data, such as temperature, flow rates, pressure drops, and variables related to product quality, using AI-driven algorithms. The AI system was able to identify optimal configurations for the heat transfer surfaces and flow patterns in the heat exchangers by fusing real-time monitoring with predictive analytics. As a result, the following benefits have been obtained.

- Minimize unplanned downtime
- Extended equipment life
- Enhanced Process Reliability:
- Cost saving
- Energy savings

1.6.4 Importance of corrugated pipes in micro HX: food and pharmaceutical Applications

Corrugated pipes are useful in micro heat exchangers, particularly where compact design and improved surface area for heat transfer are desirable. Numerous heat transfer enhancement approaches have been developed to increase the heat transfer devices' efficiency and decrease the size of the heat exchanger. The two primary methods used to improve heat transfer are passive and active. It will explain in detail in the later sections. Corrugated pipes are a passive technique and provide a more efficient alternative to classic micro heat exchangers, which can have complex microchannel shapes. They are constructed from a wide range of materials, including high-density polyethylene, polyvinyl chloride, iron, and stainless steel. There are a variety of benefits of corrugated due to their small size, ease of manufacture, thin boundary layer, effective heat transfer, and suitability for hygienic conditions. Moreover, the unique design of corrugated pipes causes low-frequency fluid micro-vibration, which has a broad range of potential applications and prevents the deposit problem.

There are several benefits of corrugated pipe in micro heat exchanger for both food and pharmaceutical industries. These benefits are improved heat transfer, compact design, enhanced efficiency, hygiene design, and prevention of fouling making them a valuable section in both industries. Medical devices, including laser systems and diagnostic equipment, use a microchannel to dissipate heat produced by electronic components. Therefore, microchannels

are the perfect choice for use in portable medical equipment because of their compact size and great efficiency. However, there are various challenges when using corrugated pipes in a micro-scale such as manufacturing precision and accuracy of micro channels, achieving uniform flow distribution inside the micro pipe, maintenance, and cleaning. Therefore, the production of corrugated pipes with exact corrugation patterns and microscale dimensions is a technically complex process that involves advanced manufacturing methods as discussed above in the manufacturing aspects of the micro channel heat exchanger section. Furthermore, corrugated pipes have complex geometry and microscopic dimensions usually below 1mm makes cleaning and maintenance difficult, especially in applications where deposition or fouling is a problem.

It needs innovative cleaning techniques or self-cleaning systems to make certain that these pipes do not become blocked or foul with the passage of time. The small size of microscale corrugated channels makes it harder to manage flow dynamics, which can lead to flow instabilities and maldistribution. It is also more difficult to achieve uniformity and distribution. Corrugations increase surface area and create turbulence, which improves heat transfer, but they also usually increase pressure drop. It is essential to achieve a balance between enhancing heat transfer and acceptable pressure drop levels to maximize system efficiency and operating expense. Furthermore, microscale corrugated pipes can be expensive to produce because they require advanced manufacturing techniques and high levels of accuracy and precision. Therefore, in this study we use six different types of corrugated pipes having variation in pitch size including transversal, helical and cross helix are utilized in conventional double pipe heat exchanger to enhance their efficiency. We examine the improvement of heat transfer both locally and globally in all corrugated pipes and compare results with smooth pipes. We also examine how the heat transfer enhancement affects pressure drop in both the turbulent and laminar regimes.

1.7 Heat transfer enhancement

Heat transfer enhancement is a major challenge for engineers and researchers as it involves improving efficiency while simultaneously reducing cost and optimizing the size of heat exchangers[116]. Heat exchangers play a major role in the efficient generation of energy and have a significant impact on the system's size and overall efficiency. Heat exchanger (HE) designs must equilibrium the effectiveness of the HE with the pressure drops (ΔP) in order to obtain the best tradeoff between efficiency and system size. The potential applications of heat transfer enhancement are numerous such as food processing [117], air conditioning [118],

electronics cooling [119], automotive cooling systems [120], aerospace industry [121], power generation [122], biomedical applications [123], chemical processing [124] and pharmaceutical [125]. Therefore, it is a great research argument in the field of heat transfer to enhance the efficiency of heat transfer devices as it can lead to significant savings in energy, materials, and costs. This is particularly crucial for industrial applications where thermal processing of fluids with medium to high viscosity fluids is needed. This has been demonstrated in recent decades by a significant number of scientific papers and an increasing number of registered patents about heat transfer enhancement technology.

1.7.1 Heat Transfer enhancement techniques

In general, there are three types of heat transfer enhancement: passive techniques, active techniques and compound techniques, are shown in Figure 1.18. Active techniques are those techniques that require external power for the enhancement of heat transfer performance while passive techniques do not require external power [126]. Passive techniques are considered generally energy efficient and cost-effective than active techniques due to their simplicity, reducing the potential points of failure, fewer moving parts, easier implementation, and less maintenance requirements. However, the choice between both techniques depends on the specific application and the desired level of control and customization. In recent years, most researchers and scientists have concentrated on enhancing heat transfer through passive techniques rather than other methods. On the other hand, compound techniques involve the combination of both passive and active techniques[127].

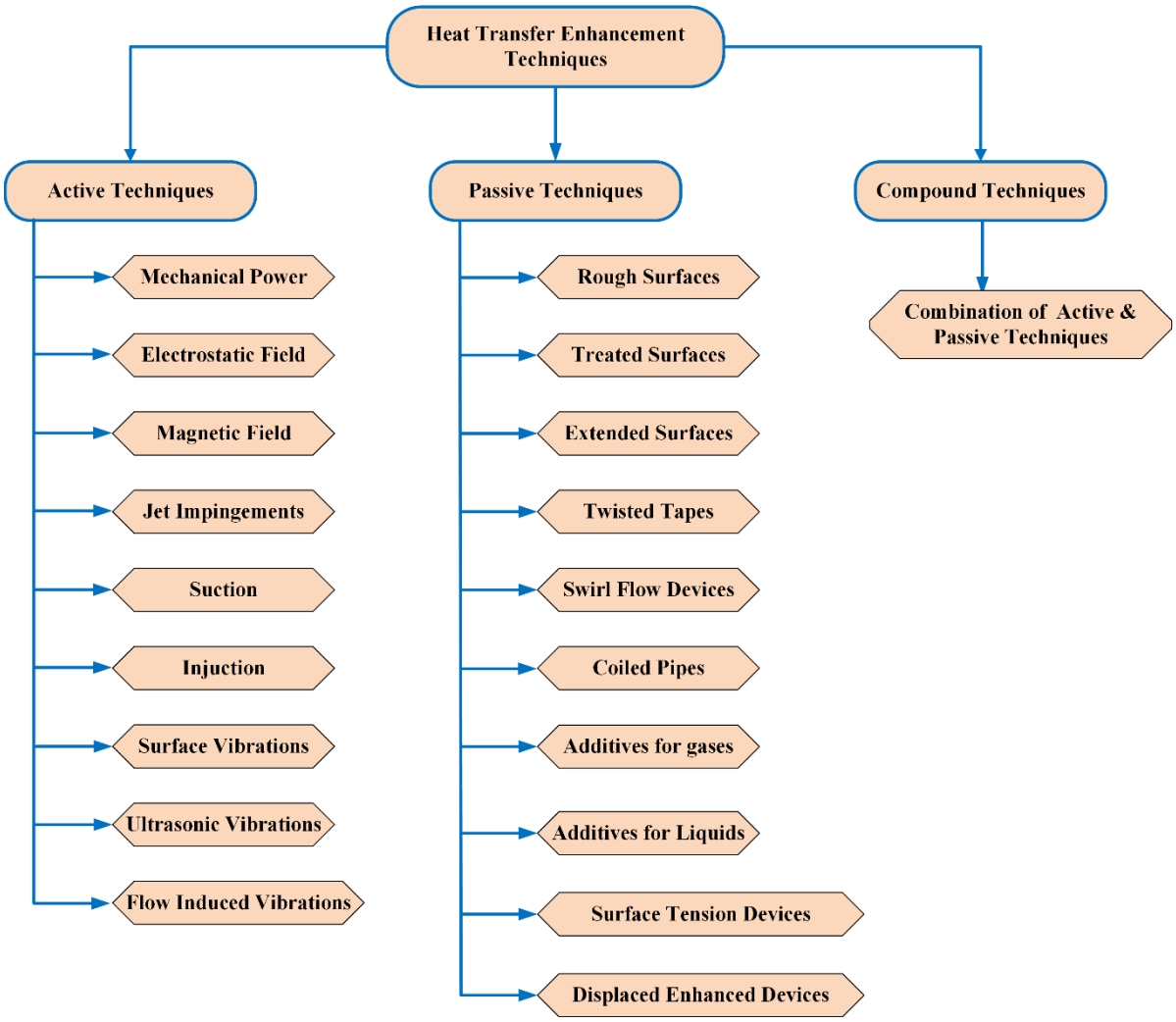

Figure 1. 18 Various techniques for heat transfer enhancement

1.7.1.1 Active techniques

Active techniques are defined as they require external power or force to enhance or maintain heat transfer. Examples of such techniques are mechanical power, electrostatic field, magnetic field, suction, injection, ultrasonic, and surface vibrations [128]. Active techniques require high energy consumption, which makes them more complex and less popular as compared to passive techniques. These techniques are used in various engineering applications such as electronics cooling, heat pipes, active thermal management, electro-thermal techniques, and forced convection[129]. Mechanical power or aid is one of the interesting methods of active techniques to enhance heat transfer. In this method, mechanical components are added to disturb the thermal boundary layer, surface rotation, and scraping of the surfaces, resulting in improved heat transfer performance. Highly viscous fluids are utilized with scraped surfaces in the chemical, food, and pharmaceutical sectors. This technique was applied by Hagge and

Junkhan [130] in an air heat exchanger to enhance the convective heat transfer of low viscous fluids. Figure 1.19 depicts a sketch of the scraped surface heat exchanger, which is composed of three components: a rotating shaft, a shell, and scraping blades known as scrapers. In the scraped surface heat exchanger, the scrapers play a crucial role by continuously mixing the working fluid which flows in the annular space between the shell and the shaft. Simultaneously, they remove the fluid from the inner side of the shell resulting in a clean heat transfer surface and heat transfer enhancement. Rainieri et al. [131] experimentally and synthetically investigated the performance of a scraped surface heat exchanger pilot plant specifically designed for highly viscous products (food industry) in a laminar regime, enabling the estimation of a heat transfer correlation.

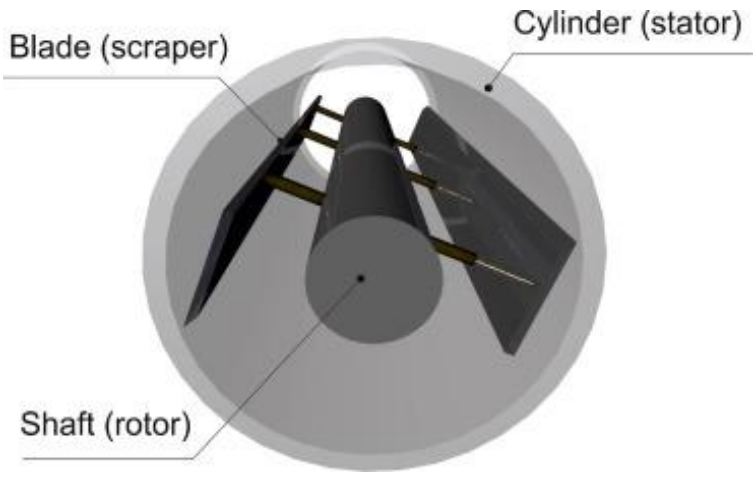

Figure 1. 19 Sketch of scraped surface heat exchanger with dual scrapers [130]

1.7.1.2 Passive technique

Passive techniques are those techniques that do not require external power or force to enhance or maintain heat transfer. Examples of such techniques are rough surfaces, treated surfaces, extended surfaces, coiled tubes, twisted tapes, etc. [132]. Passive techniques are preferred among active techniques because they have less maintenance cost, ease of implementation, environmentally friendly, energy efficiency, simplicity, and reliability. However, these techniques increase heat transfer by changing the flow treatment, which also raises pressure drop. Moreover, it's important to note that the choice between passive and active techniques depends on different factors such as desired performance results, available resources, and requirements of applications [133]. These techniques are used in various

engineering applications such as heat exchangers, electronics cooling, automotive cooling systems, building materials, heat recovery systems, etc.

Rough/Corrugated surfaces

In recent decades, rough or corrugated surfaces have been widely recognized as one of the most effective passive methods to improve heat transfer for many systems. Generally, it creates disturbances in the fluid flow, which causes turbulence as a result increases fluid mixing, and improves convective heat transfer between the fluid and the surface. The thermal performance of the system can be affected by different parameters such as the pitch, shape, arrangement, length, and height of rough surfaces[134]. Zhong et al. [135]experimentally investigated the effect of rough surfaces on heat transfer enhancement in a turbulent regime on round jet impingement. They observed that heat transfer enhancement varies from 2.53% to 6.08% respectively, due to roughness when compared with a smooth surface. Moreover, shear stress on the wall can be reduced with the increase of roughness height. Moita et al. [136] conducted a study, utilizing both numerical and experimental methods to investigate the pressure drops and heat transfer performance of helical corrugated tubes. They found that the thermal performance of helical corrugated was up to five times higher as compared to smooth tubes. Moreover, lower-pitch corrugated pipes have better performances in transitional and turbulent regimes as compared to longer corrugated and smooth tubes. Figure 1.20 depicts a sketch of the helical corrugated pipe, d, p, h represents diameter, pitch size and corrugation depth of pipe. Various corrugated techniques will be deeply explained in the following section, as it is main topic of the thesis.

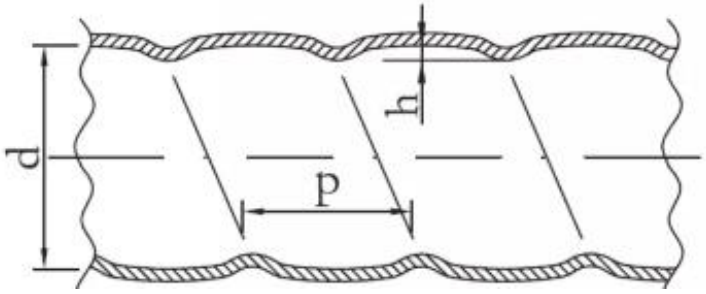

Figure 1. 20 Helical corrugated pipe [137]

Treated and coated surfaces

To enhance the heat transfer of a material, its surface characteristics can be modified through various treatments and coatings. These treatments and coatings ultimately lead to improved heat transfer efficiency of the material [138]. They involve metallic and non-metallic

coating of the surface. There are several ways in which treated and coated surfaces can improve heat transfer such as enhanced wettability, selective surface emissivity, improved roughness of surface, and increased thermal conductivity. Moreover, this technique features fine-scale alterations to their finish or coating, which are used to enhance heat transfer, particularly in boiling and condensing applications. The roughness is significantly smaller than that affecting single-phase heat transfer [139]. Rainieri et al. [140] evaluated how the wall's surface wettability affects the two-phase heat transfer throughout the dehumidification process. In this study, the critical angle of water droplets on an aluminum plate with hydrophobic coating was measured. The hydrophobic coating enhances the droplet mobility and heat transfer rate. The result revealed that a 25% convective heat transfer coefficient was enhanced with the use of hydrophobic coating with respect to the uncoated case. Ding et al. [141] studied the effects of hydrophilic coating on wavy fin and tube heat exchangers in dehumidifying conditions. When there is plenty of condensation water on the surface, hydrophilic coating can enhance heat transfer performance by facilitating the formation of a thin layer of water. However, when there is a limited amount of condensation water available, their effectiveness may be decreased. They observed that hydrophilic coatings can reduce the pressure drop and 9.9% heat transfer enhancement with reference to the uncoated surface.

Extended Surfaces

The other common name for extended surfaces is finned surfaces, which significantly increase heat transfer. Extended surfaces or fins are commonly used when the available surface area is insufficient to transfer the required amount of heat given the temperature drop and the convective heat transfer coefficient.

There are different geometrical configurations of extended surfaces shown in Figure 1.21. The extended surfaces or fins are generally made with high thermal conductivity that allow heat transfer between the outer surface and base of the fin. Coatings on fins can improve their efficiency by increasing surface area, altering surface properties (such as emissivity), or improving heat conduction. These coatings are designed to optimize heat transfer performance for specific applications and operating conditions. Fins help in dissipating heat by increasing the surface area available for convection, which allows for more efficient heat transfer to the surrounding fluid or environment. Fins can also reduce the system's temperature gradient, which could improve thermal performance and result in a more uniform distribution of temperature. The application of extended surfaces is extensively used in industrial applications i.e., engine cooling and heat exchangers. When heat exchangers with a high surface area to

volume ratio are required, fins are an extremely useful solution that has made it possible to achieve an increasing number of compact models. Moreover, it can be used in electrical appliances and electronics such as on computer processors and power supplies.

Majel et al. [142] conducted a numerical investigation in a finned double pipe exchanger on the inner tube outside surface to enhance the heat transfer. It was observed that heat transfer enhancement was 1.6 to 2 times more effective than a smooth pipe. Moreover, the heat transfer coefficient of the heat exchanger was 20% enhanced by the addition of nanoparticles (alumina) having 5% concentration. Kim et al. [143], was experimentally investigated the free convection from tubes with extended surfaces that are radially curved and oriented vertically. According to the experimental findings, the heat resistance of tubes with curved extended surfaces is 20% lower than that of tubes with straight extended surfaces. Mokheimer explored the effects of dust deposition on frosting properties on fin surfaces and discovered that as the amount of dust deposition on the fin surface increased, the frost layer's density and thickness gradually decreased [144].

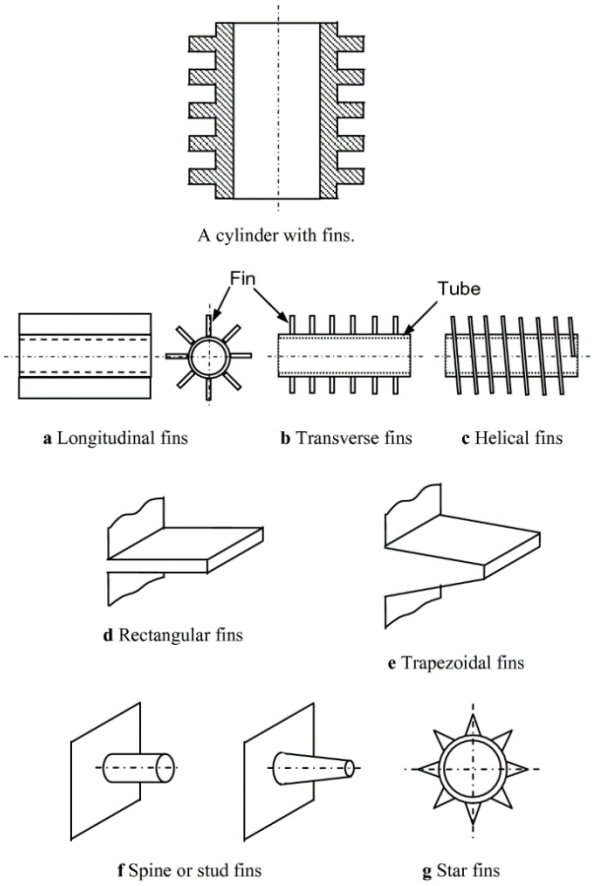

Figure 1. 21 Example of extended surfaces [145]

Twisted Tape

Twisted tape is a device that is inserted into a pipe or vessel's fluid flow path that disrupts the fluid flow and induces turbulence. This turbulence helps to improve the mixing of the fluid and enhances the rate of heat transfer between the fluids and surrounding surfaces [146]. Different types of twisted tape are used to generate turbulence such as helical, screw helical, V-cut, U-cut, overlapped multiple and trapezoidal-cut twisted tape.

During the design stage the twisted tape's width must be smaller than the inner diameter of the tube, and its thickness and twist ratio are inter-dependent correlations that need to be specified [147]. The schematic representation of twisted tape as shown in Figure 1.22. Vaisi et al. [148] conducted an experimental study to investigate thermal performance of perforated twisted tapes turbulator in double pipe heat exchanger. In this study, nine holes of various geometries, including square, rectangular, circular, and triangular with triangle arrangement, have been made on the flat surfaces of a discontinuous twisted tape turbulator. The result showed that in comparison to a continuous turbulator, a discontinuous turbulator without a hole indicates a 9.8% decrease in the pressure drop and an 8.2% increase in heat transfer.

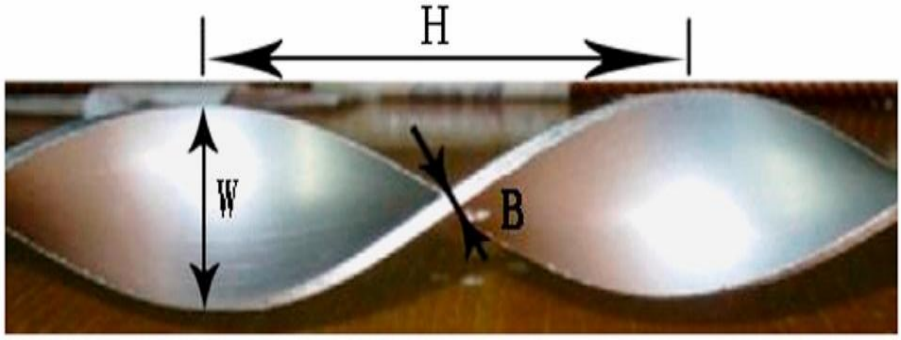

Figure 1. 22 Schematic representation of twisted tape [147]

The maximum heat transfer enhancement with circular perforated discontinuous turbulator resulted in 20.8% and 27.7% decrease in pressure drop coefficient, respectively. Wang et al. [149] experimentally investigated the thermal-hydraulic performance of self-rotated twisted tape in double pipe heat exchanger. To solve passive motion and acquire the force distribution in the frequency and time domain, dynamic mesh and the Six Degrees of Freedom approach were combined in the experiment to conduct thermal performance under various flow rates. The Nusselt number increases by 22.67% and the friction factor decreases by 26.25% when comparing the thermal-hydraulic performance of assembled self-rotating twisted tape to stationary twisted tape.

Displayed Enhanced Devices

These are the insert methods that are frequently used in restricted force convection. These techniques involve moving bulk fluid to the center of flow from the duct's or pipe's heated or cooled surface. By doing so, the heat exchange surface is indirectly improved, resulting in better energy transfer [150]. Experimental study have been performed by Promvonge [151] analyzed the impact of a conical ring turbulator on the friction factor and heat transfer enhancement in the circular tube. Three different configurations of rings such as diverging, convergent, and convergent-diverging conical rings were studied in this research. The studies, which were carried out between Reynolds numbers 6000 and 26000, used air as the working fluid. The result showed that the diverging ring has better heat transfer performance in terms of Nusselt number 330% than that of the plain tube surface. Moreover, both the converging and converging-diverging configurations are highly effective in increasing the Nusselt number, with improvements of approximately 197% and 237%, respectively. However, using conical rings also results in a significant rise in the friction factor. Figure 1.23 depicted the example of diverging conical ring.

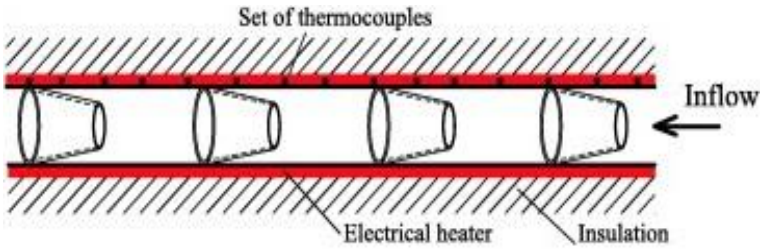

Figure 1. 23 Example of diverging conical ring [151]

Bozzoli et al. [152] investigated butterfly-shaped inserts to evaluate their thermal performance both locally and globally by applying an inverse problem approach to infrared images. An uneven distribution of the wall heat flux along the circumferential coordinate results from the velocity profile distortion caused by the insert of these butterflies. In the turbulent flow regime, the inverse analysis technique was used within a range of Reynolds numbers: $5000 < Re < 12000$. The findings showed that the front part of the insert had the greatest heat transmission, while the center of the insert, where the fluid is nearly trapped in the narrow space between the pipe wall and insert had the lowest heat transfer. Moreover, the results revealed that, it can be applied to the development of novel heat exchangers for the food industry.

Swirl Flow Devices

Swirl flow devices can be used to induce secondary recirculation in axial flow for both single and double-phase flows in heat exchangers. Examples of such devices are helical or cored screw-type tube inserts and twisted tapes. These devices utilize a tangential velocity component to the fluid, resulting in the fluid swirling, or rotating while passing through the device. This swirling motion changed the flow dynamics, which resulted in the formation of secondary recirculation zones in the fluid. These changes can have significant impacts on the system's overall performance [153][154].

Hussin et al. [155] utilized CuO-based nanofluid to improve the mixing flow inside the tube by employing swirl flow devices such helical tape with exterior inserts. The studies were carried out between Reynolds numbers (5×10^3 and 2.6×10^4) using CuO as the working fluid. The Nusselt number increases by 204% without external inserts in the twisted tapes. On the other hand, the Nusselt number increases by 202% with external inserts in the twisted tapes. Moreover, the authors reported that twisted tapes and nanofluids in heat exchangers reduce energy losses and improve heat transfer efficiency as a result of a decrease in thermal boundary layer. Similarly, Promvonge and smith [156] also examined the heat transfer enhancement by helical tapes that were placed within the tube to create swirl flow in a double pipe heat exchanger. Three different configurations including helical tape with and without rod, and regularly helical tape were studied. The authors reported that the maximum Nusselt number increases by 160% in helical tape with rod in comparison with plain tube. In the other two scenarios, the result showed that significant increase in terms of Nusselt number for helical tapes without rods and regularly spaced helical tapes were 150% and 145%, respectively. Moreover, visualization techniques showed that tubes with helical tape had strong swirling flows, in contrast to axial flow and small swirling flows in free-spacing tubes with regularly spaced helical tape without rods.

Coiled pipes

Coiled tubes are a commonly utilized passive heat transfer improvement technology. The applications of this technique in various areas including heat exchangers, air conditioning and refrigeration systems, chemical reactors, pharmaceuticals, food, and the cosmetics industries. Figure 1.24 depicts the geometry of the coiled pipe. Bozzoli et al. [157] researched to estimate the local heat transfer coefficient in the coiled pipe by IHCP on the solid wall. These geometries impact the effectiveness of fluid thermal treatment because they produce an uneven

distribution of convective heat flux at the wall along the circumferential coordinate. To find an appropriate regularization parameter, they employed the fixed-point iteration methodology in conjunction with the Tikhonov regularization method. They found that the Nusselt number was five times higher than smooth pipe. Rainieri et al. [158] researched to analyzed the performance of corrugated coiled pipes for highly viscous fluids in laminar regime. The highly viscous types of fluids are essential for applications requiring the thermal processing of fluids with a high Prandtl value. At lower Reynolds numbers, corrugated coiled pipes proved inefficient; however, at higher Reynolds numbers, wall corrugation enhances the heat transfer compared to smooth pipe.

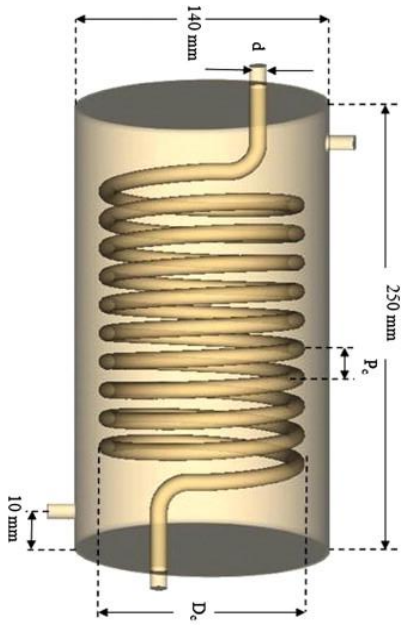

Figure 1. 24 Geometry of coiled pipes [159]

Coiled tubes are a commonly utilized passive heat transfer improvement Bozzoli et al. [160] used a coiled pipe to investigate how wall corrugation affected the local heat transfer coefficient. According to experimental data, coiled tubes with corrugated walls have a critical Dean number at which the wall curvature and corrugation together increase additional heat transfer. The distributions of convective heat transfer coefficients for low Dean numbers for smooth and corrugated walls are equivalent, on the other hand, the corrugation effect at high Dean number values significantly enhances the heat transfer. However, the more uneven dispersion of the convective heat transfer coefficient is a disadvantage of this improvement over the smooth wall coil.

Surface tension devices

Surface tension techniques that control liquid distribution and facilitate phase transition processes microgrooves, capillary-driven flows and improve heat transfer. By utilizing surface tension forces, these devices enhance the dispersion and evaporation of liquids, resulting in enhanced thermal efficiency. Kulankara and Herold [161] investigated the effect of surface tension of aqueous lithium bromide with additive that provide heat transfer enhancement. They used the drop weight method, and the surface tension of aqueous lithium bromide was determined both with and without different surfactant additions. One of the main findings of study is that the vapor concentration of the additive is a crucial factor that influences the surface tension. The findings seem to indicate that the additive in the vapor has a greater impact on surface tension than the additive in the liquid. Yong et al. [162] carried out an experimental study to determine the dynamic behaviour of the surface tension of solutions containing three different additives with different concentrations. The result showed that the addition of heat transfer additives reduced the static surface tension of deionized water. Moreover, it was found that as the concentration increased from zero to a specific amount, the surface tension's dependability on the surface increased.

1.7.1.3 Compound Techniques

A compound technique is the combination of multiple passives as well as active techniques for heat transfer enhancements. According to preliminary research, it appears quite promising to use a compound technique for heat transfer enhancement, which simultaneously improves system performance more efficiently than either technique working individually [153]. Chinaruk et al. [163] conducted an experimental study by employing a twisted tape swirl generator to improve the compound heat transfer with the effects of the pitch and twist ratio in a dimpled tube. The experiments were performed on three twisted tapes having different twist ratio and two dimpled tubes with dimpled surface pitch ratios. Moreover, the Reynolds number was in the range of 12000 to 44000, and the fully developed flow. According to the results, the dimpled tube had higher heat transfer coefficient and friction factor than the plain tube. Furthermore, as the pitch ratio and twist ratio decrease, the heat transfer coefficient increases because the fluid flow becomes more turbulent and has a greater surface area for heat exchange. The more complex flow path produced by the reduced pitch and twist, resulted in a higher friction factor. Hussein et al. [164] experimentally investigated how compound techniques effect on the performance of double pipe heat exchangers. They utilized both active and passive methods, such as air injection or the generation of bubbles, on the hand packing the shell side

with small, cylindrical pieces of aluminium. The outcomes show that utilizing both techniques (active and passive) increased the heat exchanger's performance by about 15%.

2. Inverse heat transfer problems

Inverse heat transfer problems estimate unknown quantities or boundary conditions that occur in the mathematical calculation of physical processes in thermal engineering using evaluations of temperature and heat flux. As an example, inverse heat conduction problems are typically related to the temperature measurements obtained below the boundary surface that are usually used to estimate an unknown boundary heat flux. In many engineering applications, this method is essential for precisely calculating heat transfer rates. As a result, the inverse problem requires estimating the reason from knowing the effect. In contrast, the conventional direct heat conduction problem has a defined cause (boundary heat flux) and a known effect such as body temperature. IHTP has the advantage of enabling closed collaboration between theoretical and experimental investigators to optimize the amount of evidence acquired on the real problem being studied. In thermal analysis, this integrated method provides more precise and accurate findings [165].

It is important to acknowledge that Inverse Heat Transfer Problems (IHTP) have been classified as mathematically ill-posed because of the possibility of solution instability due to internal measurement errors, whereas the direct problems are generally well-posed. The challenges provided by solving Inverse Heat Transfer issues (IHTP) should be recognized because, at first, inverse issues were considered to be ill-posed and therefore not of physical concern. Hadarnard first proposed the idea of a well-posed problem, that requires for a solution to meet the following three requirements [165]:

- Uniqueness.
- Existence.
- Must remain stable, under minor changes to the input data.

Regarding, physical reasoning could ensure that an inverse heat transfer problem has a unique solution and that it exists. As an example, it is necessary to determine a causative characteristic, such as the boundary heat flux if the measured temperature values vary in the transient situation. On the other hand, it is challenging to prove that a solution to an inverse problem exists and is unique.; this has been proven for a specific case. Moreover, random errors in the measured input data have a significant impact on the inverse problem [166]. Therefore, in order to satisfy the stability criterion, specific techniques must be used in its solution.

It was long believed that if any of the requirements for well-posedness had not been fulfilled, either the problem could not be solved or the conclusions obtained from a solution would be useless, indicating that the problem would have no meaningful significance. However, in the 1950s, certain heuristic approaches to solving inverse issues developed. These approaches focused more on pure intuition than on formal mathematically. Most of the approaches that are still widely used today were established later in the 1960s and 1970s based on their effectiveness in addressing unstable problems with ill-posed solutions. The basis of such formal methods such as those developed by Alifanov [167], J. V. Beck [168], and A. N. Tikhonov [169] are based on reformulating the inverse problem into an approximate solution to a well-posed problem by the use of regularization techniques.

With the development of new complex materials, conventional techniques to evaluate thermophysical qualities have become inadequate since thermophysical values vary significantly with temperature and position. Similarly, modern companies are operating at an increasingly advanced level. IHTP's primary benefit is that it enables experiments to be carried out in conditions as close to real life as is possible. Currently, inverse heat transfer problems have been implemented in a variety of real-world applications, including

- estimating the conditions of the inlet temperature in a parallel plate duct that vary over time. [170],
- estimation of boundary heat flux [171]
- surface heat flux estimation in a three-dimensional inverse forced convection problem [172],
- estimations of unknown parameters in cylindrical fin in genetic algorithm[173],
- Estimating the transient boundary flux in a parallel plate duct during developing flow.[174],
- estimation of local convective heat transfer coefficient [160],
- 2D inverse heat conduction problem: estimation of two-sided boundary conditions [175],
- estimation of both space and time-changing thermal properties [176],
- solution of IHCP using a hybrid techniques [177],
- surface condition estimation for nonlinear inverse heat conduction problems [178] and so forth.

It is very difficult or impossible to estimate such quantities using conventional approaches. However, these problems can be solved, and the experimental work can be expedited by applying inverse heat transfer analysis, which also increases the research's value for information.

Numerous different strategies for solving the IHTP problems have been established. Several criteria can be used to categorize these techniques: one of them could be the ability to handle both linear and nonlinear problems. The second method consists of the dimensionality of the IHTP and the heat transfer equation solution method including, the quadruple approach, finite differences and elements, finite control volumes, and Duhamel's theorem. The time-based domain over which the inverse analysis's measurements are used is another potential criterion.

It is possible to consider three different time domains: the present time, the present time plus a few time steps, and the entire time domain. The present-time domain, which can be connected to the same temperature sensor, provides a precise agreement between the estimated and measured temperatures. The second method is sequentially in nature and is based on the first two-time domains., where the related algorithms become more stable when a few more temperatures about the next time steps are used in the second-time domain. By allowing for significantly smaller time steps and reducing sensitivity to measurement error, the second method offers more precise details on the time fluctuation of the estimated variables.

In all cases, caution must be taken to avoid employing time increments that are too small, which could lead to instability in the situation. Finally, the ability to estimate time-dependent unknown functions with acceptable resolution is another powerful feature of the whole domain estimation technique, which is the ability to take extremely small-time steps.

Different criteria must be used in order to assess the various IHTP approaches. A list of potential ones was proposed by Beck [168]:

- The method used needs to be stable in terms of measurement errors.
- It should be acceptable to use one or more sensors to monitor temperature.
- The approach shouldn't require that the input data be smoothed prior.
- In comparison with large time steps, the approach should be stable for small time steps, allowing for the acquisition of more data and an improved time-varying resolution.

- Several measurement error assumptions should be confirmed by the statistical basis of the approach.
- There should be minimal computational cost.
- The method should enable the extension to several unknown.
- The entire process needs to be simple to program.
- It shouldn't be necessary to have extensive mathematical knowledge in order to apply the method.
- The use of continuous first derivatives for unknown functions should be prevented
- The method shouldn't be limited to a certain number of observations.
- Complex physical conditions such as mixed modes of heat transfer, moving boundaries, temperature-variable properties, composite materials, multi-dimensional challenges, and irregular geometries should be taken into consideration by the method.
- It may also be uncertain exactly when at which significant modifications to the unknown function occur.
- The precise timing at which an unknown surface heat flux is applied shouldn't need to be recognized.

The classification of inverse heat transfer problem based on the characteristics of the heat transfer process as follows:

- IHTP of conduction
- IHTP of forced or natural convection
- IHTP of surface radiation
- IHTP of simultaneous conduction and radiation
- IHTP of radiation in participating medium
- IHTP of continuous radiation and conduction
- IHTP of a phase change (solidification or melting)

Another classification is according to the type of causal characteristic that needs to be estimated as well. Example, be as follows

- IHTP of the conditions
- IHTP of the nonphysical characteristics
- IHTP of initial condition

- IHTP of a heated body's geometric properties
- IHTP of source term

The basic ideas of an inverse problem can be explained more clearly by using an IHTP with a function estimation. For this, the example given by Özisik and Orlande can be referenced [165]. Initially, the slab's temperature distribution is $F(x)$ with the boundary at $x = \mathrm{L}$, maintained at a constant temperature T_L , boundary $x = \mathrm{L}$. At the same time, a transient heat flux *f(t)* is used to the boundary $x = 0$ for times f > 0. This problem is expressed mathematically as follows:

$$\frac{\partial}{\partial \mathrm{x}}\left(k\frac{\partial \mathrm{T}}{\partial \mathrm{x}}\right) = \rho\, c_p \frac{\partial \mathrm{T}}{\partial \mathrm{t}} \qquad in\ 0 < x < L \qquad for\ t > 0 \qquad (2.1)$$

$$\left(-k\frac{\partial \mathrm{T}}{\partial \mathrm{x}}\right) = f(t) \qquad at \quad x = 0 \qquad for\ t > 0 \qquad (2.2)$$

$$T = T_L \qquad at \quad x = 0 \qquad for\ t > 0 \qquad (2.3)$$

$$T = F(x) \qquad for\ t = 0, \qquad in\ 0 < X < L \qquad (2.4)$$

If we consider the direct problem, which is given the specified thermophysical properties ρ, cp, and k, initial condition $F(x)$, and boundary conditions *f(t)* and T_L, the basic problem is to determine the temperature distribution $T(x, t)$ within the solid's internal portion with respect to both position and time. On the other hand, the heat source releases with varying power over time on the plane. *f(t)* at the surface $x = 0$ must be assumed to be unknown if we examine the inverse problem while all other parameters including T_L, $F(x)$, ρ, $\mathrm{c_p}$, k are known. The next step is to determine the measured temperatures $T(x_{means}), t_i = Y_i$ and the unknown boundary condition $f(t)$ are provided at an internal point x_{means} at various times $t_i(i = 1,2,3, \ldots \ldots, I)$, throughout a certain time interval $0 < t \leq t_f$, where t_f is the final time. The fact that this problem is classified as an inverse one since it requires to estimate the unknown surface condition *f(t).*

Afterward, this Inverse Problem's mathematical formulation can be obtained by,

$$\frac{\partial}{\partial \mathrm{x}}\left(k\frac{\partial \mathrm{T}}{\partial \mathrm{x}}\right) = \rho\, c_p \frac{\partial \mathrm{T}}{\partial \mathrm{t}} \qquad in\ 0 < x < L, \qquad for\ 0 < t \leq t_f \qquad (2.5)$$

$$\left(-k\frac{\partial \mathrm{T}}{\partial \mathrm{x}}\right) = f(t) = ?\,(unknown) \qquad at\ x = 0, \quad for\ 0 < t \le t_f \tag{2.6}$$

$$T = T_L \qquad at\ x = L, \quad for\ 0 < t \le t_f \tag{2.7}$$

$$T = F(x) \qquad for\ t = 0, \quad in\ 0 < x < L \tag{2.8}$$

Moreover, measurements of temperature at various times t_i at an interior position x_{means} are provided by

$$\frac{\partial}{\partial \mathrm{x}}\left(k\frac{\partial \mathrm{T}}{\partial \mathrm{x}}\right) = \rho\, c_p \frac{\partial \mathrm{T}}{\partial \mathrm{t}} \qquad in\ 0 < x < L, \quad for\ 0 < t \le t_f \tag{2.9}$$

Inverse heat transfer problems can be divided into different categories of heat transfer involved, such as conduction, convection, surface radiation, simultaneous convection and radiation, or phase change. The primary objective of the direct problem is to determine the temperature distribution $T(x,t)$ inside the solid, given that all the initial condition, thermophysical parameters, and IHTP of boundary condition are identified. On the other hand, the inverse problem's objective is to estimate one or more of these unknown causative qualities. This is achieved by utilizing the measured temperature at a specific portion of the medium. In In the inverse problem, the effect is given, and its causes are estimated; while in the direct problem, the causes are given, and the effect is estimated. Moreover, IHTPs can be linear or nonlinear, one, two, or three-dimensional, depending on the complexity of the system under investigation.

It is possible to address inverse problems using a function estimation or a parameter estimation approach. The difference between parameter and function estimation is a typical general classification used for inverse problems. The lowest possible number of factors that define parameter estimation are often associated with a physical asset, for example, a material's thermal conductivity at a specific temperature. Whereas function estimation requires determining a large number of parameters because no information about the functional form is known; these problems are typically ill-posed and can be either linear or nonlinear. To study the boundary inverse problem, let's consider that the unknown function $f(t)$ can be expressed as a polynomial over time, such as,

$$f(t) = P_1 + P_2 t + P_3 t^2 + \cdots + P_N t^{N-1} \tag{2.10}$$

Alternatively, it can be expressed in the form of a more general linear,

$$f(t) = \sum_{j=1}^{N} P_j \, C_j(t) \tag{2.11}$$

where $C_j(t)$ represents the known trial functions and j $= P_j$, j $= 1, \ldots,$ N, are unknown constants. As a result, the estimation of the unknown function *f (t)* the inverse problem transforms into estimating the finite set of parameters P_j, whereas N is considered to be predetermined.

The minimization of an object function is typically on the basis for solving an inverse problem. The inverse problem's solution could become extremely dependent on measurement errors in the input data. Therefore, it is important to briefly describe the eight common assumptions proposed by Beck [168],[179] for the statistical description of temperature measurement errors because each one has an impact on the precision of the solution that results from an inverse analysis. These eight assumptions are as follows,

- The measurement errors are additive,

$$Y_i = T_i + \varepsilon_i \tag{2.12}$$

Where $T_i =$ actual temperature, $Y_i =$ measured temperature, and $\varepsilon_i =$ random error.

- The temperature errors ε_i have an average value of zero indicating that

$$E(\varepsilon_i) = 0 \tag{2.13}$$

The expected value operator is denoted $E(.)$. When an error is random, it is one that changes with each measurement but whose mean does not always equal zero due to bias. Based on this assumption, the error occurs to be as neutral or unbiased.

- • The errors' variance is constant, indicating that

$$\sigma^2 = E\{[Y_i - E(Y_i)]\}^2 = \sigma^2 = constant \tag{2.14}$$

This implies that Y_i variance is independent by the measurement.

- There is no correlation between the measurement errors. If the covariance of ε_i and ε_j is 0, then to find if two different errors, ε_i and ε_j, where $i \neq j$, are uncorrelated.

$$cov(\varepsilon_i, \varepsilon_j) = E\{[\varepsilon_i - E(\varepsilon_i)][\varepsilon_j - E(\varepsilon_j)]\} = 0 \qquad for\ i \neq j \tag{2.15}$$

This scenario occurs when there is no correlation or effect between errors ε_i and ε_j to the other.

- The distribution of the measurement errors is normal (Gaussian), Considering the previous presumptions (2.13), (2.14), and (2.15), the probability distribution function of ε_i is obtained as follows:
- $$f(\varepsilon_i) = \frac{1}{\sigma\sqrt{2\pi}} exp\left(\frac{-\varepsilon_i^2}{2\sigma^2}\right) \quad (2.16)$$ is known which statistical parameters describing ε_i, such as σ.
- The measured temperatures are the only variables that are subject to random error. All of the quantities that occur in the formulation of the inverse problem with precision, including the heated body's dimensions, measurement positions, and times.
- The quantities that need to be estimated which could be functions or parameters have not been previously determined. If such data is obtainable, it can be used to attain more precise estimates.

Usually, inverse problems are resolved by applying a stabilization approach to the estimation procedure to minimize an objective function. Assuming the above mentioned eight assumptions are acceptable, then the objective function represented as S, the ordinary least squares norm is defined as the one that provides the lowest variance estimations [180][168]

$$S = (Y - T)^T (Y - T) \quad (2.17)$$

where the superscript T denotes the vector's transpose while the vectors Y and T, respectively, stand for the estimated and measured temperatures. The direct problem involving estimates of unknown quantities is solved by achieving estimated temperatures. Let's analyze several possible scenarios:

- Time-dependent study in which the inverse heat transfer problem is solved using various measurements of a single sensor, read at various times $ti, where\ i = (1,2,3 \dots l)$. The residuals transpose of the vector $(Y - T)^T$ in this specific case are as follows:

$$(Y - T)^2 = (Y_1 - T_1, Y_2 - T_2, \dots, Y_1 - T_1) \quad (2.18)$$

and this could be used to express the objective function as:

$$S = (Y - T)^T (Y - T) = \sum_{i=1}^{I} (Y_i - T_i)^2 \quad (2.19)$$

For a steady study, the equivalent expression remains valid when multiple measurements $Y_n$are acquired by different sensors at different locations at the same time:

$$S = (Y - T)^T (Y - T) = \sum_{n=1}^{N} (Y_n - T_n)^2 \quad (2.20)$$

- In the case of inverse analysis using transient measurements from multiple sensors, the transpose vector of the residuals is then determined as:

$$(Y - T)^T = \left(\overrightarrow{Y_1} - \overrightarrow{T_1}, \overrightarrow{Y_2} - \overrightarrow{T_2}, \dots, \overrightarrow{Y_I} - \overrightarrow{T_I}\right) \quad (2.21)$$

where $\overrightarrow{(Y_i} - \overrightarrow{T_i})$ corresponds to a row vector whose length is the number of sensors and denoted as N, for time t_i.

$$\overrightarrow{(Y_i} - \overrightarrow{T_i}) = (Y_{i1} - T_{i1}\ , Y_{i2} - T_{i2}\ , \dots , Y_{iN-}T_{iN}) \quad (2.22)$$

Where time t_i is denoted by the first subscript, while the sensor number is denoted by the second. Thus, the objective function could be written as follows:

$$S = (Y - T)^T (Y - T) = \sum_{n=1}^{N} \sum_{i=1}^{I} (Y_{in} - T_{in})^2 \quad (2.23)$$

- The ordinary least squares method generates the lowest variance estimates if the measurement standard deviations are significantly different. In this scenario, the weighted least squares norm, S_W, which can be written as

$$S_w = (Y - T)^T W (Y - T) \quad (2.24)$$

Where, W= diagonal weighting matrix

This matrix is usually considered as the inverse of the measurement errors' covariance matrix when the other statistical theories are fulfilled. subsequently, the weighting matrix W obtained by considering the measurements of the one sensor are given by

$$W = \begin{bmatrix} \frac{1}{\sigma_1^2} & 0 & 0 & 0 & 0 \\ 0 & \frac{1}{\sigma_2^2} & 0 & 0 & 0 \\ 0 & 0 & \frac{1}{\sigma_3^2} & 0 & 0 \\ 0 & 0 & 0 & \ddots & 0 \\ 0 & 0 & 0 & 0 & \frac{1}{\sigma_I^2} \end{bmatrix} \tag{2.25}$$

and S_w. can be represented precisely as follows:

$$S_w = \sum_{i=1}^{I} \frac{(Y_i - T_i)^2}{\sigma_i^2} \tag{2.26}$$

consequently σ_i ; is the measurement's standard deviation Y_i at time t_i.

In the scenario of a steady-state study including several measurements, obtained simultaneously but from various locations using various sensors:

$$S = \sum_{n=1}^{N} \left(\frac{Y_n - T_n}{\sigma_n^2}\right)^2 \tag{2.27}$$

In the same way, scenarios involving M sensors may be represented as

$$S = \sum_{m=1}^{M} \sum_{i=1}^{I} \left(\frac{Y_{in} - T_{in}}{\sigma_n^2}\right)^2 \tag{2.28}$$

where σ_n is the measurement′s standard deviation Y_{in} of sensor n at time t_i.

When the inverse heat transfer problem requires estimating a small number of unknown parameters such as thermal conductivity from transient temperature readings in a solid then the ordinary least squares norm is appropriate. This technique provides effective estimation for such particular parameter identifications with the least amount of determining complexity. However, the solution may exhibit excursion and oscillation, if the inverse problem requires the estimation of numerous parameters, like the estimation of the unknown transient heat flow components $f(t_i) = f_i$, at time $t_i = 1,2,3, \dots, I$.

Levenberg-Marquardt method

This is an iterative technique for resolving parameter estimation nonlinear least squares problems. In 1944, this method was first developed by Levenberg through modification of the

ordinary least square norm. Afterward, in 1963, Marquardt also contributed to its development by using a different approach. This technique, which was initially developed for use in nonlinear parameter estimation problems has also proven effective when used to solve linear problems. Frequently, these linear problems are too ill-conditioned to allow linear algorithms to be used.

The Levenberg-Marquardt approach can be used to solve inverse heat transfer problems by appropriately arranging the following basic steps:

- Direct Problem
- Inverse Problem
- Iterative Procedure
- Stopping Criteria

i. Direct and inverse Problem

The processes required for solving an IHCP, which involves an additional physical scenario, are explained in detail. Let's consider the unitary dimensionless thickness of a plate with linear transient heat conduction. The plate initially remains at zero temperature, with insulation maintained at both the $x = 0$ and $x = 1$ limits. There exists a plane heat source with a strength$g_p(t)$ per unit area positioned in the mid-plane $x = 0.5$ for times $t > 0$.

The heat conduction problem is formulated in a dimensionless mathematical representation as follows:

$$\frac{\partial^2 T(x,t)}{\partial \mathrm{x}^2} + g_p(t)\delta(x-0.5) = \frac{\partial \mathrm{T}(x,t)}{\partial \mathrm{t}} \qquad in\ 0 < x < 1, \quad for\ t > 0 \tag{2.29}$$

$$\frac{\partial \mathrm{T}(0,t)}{\partial \mathrm{x}} = 0 \qquad at\ x = 0, \quad for\ t > 0 \tag{2.30}$$

$$\frac{\partial \mathrm{T}(1,t)}{\partial \mathrm{x}} = 0 \qquad at\ x = 1, \quad for\ t > 0 \tag{2.31}$$

$$T(x,0) = 0 \qquad for\ t = 0, in\ 0 < x < 1 \tag{2.32}$$

and the Dirac delta function is denoted by $\delta(.)$

The above-described physical problem is categorized as a Direct Problem because the time-varying strength $g_p(t)$ of the plane heat source is specified. The second objective of the

direct problem is to find the plate's transient temperature field $T(x,t)$. On the other hand, In the Inverse Problem under consideration, the plane heat source's time-varying strength $g_p(t)$ is assumed to be unknown. For the estimation of $g_p(t)$, more information obtained from transient temperature measurements at a position $x = x_{means}$ at time $t_i = 1,2,3,\dots,I$, is subsequently used.

To solve the current inverse problem, let's consider the unknown energy generation function $g_p(t)$ to be represented in the following general linear form:

$$g_p(t) = \sum_{j=1}^{N} P_j C_j(t) \tag{2.33}$$

At this point $C_j(t)$ represents the known trial functions (polynomials etc.) and P_j, are the unknown parameters. Furthermore, N, the total number of parameters, is given as well. Afterward, the estimation of the unknown parameters *(N)* in this inverse heat conduction problem, $P_j, j = 1,\dots,N$, is based on the minimizing of the ordinary least squares norm, which can be obtained by:

$$\mathrm{S}(\mathbf{P}) = \sum_{i=1}^{I} [Y_i - T_i(\boldsymbol{P})]^2 \tag{2.34}$$

Where, S = objective function or sum of squares error

P^T unknown vector parameters, defined as $[P_1 P_2, \dots P_N]$.

$T_i(P) \equiv T(P, t_i) =$ expected temperature at time t_i

Temperature measured at time t_i , $Y_i(P) \equiv Y(t_i)$

N = the complete set of of unknown parameters

I is the total number of measurements, while $I \geq N$.

At the measurement point, x_{means} the direct problem is solved by utilizing the current estimate for the unknown parameters $P_j, j = 1,\dots,N$, to get the estimated temperatures $T_i(P)$.

Equation (2.33), can be written as in matrix form as

$$S(\boldsymbol{P}) = [\boldsymbol{Y} - \boldsymbol{T}(\boldsymbol{P})]^T [\boldsymbol{Y} - \boldsymbol{T}(\boldsymbol{P})] \tag{2.35}$$

where the superscript $T =$ transpose, while $[\boldsymbol{Y} - \boldsymbol{T}(\boldsymbol{P})]^T$ can be written as follows,

$$[\boldsymbol{Y} - \boldsymbol{T}(\boldsymbol{P})]^T \equiv [Y_1 - T_1, Y_2 - T_2, \dots, Y_I - T_I] \tag{2.36}$$

In order to minimize the least squares norm, we must zero the derivatives of S(P) with respect to each of the unknown parameters $[P_1, P_2, \dots, P_N]$

$$\frac{\partial S(\boldsymbol{P})}{\partial P_1} = \frac{\partial S(\boldsymbol{P})}{\partial P_2} = \cdots = \frac{\partial S(\boldsymbol{P})}{\partial P_N} = 0 \tag{2.36}$$

The gradient of S(**P**) with respect to the vector of parameters $\boldsymbol{P}$ can be equivalent to zero in matrix notation to represent this essential requirement for the minimization of S(**P**), that is,

$$\nabla S(\boldsymbol{P}) = 2\left[-\frac{\partial \boldsymbol{T}^T(\boldsymbol{P})}{\partial \boldsymbol{P}}\right][\boldsymbol{Y} - \boldsymbol{T}(\boldsymbol{P})] = 0 \tag{2.37}$$

Where,

$$\frac{\partial \boldsymbol{T}^T(\boldsymbol{P})}{\partial \boldsymbol{P}} = \begin{bmatrix} \frac{\partial}{\partial P_1} \\ \frac{\partial}{\partial P_2} \\ \vdots \\ \frac{\partial}{\partial P_N} \end{bmatrix} [T_1\ T_2\ \dots\ T_I] \tag{2.38}$$

The above Equation (2.38) is transposed to define the Sensitivity, or Jacobian matrix, $\boldsymbol{J}(\boldsymbol{P})$.

$$\boldsymbol{J}(\boldsymbol{P}) = \left[\frac{\partial \boldsymbol{T}^T(\boldsymbol{P})}{\partial \boldsymbol{P}}\right]^T \tag{2.39}$$

Written as the sensitivity matrix in explicit form:

$$(\boldsymbol{P}) = \left[\frac{\partial \boldsymbol{T}^T(\boldsymbol{P})}{\partial \boldsymbol{P}}\right]^T = \begin{bmatrix} \frac{\partial T_1}{\partial P_1} & \frac{\partial T_1}{\partial P_2} & \frac{\partial T_1}{\partial P_3} & \cdots & \frac{\partial T_1}{\partial P_N} \\ \frac{\partial T_2}{\partial P_1} & \frac{\partial T_2}{\partial P_2} & \frac{\partial T_2}{\partial P_2} & \cdots & \frac{\partial T_1}{\partial P_N} \\ \vdots & \vdots & \vdots & \ddots & \vdots \\ \frac{\partial T_I}{\partial P_1} & \frac{\partial T_I}{\partial P_2} & \frac{\partial T_I}{\partial P_3} & \cdots & \frac{\partial T_I}{\partial P_N} \end{bmatrix} \tag{2.40}$$

Where,

$N =$ is the total number of unknown parameters in this case.

$I =$ is the total number of measurements

.

According to its definition, the sensitivity coefficients $J_{ij}$are the components of the sensitivity matrix that represents first derivatives of the estimated temperature at time t_i with respect to the unknown parameter P_j can be written as,

$$J_{ij} = \frac{\partial T_i}{\partial P_j} \tag{2.41}$$

ii. Iterative procedure

Using the sensitivity matrix definition that was given,

$$-2\boldsymbol{J}^T(\boldsymbol{P})[\boldsymbol{Y} - \boldsymbol{T}(\boldsymbol{P})] = 0 \tag{2.42}$$

The sensitivity matrix for linear inverse problems is not dependent on the unknown parameters. In such a scenario, the vector of unknown parameters P can be solved in explicit form,

$$\boldsymbol{P} = (\boldsymbol{J}^T\boldsymbol{J})^{-1}\boldsymbol{J}^T\boldsymbol{Y} \tag{2.43}$$

In the case of a nonlinear inverse problem, the sensitivity matrix has some functional dependence on the vector of unknown parameters $\boldsymbol{P}$. Iterative processes are required in order to solve nonlinear estimating problems, achieved by linearizing the vector of estimated temperatures, $T(P)$, with a Taylor series expansion around the present answer at iteration $\boldsymbol{P}^k$, the nonlinear estimation problem can then be solved iteratively. This linearization is provided by,

$$\boldsymbol{T}(\boldsymbol{P}) = \boldsymbol{T}(\boldsymbol{P})^{\boldsymbol{k}} + \boldsymbol{J}^{\boldsymbol{k}}\left(\boldsymbol{P} - \boldsymbol{P}^{\boldsymbol{k}}\right) \tag{2.44}$$

where $\boldsymbol{J}^k$ is the sensitivity matrix evaluated at iteration k and $\boldsymbol{T}\left(\boldsymbol{P}^{\boldsymbol{k}}\right)$ is the estimated temperatures. According to Beck and Arnold, iteratively estimating the vector of unknown parameters can be obtained by rearranging the equation and replacing it in equation (2.42),

$$\boldsymbol{P}^{\boldsymbol{k+1}} = \boldsymbol{P}^{\boldsymbol{k}} + \left[\left(\boldsymbol{J}^{\boldsymbol{k}}\right)^{\boldsymbol{T}}\boldsymbol{J}^{\boldsymbol{k}}\right]^{-\boldsymbol{1}}\left(\boldsymbol{J}^{\boldsymbol{k}}\right)^{\boldsymbol{T}}\left[\boldsymbol{Y} - \boldsymbol{T}(\boldsymbol{P})^{\boldsymbol{k}}\right] \tag{2.45}$$

In fact, the Gauss technique refers to the iterative process based on this equation. This approach resembles a Newton (or Newton-Raphson) approximation. There is a possibility of oscillations in the solution since the inverse issues are ill-posed. Levenberg and Marquardt

proposed a dampening term be added to equation (2.45) in order to minimize the instability in the solution brought on by the inverse problems ill-posedness:

$$\boldsymbol{P^{k+1}} = \boldsymbol{P^k} + \left[\left(\boldsymbol{J^k}\right)^{\boldsymbol{T}}\boldsymbol{J^k} + \boldsymbol{\mu^k\Omega^k}\right]^{-1}\left(\boldsymbol{J^k}\right)^{\boldsymbol{T}}\left[\boldsymbol{Y} - \boldsymbol{T}(\boldsymbol{P})^k\right] \tag{2.46}$$

Where, Ω^k is a diagonal matrix, and

μ^k = is a scalar that is positive and called a damping parameter.

The objective of the matrix term, $\mu^k\Omega^k$ is to reduce oscillations and instabilities caused by the problem's ill-conditioned nature by increasing its components relative to those of $\boldsymbol{J^TJ}$ as required. The damping parameter is become large at the initial stage of the iterations, considering the problem is typically ill-conditioned in the area surrounding the first guess used for the iterative approach, which can be quite different from its actual parameters. The Levenberg-Marquardt Method then tends to the Gauss Method as the iteration process moves to address the parameter estimation problem's solution. Afterward, the parameter μ^k is steadily reduced.

iii. Stopping Criteria

Dennis & Schnabel [181] proposed the following criteria to stop the Levenberg-Marquardt Method's iterative process.

$$S(\boldsymbol{P}^{k+1}) < \varepsilon_1 \tag{2.47}$$

$$\|(\boldsymbol{J}^k)^T[Y - T(P^k)]\| < \varepsilon_2 \tag{2.48}$$

$$\|P^{k+1} - P^k\| < \varepsilon_3 \tag{2.49}$$

Where, $\varepsilon_1, \varepsilon_2$ and ε_3 are tolerances suggested by the user and $\|\ .\ \|$ is the Euclidean norm of vectors.

2.1 Filtering Technique

In order to stabilize the solution and ensure its significance, filtering techniques are frequently needed while addressing ill-posed inverse problems. To address the ill-posed nature of the IHCP, it is competitive and challenging to modify the raw input temperature data using suitable filtering algorithms. This method focuses on the system response's instability in relation to random errors in the input data. The signal's frequency components can be either entirely or partially suppressed by the filter. This indicates that the filter has the ability to

minimize or eliminate specific frequencies from the temperature data, which lowers noise and stabilizes the solution, making it reduce noise to errors and input variations.

The experimental errors in actual measurements are typically represented as Gaussian noise with spectral components that are evenly spaced throughout the frequency range. On the other hand, important information is usually limited in nature, with a concentration of frequency components inside the lower frequency range of the electromagnetic spectrum. Choosing the right number of frequencies to cut in order to solve the inverse problem's ill-posedness while conserving a sufficient amount of signal information is a key consideration in the application of filters. Therefore, cutting frequencies too much can lead to the loss of important information while reducing frequencies too little can make the solution unstable and too noise sensitive. When determining the ideal number of frequencies to cut, integrate advanced methods such as adaptive filtering and regularization with empirical techniques. A key technique in signal processing and inverse problem solving, the ideal low-pass filter is one of the most often used filtering strategies. An ideal low-pass filter is designed to fully block frequencies over a specific threshold while allowing signals with frequencies below it to pass through. High-frequency noise is removed from a signal using this type of filter while the crucial low-frequency components remain unaffected.

Another popular filtering technique is the Gaussian filter, whose impulse response is a Gaussian function, and in this thesis, this technique is used for smoothing and reducing noise in images. Noise filtering is an essential process in image processing, with its primary objective to minimize distortion while eliminating noise and its effects from the original image. The Gaussian filter is an essential tool for noise reduction and smoothing in image processing. As the Fourier transform of a Gaussian is also a Gaussian function, as it reduces the high-frequency components of the information. The level of flattening is determined by the standard deviation σ. The filter will mostly evaluate pixels near the central pixel when the standard deviation σ value is smaller, resulting in a narrower Gaussian function and less blurring. On the other hand, a higher value results in a wider Gaussian function, which requires the filter to average across a greater range of nearby pixels. The benefits of this filters are given below in image processing,

- Noise reduction: An image is smoothed considerably when high-frequency noise is efficiently reduced using the Gaussian filter.

- Edge preservation: It maintains edges better than some other smoothing approaches.
- Isotropic Filtering: Directional bias is avoided since the filter is isotropic, which smoothest in all directions equally.

The Wiener filter is another effective filter that has been proven to eliminate unwanted noise from experimental temperature. It can minimize noise while maintaining essential elements of the signal because it can differentiate between the signal and noise components with effectiveness. Therefore due this, Wiener filter particularly suitable for applications maintaining the original data while minimizing noise [182].

It is interesting that the filtering method for solving Inverse Heat Conduction Problems (IHCPs) works best with input signals that are highly resolved temperature maps, either spatially or temporally. On the other hand, when signals are represented by a small number of input variables, this method is impracticable. Filter techniques, particularly Gaussian filters, offer a significant advantage due to their very low computational cost compared to other methods.

3. Pipes Geometry

3.1 Corrugated pipe:

Pipes facilitate the transfer of energy and fluid in numerous applications such as buildings, heating, cooling, power plants, fire departments, and plumbing. Generally, smooth pipes are used in large-scale facilities with space constraints. However, the smooth pipe is inappropriate in areas with limited space, such as fire or disaster sites, therefore in these areas, flexible corrugated pipes are frequently utilized [183]. Wall corrugation is a passive technique among various passive techniques used to enhance the convective heat transfer coefficient explained in the Chapter 1. Among these approaches, corrugated pipes are most widely used in industrial applications and extensively studied in the scientific literature.

Wall corrugation has been extensively investigated because it works as a source of disruption in the primary flow, leading to an early transition to turbulent regimes. This transition showed significant improvements in performances from the thermal point of view for the tube section and, at the same time, it limited the increase of pressure drop in comparison to different passive techniques, like the use of insert devices. The use of pipes with corrugated walls significantly enhances the performance from the thermal point of view compared to smooth pipes. Moreover, wall corrugations have shown to be able to disrupt the thermal boundary layer, increase the mixing of flow due to the generation of secondary swirl, and increase the heat exchange area. These pipes are widely used in heat exchangers and various industrial fields due to numerous benefits. However, their design leads to the formation of vortexes within the groove, which can cause other issues and originate complex flow phenomena within the pipe [184].

Various geometries have been investigated, such as transversal grooved pipes [185], converging and diverging pipes [186], dimpled pipes [187], spirally corrugated pipes [188], internally corrugated pipes [189], and wavy channels [190]. When discussing the enhancement capabilities of corrugated tubes, the available scientific literature mainly focuses on the average heat exchange behavior across the pipe section or the entire heat exchange surface region [191], [192]. This simplified method, suitable for many practical applications, arises from the challenges of locally assessing the heat flux on the inner surface of a duct. The dimensions of the sensors, inaccessibility of the surface due to its geometry, or harsh conditions hinder the placement of sensors on the inner surface of the pipe.

There are different methods used to calculate the local heat transfer coefficient as depicted in the Figure 3.1.

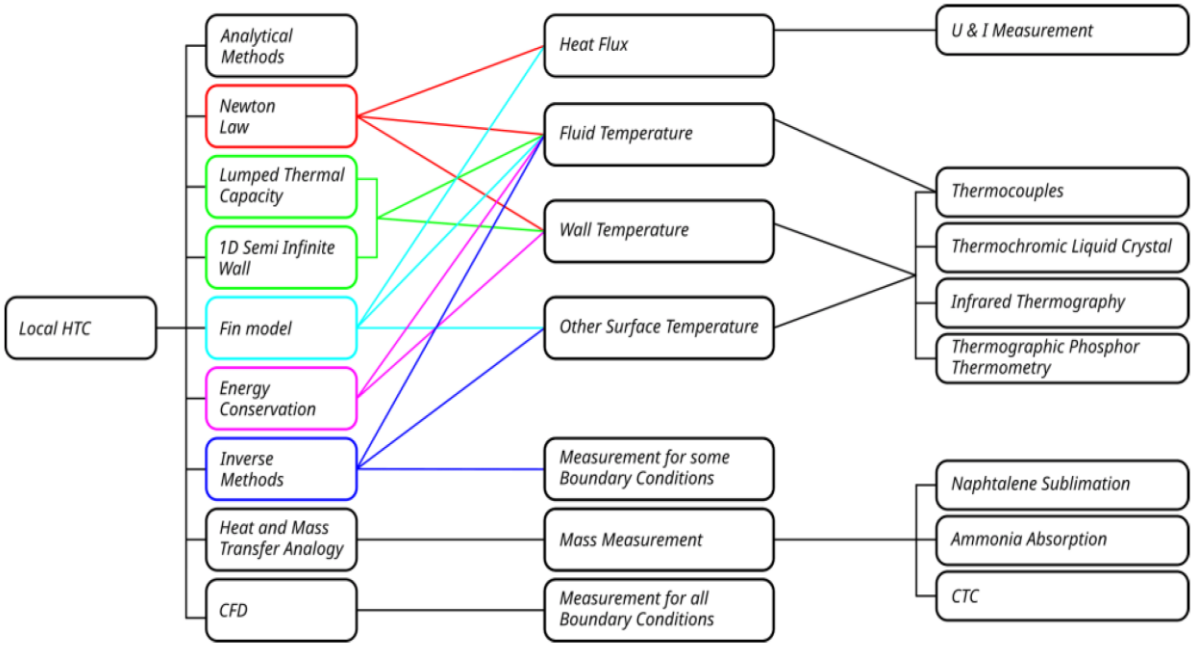

Figure 3. 1 Different methods for calculation of local heat transfer coefficient [193]

However, in certain practical industrial cases, knowledge of the performances from a local point of view is crucial. For example, in food pasteurization, irregular temperature distributions could negatively impact bacteria heat destruction or cause local overheating of the product. Additionally, experimental information on the local behavior of the heat transfer coefficient of convection over the area of heat exchange can provide deeper insights into increasing mechanisms. It also helps in understanding the causal connection between modifications to the shape of the area of heat exchange and the improvement of convection.

Inner corrugation is one of the most widely used techniques in the food and pharmaceutical industries. It is important to demonstrate some of the characteristic parameters in order to better explain this kind of corrugated geometry as shown in Figure 3.2.

- Pitch (p): The distance between two consecutive peaks or troughs of a corrugated surface is referred to as a corrugation pitch. It is an important parameter for defining the geometry of corrugated pipe, influencing performance and mechanical properties of pipe including structural stability and heat transfer. Moreover, this parameter has significant effects on the degree of turbulence in the flow.

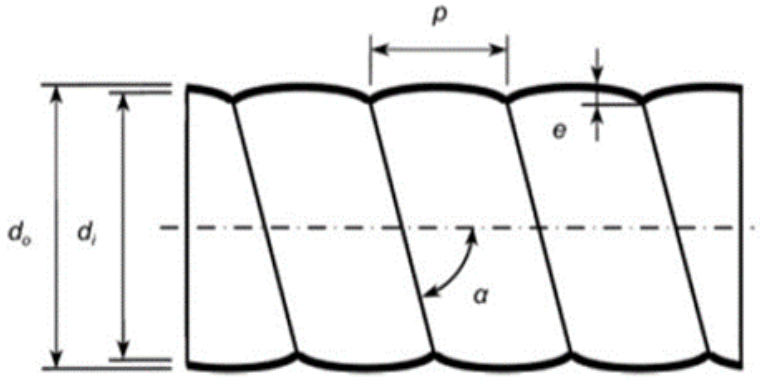

Figure 3. 2 Characteristic parameters of corrugation geometry

- The external and interior diameters of pipe are denoted by d_o and d_i, respectively.
- Depending on whether the corrugation is outer or inner, the depth (e) or height of the corrugation should be varied.
- The angle of inclination of the corrugation with respect to the pipe longitudinal axis is represented by α.

Corrugated pipes can be manufactured from a range of materials, such as metals (stainless steel, aluminium, copper), composite materials (Fiber-Reinforced Polymers), and elastomers depending on their application. Unlike conventional solid wall pipes, the corrugated outer wall design increases the strength of the pipe structure rather than the wall thickness. Most commonly, using metals in corrugated pipes offers a balance of high thermal conductivity, strength, durability, heat, and corrosion resistance. These pipes have several key properties that make them attractive for different applications. Due to their high flexibility, they can easily bend around corners and other obstacles without increasing the risk of damaging what is being transported safely. Moreover, they have high tensile strength, allowing them to withstand significant internal pressures and external forces without deforming or failing. This property makes them effective for applications in industries such as food and pharmaceutical etc. Furthermore, they are highly resistant to a wide range of chemicals, for transferring liquids that could corrode or deteriorate other materials.

We use stainless steel pipes AISI 304 in our research because they are made from ultra-low carbon steel and offer excellent corrosion resistance. These pipes are flexible metals with a series of corrugations that offer strength and flexibility and are commonly used in various industrial sectors such as the food and pharmaceutical industries, power plants, oil refineries,

and chemical plants. Recent market trends in the stainless-steel corrugated pipe industries demonstrate the development of advanced stainless-steel grades with better quality properties and innovative pipe designs to enhance performance [194]. Furthermore, the use of environmentally friendly and sustainable materials is becoming more and more popular within the industries.

Corrugated pipes offer various benefits; however, it is important to highlight the potential drawbacks of corrugated pipes, particularly the challenges during manufacturing. These challenges include material waste, manufacturing complexity, quality control challenges, installation difficulties, and market acceptance [195],[196].

Specialized tools/equipment: More advanced techniques and specialized tools are often required to manufacture or produce corrugated pipes than conventional pipes. These tools or equipment could be advanced extrusion lines or moulds used for shaping the material into the required corrugation pattern. However, the drawbacks of these specific tools require higher initial costs and maintenance expenses.

Precision requirements: Precise designs are developed in corrugated pipes during the fabrication process to ensure both strength and flexibility. It is very important that during the manufacturing of these pipes, there is precise control over a number of factors, including temperature, pressure, and speed. Achieving precise specifications can be challenging as minor modifications can cause problems with the finished product. To keep the structural integrity (to withstand pressure or external stresses) and flexibility (for bending or movement) in equilibrium, the pitch size, depth, and width of the corrugations must be precise.

Material considerations: Corrugated pipes need to be fabricated of materials that are appropriate for both the primary goal and the corrugation process. This could constrain the selection of materials available, and manufacturers might have to spend money finding particular kinds of metals or plastics that are suitable for corrugated patterns. The selection of materials depends on their applications in the food and pharmaceutical industries stainless is better due to its lightweight, corrosion resistance, and withstand high temperature. Moreover, plastics like HDPE (High-Density Polyethylene) are commonly used in underground drainage systems because of their low weight, water resistance, and durability under challenging conditions [197].

Material waste: When compared to the production of conventional pipes, the corrugated pipe manufacturing method can result in a higher material waste rate. This is because the

material must be trimmed or shaped in order to the get desired corrugation design/pattern, which can raise costs and cause environmental issues. Moreover, the complex design of corrugated pipes often results in scrap materials, particularly when tools are changed, or manufacturing settings are modified. Therefore, minimizing material waste is a challenge because it directly increases the production cost.

Increased production time: Production times of corrugated pipes increase due to the complicated nature of the manufacturing process. Compared to ordinary/conventional pipes, there may be a delay in every stage/step including raw material preparation, corrugation pattern/design, cooling, and quality control needs accuracy and attention to detail. The structural stability of the pipes depends on checking that the material is completely cooled before going on to the next stage, although doing so gets longer the production cycle overall. As a result, customers may have to wait longer for their orders, which can be a drawback for industries that need products quickly.

Training and expertise: As corrugated pipe production needs specialized tools therefore it requires highly trained employees who understand the complexities of the equipment and the production techniques are needed to manufacture it. This might mean that employees need more training, which would raise the overall complexity and cost of production. Training programs include the characteristics of the materials being used, the advanced procedures required to provide consistent results, and the particular machinery. Moreover, hiring employees with the required expertise, and training programs can be time-consuming as well as expensive.

Many researchers have investigated various inner corrugation geometries in previous literature. The most adopted technique among inner corrugation geometries is the helical design in order to enhance the average Nusselt number and find out novel geometry. Regarding this, Rainieri et al. [198] conducted an experimental study to investigate the heat transfer enhancement and pressure drop in the helical corrugated pipe with different pitch sizes and corrugation depths. The working fluid was ethylene glycol in the range of Reynolds $300 < Re < 1800$. They observed that the transitional regime occurred in helical corrugation between Reynolds Number 700 and 800. Due to this early transition, they observed a significant enhancement in heat transfer, with values ranging from 1.1 to 6 times higher than those of a smooth pipe. However, the increased pressure drops were one of the drawbacks of heat transfer enhancement. Aliabadi and Feizabadi [199] carried out numerical studies with helical

corrugated walls to enhance the overall hydrothermal performance. Initially, in order to evaluate the accuracy and dependability of the present study, the obtained results for the smooth model were compared with existing empirical correlations from the literature. After that, the performance of the corrugated structure was tested individually to see how well it performed. The result revealed that continuously varying the position and size of developed secondary flows and velocity contours led to more uniform temperatures. This was achieved by corrugating the side walls of the helical channel, which prevented the development of thermal boundary layers along the flow direction. Moreover, correlations have been established for various scenarios that correspond to the observed data with a mean absolute error of 7.43% for the friction factor and 4.43% for the Nusselt number.

Huang et al. [200] investigated the heat transfer enhancement and thermal performance of the coiled helical corrugated pipe. The effects of different corrugation pitches and depths on the friction coefficient and Nusselt number are investigated numerically, taking into consideration a range of mass flow rates. The Kriging model was used for efficiency calculation instead of the numerical calculation technique for estimating the Nusselt number. The results showed that the Kriging models estimated the Nusselt number and evaluated the reliability of heat transfer exhibited exceptional accuracy and efficiency. Moreover, it was found that, 99.28% heat transfer reliability, with an error limit of 7.5% of the mean value. Furthermore, as the corrugation depth increases and the corrugation pitch decreases, the Nusselt number moves upwards. Similarly, another study conducted by Yiran et al. [201] performed a numerical simulation to investigate the heat transfer performance of a helically coiled corrugated tube in a shell-and-tube heat exchanger. They also investigated the effects of corrugation length and height on the Nusselt number, friction factor, and the performance evaluation criterion (PEC) number. The findings indicate that the average Nusselt number was 2.33 times higher in a helical corrugated coiled tube than that of a smooth tube heat exchanger. It was observed that, the Nusselt number significantly rises with increasing corrugation height and decreasing corrugation length.

Safak et al. [202] numerically investigated the combination of both helically coiled tubes and corrugated surfaces for flow and heat transfer enhancement. At various Reynolds numbers, the parametric investigation analyzes the impact of pitch and depth of corrugation on the Friction Factor, Nusselt number, and performance evaluation criteria. According to the results, corrugated helically coiled tubes demonstrate much better thermal and hydraulic characteristics between $200 < Re < 2300$. The intensity of secondary flow increases

proportionately with a helically coiled corrugated tube. This effect was further enhanced by decreasing the corrugation pitch and increasing the corrugation depth. Wang et al. [203] conducted numerically researched in order to find the equilibrium performance in terms of energy efficiency, pressure drop, and heat transfer for a unique outward helically corrugated tube. Numerical experiments including three objective functions *(Re, f, PEC)* and three factors *(Re, pl/D, and Hl/D)* were designed using the response surface approach. Variance and sensitivity studies were performed to confirm the accuracy of the model and also explain the influence of each component on the outcomes. The results indicated that the regression model generated after the insignificant components were eliminated and showed good agreement with the numerical data, with an error of ±10%. Moreover, it was observed that the Nusselt number was most significantly affected by the Reynolds number. As its sensitivity coefficient was five times higher compared to the corrugation pitch-to-diameter ratio and the corrugation height-to-diameter ratio, indicating that the Reynolds Number (Re) has a significant impact on evaluating the Nusselt Number (Nu). Furthermore, when designing heat exchangers, parameters including a higher corrugation height, a lower pitch, and a higher Reynolds number are important.

Dong et al. [204] carried out an experimental study to investigate the turbulent friction and heat transfer parameters of different helical corrugated geometries. The experiments were conducted using water and oil as the working fluids, with Reynolds number ranging from 6000 < Re < 93000 for water and for oil 3200 < Re < 19000. It was observed that, in comparison to smooth pipe, heat transfer enhancement ranges from 30 to 120%. On the other hand, friction factor enhancement ranges from 60-120% as compared to smooth pipe. Cui et al. [205] investigated the performance of w-type spirally corrugated tubes in terms of heat transfer enhancement. Measurements were performed between the pressure drop and heat transfer properties of corrugated tubes with different geometric parameters within a Reynolds number range of 8000 < Re < 15000. The experimental results demonstrated that the heat transfer coefficient increased by 53-160% while the pressure drop decreased by 20-300%. Moreover, they developed an experimental correlation for the pressure drop and the heat transfer coefficient from a significant number of observations for this particular corrugation profile. According to performance evaluation criteria, the heat transfer rate can be increased up to 30% or more by modifying the smooth tubes with w-type spirally corrugated tubes.

Rainieri and Pagliarini [206] experimentally investigated the thermal performance of multiple helical corrugated pipes for various industrial applications specifically focusing on the

food industry. The working fluid was ethylene glycol with the range of Reynolds number $90 < Re < 800$, and that fluid was an extremely viscous liquid whose viscosity coefficient was strongly dependent on temperature. The local Reynolds number for the helical corrugation was directly related to the dimensionless corrugation pitch and was determined using the axial coordinate from the thermal inlet section. It was found that the Nusselt number in turbulent flow was essentially unaffected by the corrugation shape. For the helical corrugation wall close to the thermal entrance, the local Nusselt number rise seems to be mostly caused by the fluid viscosity variation. Moreover, it was observed that, below 200 Reynolds numbers, helical corrugation generates significant swirl components; however, this has a small impact on heat transfer enhancement. The Nusselt number gradually rises for Reynolds numbers higher than 200, primarily as a result of variations in fluid properties.

Jin et al. [207] conducted experimental studies on the friction factor and pressure drop for turbulent slush nitrogen in the helical corrugated pipe. In order to determine pressure drops and friction factors, slush nitrogen flows in corrugated pipes under various operating conditions such as inlet velocity (0-4 m/s) and solid fraction (0-20%). Empirical correlation explains how the friction characteristics were affected by the flow conditions such as fluid velocity and physical properties and structural characteristics such as inner diameter and pitch of the corrugated pipes. It was observed that, when liquid nitrogen was used in a helically corrugated pipe, the pressure drop was 5 to 12 times higher than smooth pipe having the same diameter and flow velocity. In helical corrugated pipes, the friction factor of slush nitrogen increases as the slush Reynolds number increases, whereas in smooth pipes, it decreases. Furthermore, slush nitrogen's friction factor very slightly increases when the solid percentage increases (such as 20%).

Another commonly adopted technique among inner corrugation geometries is the transverse design. A transversal corrugated pipe is designed with a series of ridges and grooves transversely around its circumferential pattern, that are perpendicular to the length of the pipe. Numerous researchers have investigated this type of corrugation in detail: Hwang et al. [208] conducted an experimental study to evaluate the performance of various transversal corrugated pipes in terms of heat transfer and pressure drop measurements of single-phase turbulent regime. The four titanium tubes had pitch sizes (such as 4, 4.5,5, and 5.5 mm), and water was used for the experiment as the working fluid. The experiments were conducted with Reynolds numbers varying between 15,000 and 65,000, respectively. Among the corrugated tubes, the one with a 5.5 mm pitch size had better performance, and 2.5 times higher than that of a smooth

tube. Moreover, the result allows for the heat exchanger's practical design to be accomplished through the use of corrugated titanium tubes. Furthermore, these results facilitate the practical and efficient design of heat exchangers through the use of corrugated titanium tubes, which improves the heat exchangers overall durability and performance.

Poredos et al. [209] carried out a study to investigate the thermal performance of concentric-tube heat exchangers using transversal corrugated tubes. The result revealed that corrugated tubes with a corrugation ratio of less than 1.648 had an increase in the convective heat-transfer coefficient when compared to a smooth tube. However, the heat transfer was more effective for corrugated tubes by 65 to 90%, because of the larger heat-transfer surface area. Moreover, in comparison to a smooth tube, a corrugated tube improves heat transfer and pressure drop by 3.95 and 3.5 times, respectively.

Dordevic et al. [210] conducted an experimental study to analyzed the pressure drop and flow stability in an Archimedean spiral tube with the straight transverse corrugated pipe. The transverse corrugated straight pipe under evaluation was found to demonstrate four different flow zones: laminar at $Re < 1300$, critical between $1300 < Re < 1600$, transitional between $1600 < Re < 4000$, and turbulent at $4000 < Re$. At higher Reynolds numbers, the friction factor asymptotically tends to a constant value. The friction factor increases significantly at the critical zone, then decreases for a range of Reynolds numbers in the transition zone, and then increases once more to reach the friction factor for turbulent flow in the fully rough zone. Bashtani and Esfahani [211] numerically studied the performance of a double-pipe heat exchanger using corrugated and smooth tubes with three different wave amplitudes. The average Nusselt number and friction coefficient were analyzed to demonstrate how corrugation improves heat transfer and the flow patterning turbulent regime. At the point of the bottleneck, the Nusselt Number and friction coefficient achieve their maximum levels, whereas, during reverse flow, both attain their lowest values. The corrugated heat exchanger attained ratios of 1.73 for effectiveness and 1.17 for thermal efficiency when compared to the simple heat exchanger.

Ahmad et al. [187] evaluated the thermo-hydrodynamic efficiency in double-dimpled corrugated tubes by utilizing nanofluids. Numerical simulations were performed at Reynolds numbers ranging from 10,000 to 30,000, assuming a constant heat flux of 10,000 $\frac{W}{m^2}$. The heat transfer coefficient for the double-dimpled pipe was found to be 20–25% higher for different nanoparticle compositions when compared to the smooth one, demonstrating a significant

increase in thermal performance. The complex design of the corrugations gives a higher Nusselt number and the increased volume fractions of nanoparticles enhance both heat transfer as well as pressure drop. Moreover, it was observed that an increase in the channel aspect ratio lowers an adequate amount of instability for an increase in heat transfer. Another study conducted by Gong et al. [212] numerically and experimentally investigated to enhance the heat transfer by the spiral wound corrugated tube heat exchanger. Moreover, they also analyzed the effects of corrugated height and pitch on overall heat transfer performance with a decrease in the corrugated pitch and an increase in the corrugated height. The results show that the increase of Nusselt number and pressure drop was 40% and 55% respectively, while overall heat transfer performance improves between a range from 7-21%.

One of their most challenging applications arises from their need to observe the temperature distribution on the devices outside surface to determine what happens inside the heat transfer devices. In order to do this, contactless experimental approaches are utilized frequently. Therefore, several data-processing-based methods have been presented in the literature for this contactless experimental approach to measuring temperature through infrared thermography. Among them, it is possible to include the iterative method of conjugate gradient, the method of Laplace transformation, the method of the sequential function specification, methods of regularization like the Tikhonov one, the method of mollification, the approach of function reciprocity, the method of the truncated singular value decomposition, and the technique of filtering [213]. When employed in non-destructive testing (IRNDT), infrared thermography generates images, or thermograms, that are used to indicate zones of interest, such as surface nonuniformity and IR camera self-emission. Certain techniques, including vibro-thermography, step heating, locking thermography, pulsed thermography, and modulated thermography, improve infrared thermography in non-destructive testing (IRNDT) capabilities by making small error signals visible. Advancements in more sensitive as well as faster IR cameras, combined with increasingly powerful computers capable of efficiently processing complex algorithms and large datasets, this could be pushed even further by developments [214]. Cattani et al. [215] used a 2D thermal quadrupole model (QM) and the truncated singular value decomposition method for estimating the local internal convective heat transfer coefficient of a tube's flow. This technique has several benefits over the other traditional domain (or boundary) discretization techniques, including meshless computing, and lowers computational costs. Xiong et al. [216] adopted the sequential function specification to concurrently determine the spatially and temporally varying internal fluid temperature and

convective heat transfer coefficient of two-dimensional pipes. The temperature estimation results a good agreement found with the numerical experiment results on natural cooling, and the relative error was less than 4%. However, the convective heat transfer coefficient was slightly poor because of the variations in the extraction positions. Moreover, the proposed inverse approach should be used to efficiently determine the fluid temperature and convective heat transfer coefficient of natural cooling.

Delpueyo et al. [217] used a regularization approach based on an optimized derivative Gaussian filter starting from noisy temperature fields to obtain a heat source reconstruction. Since the temperature fields under consideration were unavoidably noisy, filtering and differentiating are essential and strongly associated challenges. The result helps to observe how a heat source's position, magnitude, and amplitude impact the filter's unique parameter (standard deviation σ). Moreover, the results that were obtained demonstrate how useful the derivative Gaussian filter is for identifying heat sources in temperature fields with noise. Colaço et al. [218] used the so-called “reciprocity function approach” for the non-intrusive estimation of internal heat transfer coefficients in ducts. The reciprocity function approach avoids the requirement for any intrusive measurements and is computationally low resource eliminating the need for iterative processes. The numerical outcomes, demonstrate the stability method with a range of noisy functions. Excellent results were obtained when the method was analyzed and compared with a standard technique using data obtained by an infrared camera. They also suggested that in order to determine the local heat transfer coefficient in those improved geometries requires a three-dimensional numerical model instead of a two-dimensional one.

Daniel et al. [219] used Tikhonov regularization to investigate the characteristics of a regularization technique. This technique is based on the well-known result that Tikhonov regularization approximates the exact solution that is unknown within the range of the forward operator's adjoint. Ngendahayo et al. [220] adopted the Tikhonov regularization method for the estimation of surface temperatures from interior measurements. The novelty of the proposed method was that it could use several measurements obtained from different locations inside a material, which allowed for a much more accurate estimation of temperature on the surface. They observed that the Tikhonov regularization method could be utilized better if the main objective was to compute the surface heat flux instead of the temperature. Similarly, Bozzoli et al. [221] applied the Tikhonov regularization method for estimating the local heat transfer coefficient in coiled pipes. An experimental evaluation of the proposed estimation technique

was conducted in a fully formed laminar flow regime in coiled tubes, taking into account Reynolds numbers ranging from 100 to 1100. The findings demonstrate significant variation in the convective heat transfer coefficient along the pipe cross-section boundary. Patricia et al. [222] investigated the First-kind Volterra problems, which include inverse heat conduction and are frequently ill-posed because solutions don't depend continuously on the data. After that. They used a traditional regularization technique such as Tikhonov regularization. Moreover, they demonstrated by this numerical investigation, that the Tikhonov regularization method allows the use of significantly smaller approximation step sizes than those required for a stable solution of the initial equation. Furthermore, it also explained how to achieve a "predictor-corrector" type of numerical regularization.

Herchang et al. [223] carried out an experimental investigation using an infrared camera to measure the temperature distribution over a plate finned-tube heat exchangers by lumped conduction method. The result revealed that the staggered geometries' average heat transfer coefficient was 32% higher when compared to the in-lined configuration. Charles and John [224] used an external laser heating and infrared camera-based temperature measurement setup to provide a few percent accurate internal heat transfer coefficient for the thin-wall plastic model. It was observed that the heat transfer coefficient in fully developed pipe flow was lower than in the majority of complex internal passages, where secondary flows and higher turbulence levels typically resulted in higher values. Bougeard [225] conducted an experimental study to determine the local heat transfer coefficient in a plate fin-tube with an IR camera by using the lumped capacitance method. The ability to monitor surface temperatures using infrared thermography in a transient method, accounting for inaccuracies caused by tangential conduction and radiation of the investigated fin. They concluded that, when evaluating the distribution of heat transfer in complex geometries, this approach is especially interesting. Bazzoli et al. [226] Wiener filtering methods that use the temperature distribution as input data to estimate the heat flux distribution on a particular surface.

Chantasiriwan et al. [227] compared three different methods for estimating the heat flux including a piecewise consistent function, linear function, and uniform slope function. According to the comparison results, the method that divides the heat flux into portions that vary linearly that was, the one that uses a linear piecewise function performs significantly better than the other two algorithms. Additionally, this specific technique assumed that in the future, the heat flux or how much heat flows through a surface was vary linearly with time. Baldauf et al. [228] investigated local heat transfer coefficients in Discrete-Hole Film Cooling by using

high-quality resolution IR thermo-camera. They were utilized to calculate the wall temperature-independent local heat transfer coefficients of the high-density ratio flow, by considering all effects of variable properties inside the cooling film. Rathor and Aharwal [229] used liquid crystal thermography to investigate experimentally the heat transfer and flow geometry in a rectangular duct. By using thermochromic liquid crystals, one can visualize the surface temperature distributions inside a specified zone on a roughened surface, therefore acting as a thermal imaging tool.

Among these estimation approaches, the one that best fits many unknown variables and input signals, like temperature maps with high resolution, i.e., infrared maps, is the filtering approach. IR thermography can be effectively used with both steady and transient techniques to determine convective heat flux distributions by selecting the right thermal sensor. The non-intrusive characteristic of the IR camera proves especially beneficial when compared to traditional transducers. It has unique properties such as low response time and great sensitivity. Furthermore, its full two-dimensionality enables more accurate measurements of errors resulting from tangential conduction within the sensor [230]. Furthermore, by using a noise-filtered temperature distribution for solving heat conduction equations for the calculation of the internal convective heat transfer coefficient, it is possible to avoid complex algorithms for solving the related inverse problem.

The aims of this research is to address this gap by introducing and assessing an experimental technique for evaluating the local heat transfer coefficient in ducts with different corrugation profiles. However, the current literature has only evaluated the thermal enhancement performance of corrugation in straight pipes from an average point of view. These measurements consider only the heat transfer performance averaged over the entire heat transfer surface area. In this work, we investigated six different corrugated pipes in terms of both average and local heat transfer enhancement. The local analysis of the convective heat transfer coefficient is essential for some specific industrial processes, such as sterilization and pasteurization treatments of food. The performance of these processes can be significantly affected by an unequal distribution of temperatures on the inside of the corrugated wall. Localized heat transfer analysis becomes essential because achieving an optimal level of pasteurization or sterilization requires maintaining a consistent temperature.

The estimation procedure utilized in this study involves solving the inverse heat conduction problem (IHCP) inside the domain of the pipe wall, employing the distribution of

the temperature on the outer surface as starting data. By considering the distribution of the convection coefficient on the interface between the internal wall and the fluid as unknown. This method allows for a more detailed and precise evaluation of heat transfer performance, especially in complex systems where the convection coefficient varies significantly [179].

Since the wall temperature distribution exhibits significant variations over space, as a consequence of the complicated outcome of surface corrugation on the flow arrangement. The proposed method demands a high-resolution temperature measurement technique, which was attained using a liquid-cooled infrared camera. It is important to note that the applications of IR devices to IHCPs primarily rely on cameras with cryogenic cooling due to their excellent performance in terms of their noise-equivalent temperature difference. As a result, they are very useful for controlling and monitoring temperature in various industrial processes [231]. As recognized, IHCPs present challenges as they are ill-posed and highly sensitive to variations in input data, including those arising from experimental noise. The IHCP of an ill-conditioned nature is addressed using a filtering technique with the distribution of temperature obtained with infrared acquisition, enabling the determination of the distribution of the coefficient of convection in corrugated pipes. Moreover, the obtained results provide valuable insights for the design and optimization of heat exchangers utilizing corrugated tubes.

3.2 Tested Pipe profiles

In this study, we conducted experimental investigations on six different stainless-steel pipes made of AISI 304. Each pipe was characterized by unique geometrical characteristics and corrugation profiles. These variations allowed us to investigate how different designs affected the performance of the pipes. All the tested pipes had a uniform wall thickness of 1 mm, an outer envelope radius (r_o) of 8 mm, and a length of 3 m. The corrugation profile of the pipes varied, including the helical, transversal, and cross-helical profiles. For each corrugation profile, we considered two different corrugation pitch values: 16 mm and 32 mm. Furthermore, the smooth pipe was tested to determine a baseline reference to compare the performance of the corrugation patterns. Table 3.1 provides a summary of the geometric characteristics of the six corrugated pipes under the investigation.

Table 3. 1 Dimensions of the studied corrugated pipes

Pipe Name	Corrugation Profile	Pitch *(p)* mm	Depth *(e)* mm	D_i mm	D_o mm

T32	Transversal	32	1	14	16
T16	Transversal	16	1	14	16
H32	Helical	32	1	14	16
H16	Helical	16	1	14	16
C32	Cross-helix	32	1	14	16
C16	Cross-helix	16	1	14	16

Helical corrugation is the most used in industrial applications due to its ease of production compared to transversal corrugation. Helical corrugation involves continuous rotation of the pipe, resulting in an internal helical groove and a corresponding external helical one obtained by embossing a smooth tube. The Flexibility and structural strength of the pipe are increased by this helical pattern, which also makes it more resistant to deformation under pressure. Consequently, cross-helical corrugated pipes can also be produced by rolling the same tube two times, incorporating two helical corrugations in reverse directions. This produces a cross-helical pattern where they cross each other, further improving the structural flexibility and integrity of the pipe. On the other hand, transversal corrugation develops through a more discontinuous process, which means that rather than continuous, the corrugations are generated through intermittent or stepwise operations. Figure 3.3 provides a representation of the six corrugated tubes, highlighting the differences in corrugation profiles and pitches.

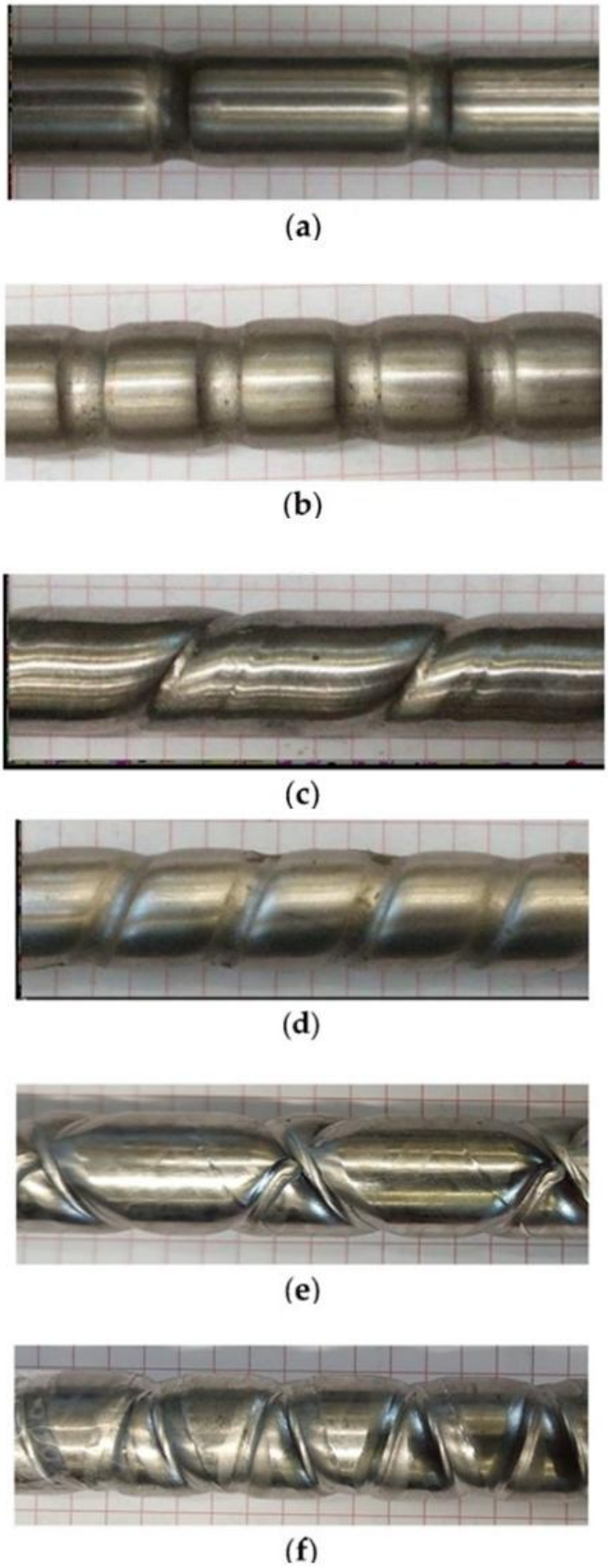

Figure 3. 3 The tested corrugated pipe's geometries: (a) T32, (b) T16, (c) H32, (d) H16, (e) C32, and (f) C16

The entire length of all tested pipes was three sections such as inlet, heating, and outlet section. A heated 1.84 m portion was developed in order to provide a heating section throughout the length of the pipes. This was achieved by applying two steel electrodes electrically connected to a power supply. The power supply used was an HP 6671A, operating within the ranges of 0–8 V and 0–220 A.

The heat flux was generated by the Joule effect on the wall of the pipe, and it was assumed to be uniform across the heating section. It was determined by dividing the provided electrical power (adjusted for heat losses to the ambient environment) by the solid volume of the pipe. To minimize heat losses to the ambient environment, the pipes were thermally insulated with a double layer of expanded polyurethane. We gave special attention to the impacts associated with buoyancy forces, so we carefully chose the applied heat flux to the working fluid to minimize these forces when compared to the inertia forces at the fluid velocity values examined here. To assess whether the natural convection effects were significant in comparison to the forced convection effects, we calculated the Grashof-to-Reynolds number ratio, denoted as Gr/Re^2 [232]. Since this ratio is considerably smaller than 1 for all the experiments conducted, we could conclude that the buoyancy forces can be regarded as negligible when compared to inertial forces. Consequently, the measurements obtained in a single section can be considered representative of the thermally developed conditions for forced convection flows.

4. Experimental Setup

4.1 Average experimental setup

The initial focus of this investigation was to measure the performance of the corrugated pipes from an average point of view in terms of heat transfer effects and fluid-dynamic penalties. The pipes were horizontally placed in a specifically designed setup, as depicted in Figure 4.1. This figure is also representative of the outlet section since the two sections are specular. Water was used as the working fluid, which was pumped from a holding tank to a heat exchanger whereas in the service section was fed with city water. A volumetric pump transfers the working fluid from the tank to a shell-and-tube heat exchanger. A volumetric pump is used in this system to transfer the fluid that is stored in the tank, ensuring a precise and steady flow rate. The pump used in these experiments is a volumetric pump (Product Type: T100LB4, IEC: 60034) manufactured by Motovario S.p.A as shown in Figure 4.2. This kind of pump provides excellent flow rate stability, which means it continuously provides a precise and steady fluid volume with respect to time. This pump maintains a constant output, compared to other pumps that may experience variations in flow rate as a result of changing conditions or operating variables.

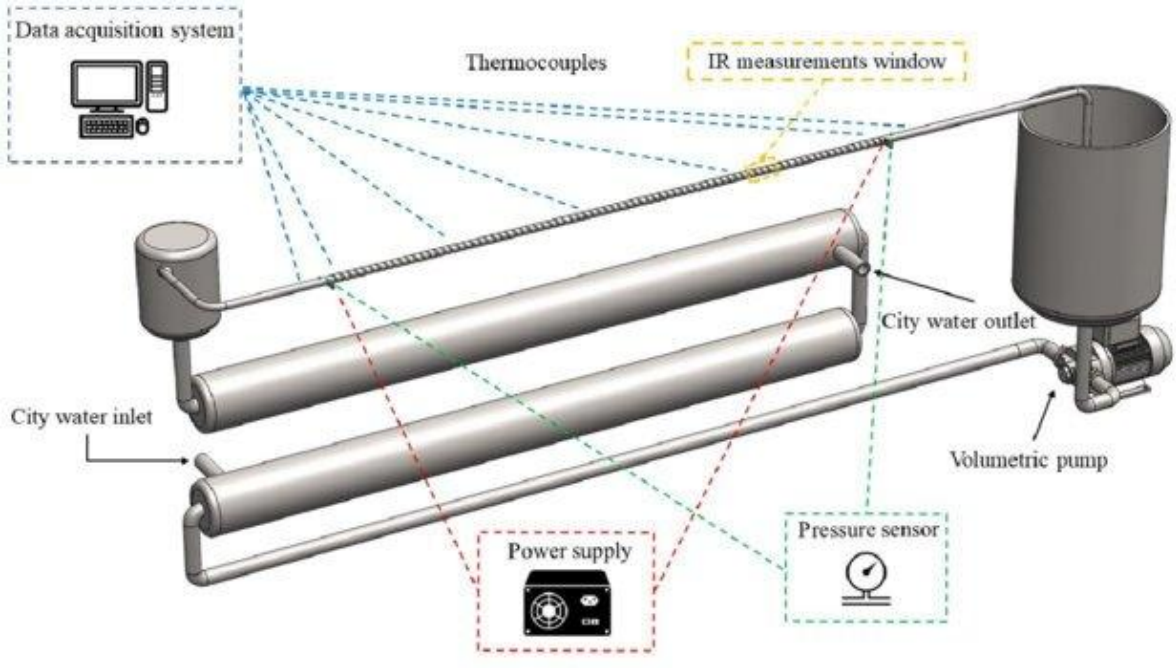

Figure 4. 1 Schematic representation of the average experimental setup

A small vent valve at the top of the tank was designed to remove any air that may have accidentally entered the fluid circuit. Trapped air can be released by opening this valve when the system is being filled or being operated. This setup maintained a constant inlet temperature for the fluid entering the tested pipes. Air bubbles can damage system components and also effect pump performance and disrupt fluid flow. To measure the temperatures, forty T-type thermocouples were calibrated and connected to an ice multipoint reference (type KAYE K170-50C). To minimize heat losses to the ambient environment, the pipes were thermally insulated with a double layer of expanded polyurethane, of 9 mm and 32 mm respectively.

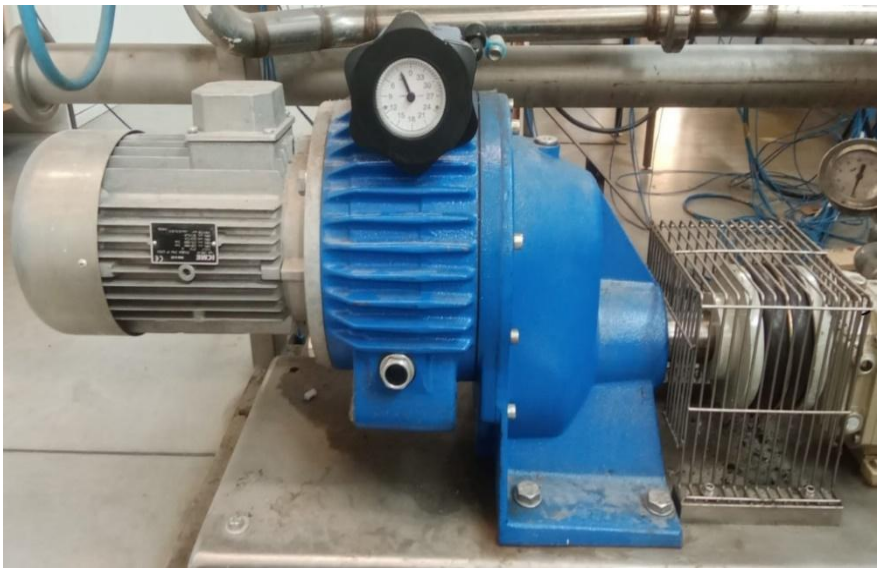

Figure 4. 2 Volumetric pump and Mechanical reducer

These thermocouples were positioned at different axial and circumferential locations on the outer side of the pipe in three sections of the pipe such as inlet, outlet, and heated section. The bulk temperature at any place in the heat transfer section was determined based on the power supplied to the pipe, which was assumed to be uniformly distributed per unit length over the heat transfer surface area. This calculation also considered the heat losses through the insulation. Moreover, placing a thermocouple at the end of the heated area allowed for an additional confirmation of the outlet temperature.

For each axial distance, two thermocouples were placed diametrically opposite each other, with one on the top and one on the bottom of the tube's cross-section. To calculate the temperature of the internal side of the wall, the problem related to the heat generation in the pipe wall of the steady-state heat conduction was solved [233]. The temperature of the fluid at

the inlet and outlet section was measured by thermocouple probes placed on the pipe's wall before and after the heated section, respectively. In Figure 4.3, a detail of the inlet section of the corrugated portion of the studied tubes is reported.

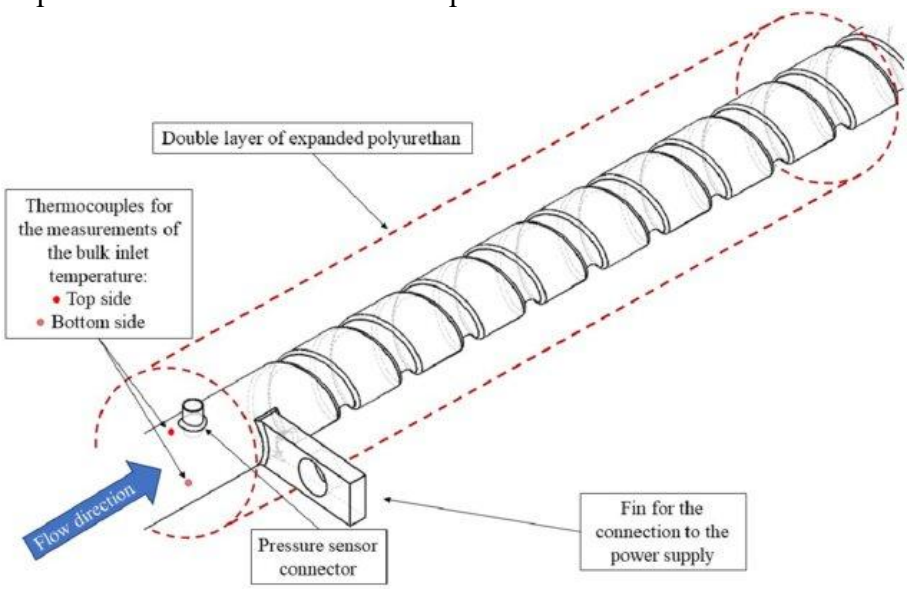

Figure 4. 3 Detail of the corrugated pipe inlet (and outlet) section

The product temperature along the heat transfer area of the pipe was obtained based on the power generated in the pipe wall, assuming it was uniformly distributed along the total length of the section. Volumetric flow rates were calculated by weighing the quantity of product exiting the test section and relating it to the time taken. Using this method, the fluid that discharged was collected in a calibrated container, and the weight was recorded at regular time intervals. The mass flow rate was then converted into volumetric flow rate by considering the fluid's density, which was either measured experimentally. Three measurements were taken in order to ensure precision and repeatability, and an average value was chosen for analysis. Data acquisition was performed using a high-precision multi-meter controlled by a computer/Laptop. The commercial software LabVIEW was utilized for real-time temperature sensor data collection, processing, and monitoring of temperature sensors, ensuring precise and efficient experimental measurements. A graphical programming environment called LabVIEW enables users to create personalized virtual instruments (VIs) for collecting, analyzing, and visualizing data. This software is user-friendly interface that allows users to activate or deactivate the various channels of collecting data, each of which corresponds to a thermocouple, and to monitor the temperature. For better understanding, we displayed the data (Temperature) in both a table format and a graphical plot. The interface of LabView is shown in Figure 4.4.

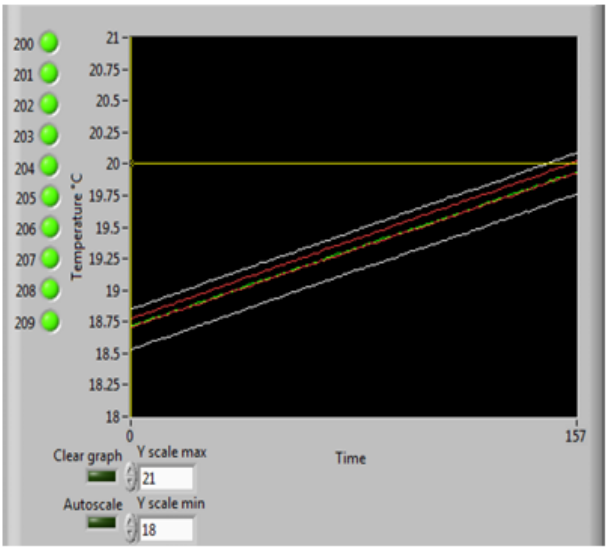

Cycle	Time, s	100	101
153	141	20.042602	19.976957
154	142	20.051237	19.984861
155	143	20.063897	19.997962
156	144	20.069641	20.007146
157	145	20.077690	20.009122

Figure 4. 4 LabVIEW interface

Pressure drops across the corrugated pipes were measured using an Emerson (Italy) Rosemount 3051S pressure transducer based on the differential signal under isothermal conditions. The Rosemount 3051S is a high-performance pressure transducer with outstanding accuracy, stability, and advanced measurements that is designed for use in industrial and laboratory applications. It can be used for a number of tasks, including level measurement, flow monitoring, and pressure control in complex structures, because it can measure gauge, absolute, and differential pressure.

Finally, temperature data were acquired for a duration of 5 min at a frequency of 0.33 Hz after reaching a steady state for Reynolds number values ranging from 4×10^3 *to* 16×10^3.

The heat transfer performances were determined by using the Nusselt number, defined as:

$$Nu_z = \frac{h_z \cdot D_i}{k_f} \tag{4.1}$$

$$Nu = \frac{1}{h} = \int_0^{L_H} Nu_z dz \tag{4.2}$$

where k_f represents the thermal conductivity of the fluid at the local fluid temperature, and h_z is the local convective heat transfer coefficient averaged on the circumference. The latter was calculated using the formula:

$$h_z = \frac{q}{(\bar{T}_w - T_b)} \tag{4.3}$$

Emerson where $\bar{T}_w$ and T_b are the wall temperatures averaged on the circumference and the local bulk fluid temperature, respectively; T_w was obtained by averaging the values obtained by the two thermocouples located along the top and bottom axial extremities of the cylindrical external surface at each position of measurement. To evaluate the heat exchanged in the unitary area (q), the surface of the heat exchange of the pipe was considered to correspond to the one of a cylinder with the same diameter. The fluid properties were estimated using the previously described method to compute the local fluid bulk temperature based on the energy balance. The friction factor of Darcy, evaluated as reported in Equation (3), was adopted for the evaluation of the pressure drops in the pipes studied:

$$f = \frac{\Delta p}{\rho} \frac{D_i}{L} \frac{2}{w^2} \tag{4.4}$$

where Δp is the pressure drop over the test section with length L. For the evaluation of the pressure drops induced by the corrugation and assessing the improvements and potential drawbacks, two dimensionless quantities commonly used in the evaluation of enhanced geometries were considered [234], the friction factor enhancement and heat transfer enhancement, calculated with the following definitions:

$$\varepsilon_f = \frac{f_e}{f_o} \tag{4.5}$$

$$\varepsilon_h = \frac{Nu_e}{Nu_o} \tag{4.6}$$

where e and o refer the enhanced and reference pipes, respectively. As the reference geometry, a straight and smooth pipe was used, as commonly assumed in literature [5], and the correlation of Dittus-Boelter for smooth wall pipes in turbulent regimes was considered valid [230]. Moreover, the efficiency of the enhancement was evaluated following one of the most

adopted definitions infrared image filtering applied to the restoration of the convective heat transfer coefficient distribution in coiled tubes [221], [5]:

$$\eta = \frac{\varepsilon_h}{\varepsilon_f^{\frac{1}{3}}} \tag{4.7}$$

Where, ε_f = Friction factor enhancement, ε_h = Heat transfer enhancement as defined above Eq. (4.5) and (4.6). Finaly, we have calculated the Nusselt number value by changing the Reynolds number, which has the following definition:

$$Re = \frac{\rho . v . D_i}{\mu} \tag{4.8}$$

Where, D_i =Internal diameter of pipe, v = mean fluid velocity inside the pipe, ρ =density of the working fluid and μ = dynamic viscosity of the working fluid.

4.2 Local Experimental Setup

This section of the thesis provides a local analysis based on the solution of the inverse problem and filtering technique described in Chapter 2 for the stability of the solution. For the local heat transfer estimation, the thermal insulation layer was completely removed approximately 14 cm from the heating section. The insulation layer was removed along a section of the external pipe wall to make the outer surface of the pipe accessible for measurement by the infrared camera. This removal of insulation allowed for accurate thermal measurements of the pipe's external surface. It is important to note that accurate analysis

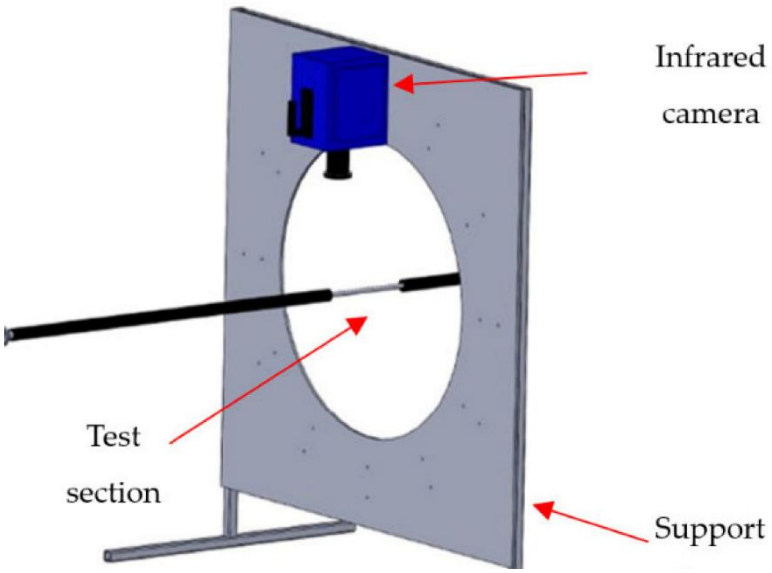

Figure 4. 5 Sketch of the infrared thermographic system to estimate

requires capturing the entire rotational period of the corrugation. After that, the portion where insulation was removed was painted with a thin film of opaque acrylic colour with a known and uniform emissivity (i.e., 0.95).

The camera used for capturing the images was a FLIR SC7000 with a 640 × 512-pixel sensor, a sensitivity of 20 mK at 303 K, and an accuracy of ±1 K. These characteristics of the IR camera ensured precise measurements and accurate thermal imaging. By moving the IR camera around the axis of the section painted, multiple images were collected to obtain a temperature map of the entire external wall of the pipe as shown in Figure 4.5. After the thermal steady state condition was achieved, images were captured for each pipe at different Reynolds Number such as $4 \times 10^3, 10^4, 16 \times 10^3$. Each image was captured at a frame rate of 25 Hz and an exposure length of 3 seconds in order to minimize acquisition noise.

This configuration ensured that each image was an average of 75 individual frames, thereby improving the visibility as well as precision of the final captured images. A support, created to keep the optical axis of the camera in a perpendicular position with respect to the tube axis in all the shots as shown in Figure 4.8 such as (A, B, C, D, E, F), was used for reducing the perspective artifacts during the acquisition. In this experimental setup, the angle of view was lower than ±30◦, considering the pipe surface was like a diffuse grey emitter [217],[235]. The image processing procedure utilized in a previous study was employed to rectify the optical deformations caused by the surface curvature of the observed target surface.

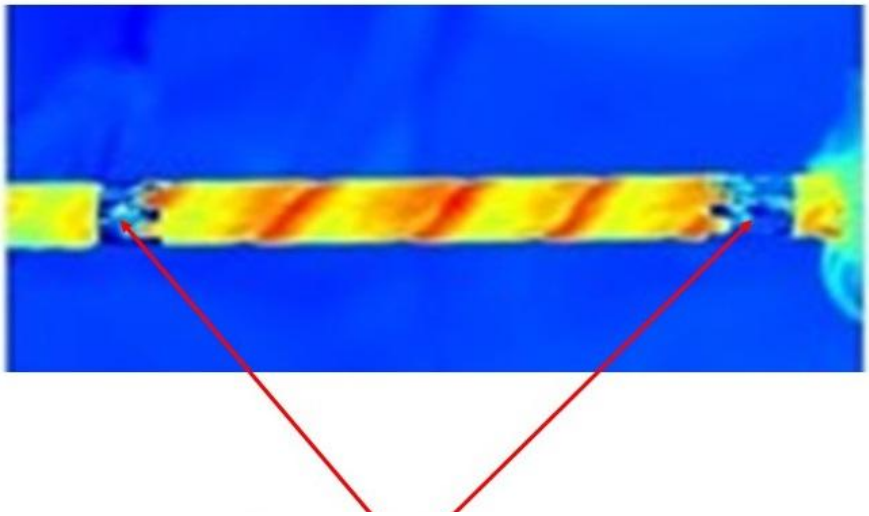

Figure 4. 6 A representative infrared image of one of the six pictures (labelled A–F) captured around the external surface of the test section

The captured images as shown in Figure 4.6 were processed to generate a continuous temperature distribution on the external pipe wall by using appropriate references. These references were fixed on the tube wall, for the correct positioning of every shot. These visual references were placed at the ends of the surface captured by the camera and served to identify the specific areas of interest in each obtained image. Each image provided 1/6 of the total surface under investigation as illustrated in figure 4.7.

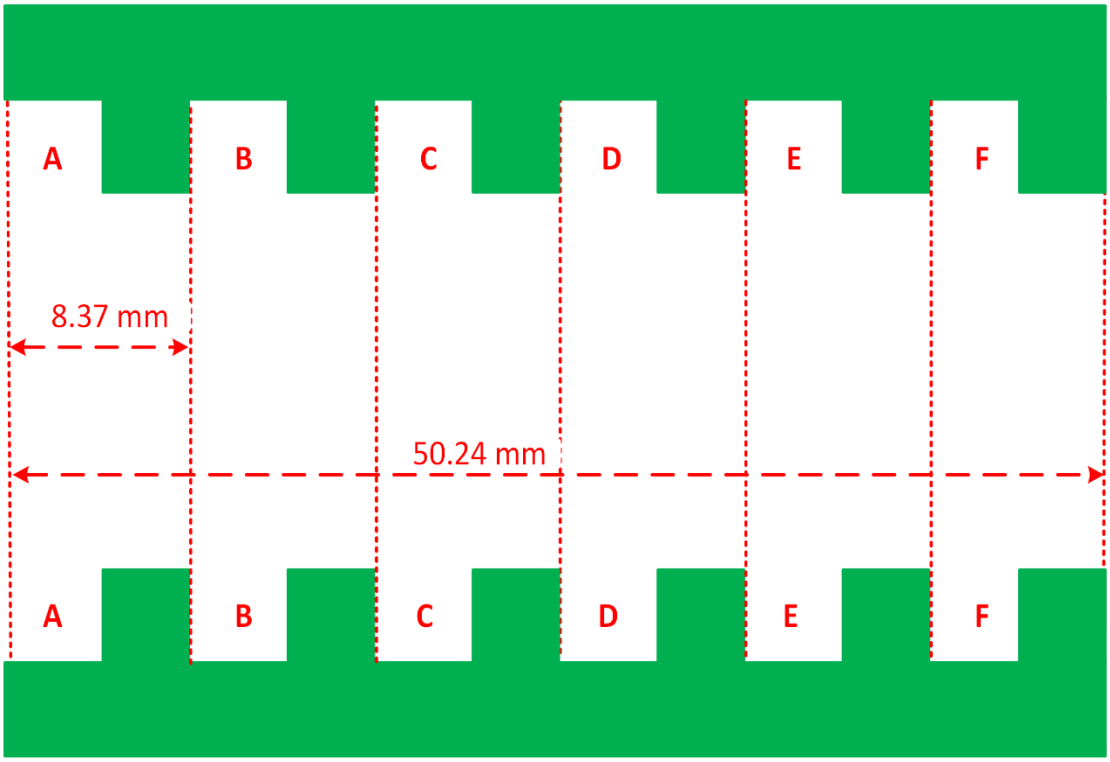

Figure 4. 7 Scheme of the unwrapped six images, with references for reconstructing the external surface of the corrugated pipe

The first step to start the process, six raw infrared images (can be seen figure 4.8) were taken from different perspectives around the external surface of corrugated pipe.

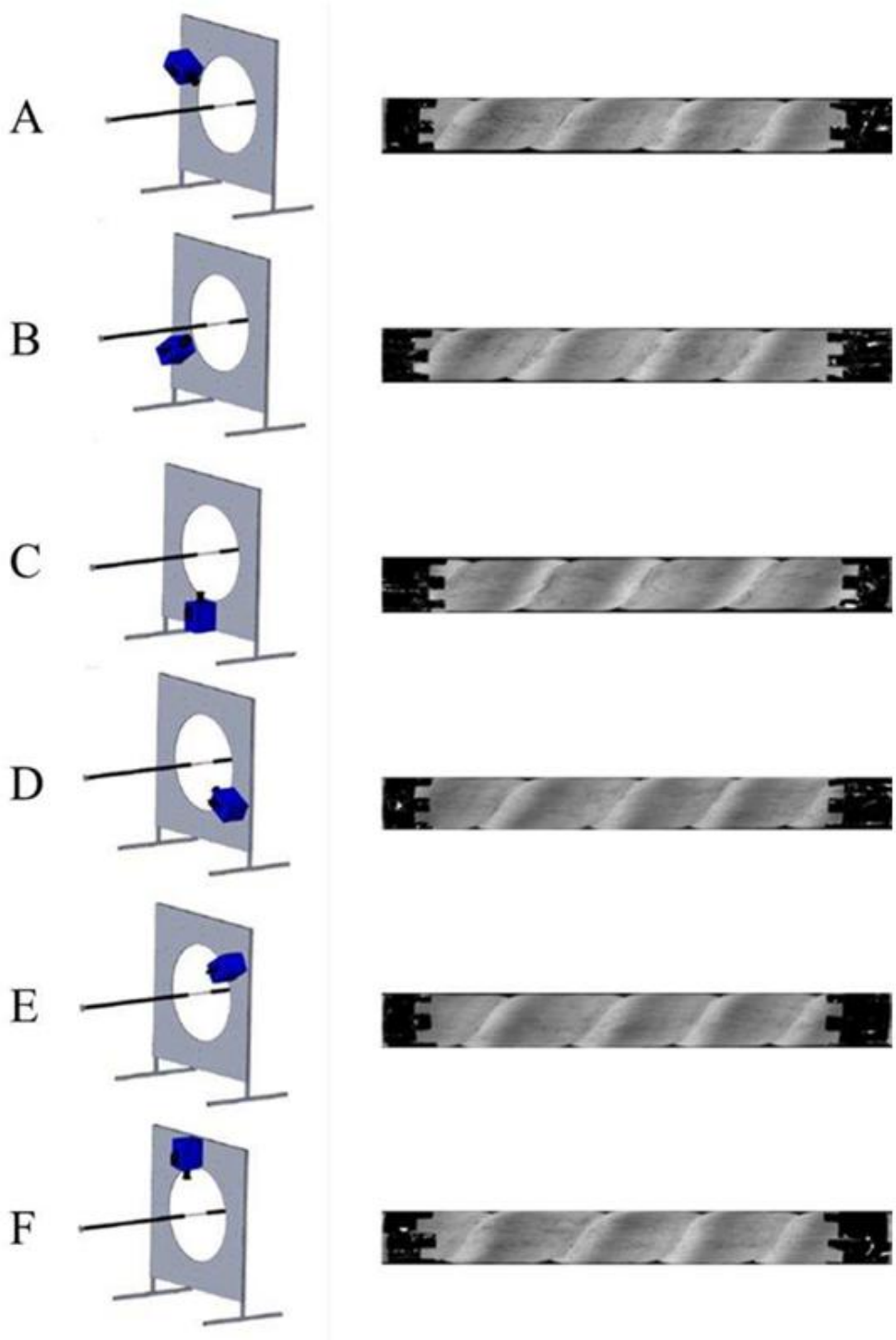

Figure 4. 8 Six raw IR images around the pipe before unwrapping and merging

The coordinates (x, y) of a point of an image in a planar reference system can be transferred into cylindrical coordinates, provided the camera is sufficiently far away from the pipe. This is achieved by using following specific equations,

(4.9)

$$\begin{cases} z = \Omega . y + z_0 \\ \alpha = \arctan\left(\frac{x}{\Psi}\right) + \alpha_0 \end{cases} \quad (4.10)$$

where Ψ, x, z_0 and α_0 are parameters determined by the relative position and lenses of the camera. It is easy to find these parameters by calibrating the acquisition system with a known sample pattern that is fixed onto the tube wall [236],[237]. In order to ensure that the IR camera captures the images by the proper coordinates for transformation, this procedure enables precise measurement and adjustment. It has been feasible to unravel the six infrared raw images captured by the infrared camera by using this system of equations 4.9 and 4.10.

After successfully completing this procedure, all the wrapped images had their top and bottom portions clipped, as seen in Figure 4.9. In order to ensure that the images were more accurate and consistent for subsequent analysis, this step was required to remove any distortions and deformations present at the edges.

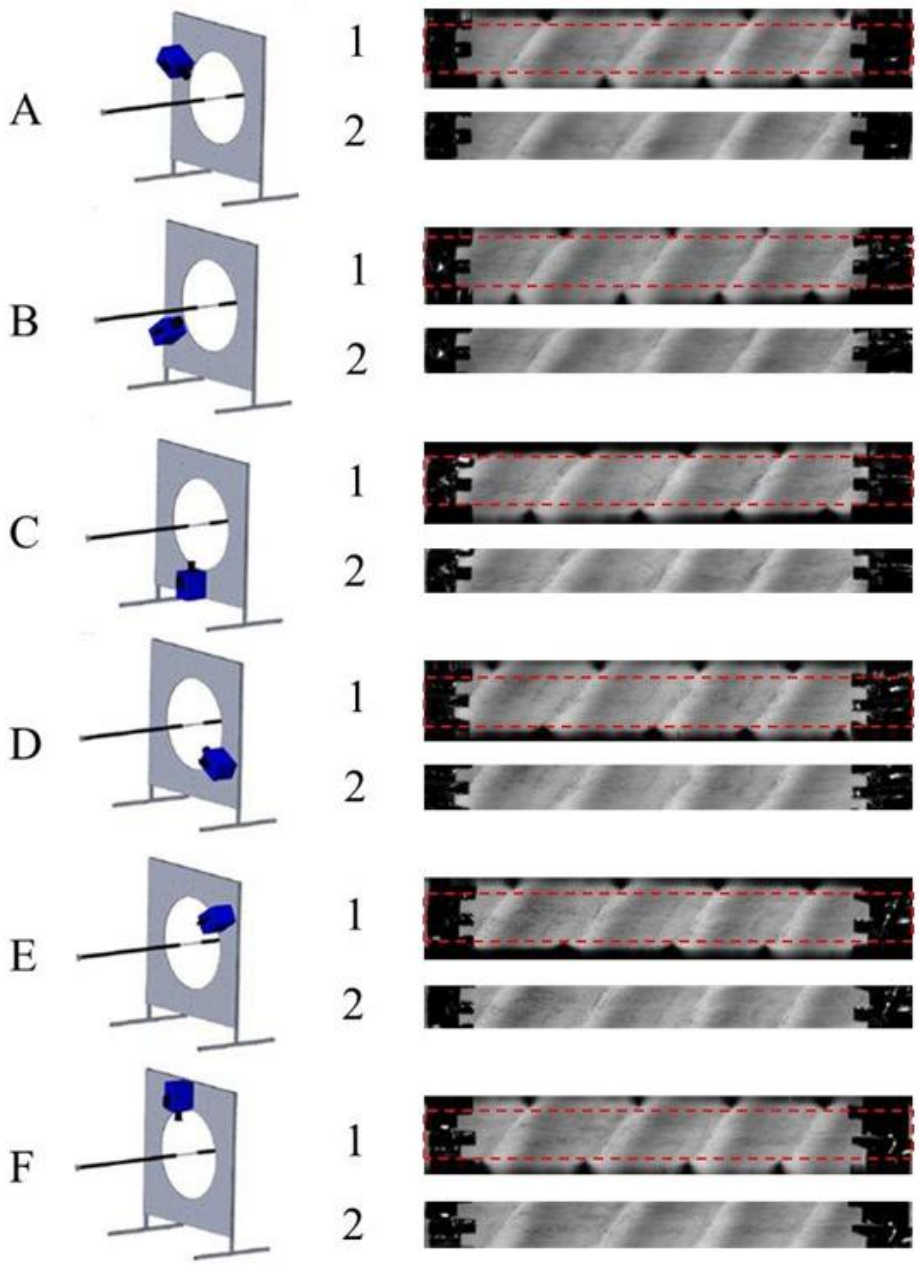

Figure 4. 9 : Each IR raw image (A, B, C, D, E, and F) as a representation of two-step (1) images that were wrapped and show how to cut borders to obtain them (2) central sections for executing the subsequent merging process

Finally, the acquired images are combined to reconstruct the flat (planar) representation of the pipes outside surface as seen in Figure 4.10. To ensure the correct positioning of the images throughout the merging process, reference points are positioned at both corners. By doing this, the resulting combined image precisely represents the relevant regions of interest on the pipe's surface, enabling a thorough examination of the surface.

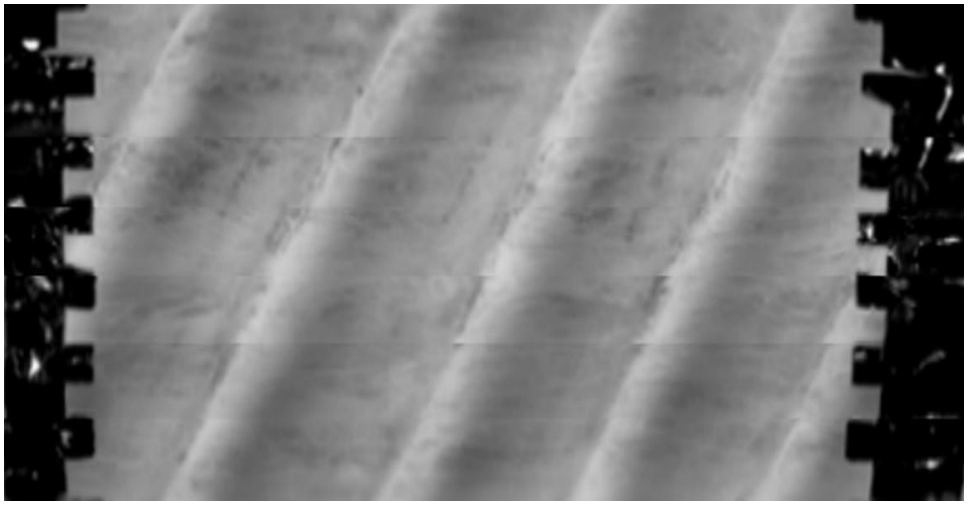

Figure 4. 10 Example of a reconstructed external surface after the merging operation

4.3 Estimation procedure

To determine the local convective heat transfer coefficient based on the obtained temperature distribution image from the IR camera, the Inverse Heat Conduction Problem (IHCP) within the tube wall domain was solved. The physical problem involves heat conduction in the wall of a cylindrical pipe (as depicted in Figure 4.11), and the steady-state

$$k\nabla^2 T + q_g = 0 \tag{4.11}$$

energy balance equation in this domain is given by:

where q_g represents the heat generated per unit volume within the tube wall, and k is the thermal conductivity of the wall material. Two boundary conditions are included to the energy balance equation:

$$-k\frac{\partial T}{\partial r} = \frac{(T - T_{env})}{R_{env}}, \qquad r = r_{ext} \tag{4.12}$$

$$-k\frac{\partial T}{\partial r} = h_{int}(T - T_b), \qquad r = r_{int} \tag{4.13}$$

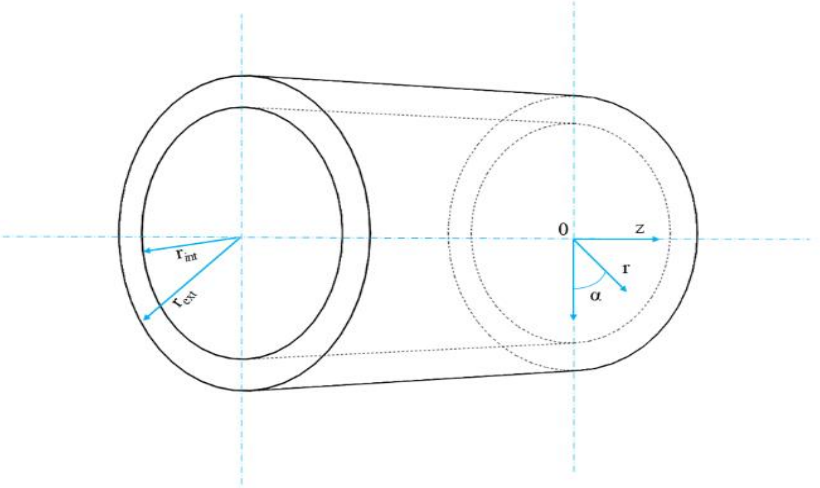

Figure 4. 11 Geometrical domain with coordinate system

where T_{env} is the surrounding environment temperature, R_{env} is the overall heat transfer resistance between the environment and the tube wall, and T_b is the local bulk fluid temperature.

Under the assumption of thin-wall approximation, the temperature on the external surface is considered to be equal to that on the internal surface:

$$T(\alpha, r, z) \cong T(\alpha, r_{int}, z) \cong T\ (\alpha, r_{ext}, z) \tag{4.14}$$

The thin-wall approximation is valid when the Biot number, defined as the product of the convective heat transfer coefficient, tube thickness, and inverse of the tube wall thermal conductivity, is less than 0.1. This condition was verified for the cases studied.

Referring to the infinitesimal cylindrical sector as shown in Figure 4.12, the steady-state local energy balance equation can be expressed as:

$$Q_{\alpha+d\alpha} + Q_\alpha + Q_{r_{int}} + Q_{r_{ext}} + Q_{z+dz} + Q_z + Q_g = 0 \tag{4.15}$$

The heat flux with the angular coordinates (α) are defined as:

$$Q_\alpha = \int_{r_{int}}^{r_{ext}} -\frac{k\partial T}{r\partial\alpha} dr dz = -\frac{k dT}{d\alpha} \ln\left(\frac{r_{ext}}{r_{int}}\right) dz \tag{4.16}$$

$$Q_{\alpha+d\alpha} = -k\frac{\partial T}{\partial \alpha}\ln\left(\frac{r_{ext}}{r_{int}}\right)dz + k\frac{\partial^2 T}{\partial \alpha^2}\ln\left(\frac{r_{ext}}{r_{int}}\right)d\alpha dz \tag{4.17}$$

where the internal and external radii of the pipe are denoted by r_{int} and r_{ext}. The heat flux along radial coordinate *r,* are described by the following equations.

$$Q_{r_{int}} = -h_{int}(T - T_{int})r_{int}\, d\alpha\, dz \tag{4.18}$$

$$Q_{r_{ext}} = -\frac{(T - T_{env})}{R_{env}}\, R_{ext}\, d\alpha\, dz \tag{4.19}$$

For the axial coordinates, the heat flux can be expressed as follow:

$$Q_z = \int_{r_{int}}^{r_{ext}} -\frac{k\partial T}{r\partial z}\frac{\pi r^2}{2\pi}d\alpha dr = -k\frac{\partial T}{\partial z}\left(\frac{r_{ext}^2 - r_{int}^2}{2}\right)d\alpha \tag{4.20}$$

$$Q_{z+dz} = -k\frac{\partial T}{\partial z}\left(\frac{r_{ext}^2 - r_{int}^2}{2}\right)d\alpha + k\frac{\partial^2 T}{\partial z^2}\left(\frac{r_{ext}^2 - r_{int}^2}{2}\right)d\alpha dz \tag{4.21}$$

Finally, the heat source can be defined as:

$$Q_g = q_g\left(\frac{\pi r_{ext}^2 - \pi r_{int}^2}{2\pi}\right)d\alpha dz = \frac{q_g}{2}(r_{ext}^2 - r_{int}^2)\, d\alpha dz \tag{4.22}$$

Finally, by expressing all the terms in Eq. (4.15) and simplifying [116], we arrive at the expression for determining the local convective coefficient at the internal wall-fluid interface:

$$h_{int} = \frac{k \cdot \ln\left(\frac{r_{ext}}{r_{int}}\right)\cdot\frac{\partial^2 T}{\partial \alpha^2} + \frac{k}{2}(r_{ext}^2 - r_{int}^2)\cdot\frac{\partial^2 T}{\partial z^2} - \frac{r_{ext}}{R_{env}}(T - T_{env}) + \frac{q_g}{2}(r_{ext}^2 - r_{int}^2)}{r_{int}\cdot(T - T_b)} \tag{4.23}$$

However, due to the presence of noise in the raw images of the surface temperature distribution, Eq. (4.23) may yield unreliable results [216]. Its second derivative operator makes it highly sensitive to small perturbations caused by noise in the input data, leading to inaccurate outcomes [238]. To solve this problem, a Gaussian filtering approach is applied to the raw temperature data. This filter helps in data smoothing by eliminating high-frequency

components that could lead to noise or fluctuations. The Gaussian filter, which ensures that the temperature data is more stable and easier to study without losing significant trends or patterns, essentially serves as a regularization function. The measurements of temperature can be reported in an accurate and more precise way according to this filtering method, which effectively eliminates the unwanted noise.

The efficacy of Gaussian filtering in this type of approach has been demonstrated by several researchers [179],[216]. The filter function in the 2-D frequency domain can be expressed as:

$$H(u,v) = e^{-\frac{(u^2+v^2)}{2u_c^2}} \tag{4.24}$$

where u_c is the cutoff frequency, assumed equal along the u and v coordinates.

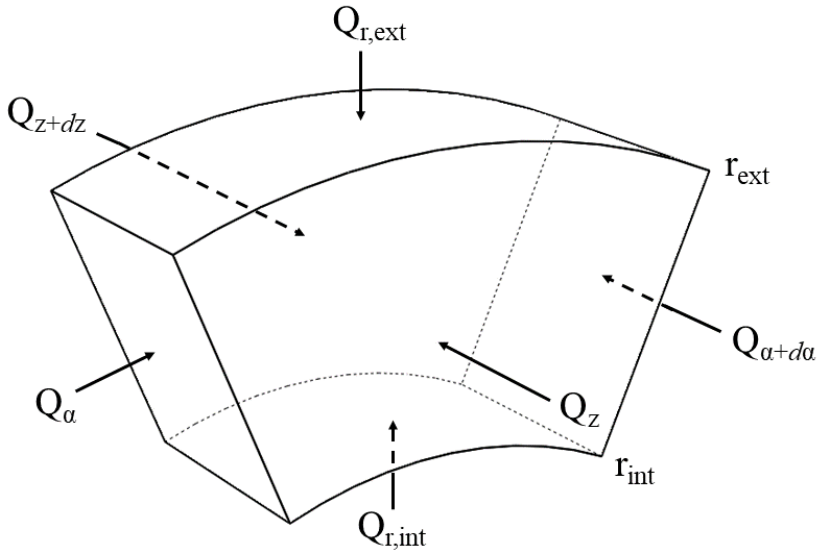

Figure 4. 12 Sketch of a portion of the test section

In real situations, it is difficult to determine the correct cutoff frequency for filtering because the perfect value isn't known in advance. The cutoff frequency is very critical since it determines whether portions of the data are considered noisy and need to be filtered. A selection criterion is required in order to efficiently carry out the regularization step, which smoothed and eliminates the noise from the data. Therefore, this criterion helps in selecting the best cutoff frequency by comparing the retention of significant data characteristics with the elimination of noise.

In this study, the discrepancy criterion proposed by Morozov [239] was adopted. According to this criterion, the solution of the inverse problem is considered accurate enough when the difference between the measured temperatures T and the filtered temperatures T_f is similar to the standard deviation of the measured temperatures T. Hence, the appropriate cutoff frequency can be determined once the following condition is satisfied:

$$\frac{\left\|T_f - T\right\|_2^2}{N \cdot M} = \sigma_T^2 \tag{4.25}$$

Where, σ_T represents the standard deviation of measured temperature, where N and M is the matrix's dimension derived from the measured temperatures. The data was obtained by measuring the surface temperature of the coil when it was kept in an isothermal condition. In this condition there are no temperature variations or fluctuations, and the measurements are more precise and reliable when this constant temperature is maintained. This stability makes sure that there are no outside influences generating distortions or inaccuracies and that the data accurately represents the surface temperature of the coil.

The specification of the uncertainties in the several major experimental measurements provides its starting point. The uncertainties of the initial measurements are the starting point, and the uncertainties can cause large differences in the final findings when they propagate through other calculations or algorithms. These uncertainties, which are a part of the entire measurement process, are caused by things including measuring error, atmosphere conditions, and instrument precision. It is essential to comprehend and measure these uncertainties because they influence modification for obtaining accurate results, as well as how confident one can be in the results itself. Therefore, by employing the error propagation method as outlined in [240], the level of uncertainty is associated with the primary parameter employed in this investigation. The upper bounds of uncertainty for the friction factor, convective heat transfer coefficient, Nusselt number, and Reynolds number were determined to be approximately ±6%, ±8%, ±9%, and ±3%, respectively.

The uncertainties in the primary measurements were first evaluated, focusing on the thermocouples' signal. The signal was captured using a high-precision multi-meter with a 10 nV resolution in the 0–100 mV range. Under the experimental conditions, the thermocouple signal was approximately 0.6 mV, resulting in an absolute accuracy of 0.05 μV. With a 40

μV/°C sensitivity for the copper-constantan thermocouple, this corresponds to a temperature accuracy of 0.008°C. To calculate the volumetric flow rate, a high-precision digital scale with a resolution of 0.1 g was used to measure the mass of the container, and the time needed to fill it at outlet of test section. A digital stopwatch with a 0.01 seconds resolution was used to record the time. The experimenter's estimated response time of 0.1 seconds accounts for the majority of the measurement's error. Because of this, the total uncertainty in the measurement of the volumetric flow rate is less than 1%.

The Rosemount 3051S Pressure Transducer was used to measure the pressure drop throughout the corrugated pipes under isothermal conditions. Because of its excellent accuracy and stability, this transducer is perfect for applications which require for precise pressure measurements. In order to ensure precise and dependable pressure drop measurements throughout the system, the manufacturer set the measurement uncertainty for the Rosemount 3051S at 3%. The heat flux generated in the wall per unit volume is influenced by the electric power supplied and the heat exchanged with the environment. The uncertainty in heat flux arises from several factors, including heat dissipation through cables and fin electrodes, power supply stability, accurate volume estimation, and axial temperature gradients in the entry region. To account for these uncertainties, a conservative error of approximately 4% was considered. Since all of the pipes had the same diameter and the tubes were mechanically fabricated, therefore, uncertainty in the pipe diameter was also calculated. The tube diameter was determined to have an inaccuracy of about 2%. The measured quantities inherent uncertainties are documented in Table 4.1.

Table 4. 1 Uncertainty of the main physical quantities involved in the estimation procedure

Sr.#	Parameters	Unit	Uncertainty Percentage
1	Temperature	K	±0.1
2	Change in temperature	K	±0.2
3	Pressure drops	Pa	±3
4	Dynamic viscosity	$Pa \cdot s$	±1
5	Density	$\frac{Kg}{m^3}$	±1
6	Internal heat generation	$\frac{W}{m^3}$	±3
7	Volume	$\frac{m^3}{s}$	±1
8	Internal diameter	m	±2
9	Reynolds Number	-	±3
10	Nusselt Number	-	±9
11	Heat transfer coefficient	$\frac{W}{m^2}.K$	±8

5. Heat Transfer Enhancement in Turbulent Regimes: Local and Average Analysis

5.1. Average Results

The initial phase of the investigation aimed to assess the average heat transfer capabilities of the tested corrugated pipes and examine the associated pressure drops. The thermal performance of the pipes was evaluated by plotting the Nusselt number against the Reynolds number for each design, as depicted in Figure 5.1. The experiments were conducted in the turbulent regime, with Reynolds numbers ranging from 4×10^3 to 1.6×10^4, using water as the working fluid. The plot also included the Nusselt number distribution for a smooth tube, obtained through experimental means, as well as the Dittus–Boelter correlation for smooth pipe operating in turbulent conditions [179]. Significant improvements in thermal behavior are indicated by a significant increase in the Nusselt number, an essential indicator of heat transfer efficiency.

The good agreement observed between the measured values for the smooth tube and the Dittus–Boelter correlation confirms the reliability of the experimental setup. The experimental values of the Nusselt number obtained for the smooth pipe can be considered in good accordance with the ones calculated with the Dittus–Boelter correlation since the difference is within ±15% which is reported in figure 5.1. From Figure 5.1, it can be observed that the transverse corrugations T16 and T32, with the cross-helix corrugation C16 with the smaller pitch, exhibited the best thermal performance, achieving Nusselt numbers approximately three times higher than that of the smooth tube and 1.5 times higher than that of the H32 corrugation. Moreover, it can be noted that the pitch size seems to have a significant influence on thermal performance. This effect is especially seen in the case of helical geometries, where the smaller pitches (H16 and C16) enhance thermal effect to a greater extent compared to the larger pitches (H32 and C32), especially at higher Reynolds number values. Furthermore, the worst performance can be seen in the helical corrugation H32 having higher pitch size than other corrugated pipes. Overall, all the studied corrugation profiles

demonstrated superior heat transfer rates compared to the smooth pipe, highlighting their effectiveness in enhancing thermal performance.

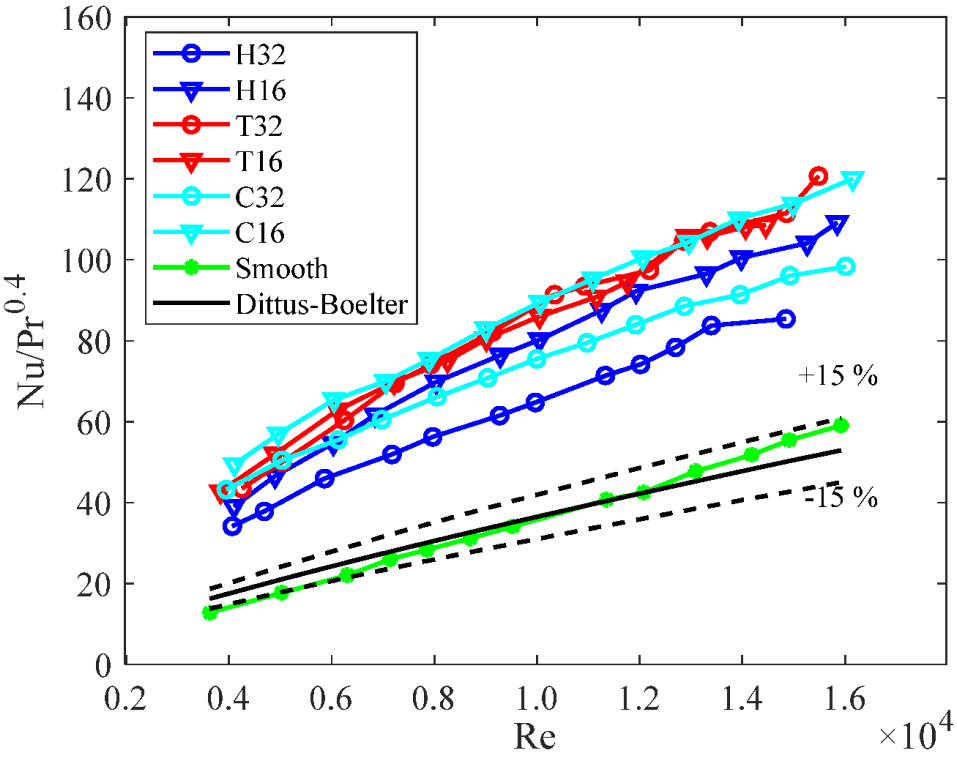

Figure 5. 1 Nusselt number vs. Reynolds number

These findings align with the observations made by Rainieri and Pagliarini [206] in laminar conditions where transverse corrugation achieved the best thermal results, demonstrating excellent thermal enhancement capabilities in straight pipes. Regarding the helical corrugation, it was observed that the lower the pitch, the higher the thermal enhancement. Moreover, the results are consistent with those obtained by Vicente et al. [241] for helical corrugation, by Mohammed et al. [242] for transversal corrugation, and by Bozzoli et al. [117] for cross-helical corrugation, as reported in Figure 5.2.

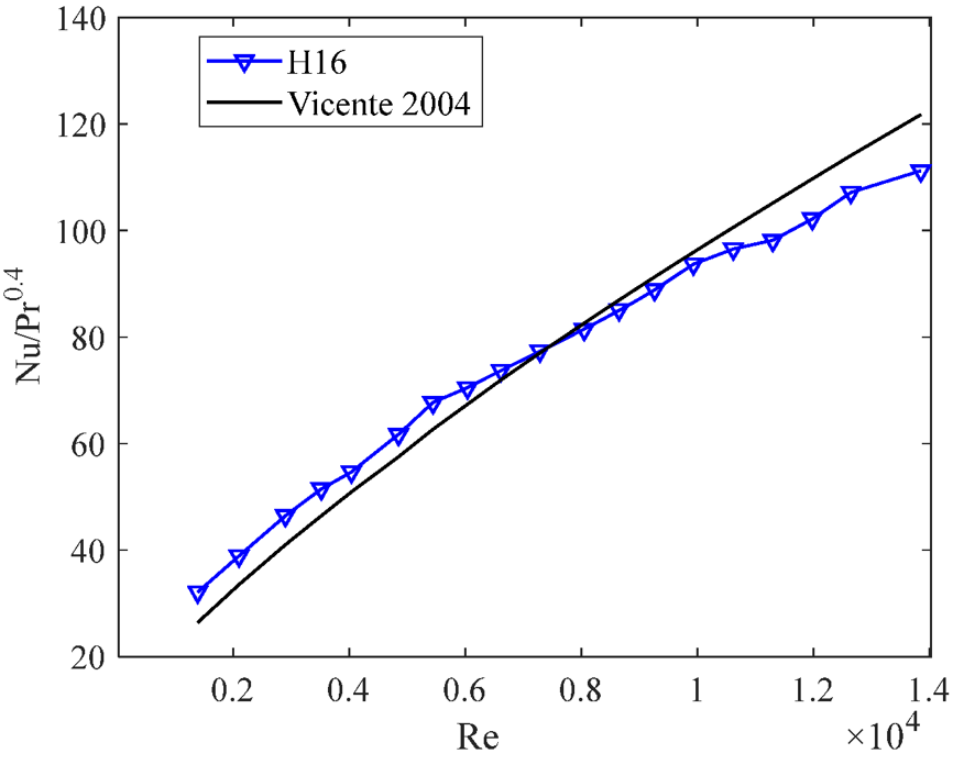
H16
Vicente 2004
Nu/Pr^0.4
Re
×10^4
140
120
100
80
60
40
20
0.2
0.4
0.6
0.8
1
1.2
1.4

(a)

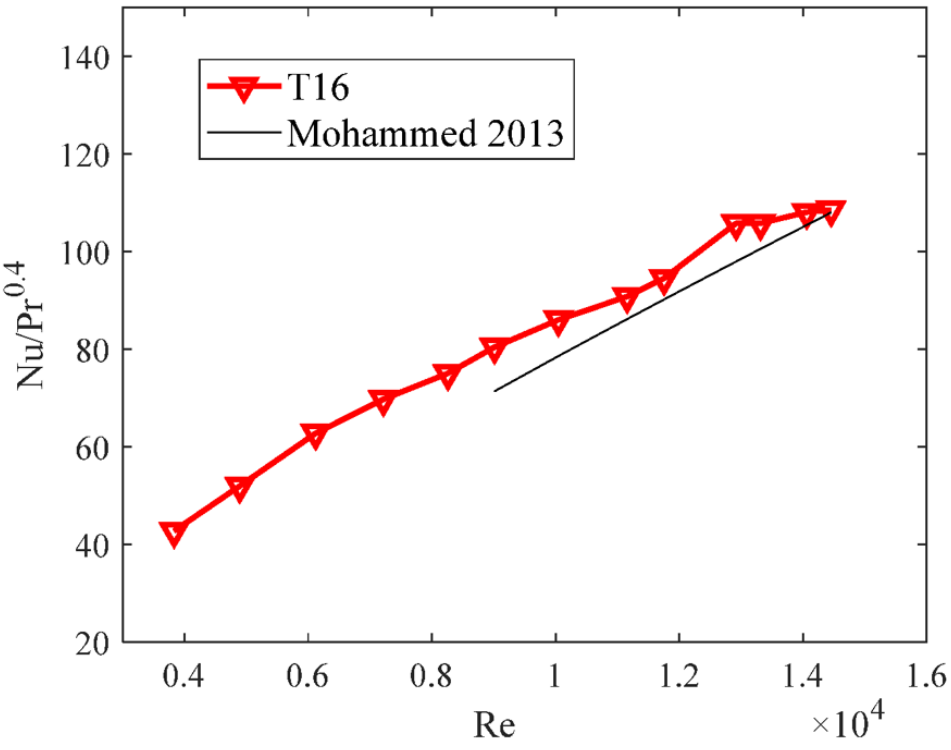
T16
Mohammed 2013
Nu/Pr^0.4
Re
×10^4
140
120
100
80
60
40
20
0.4
0.6
0.8
1
1.2
1.4
1.6

(b)

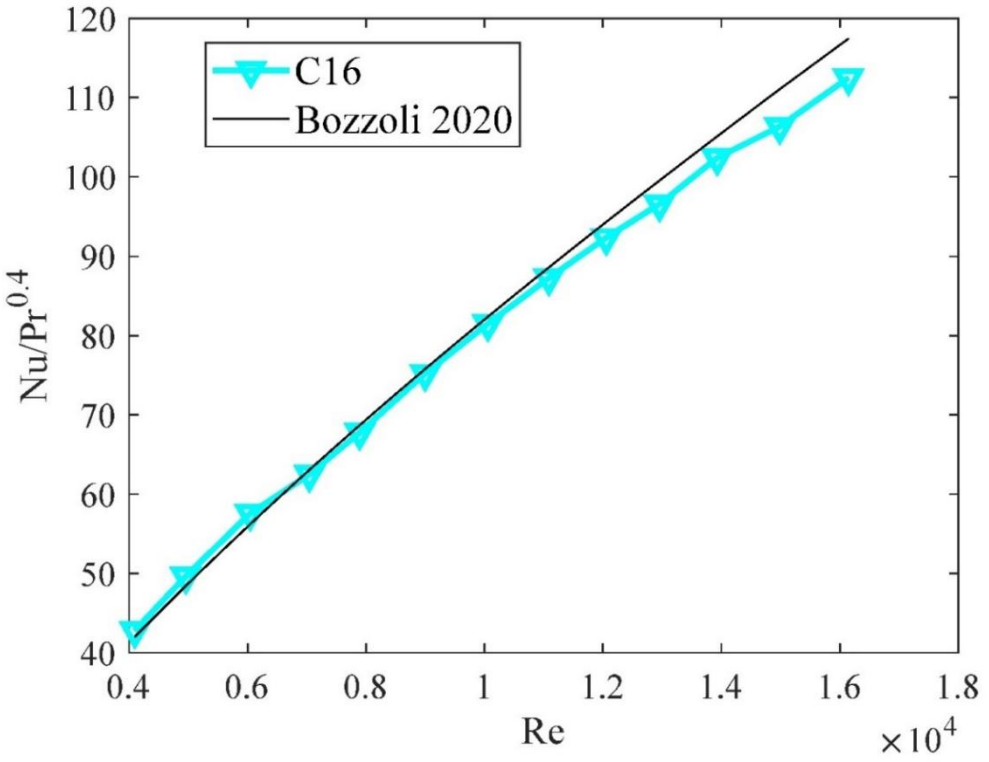

(c)

Figure 5. 2 Comparison of the experimental results with those previously obtained in the literature for (a) helical, (b) transversal, and (c) cross-helical corrugations

In this research, we used water as a working fluid in the range of Reynolds number 4×10^3 to 16×10^3. For each corrugated pipe at a different Reynolds number (4×10^3, 10×10^3, and 16×10^3), wall temperature distributions along the axial direction are shown in Figures 5.3, 5.4 and 5.5 as a function of dimensionless abscissa. This dimensionless abscissa was determined with the help of Equation 5.1. Each graph reports the temperature at the upper and lower sides of the corrugated pipe, along with the average wall temperature, which is determined by taking the mean of these two values (upper and lower temperature of the wall). Most commonly, the natural convection is negligible when $Ri < 0.1$, where $Ri = \frac{Gr}{Re^2}$. It can be observed from the tables presented in sections 5.1, 5.2, 5.3, 5.4, 5.5, and 5.6 that the Richardson number (Ri) for all corrugated cases is always less than 0.1.

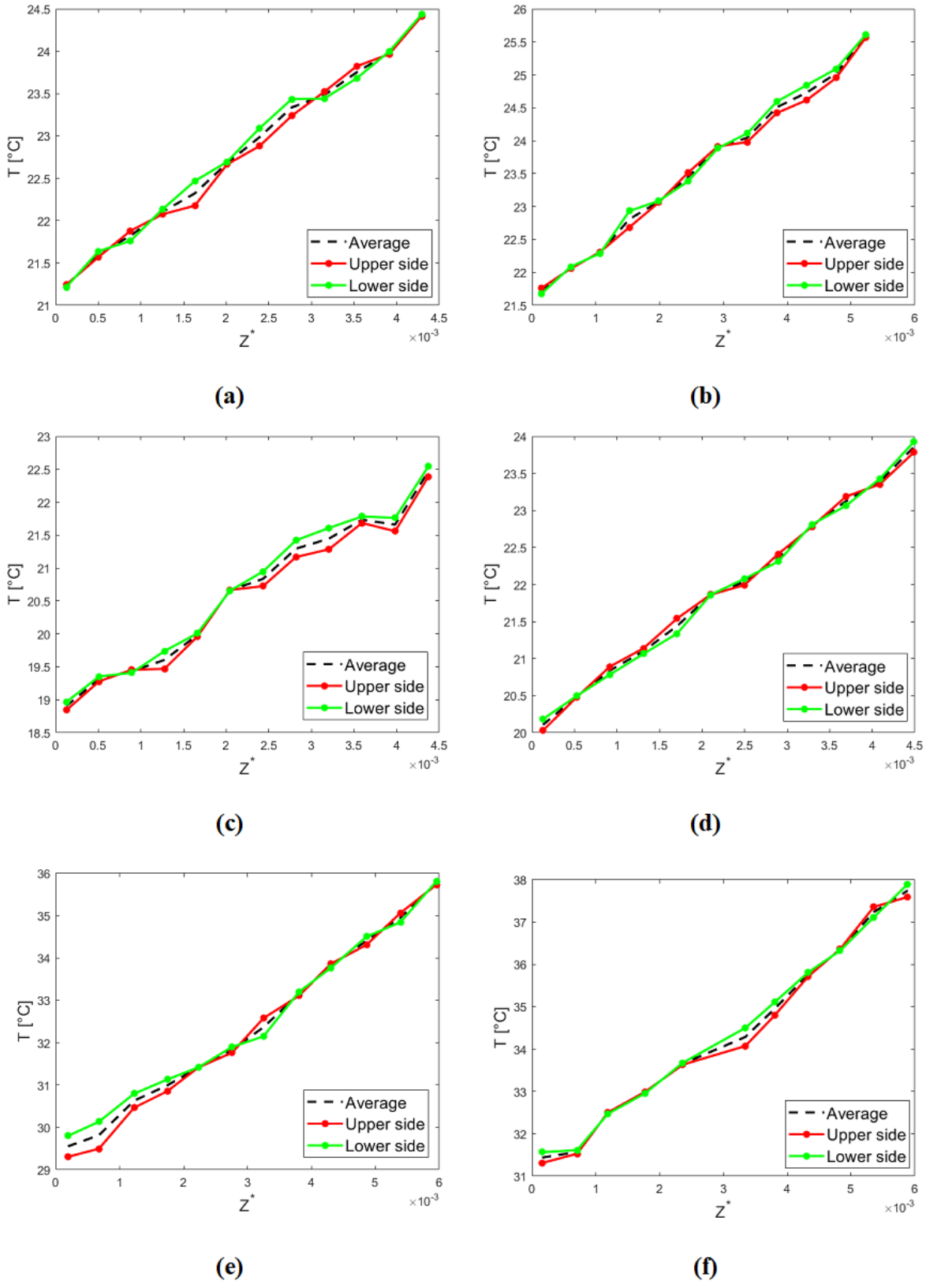

Figure 5. 3 Wall temperature distribution for all corrugated pipes at $Re = 4 \times 10^3$: (a) H32, (b) H16, (c) T32, (d) T16, (e) C32, and (f) C16

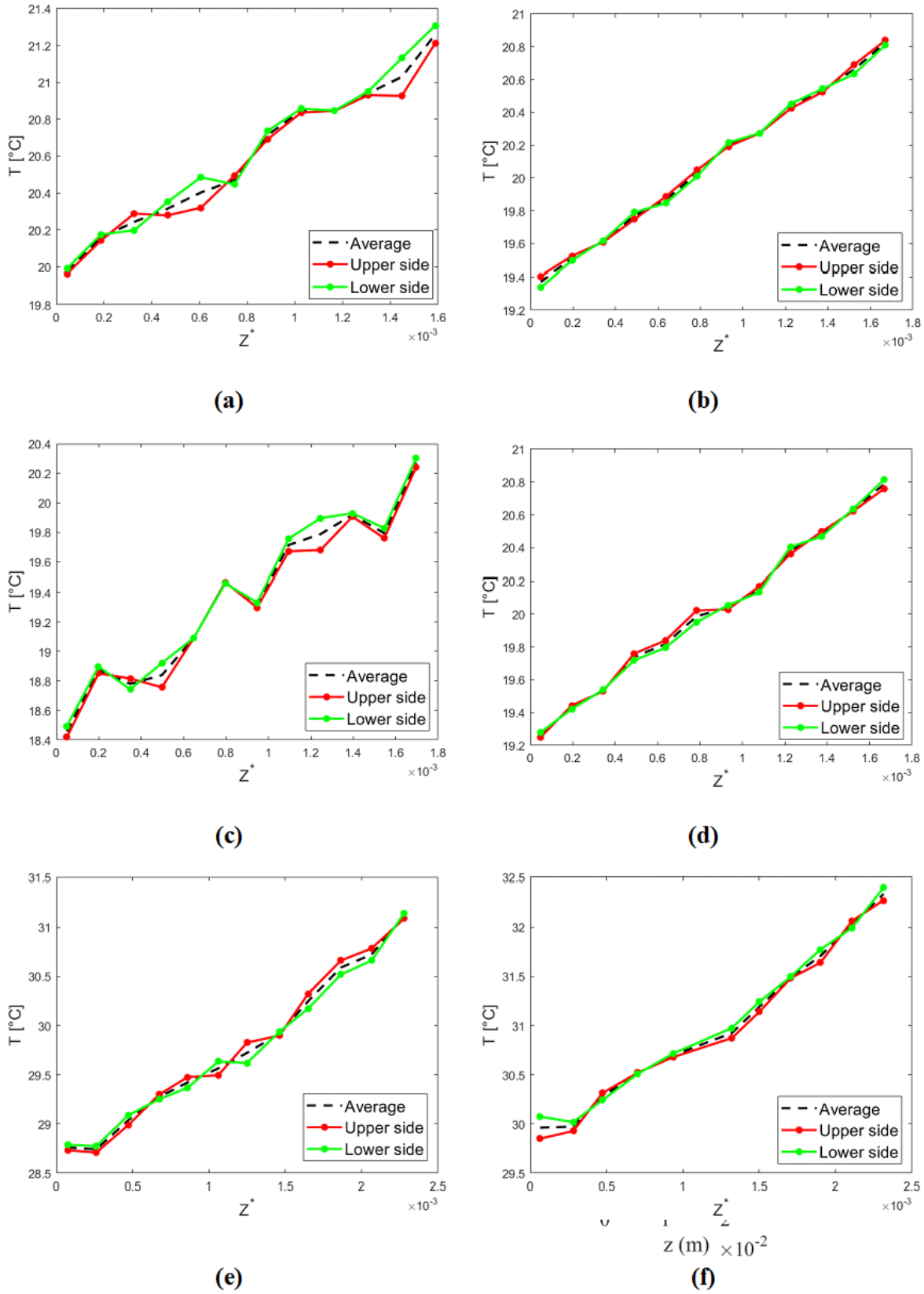

Figure 5. 4 Wall temperature distribution for all corrugated pipes at $Re = 10 \times 10^3$: (a) H32, (b) H16, (c) T32, (d) T16, (e) C32, and (f) C16.

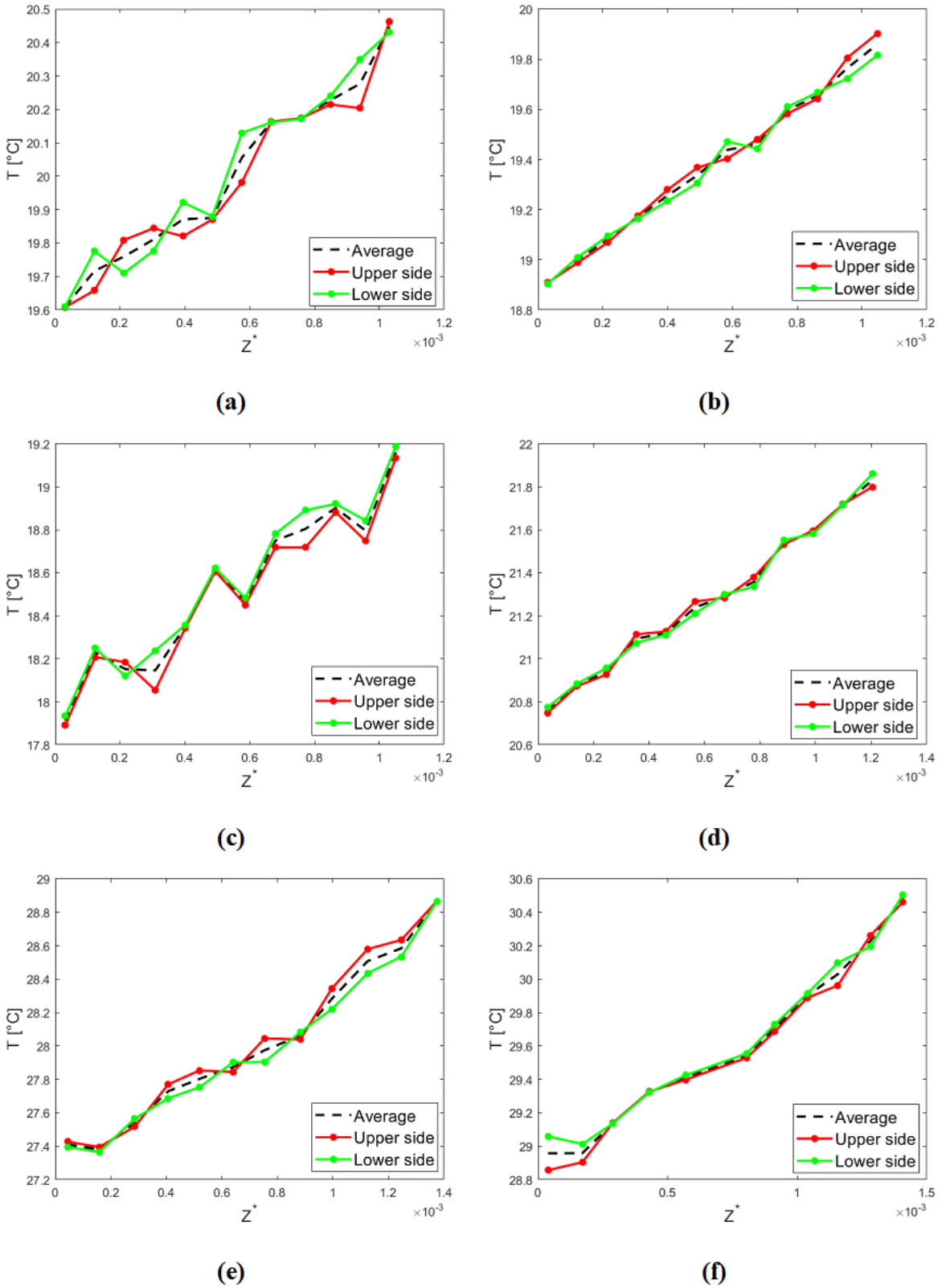

Figure 5. 5 Wall temperature distribution for all corrugated pipes at $Re = 16 \times 10^3$: (a) H32, (b) H16, (c) T32, (d) T16, (e) C32, and (f) C16

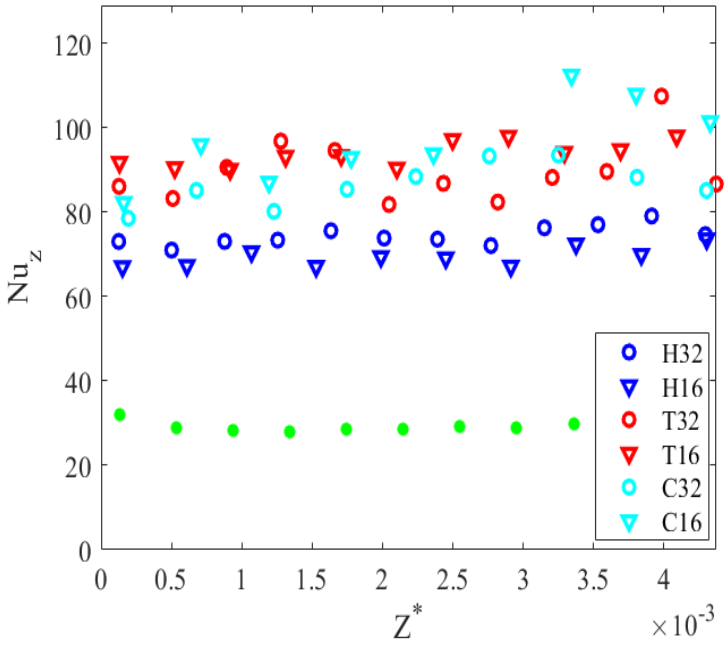

Figure 5. 6 At $Re = 4 \times 10^3$ Reynolds Number: Local Averaged Nusselt Number vs. dimensionless abscissa for all corrugated pipes

The behavior of the axial Nusselt number (Nu_z) as a function of the dimensionless abscissa is investigated in order to thoroughly how corrugation geometry affects thermal exchange and shown in Figures 5.6, 5.7, and 5.8 at various Renyolds number (4×10^3, 10×10^3, and 16×10^3). The dimensionless abscissa was determined with the help of Equation 5.1.

$$z^* = \frac{z}{Re.Pr.D} \tag{5.1}$$

It can be observed that all Figures (5.6, 5.7, and 5.8) remain consistent along the dimensionless abscissa for all corrugated pipes under thermally and hydrodynamically fully developed conditions. Furthermore, the findings regarding the overall behavior are validated as seen in Figure 5.1. The helical corrugation design resulted in 1.5 times higher thermal performance, while the transverse corrugation shows significant heat transfer enhancement, with Nu_z values almost three times higher than those for smooth pipes, due to the increased flow disruption and mixing, which lead to more efficient heat transfer. The pitch size has no impact on thermal efficiency for transverse corrugations (T32 and T16). Furthermore, the smaller pitch pipe has higher thermal performance as compared to larger pitch pipes.

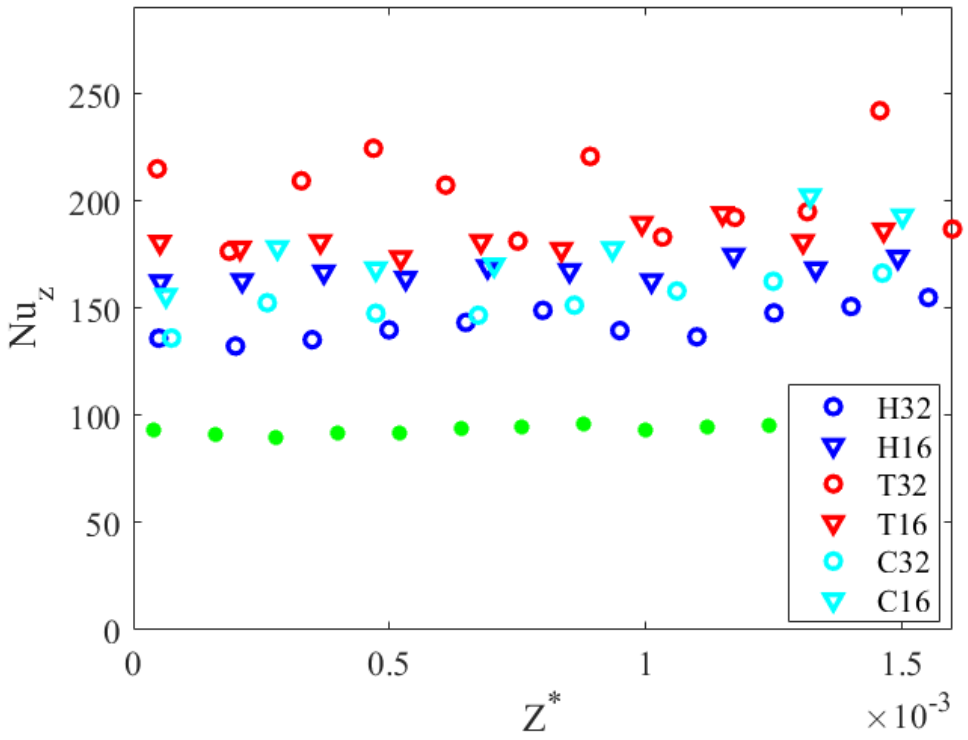

Figure 5. 7 At $Re = 10 \times 10^3$ Reynolds Number: Local Averaged Nusselt Number vs. dimensionless abscissa for all corrugated pipes

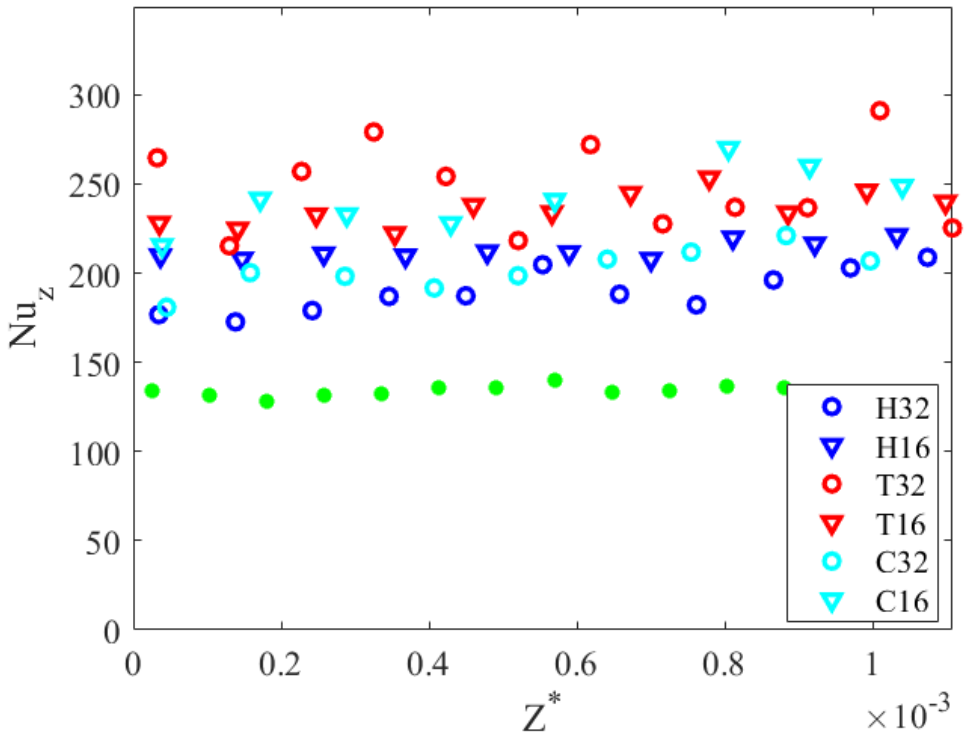

Figure 5. 8 At Re= 16×10^3 Reynolds Number: Local Averaged Nusselt Number vs. dimensionless abscissa for all corrugated pipes

Furthermore, Figure 5.9 illustrates the evaluation of the pressure drop in terms of the Darcy friction factor (f) as a function of the Reynolds number for all the pipes. It can be observed that for $Re < 8 \times 10^3$, the helically corrugated pipes exhibited a lower pressure drop compared to the transverse ones. However, for Re > 8×10^3, the profiles behaved similarly. The cross-helix corrugation C32 showed similar behavior to the helical ones, while the C16 profile demonstrated the worst performance. As expected, all the corrugated pipes had higher values of frication factor *(f)* compared to the smooth pipe.

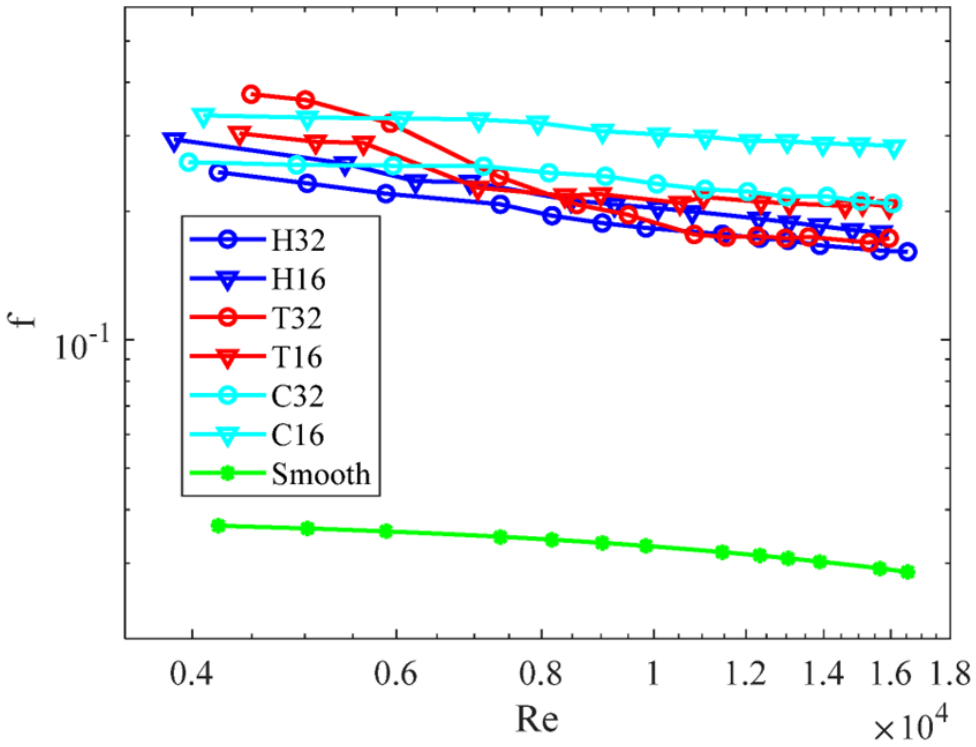

Figure 5. 9 Friction factor vs. Reynolds number

Figures 5.10 and 5.11 describe the heat transfer and friction factor enhancement effect caused by all tubes. It is possible to observe that from Figure 5.10, it can be observed that the transverse corrugations T16 and T32, with the cross-helix corrugation C16 exhibited the maximum heat transfer enhancement. In terms of facilitating effective heat transfer, these corrugations performed significantly better than others. As shown in Figure 5.11, in the case of cross-helix corrugation C16 has the maximum friction factor enhancement and C32 has the lowest. Moreover, the enhancement of the friction factor in both transverse and helical pipes remains generally consistent up to 10×10^3. However, after 10×10^3, a noticeable peak in friction factor enhancement is observed across all these corrugated pipes.

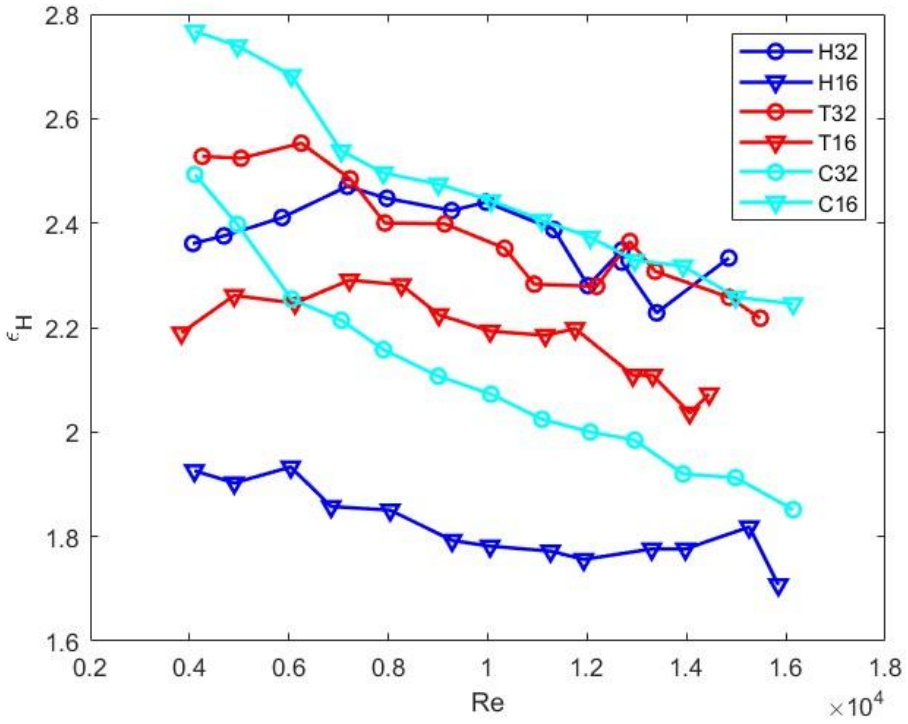

Figure 5. 10 Heat transfer enhancement

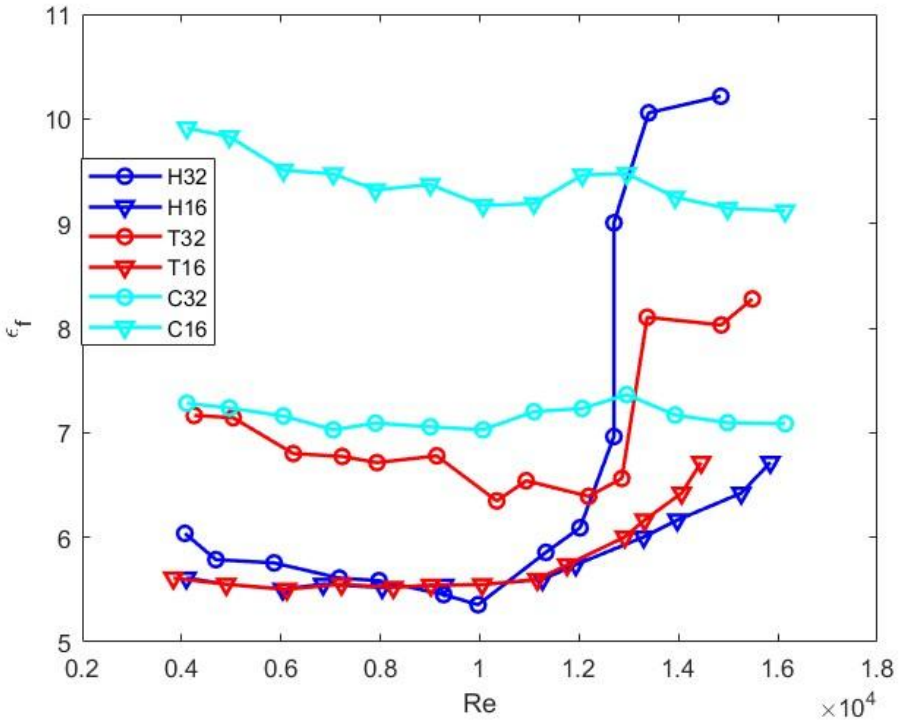

Figure 5. 11 Friction factor enhancement

To assess the effect of the different profiles, the efficiency of the geometry (η) is presented in Figure 5.12. It can be observed that, in terms of efficiency (η), for $Re < 10^4$, the

transverse geometry consistently outperformed the helical profiles, including both the single and cross-helix corrugations. Hence, it can be concluded that although transverse corrugation leads to higher friction factors, its ability to enhance thermal performance makes it more efficient. On the other hand, the H32 geometry exhibited the lowest efficiency across the entire range of tested Reynolds numbers. For $Re > 10^4$, the efficiency (η) of all the pipes did not show significant differences, except for the H32 geometry, which remains the least efficient geometry. Finally, the experimental conditions of all the tests performed for each pipe are reported in tables 5.1,5.2,5.3,5.4,5.5 and 5.6.

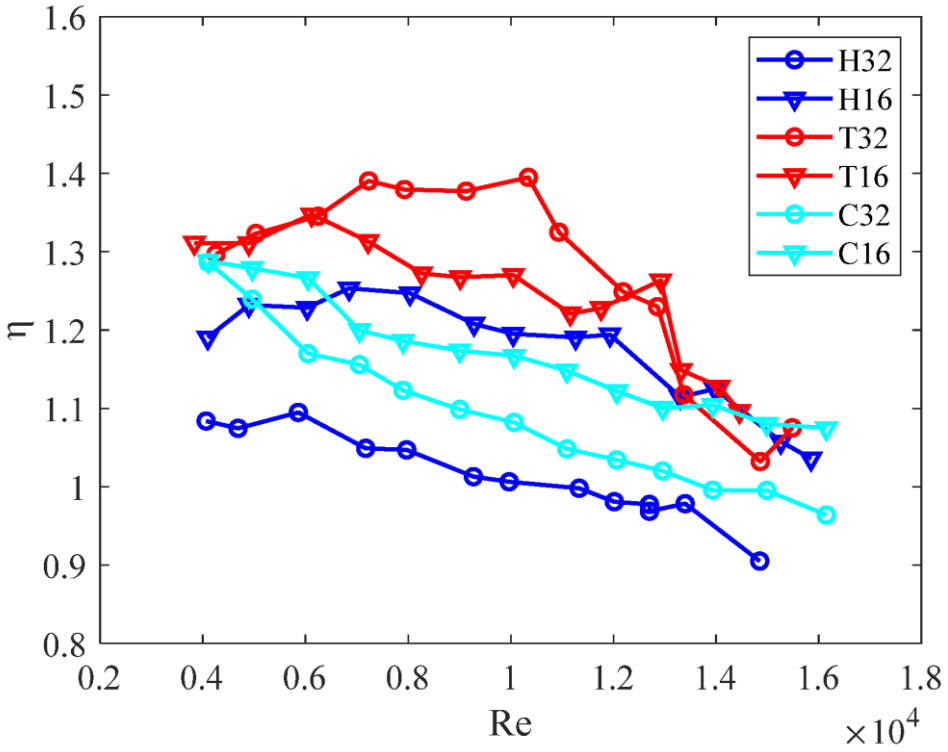

Figure 5. 12 Efficiency η vs. Reynolds number

Table 5. 1 Experimental conditions for Pipe C16

Pipe	Test no.	Re	Nu	Pr	Tb [K]	Gr/Re^2
C16	0	4139	110	5.32	304.15	3.5×10^{-3}
	1	4979	111.63	5.35	303.8	2.1×10^{-3}
	2	6051	128.49	5.4	303.42	1.2×10^{-3}
	3	7037	143.08	5.46	302.94	7.5×10^{-4}
	4	7899	148.87	5.49	302.77	5.63×10^{-4}
	5	8991	164.2	5.51	302.48	3.99×10^{-4}
	6	10054	177.49	5.54	302.31	2.95×10^{-4}
	7	11080	189.09	5.55	302.18	2.27×10^{-4}
	8	12054	199.73	5.56	302.08	1.83×10^{-4}
	9	12947	207.95	5.59	301.85	1.54×10^{-4}
	10	13925	219.95	5.63	301.55	1.01×10^{-4}
	11	14978	227.56	5.65	301.36	8.5×10^{-5}

Table 5. 2 Experimental conditions for Pipe C32

Pipe	Test no.	Re	Nu	Pr	Tb [K]	Gr/Re^2
C32	0	3937	85.85	5.58	301.96	3.9×10^{-3}
	1	5030	100.53	5.61	3134.15	2.0×10^{-3}
	2	6114	110.92	5.65	301.44	1.2×10^{-3}
	3	6965	121.03	5.67	301.27	8.5×10^{-4}
	4	8041	132.54	5.69	301.1	5.86×10^{-4}
	5	9028	142.2	5.71	300.9	4.32×10^{-4}
	6	9987	151.78	5.73	300.79	3.31×10^{-4}
	7	10965	160.41	5.79	300.3	2.58×10^{-4}
	8	11914	169.59	5.81	300.14	2.07×10^{-4}
	9	12865	179.13	5.85	299.92	1.69×10^{-4}
	10	13947	185.54	5.88	299.7	1.37×10^{-4}
	11	14926	195.57	5.91	299.49	1.13×10^{-4}
	12	16007	200.28	5.91	299.46	9.64×10^{-5}

Table 5. 3 Experimental conditions for Pipe H32

Pipe	Test no.	Re	Nu	Pr	Tb [K]	Gr/Re^2
H32	0	4111	74.34	7	293.76	2.0×10^{-3}
	1	4688	82.4	7.01	293.17	1.4×10^{-3}
	2	5400	91.29	7.02	292.59	9.63×10^{-4}
	3	5859	100.76	7.13	292.47	7.49×10^{-4}
	4	6564	108.13	7.13	292.43	5.63×10^{-4}
	5	7174	113.95	7.14	292.36	4.49×10^{-4}
	6	7970	123.51	7.14	292.35	3.43×10^{-4}
	7	8570	130.23	7.16	292.25	2.81×10^{-4}
	8	9272	135.2	7.17	292.22	2.31×10^{-4}
	9	9966	142.44	7.18	292.17	1.91×10^{-4}
	10	10652	148.2	7.19	292.08	1.60×10^{-4}
	11	11330	157.29	7.21	291.98	1.36×10^{-4}
	12	12017	163.48	7.22	291.91	1.16×10^{-4}
	13	12699	172.92	7.23	291.84	1.002×10^{-4}
	14	13398	184.81	7.23	291.84	8.60×10^{-5}
	15	14256	189.03	7.24	291.78	7.37×10^{-5}
	16	14850	188.65	7.25	291.72	6.72×10^{-5}
	17	15640	194.23	7.25	291.73	5.88×10^{-5}
	18	16283	195.48	7.24	291.82	5.36×10^{-5}

Table 5. 4 Experimental conditions for Pipe H16

Pipe	Test no.	Re	Nu	Pr	Tb [K]	Gr/Re^2
H16	0	3387	69.93	6.9	293.85	2.0×10^{-3}
	1	4096	84.76	6.94	293.6	1.9×10^{-3}
	2	4898	101.15	6.96	293.43	1.2×10^{-3}
	3	5513	112.1	6.99	293.27	8.29×10^{-4}
	4	6034	119.12	7.01	293.12	6.01×10^{-4}
	5	6848	135.1	7.01	293.14	4.59×10^{-4}
	6	7422	148.3	7.14	292.37	3.50×10^{-4}
	7	8036	153.49	7.17	292.23	2.85×10^{-4}
	8	8612	160.52	7.21	292	2.33×10^{-4}
	9	9282	168.57	7.23	291.84	1.92×10^{-4}
	10	10047	177.24	7.25	291.73	1.56×10^{-4}
	11	10650	185.44	7.26	291.69	1.33×10^{-4}
	12	11254	193.53	7.26	291.7	9.83×10^{-5}
	13	11931	204.09	7.28	291.58	8.85×10^{-5}
	14	12610	210.26	7.28	291.55	7.49×10^{-5}
	15	13299	213.75	7.29	291.49	6.54×10^{-5}
	16	13977	224.48	7.3	291.83	5.73×10^{-5}
	17	14637	235.39	7.32	291.35	5.24×10^{-5}
	18	15839	242.16	7.32	291.32	4.71×10^{-5}

Table 5. 5 Experimental conditions for Pipe T16

Pipe	Test no.	Re	Nu	Pr	Tb [K]	Gr/Re^2
T16	0	3834	93.66	7.1	292.52	2.0×10^{-3}
	1	4461	106.59	7.09	292.55	1.3×10^{-3}
	2	4897	113.82	7.11	292.45	1.0×10^{-3}
	3	6121	137.84	7.13	292.28	5.56×10^{-4}
	4	6633	144.23	7.16	292.14	4.47×10^{-4}
	5	7227	153.89	7.18	292.03	3.54×10^{-4}
	6	7740	162.47	7.2	291.89	2.94×10^{-4}
	7	8235	165.13	7.22	291.75	2.49×10^{-4}
	8	9015	177.6	7.24	291.67	1.97×10^{-4}
	9	9454	182.78	7.24	291.67	1.74×10^{-4}
	10	10049	190.05	7.25	291.59	1.48×10^{-4}
	11	10538	193.77	7.27	291.47	1.30×10^{-4}
	12	11158	200.85	7.27	291.48	1.12×10^{-4}
	13	11758	209.13	7.28	291.44	9.81×10^{-5}
	14	12829	229.02	7.04	292.79	8.02×10^{-5}
	15	13318	230.82	7.02	292.93	7.36×10^{-5}
	16	14062	235.68	7.006	293	6.49×10^{-5}
	17	14455	238.62	6.98	293.1	6.11×10^{-5}

Table 5. 6 Experimental conditions for Pipe T32

Pipe	Test no.	Re	Nu	Pr	Tb [K]	Gr/Re^2
T32	0	3807	89.47	7.35	291.29	1.9×10^{-3}
	1	4253	96.21	7.31	291.43	1.4×10^{-3}
	2	5036	110.79	7.31	291.45	9.27×10^{-4}
	3	6246	133.61	7.31	291.4	5.22×10^{-4}
	4	7231	154.48	7.38	291.05	3.46×10^{-4}
	5	8108	162.94	7.36	291.14	2.74×10^{-4}
	6	9132	182.62	7.37	291.08	1.89×10^{-4}
	7	9723	192.32	7.38	291.02	1.54×10^{-4}
	8	10341	203.04	7.36	291.09	1.35×10^{-4}
	9	10934	207.85	7.37	291.05	1.15×10^{-4}
	10	11523	223	7.38	290.99	1.01×10^{-4}
	11	12857	233	7.41	290.84	7.57×10^{-5}
	12	13368	238	7.41	290.83	6.85×10^{-5}
	13	14135	243.54	7.41	290.81	6.01×10^{-5}
	14	14859	248.16	7.39	290.93	5.31×10^{-5}
	15	15484	269.72	7.47	290.45	4.62×10^{-5}

5.2 Local results

To aid in the understanding of the results obtained from the infrared (IR) analysis, Figure 5.13 provides a schematic representation of the analyzed section of the pipes captured by the IR camera, indicating the position of the corrugations for each tested pipe and the direction of the flow. The portion analyzed to determine the coefficient corresponds to a complete pitch of the corrugation, ensuring a comparable analysis domain for the different corrugation profiles studied.

By analyzing the non-filtered temperature distribution shown in Figure 5.14 and the filtered temperature distribution depicted in Figure 5.17 on the external surface of the tested pipes, an example for the case of $Re = 4 \times 10^3$. A detailed analysis of both Figures 5.14 and 5.17 demonstrates how the temperature distribution on the wall of the investigated pipes is locally impacted by corrugations. It is evident that the corrugations had a significant influence on the temperature distribution along the pipe wall. For instance, taking the H32 case as an example, it can be observed that immediately after the corrugation, in the direction of flow (as shown in Figure 5.13), the wall temperature reached a peak. This indicates a reduction in the rate of thermal exchange between the fluid and the wall due to the disruption of the boundary layer caused by the roughness of the corrugation. As the fluid continued along the pipe, the wall temperature suddenly decreased, indicating an increase in the rate of thermal exchange. This phenomenon can be attributed to the reattachment of the fluid to the inner wall of the pipe, leading to increased turbulence. Subsequently, the wall temperature gradually increased until the next corrugation, where the process was repeated.

This gradual temperature rise could be attributed to the re-establishment of the fluid's original turbulent state, with the smooth pipe section acting as a stabilizer for the flow. The wall temperature gradually increases until it reaches the next corrugation, at this point, the cycle begins again after reaching its lowest point. Each corrugation repeats this phenomenon of a decrease in temperature afterward a gradual increase in temperature. After achieving the minimum, the fluid's temperature may gradually rise again because it may be restored to its initial turbulent state. This temperature rise may be facilitated by the smooth portion of the pipe stabilizing the fluid's flow. A similar trend of temperature drop followed by a gradual rise can be observed in scenario T32.

However, when examining the temperature distribution for smaller pitches (H16 and T16), the stabilizing effect between the corrugations seemed to diminish. This could be due to the insufficient distance between the corrugations preventing the stabilization effect and resulting in lower and more homogeneous temperatures as the distance exists between the end of one corrugation crest and the beginning of the one that comes next is less than 16mm. These lower and more homogeneous temperatures indicate an increased heat exchange ability in the pipe wall, confirming their superior thermal performance compared to pipes with larger pitch. This observation aligns perfectly with the average analysis results, further confirming the advantage over pipes with a larger pitch.

The pipes with cross-helix corrugations (C32 and C16) exhibited more complex temperature distributions due to the combined effect of the two helical corrugations that evolve in opposite directions, promoting a chaotic flow pattern. In comparison to the other corrugated pipes, the chaotic flow improves overall heat transfer but also increases the unpredictability of temperature patterns. Moreover, chaotic flow improves heat transfer but also leads to more complex temperature patterns. Similarly, the non-filtered temperature distribution and filtered temperature distribution on the external surface of the tested pipes, for the other cases such as $Re = 10 \times 10^3$ and $Re = 16 \times 10^3$ are shown in Figure 5.15, 5.16, 5.18, and 5.19. The temperature variations for these particular Reynolds numbers are presented in detail in these figures.

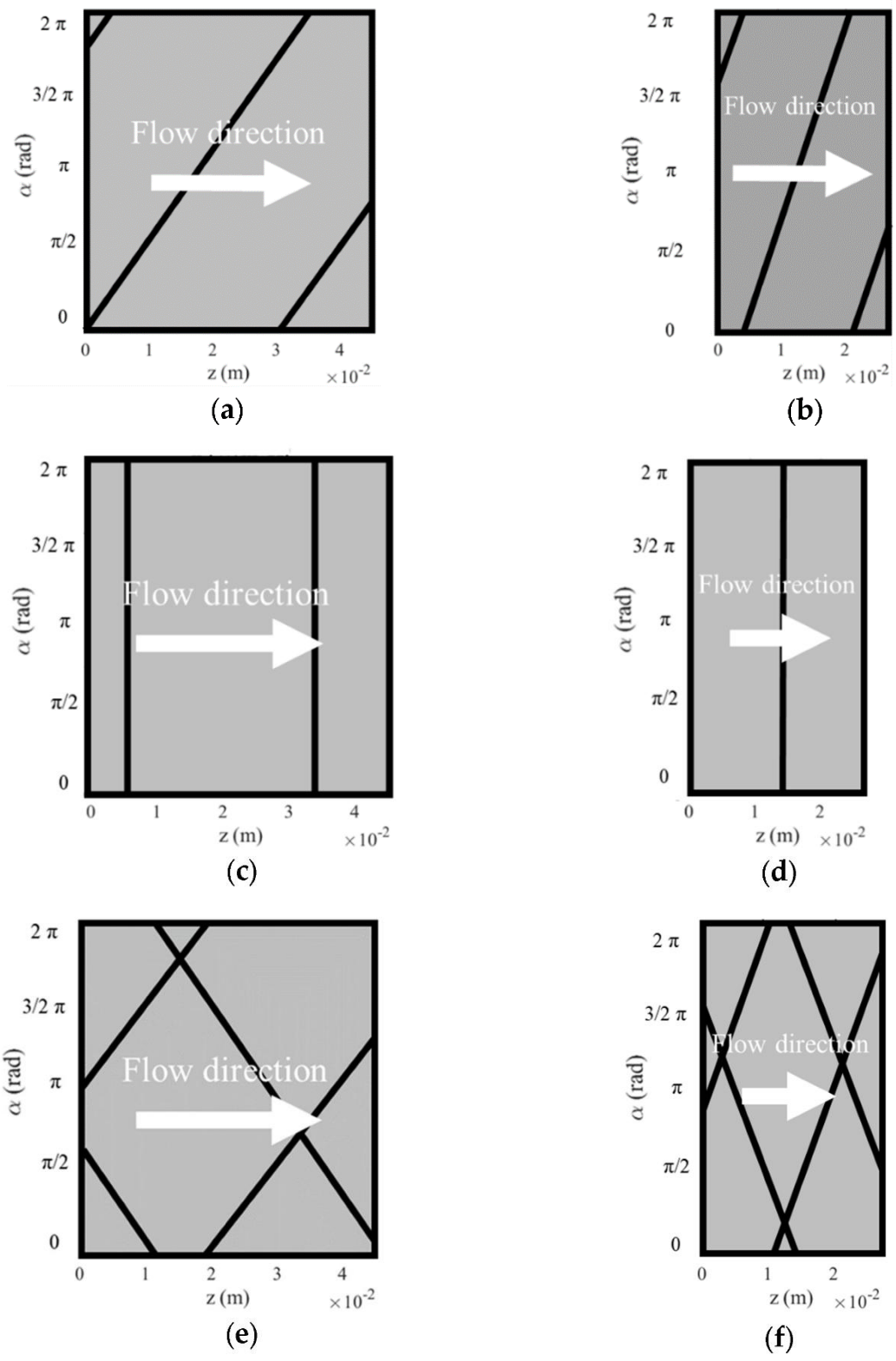

Figure 5. 13 Corrugation position and flow direction in tested pipes: (a) H32, (b) H16, (c) T32, (d) T16, (e) C32, and (f) C16

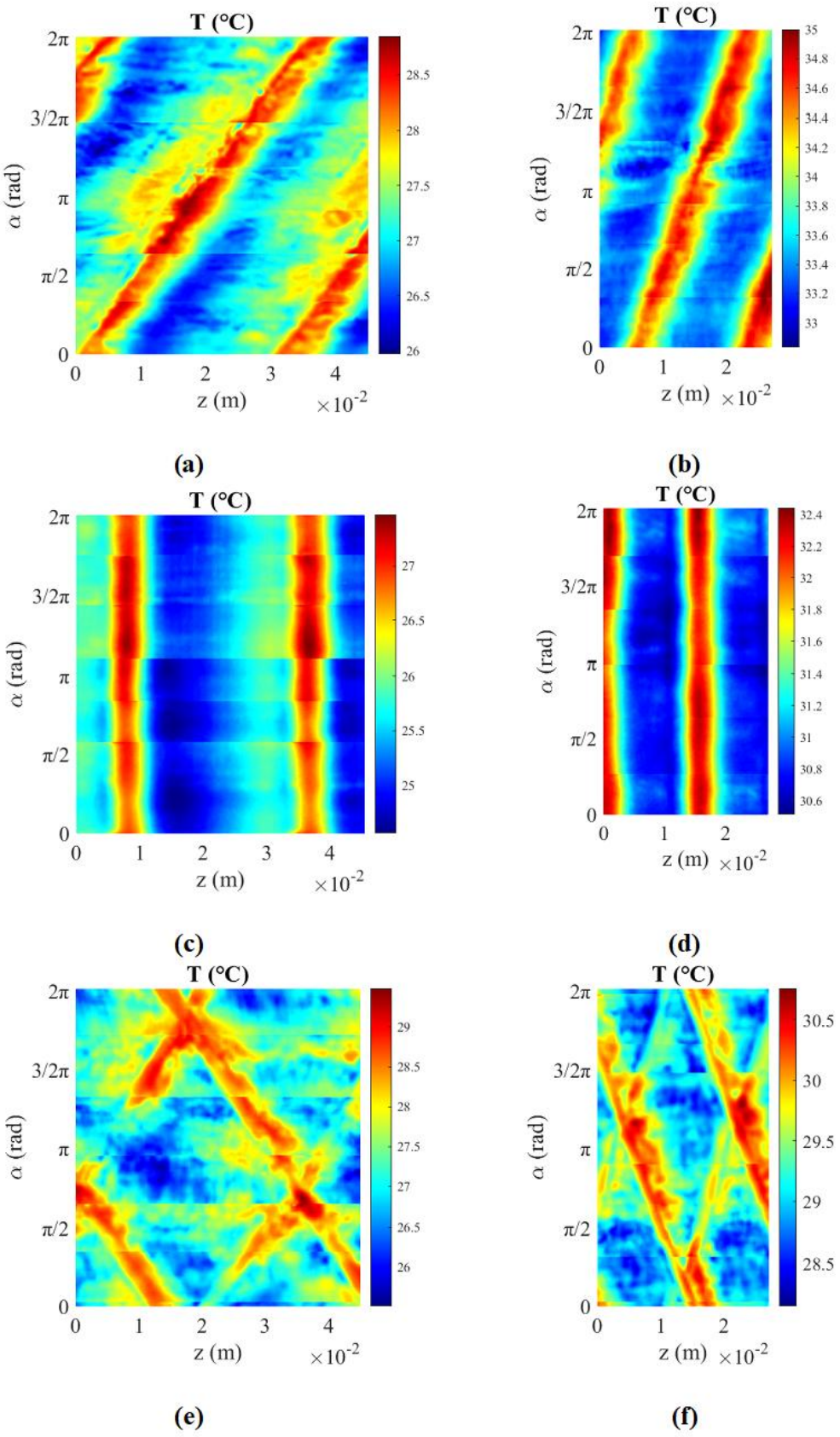

Figure 5. 14 Non-filtered temperature distributions at $\mathbf{Re = 4 \times 10^3}$: (a) H32, (b) H16, (c) T32, (d) T16, (e) C32, and (f) C16

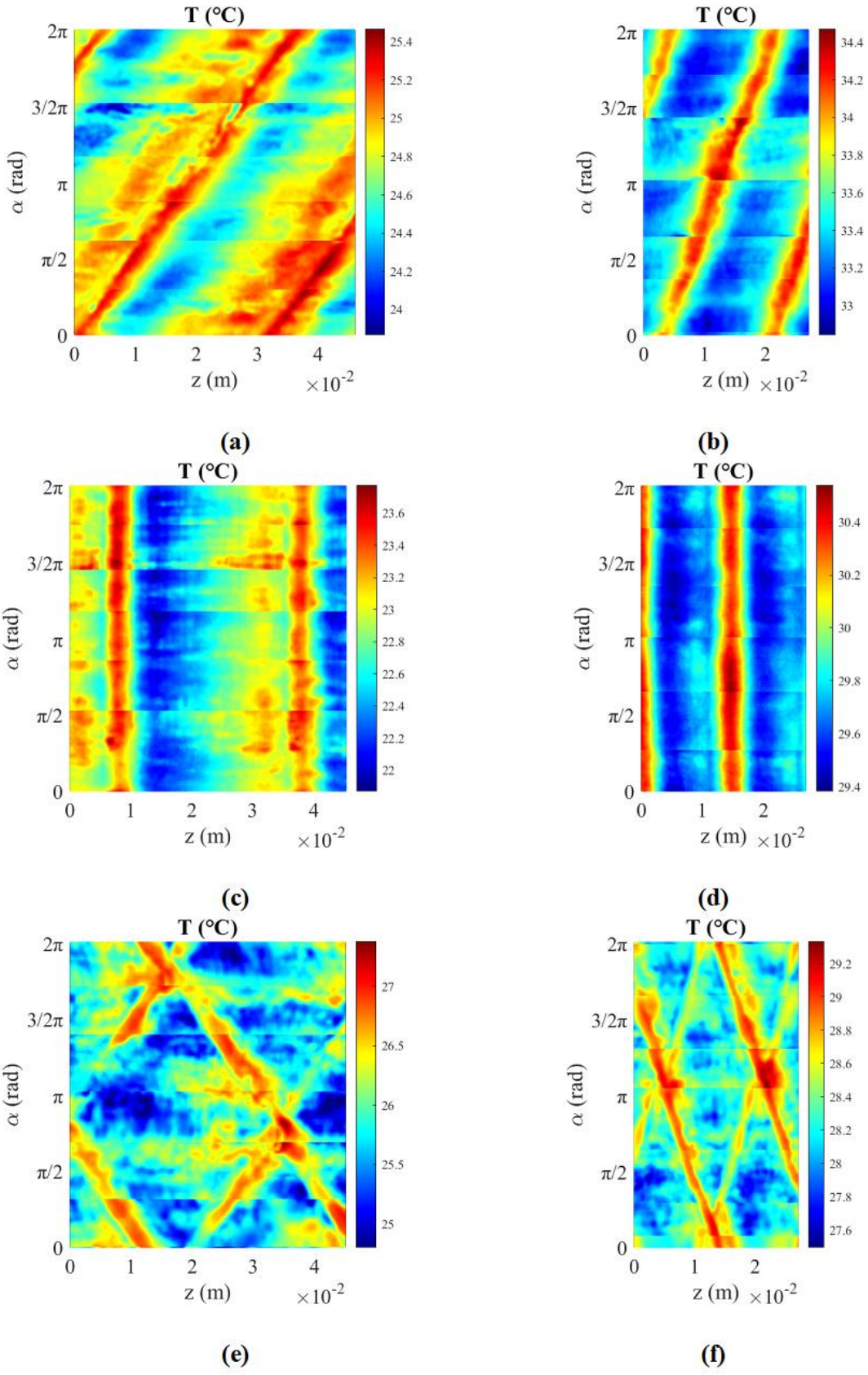

Figure 5. 15 Non-filtered temperature distributions at $\mathbf{Re = 10 \times 10^3}$: (a) H32, (b) H16, (c) T32, (d) T16, (e) C32, and (f) C16

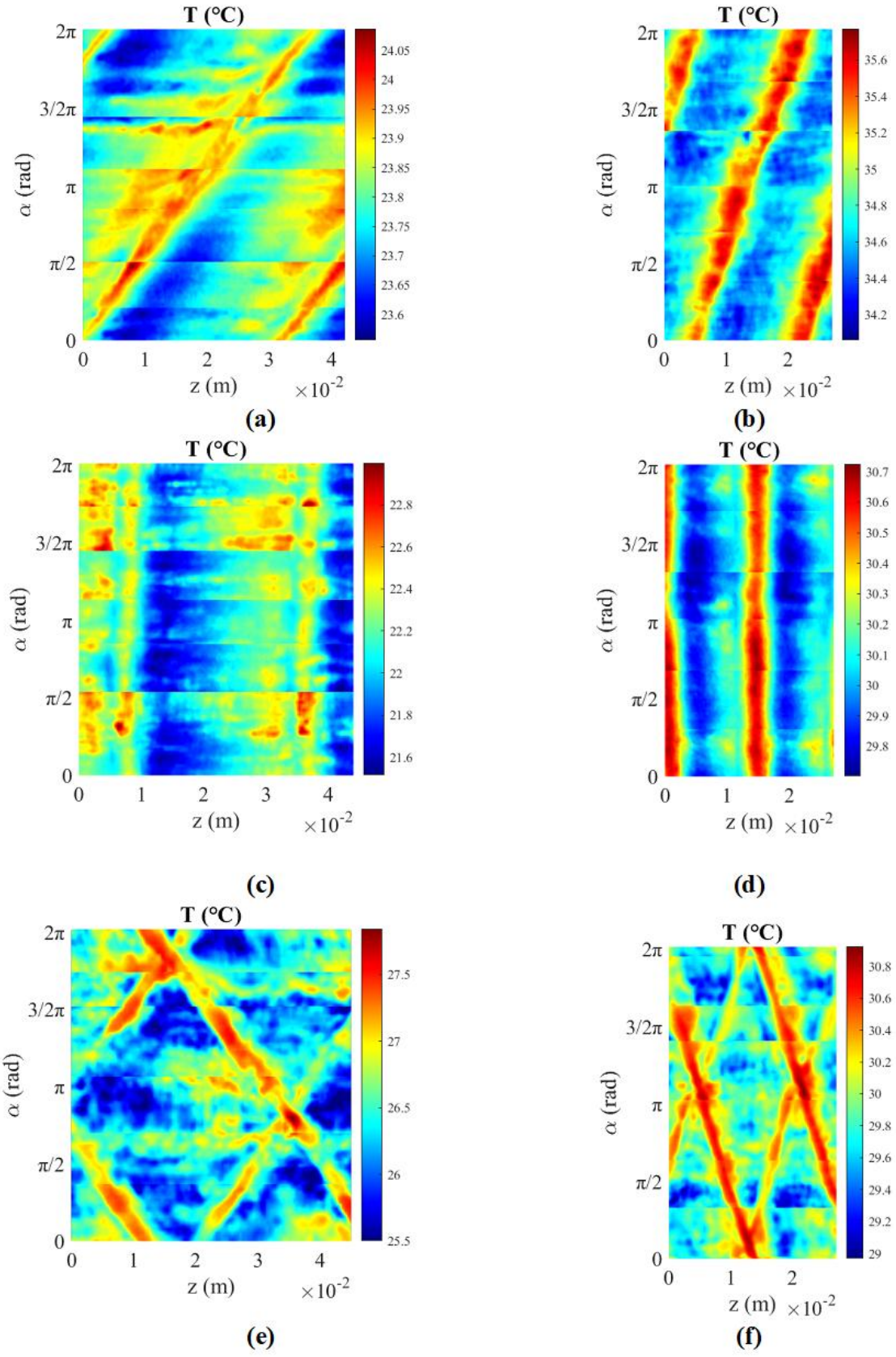

Figure 5. 16 Non-filtered temperature distributions at $\mathrm{Re} = 16 \times 10^3$: (a) H32, (b) H16, (c) T32, (d) T16, (e) C32, and (f) C16

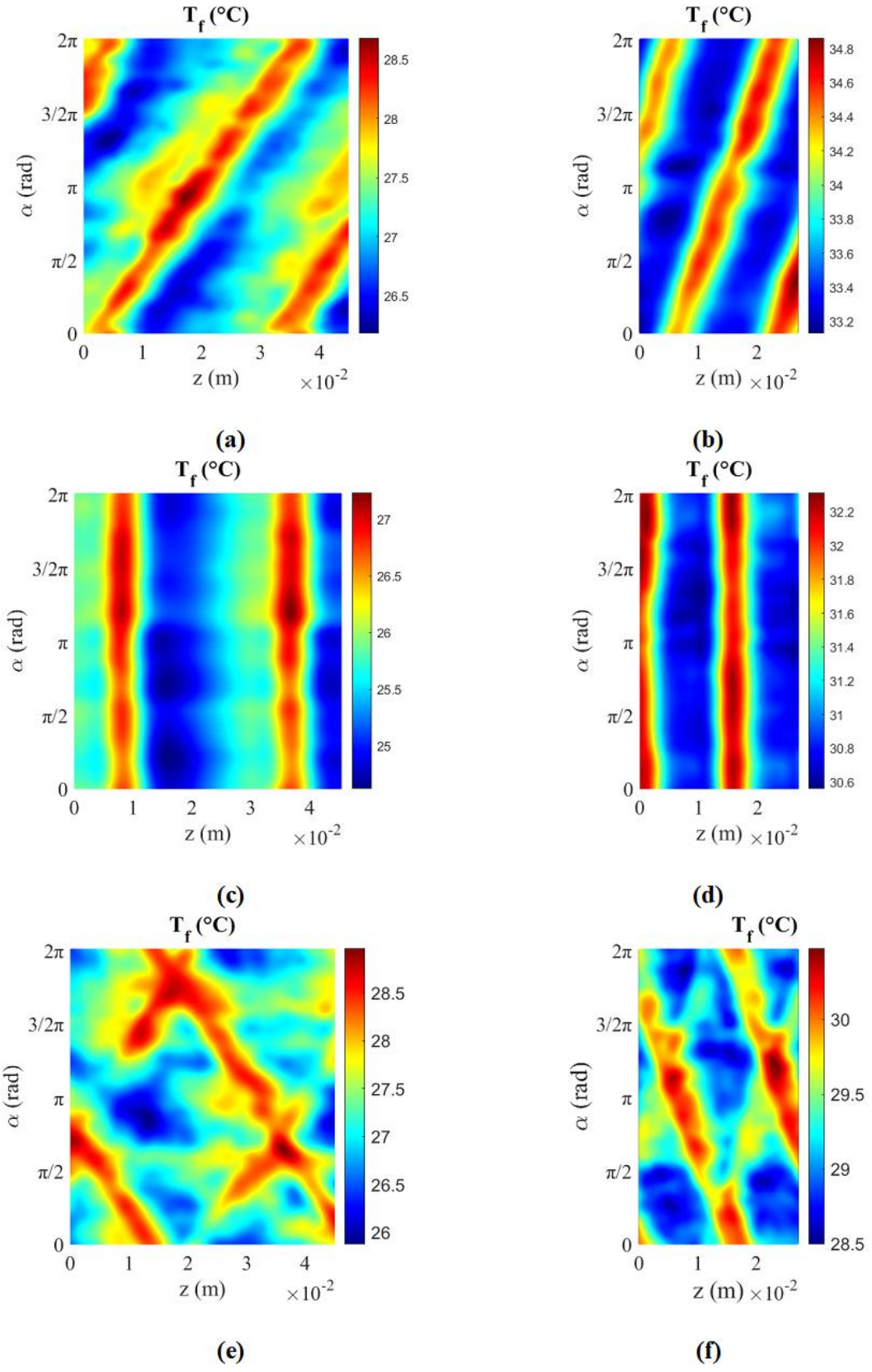

Figure 5. 17 Filtered temperature distributions at Re = 4 × 10^3: (a) H32, (b) H16, (c) T32, (d) T16, (e) C32, and (f) C16

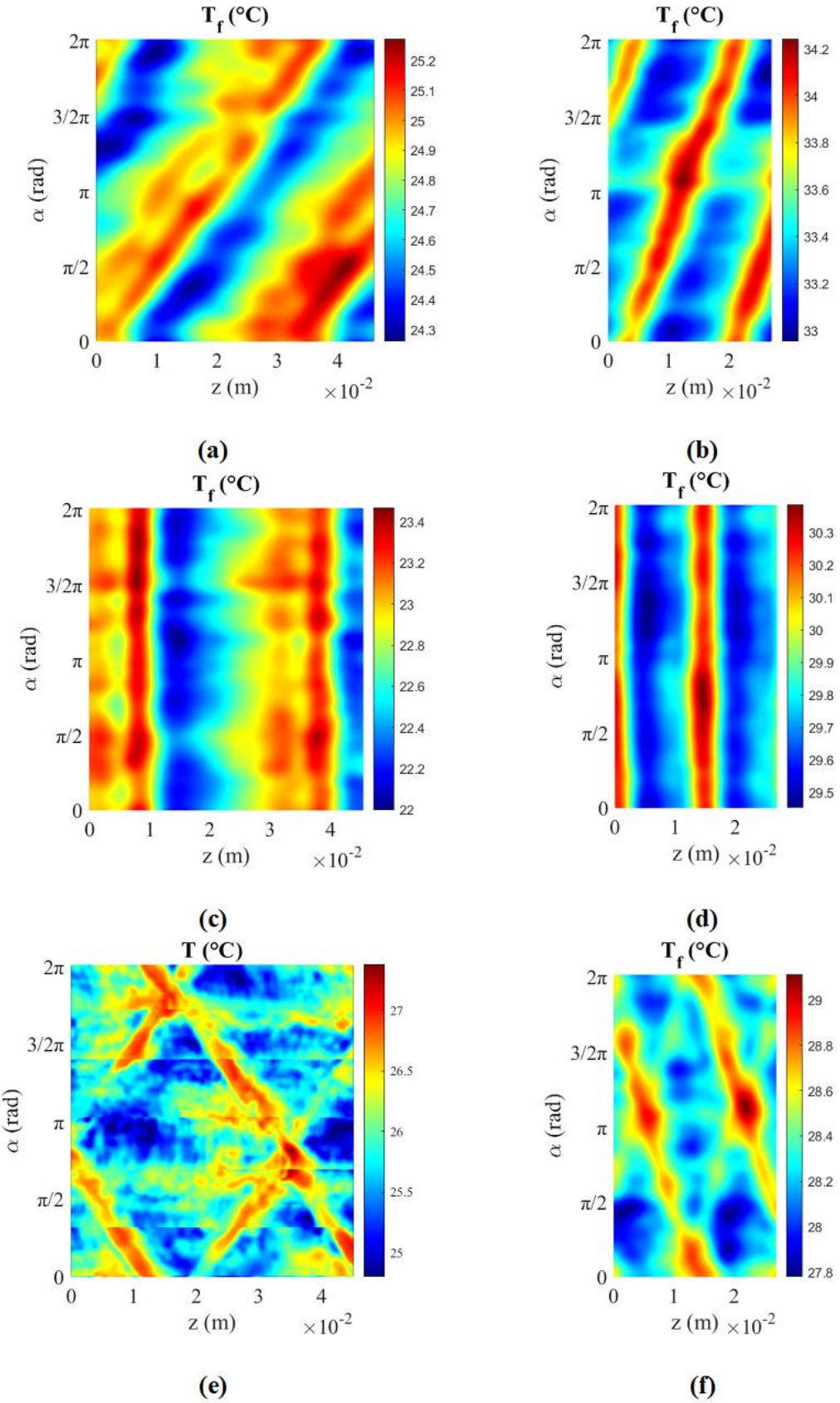

Figure 5. 18 Filtered temperature distributions at Re = 10 × 10^3: (a) H32, (b) H16, (c) T32, (d) T16, (e) C32, and (f) C16

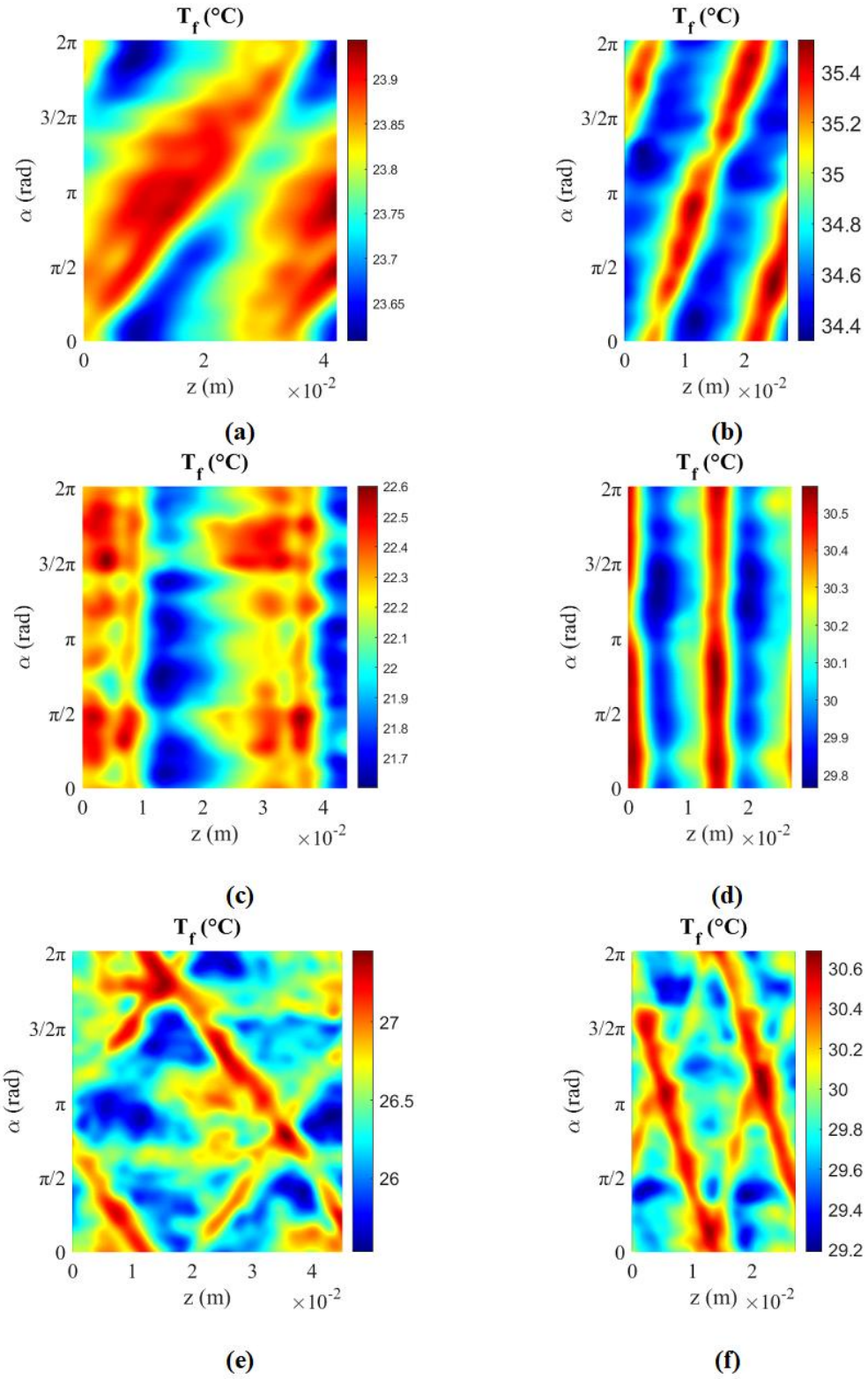

Figure 5. 19 Filtered temperature distributions at Re = 16 × 10^3: (a) H32, (b) H16, (c) T32, (d) T16, (e) C32, and (f) C16

The restored internal convective heat transfer coefficient (h) at Re = 4×10^3 for all the pipes can be seen in Figure 5.20. The behavior of (h) confirms the observations made for the temperature distributions of pipes with transverse and helical corrugations. Immediately after the corrugation, following the flow stream, the value of (h)reached a minimum and then a maximum. Corrugations with a pitch of 32 mm, (h) tended to decrease until the next corrugation after reaching a maximum, consistent with the temperature behavior previously observed for these cases. This phenomenon was particularly pronounced in the T32 case.

However, it is important to note that even immediately after the corrugation, the convective heat transfer coefficient was still greater than what can be achieved in a smooth tube. Therefore, it is more appropriate to describe this region as having a lower effect of corrugation on the (h)values compared to subsequent areas. In the pipes with corrugation pitches of 16 mm (H16 and T16), this intermediate decrease in (h) between corrugations was not observed (consistent with the temperature distributions), allowing for higher values of (h) throughout the surface between corrugations and a more homogeneous distribution of convective heat transfer. Regarding homogeneity, the best solution appears to be the pipes with helical and transverse corrugation. In the cross-helically corrugated pipes the chaotic flow distribution caused by the presence of a double helix rib promoted mass transfer in the transversal direction relative to the fluid flow, producing an increase in turbulence that generated higher peaks of (h) values.

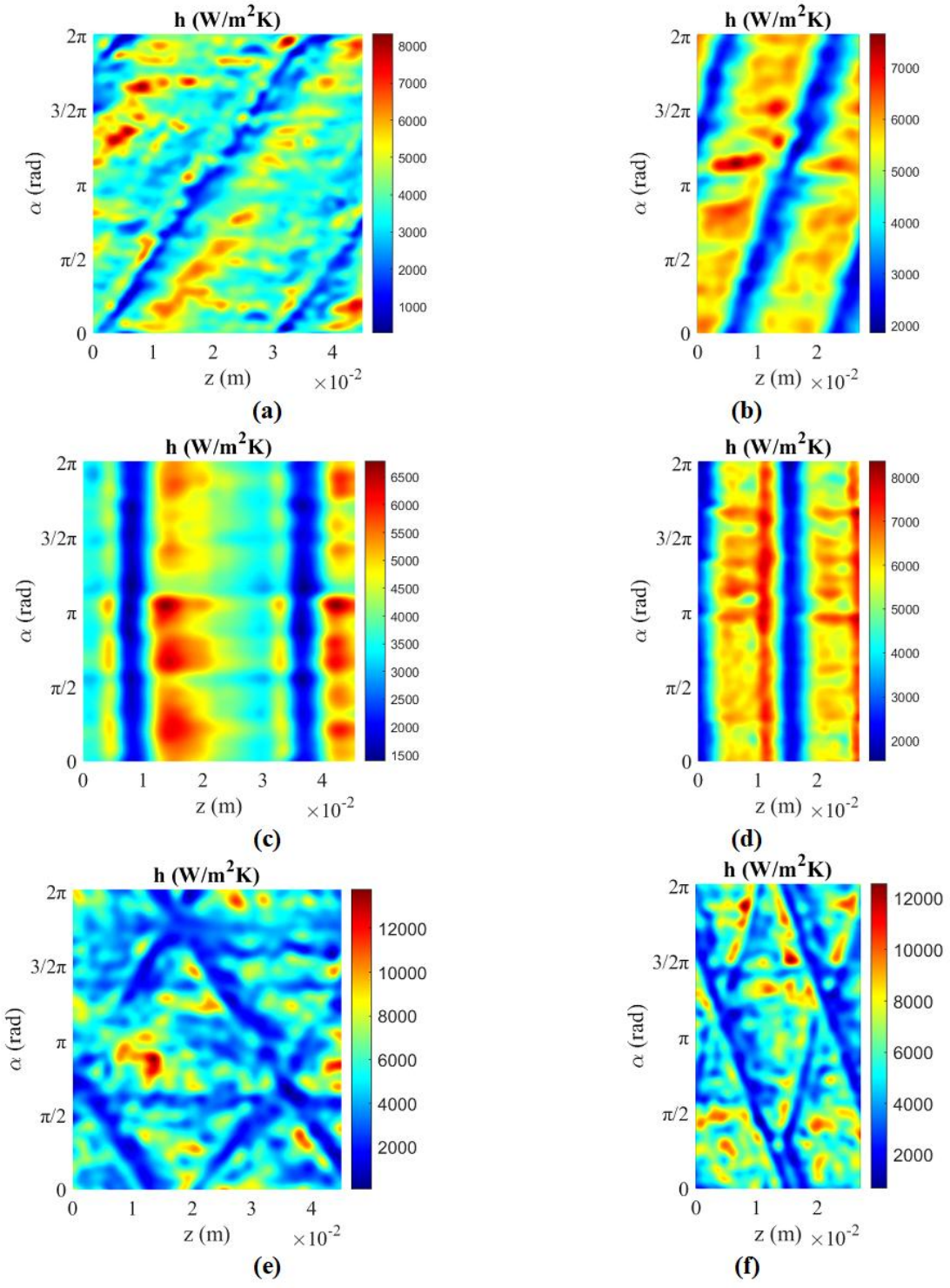

Figure 5. 20 Convective heat transfer distribution (h) at $\mathbf{Re = 4 \times 10^3}$: (a) T32, (b) T16, (c) H32, (d) H16, (e) C32, and (f) C16

This trend held true for the cases at $Re = 10^4$ (Figure 5.21) and $Re = 16 \times 10^3$ (Figure 5.22) as well. In conclusion, transverse corrugation seems to outperform helical and cross-helical corrugations in terms of enhancing thermal performance. When comparing the internal convective heat transfer coefficient (h) obtained at the same Re and corrugation pitch, the transverse geometry showed higher values. For a pitch of 32 mm, (h) values of transverse corrugations showed an average increase of 20% with respect to the helical ones and 10% with respect to the cross helical ones, while for a pitch of 16 mm, there was an average increase of about 22% with respect to the helical ones and 9% with respect to the cross helical ones.

On the other side, the distribution of the local heat transfer coefficient seems to be more uniform in the case of helical corrugation. To provide quantitative data regarding the homogeneity of the (h) distribution, the standard deviation of all the distributions reported in Figures 5.20, 5.21, and 5.22 was computed. For a pitch of 32 mm, the standard deviation of the (h) distribution of helical corrugations had an average of 60% and 65% lower than the transversally and cross-helically corrugated pipes, respectively, while for a pitch of 16 mm, it was about 10% lower than transversal one and 30% lower than the cross helical one.

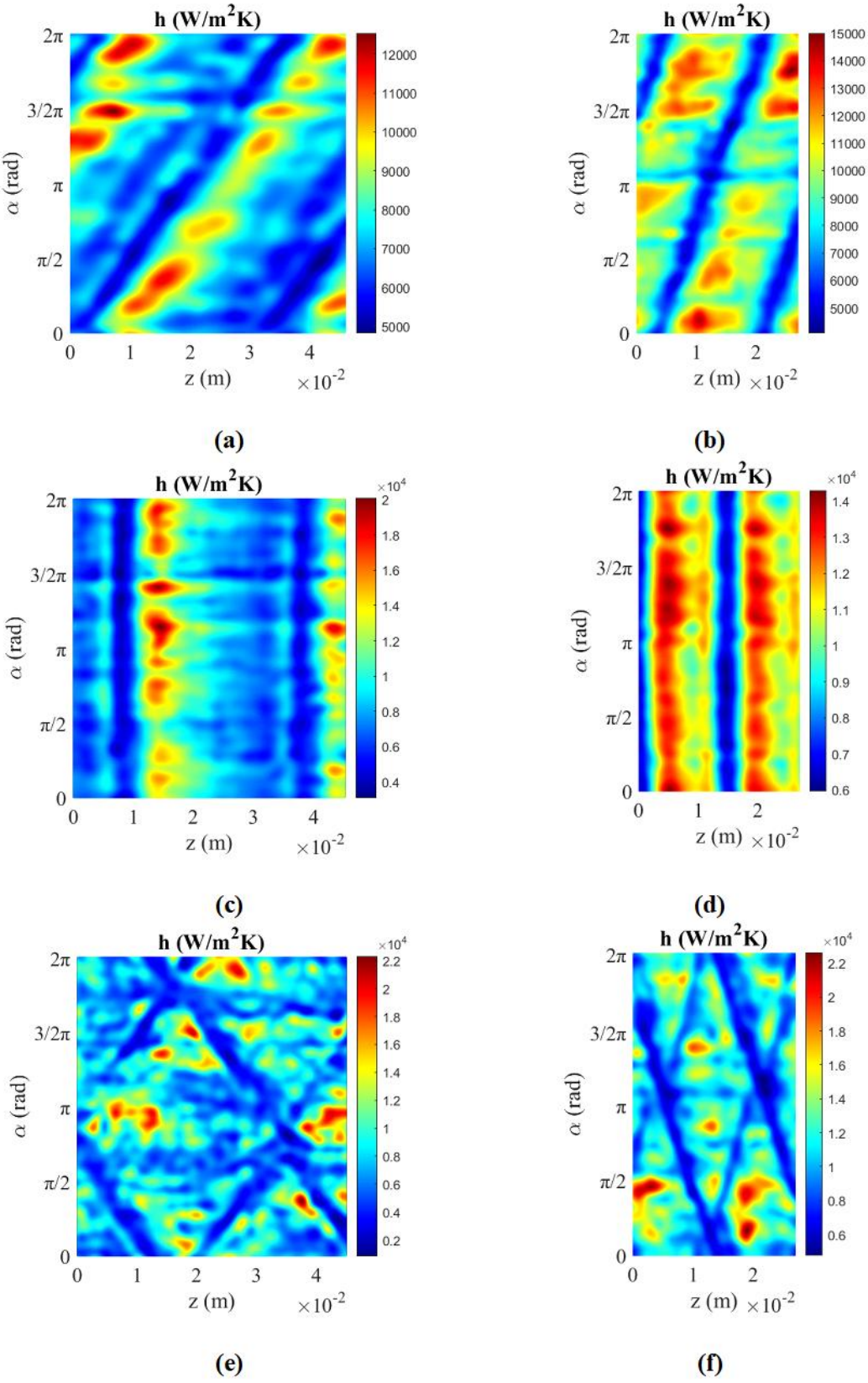

Figure 5. 21 Convective heat transfer distribution (h) at $\mathbf{Re = 10 \times 10^3}$: (a) T32, (b) T16, (c) H32, (d) H16, (e) C32, and (f) C16

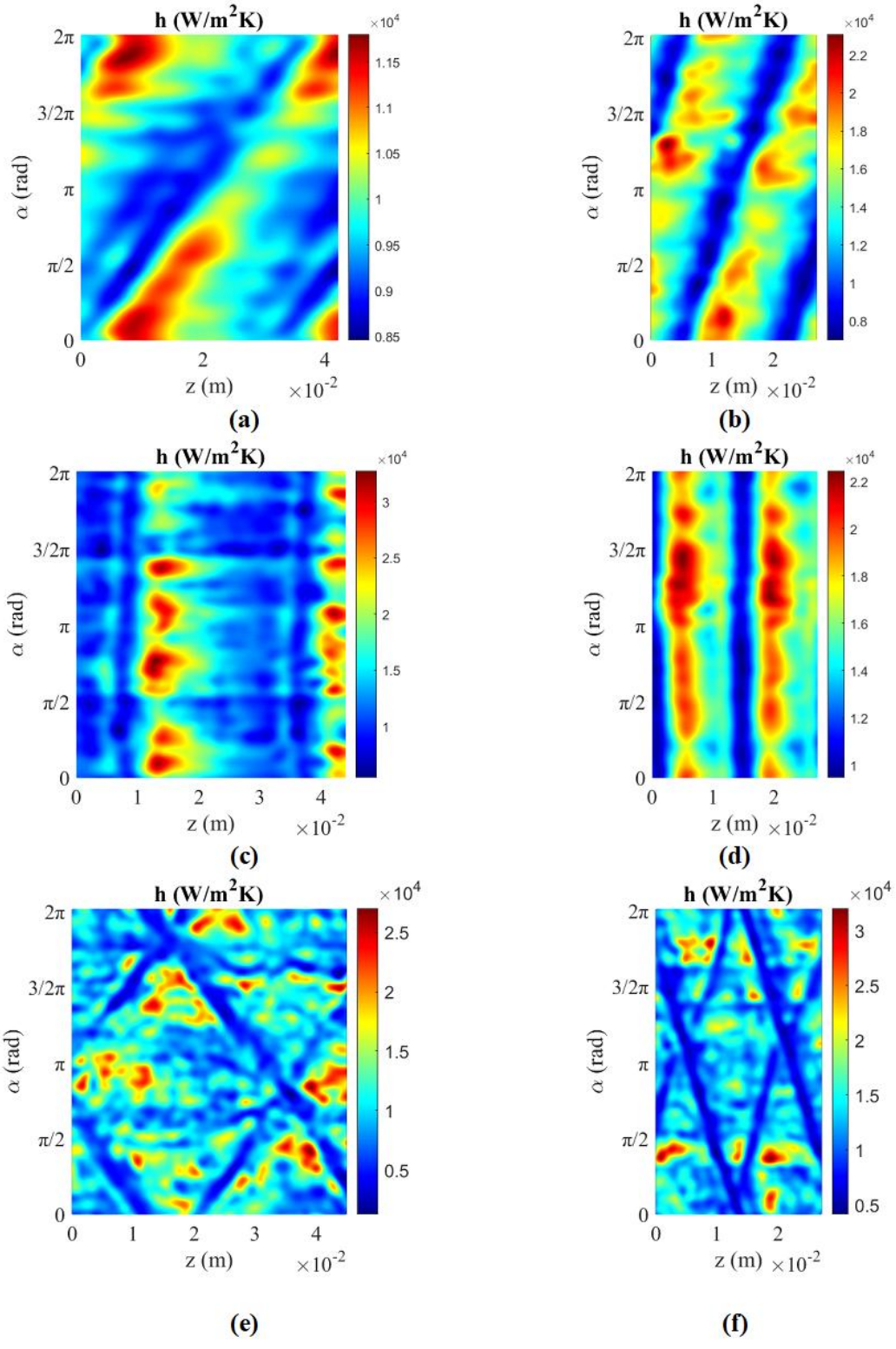

Figure 5. 22 Convective heat transfer distribution (h) at $\mathrm{Re} = 16 \times 10^3$: (a) T32, (b) T16, (c) H32, (d) H16, (e) C32, and (f) C16

Finally. the local Nu in position $\alpha = \pi$ for each pipe tested in the examples with various $Re = 4 \times 10^3$, 10^4, and 16×10^3, respectively, is reported as a function of z in Figures 5.23, 5.24, and 5.25. Comparing these images with the positions of the corrugations shown in Figure 5.13, it can be observed that, for all cases, the local Nusselt number suddenly decreased after the corrugation crest (reported in red in Figures 5.23, 5.24, and 5.25) reached its maximum value in the areas between the corrugations, where the tube wall is still smooth. It is noticed that a smaller corrugation pitch leads to a more consistent trend of the local Nusselt number in the regions between corrugations at the same corrugation type and Reynolds number. More specifically, with smaller pitches, the local Nusselt number remains closer to its maximum value, indicating a more consistent heat transfer ability. On the other hand, the local Nusselt number gradually decreases between corrugations for greater corrugation pitches, which results in significant differences in thermal performance. This decline creates regions of inhomogeneity, where the heat transfer efficiency is less consistent. This trend confirms the preceding observations and is consistent with the patterns for the heat transfer coefficient (h) that have been reported previously.

Moreover, the comparable homogeneity between helical and transverse corrugation was also confirmed in this case, showing an equivalent ratio between the maximum and minimum values of Nu. Finally, transverse geometry appears to perform better from a thermal point of view than helical geometry for the same pitches and Re number, producing a greater local Nusselt number. This indicates that the transverse configuration is more effective at enhancing heat transfer under the given conditions.

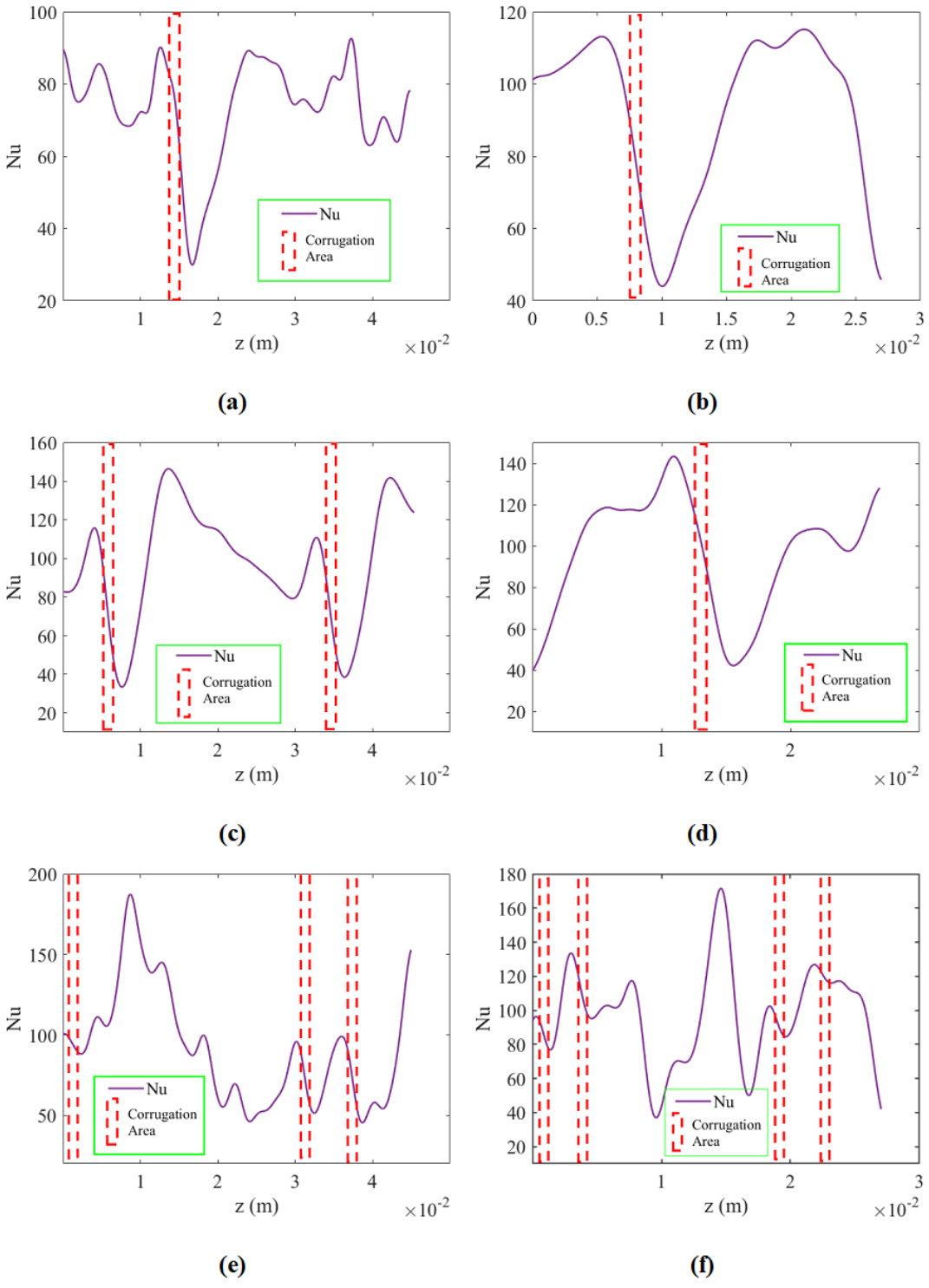

Figure 5. 23 Nu at $\alpha = \pi$ as a function of z at $Re = 4 \times 10^3$: (a) H32, (b) H16, (c) T32, (d) T16, (e) C32, and (f) C16

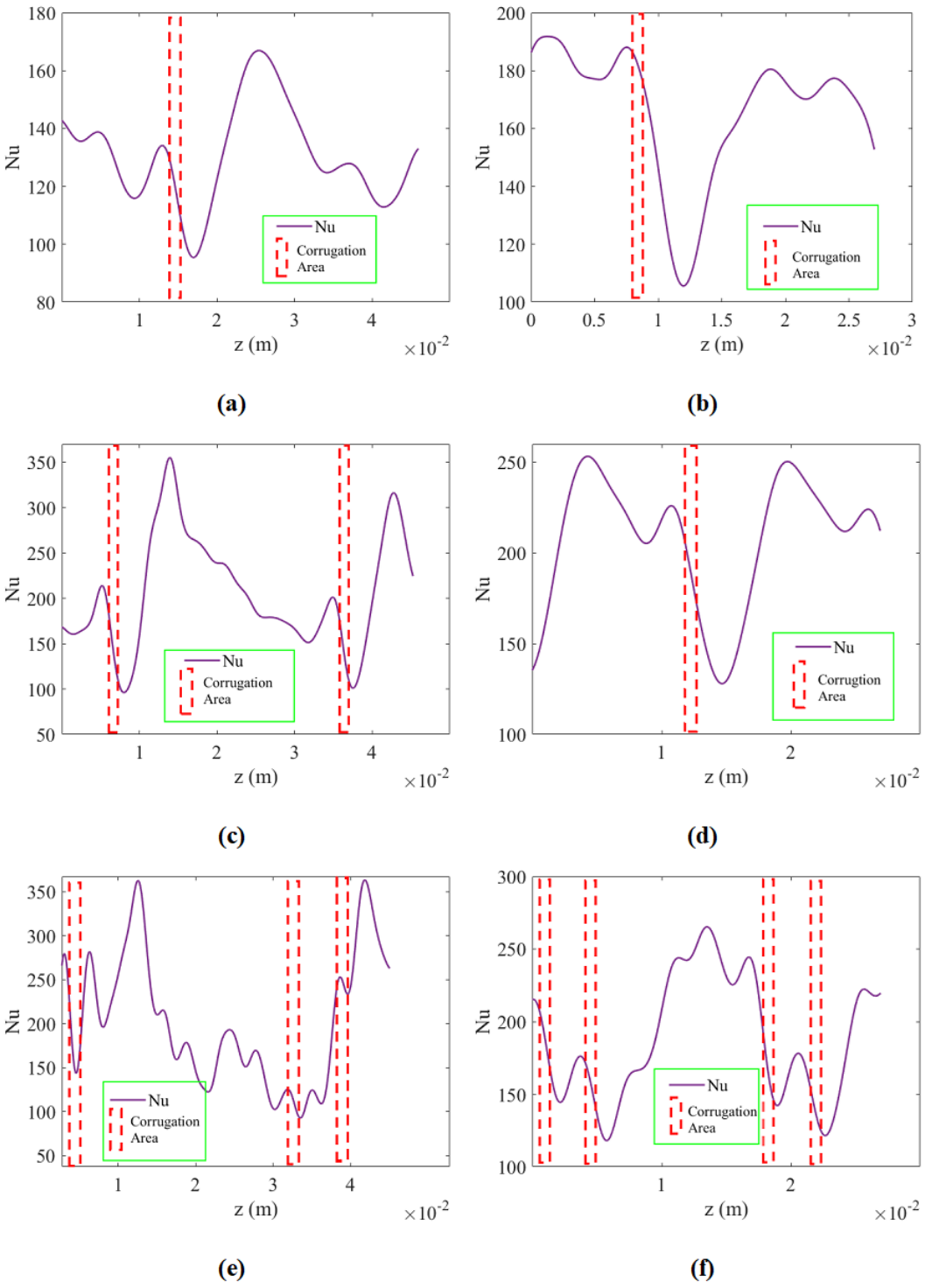

Figure 5. 24 Nu at α = π as a function of z at Re = 10×10^3: (a) H32, (b) H16, (c) T32, (d) T16, (e) C32, and (f) C16

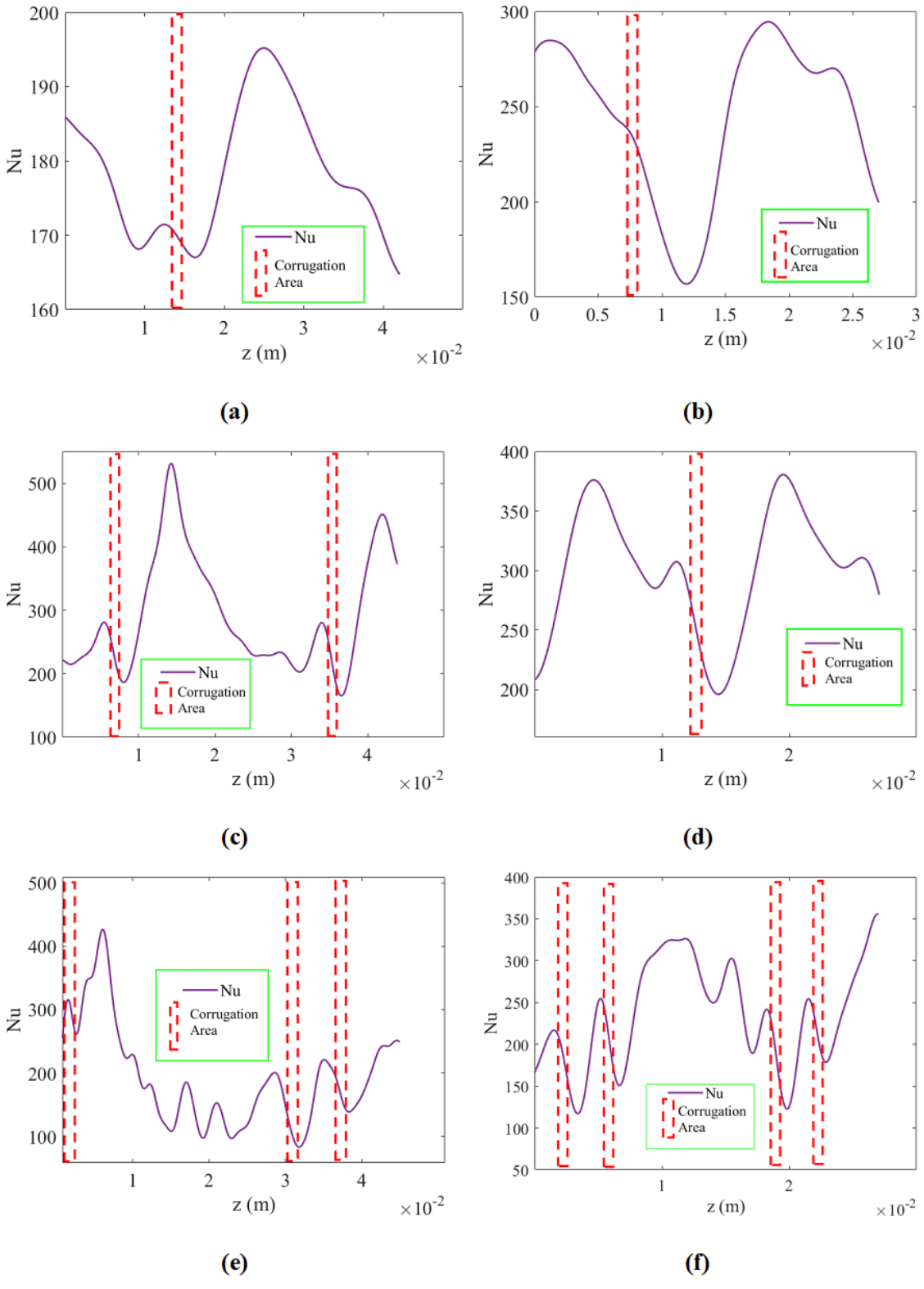

Figure 5. 25 Nu at $\alpha = \pi$ as a function of z at $Re = 16 \times 10^3$: (a) H32, (b) H16, (c) T32, (d) T16, (e) C32, and (f) C16

Therefore, in those situations where achieving the highest possible convective heat transfer is the primary requirement, transversally corrugated or cross-helically corrugated ducts with a small pitch will be preferred. On the other hand, helically corrugated pipes are the ideal choice for applications where heating uniformity is crucial. This is particularly relevant in certain food and industry, industry applications such as food pasteurization, where an excessively uneven temperature distribution could hinder effective bacteria heat killing or cause localized overheating of the product.

Therefore, precise temperature control is necessary during pasteurization in order to eliminate harmful bacteria without spoiling the product. An uneven temperature distribution can result in certain areas where the temperature is insufficient to achieve the desired for eliminating bacteria, which might be a risk to public health. On the other hand, localized temperature rise can cause food to diminish its nutritional content, flavor, and texture. Similarly, this is particularly significant for applications that need quick and efficient heat transfer, including the processing and manufacturing of products, where accurate temperature control is required. To ensure both the safety and effectiveness of the final product, uniform heating must be achieved during the pharmaceutical sterilization and formulation processes. Maintaining a constant temperature distribution throughout the process avoids possible problems like deterioration or uneven handling, which might compromise the quality of the product.

Furthermore, both local and average measurements showed that corrugation, regardless of the specific geometry tested, can effectively enhance the heat transfer capacity of the heat exchanger even under turbulent conditions. These findings indicate that whether you measure heat transfer at specific points (local measurements) or over the entire surface (average measurements), the heat-transfer efficiency of the system is continuously enhanced by the corrugations. As a result, corrugated pipes can also be considered suitable when the food fluid is flowing turbulently and there is a need to increase the heat transfer capability of the process. Efficient heat transfer could be more difficult to perform in turbulent flow because of the chaotic flow of the fluid. However, corrugated pipe design benefits in efficiently controlling such turbulence flow.

Moreover, the ease of implementation and cost-effectiveness of corrugated pipes add to their appeal for both food and pharmaceutical manufacturers. These pipes offer an economical solution for improving performance because they are easily integrated into existing

systems with minimal need for modifications. Corrugated pipes are beneficial to machinery manufacturers as well because they enhance thermal and energy efficiency, which is aligned with the objectives of minimizing operating costs and improving system performance. These pipes also help reduce carbon footprints and promote greater environmental responsibility by using less energy.

6. Heat Transfer Enhancement in Laminar Regimes: Average Analysis

After analyzing the heat transfer enhancement in the turbulent regime, the next step is to apply the same procedure to the laminar regime, focusing on both average and local analysis. The asymptotic Nusselt number distributions for the range of Reynolds numbers from 100 to 1000 are shown in Figure 6.1. The results are compared to the smooth wall tube for fully developed laminar flow in a smooth pipe with a uniform wall heat flux condition. The results presented in Figure 6.1 clearly illustrate how corrugation improves heat transfer performance by significant enhancement. Moreover, it is necessary to highlight how different types or designs of corrugations significantly improve the heat transfer enhancement of the various pipes under investigation. Furthermore, the corrugation pitch seems to have a significant impact on the thermal performance of the tested pipes.

The Nusselt number (Nu) is plotted against the Reynolds number (Re) of various types of corrugated pipe such as cross-helix, transverse, and helical corrugations, respectively, with 16 representing a smaller pitch and 32 representing a larger pitch size. Below 600 Reynolds number ($Re < 600$) it can be observed that, the smaller pitch sizes of transversal T16 with cross helix C32 and helical C32 exhibited the best thermal performance, achieving Nusselt numbers approximately three times higher than that of the smooth tube. In the case of transverse corrugation, pitch size has significant effects on performance, as evidenced by the smaller pitch (T16) performing better than the bigger pitch (T32). Moreover, it can be observed that the C32 pipes occur an earlier transition ($Re < 300$) compared to other corrugated pipes. However, in both cases of helical corrugation where the larger pitches (H32 and C32) enhance higher performance as compared to the smaller pitches (H16 and C16). Overall, all the studied types of corrugated pipes illustrated that significantly higher heat transfer enhancement than the smooth pipe.

After 600 Reynolds number ($600 < Re < 1000$) it can be seen that the Nusselt number rises sharply for all corrugated pipes. It can be observed that the C16 and C32 pipes continue to outperform the transverse and helical corrugated pipes. In the case of transversal corrugation, the performance of the smaller pitch T16 pipe consistently outperforms the larger pitch T32. Additionally, the helical and cross helix pipes perform well; bigger pitches such as

C32 and H32 continue to outperform their smaller pitch. Finally, as expected, all the corrugated pipes had higher performance in terms of Nusselt number as compared to the smooth pipe.

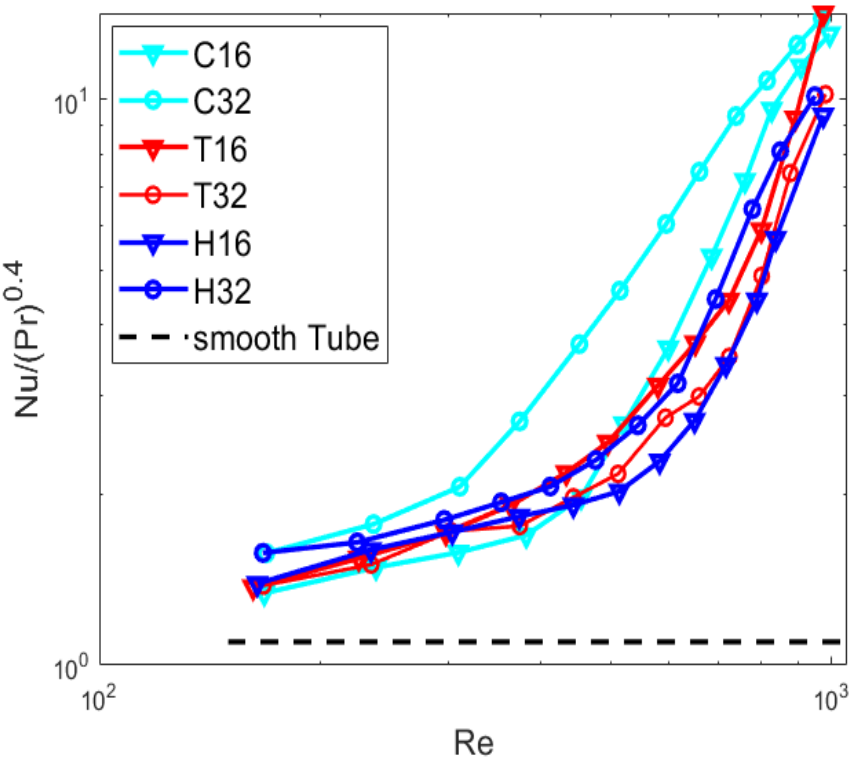

Figure 6. 1 Nusselt number vs. Reynolds number

In this section, we investigated wall temperature distributions along the axial direction of corrugated pipes using ethylene glycol as the working fluid at various Reynolds numbers (200 and 400) as shown in Figures 6.2 and 6.3. Each graph reports temperature profiles at the upper and lower sides of the pipe and the average wall temperature. Notably, the Richardson number (Ri) for all cases remained below 0.1, indicating negligible natural convection as shown in Tables 6.1, 6.2, 6.3, 6.4, 6.5, and 6.6. The axial Nusselt number (Nu_z) as a function of dimensionless abscissa for all corrugated pipes at various Renyolds numbers (Re = 200 and Re = 400) are shown in Figures 6.4, and 6.5.

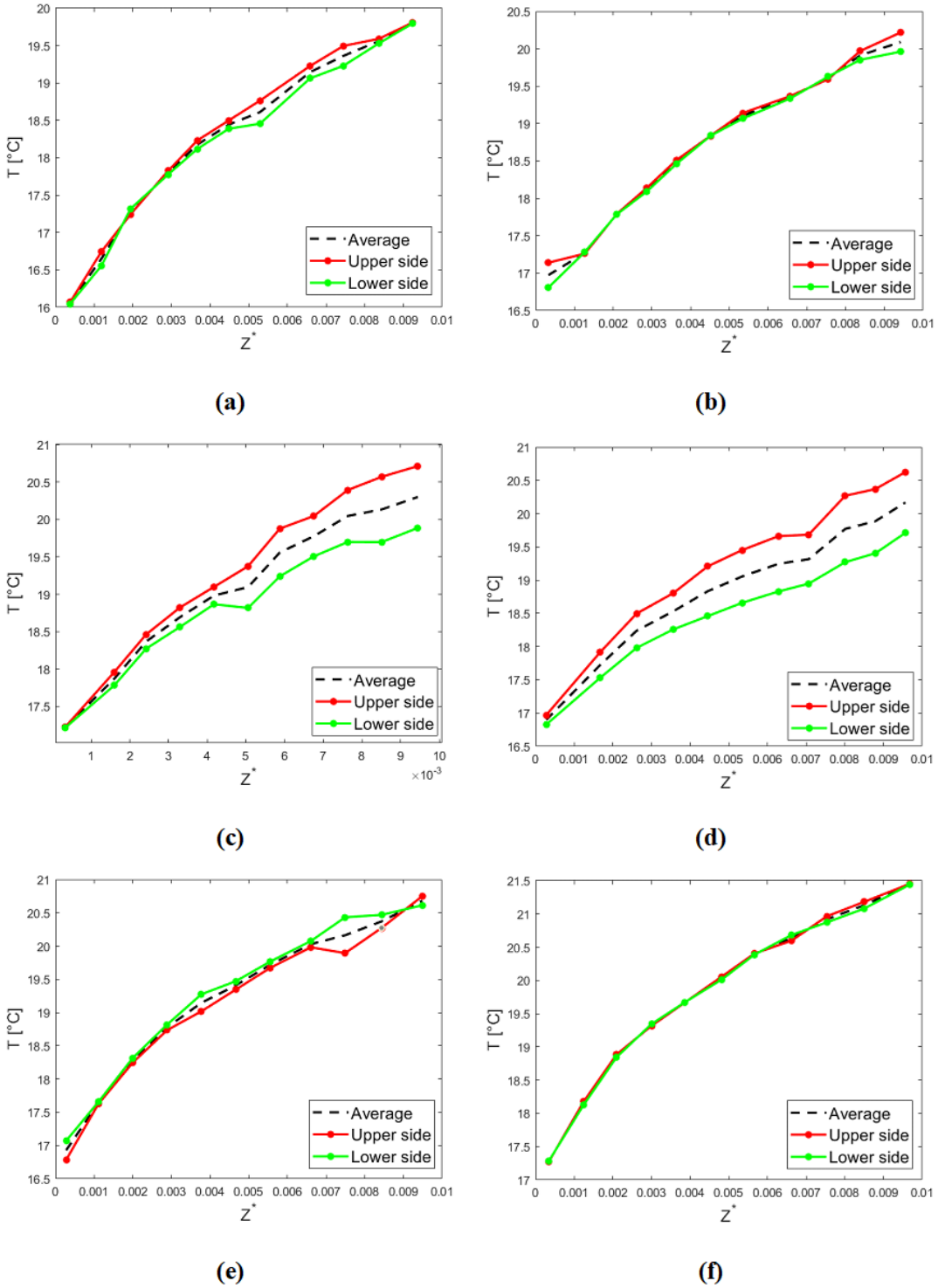

Figure 6. 2 Wall temperature distribution for all corrugated pipes at Re = 200: (a) H32, (b) H16, (c) T32, (d) T16, (e) C32, and (f) C16.

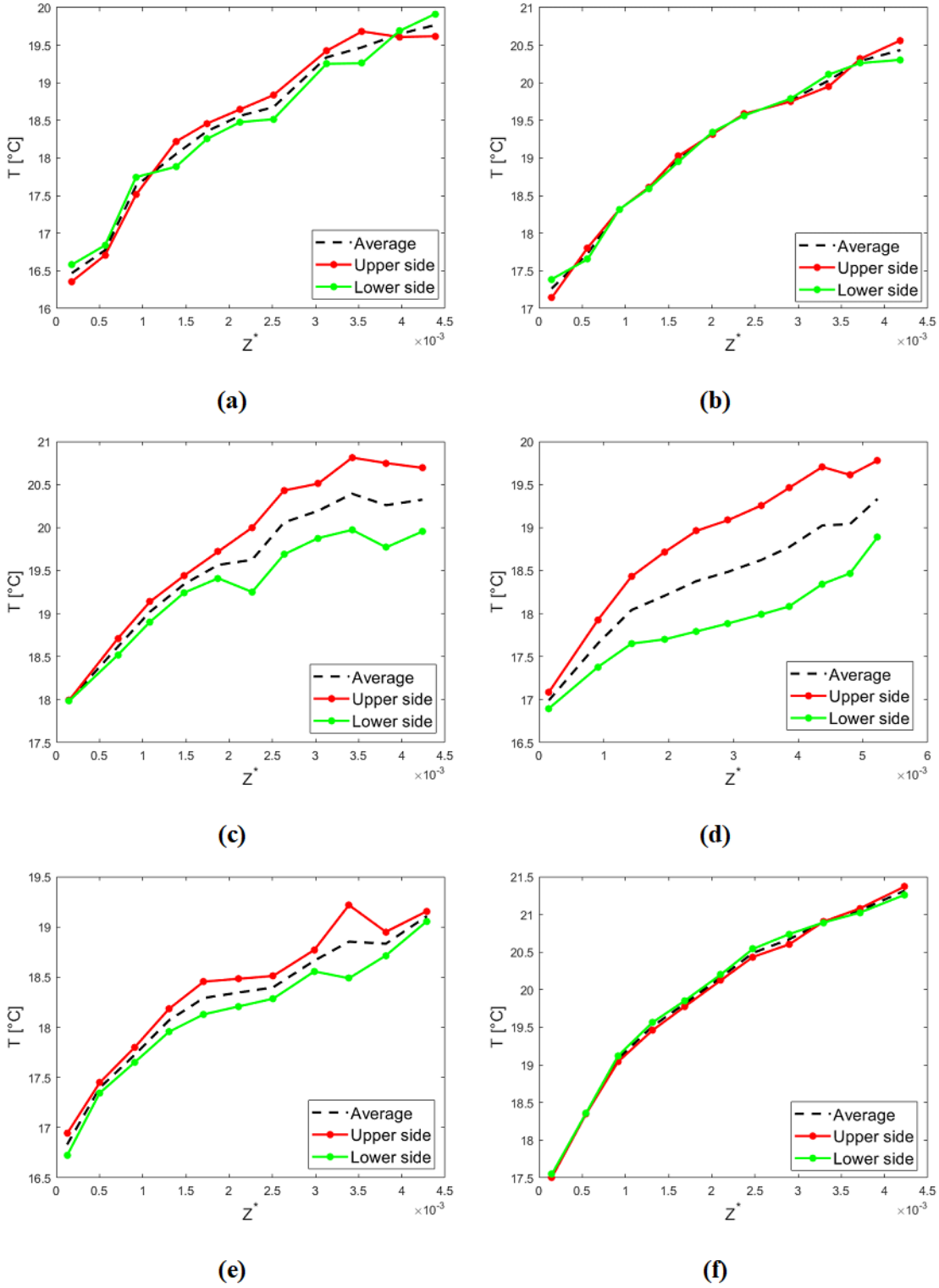

Figure 6. 3 Wall temperature distribution for all corrugated pipes at Re = 200: (a) H32, (b) H16, (c) T32, (d) T16, (e) C32, and (f) C16.

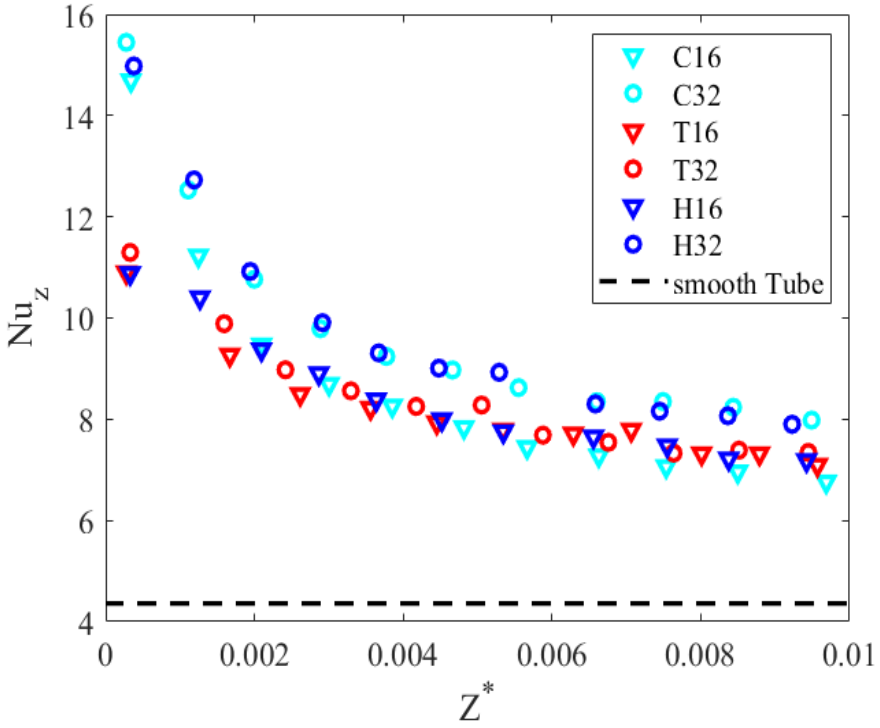

Figure 6. 4 At 200 Reynolds Number: Local Averaged Nusselt Number vs. dimensionless abscissa for all corrugated pipes

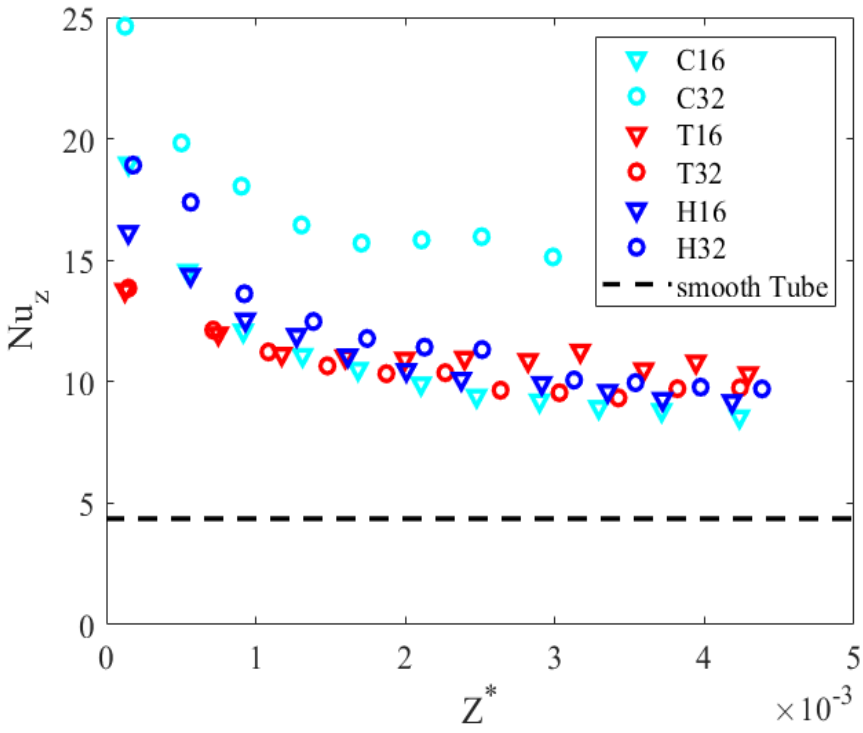

Figure 6. 5 At 400 Reynolds Number: Local Averaged Nusselt Number vs. dimensionless abscissa for all corrugated pipes

The Darcy friction factor *(f)* is used to analyze the pressure drop for each corrugated pipe as a function of Reynolds number in the range of 100 to 1000, as shown in Figure 6.6. In the same Figure, the friction factor in a smooth pipe is presented for the fully developed laminar flow. These results align with earlier findings obtained from the asymptotic Nusselt number distributions, which indicated that wall corrugation initiates an improved transitional flow regime, leading to increased heat transfer and pressure drop compared to smooth wall conditions. In the case of transversal corrugated pipes T16 exhibits a higher pressure drop than T32, despite its better overall performance. Moreover, in the case of the cross helix, as noted in the heat enhancement, the larger pitch C32 shows a greater pressure drop than the smaller pitch C16. Overall, all the corrugated pipes have significantly higher Darcy friction factor *(f)* than smooth surface.

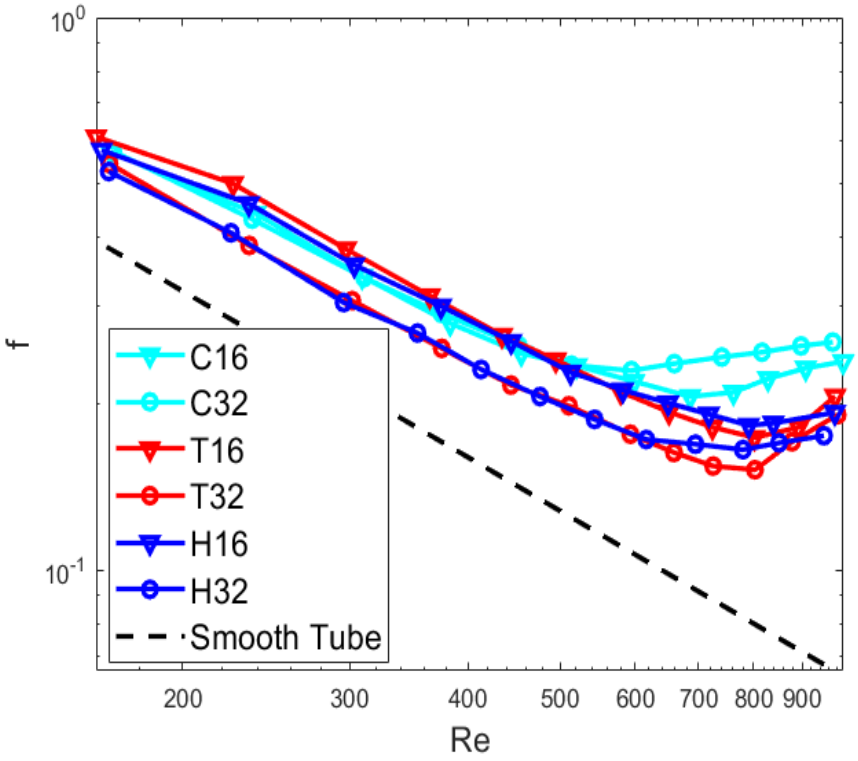

Figure 6. 6 Friction factor vs. Reynolds number

The friction factor and heat transfer enhancement were analyzed to more accurately measure the enhancement of the investigated various types of corrugated pipes compared to a smooth pipe as a reference geometry. A heat transfer enhancement of up to 14 was seen as cross-helix pipes, with a maximum friction factor increase of 4. Figures 6.7 and 6.8 describe the behaviour of both heat transfer and friction factor enhancement effect caused by all corrugated pipes between 100 to 1000 Reynolds Numbers. It can be observed that from Figure

6.7 both bigger pitches C32 and H32, along with smaller pitches C16 and T16 show better heat transfer enhancement at higher Reynolds Number. Figure 6.8 reported that at a lower Reynold number, smaller pitches T16 and H16 have a higher friction factor as compared to bigger pitches T32 and H32. However, at higher Reynolds numbers both cross helix C16 and C32 along T16 showed higher friction factor enhancement.

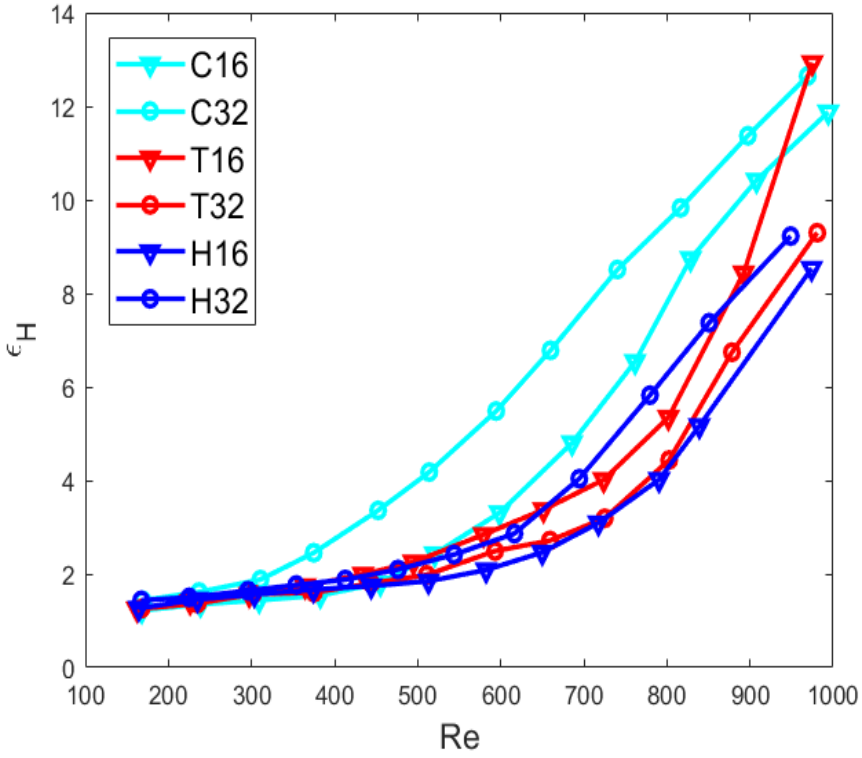

Figure 6. 7 Heat transfer enhancement

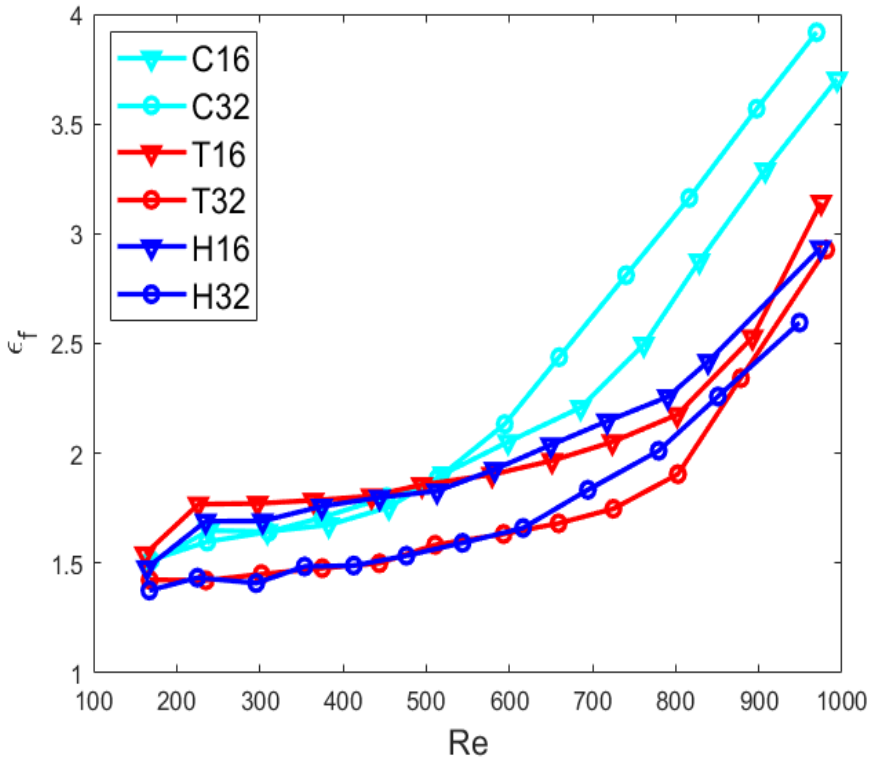

Figure 6. 8 Friction factor enhancement

Finally, the enhancement efficiency of all six corrugated tested pipes with respect to the Reynolds number are demonstrated in Figure 6.9. It is evident that C32, C16, T16, and H32 are the best pipes among all corrugated tested pipes. On the other hand, T32 and H16 exhibited the worst performance. Finally, the experimental conditions of all the tests performed for each pipe are reported in tables 6.1,6.2,6.3,6.4,6.5, and 6.6

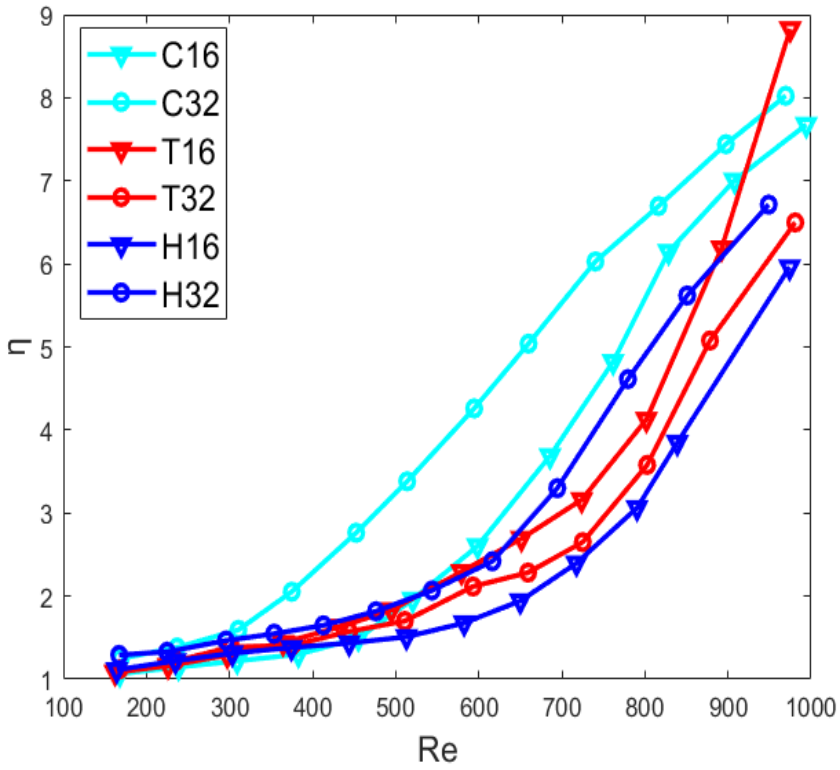

Figure 6. 9 Efficiency η vs. Reynolds number

Table 6. 1 Experimental conditions for Pipe H32

Tube	Test no.	Re	Nu	Pr	Tb [K]	$\frac{Gr}{Re^2}$
H32	1	167.2116	9.0755	79.1467	288.0463	2.3×10^{-3}
	2	224.9649	9.4826	79.3466	287.7787	1.19×10^{-3}
	3	295.711	10.3738	79.085	287.7798	7.0×10^{-4}
	4	353.7985	11.1273	78.7344	287.8703	5.148×10^{-4}
	5	412.8877	11.8557	78.5919	287.8968	4.0×10^{-4}
	6	476.2978	13.1453	77.6843	288.1941	3.0×10^{-4}
	7	543.7568	15.0639	76.6502	288.4977	2.1×10^{-4}
	8	616.525	17.8663	76.6043	288.4702	1.3×10^{-4}
	9	694.5239	25.0881	75.8606	288.7192	9.35×10^{-5}
	10	779.5393	35.9316	74.6077	289.1737	7.18×10^{-5}
	11	850.8561	45.3967	74.1986	289.2836	5.308×10^{-5}
	12	948.9318	56.4686	73.1036	289.6775	3.42×10^{-5}

Table 6. 2 Experimental conditions for Pipe H16

Tube	Test no.	Re	Nu	Pr	Tb [K]	$\frac{Gr}{Re^2}$
H16	1	164.366	7.9947	78.8563	288.121	2.5×10^{-3}
	2	234.963	9.1796	78.9112	287.928	1.18×10^{-3}
	3	303.437	9.8408	78.3039	288.073	7.8×10^{-4}
	4	374.591	10.4617	77.9211	288.136	5.2×10^{-4}
	5	444.055	10.9494	77.8025	288.125	3.7×10^{-4}
	6	513.02	11.5669	77.5308	288.205	2.9×10^{-4}
	7	582.44	13.0442	77.069	288.319	2.08×10^{-4}
	8	650.012	15.3511	76.5104	288.5	1.58×10^{-4}
	9	717.673	19.1793	75.5997	288.815	1.02×10^{-4}
	10	790.587	24.8324	74.8543	289.066	8.66×10^{-5}
	11	839.041	31.8148	74.2282	289.291	6.69×10^{-5}
	12	974.168	52.1331	72.7419	289.833	3.73×10^{-5}

Table 6. 3 Experimental conditions for Pipe T32

Tube	Test no.	Re	Nu	Pr	Tb [K]	$\frac{Gr}{Re^2}$
T32	1	167.5	7.8852	77.6294	288.523	2.54×10^{-3}
	2	235.144	8.5826	77.5149	288.438	1.13×10^{-3}
	3	301.95	9.8248	77.3476	288.363	7.79×10^{-4}
	4	375.192	10.0267	77.2696	288.358	5.5×10^{-4}
	5	443.906	11.2467	76.869	288.463	4.11×10^{-4}
	6	510.929	12.3266	76.1462	288.673	2.93×10^{-4}
	7	593.164	15.4321	75.3342	288.945	2.02×10^{-4}
	8	659.264	16.7735	74.8173	289.125	1.63×10^{-4}
	9	725.068	19.6519	74.2056	289.332	1.2×10^{-4}
	10	802.665	27.2403	73.6579	289.511	8.19×10^{-5}
	11	878.347	41.209	72.844	289.796	5.56×10^{-5}
	12	980.92	56.5512	71.978	290.089	3.50×10^{-5}

Table 6. 4 Experimental conditions for Pipe T16

Tube	Test no.	Re	Nu	Pr	Tb [K]	$\frac{Gr}{Re^2}$
T32	1	162.192	7.8934	79.1524	288.04	2.27×10^{-3}
	2	226.111	8.8827	79.3066	287.83	1.41×10^{-3}
	3	297.384	9.846	79.0747	287.764	7.42×10^{-4}
	4	364.484	10.9874	78.5237	287.919	5.09×10^{-4}
	5	434.316	12.5165	78.2052	287.999	3.54×10^{-4}
	6	494.874	14.1169	77.5463	288.194	2.60×10^{-4}
	7	579.305	17.7056	76.419	288.573	1.7×10^{-4}
	8	651.456	20.9106	75.3781	288.933	1.4×10^{-4}
	9	723.887	24.7427	74.3377	289.28	1.07×10^{-4}
	10	801.824	32.8443	73.7062	289.509	7.68×10^{-5}
	11	892.32	51.4944	72.6699	289.857	4.39×10^{-5}
	12	974.966	78.5912	71.8226	290.142	2.69×10^{-5}

Table 6. 5 Experimental conditions for Pipe C32

Tube	Test no.	Re	Nu	Pr	Tb [K]	$\frac{Gr}{Re^2}$
C32	1	169.043	8.9233	76.126	273.15	2.3×10^{-3}
	2	236.9	10.0491	76.1964	288.905	1.19×10^{-3}
	3	310.749	11.7152	76.3891	288.689	5.84×10^{-4}
	4	374.913	15.2472	75.9194	288.819	3.64×10^{-4}
	5	452.479	20.8154	75.3043	288.998	2.14×10^{-4}
	6	513.914	25.852	75.071	289.029	1.39×10^{-4}
	7	594.508	33.8253	74.5486	289.213	8.86×10^{-5}
	8	659.887	41.7595	74.1927	289.328	5.92×10^{-5}
	9	740.427	52.1768	73.434	289.6	4.48×10^{-5}
	10	816.388	60.0105	72.6575	289.862	3.5×10^{-5}
	11	897.417	69.1976	72.0537	290.065	2.84×10^{-5}
	12	969.432	76.7153	71.4566	290.265	2.38×10^{-5}

Table 6. 6 Experimental conditions for Pipe C16

Tube	Test no.	Re	Nu	Pr	Tb [K]	$\frac{Gr}{(Re)^2}$
C16	1	168.009	7.5397	75.037	289.403	2.63×10^{-3}
	2	238.735	8.3869	75.3742	289.161	1.13×10^{-3}
	3	309.233	8.9175	75.4072	289.012	7.77×10^{-4}
	4	382.925	9.5608	75.3396	288.986	5.52×10^{-4}
	5	455.162	11.1379	74.75	289.18	3.87×10^{-4}
	6	520.597	14.9818	74.5243	289.209	2.29×10^{-4}
	7	598.554	20.3291	73.8328	289.436	1.15×10^{-4}
	8	685.813	29.3347	72.6853	289.854	1.02×10^{-4}
	9	761.704	39.7907	71.9831	290.09	6.05×10^{-5}
	10	828.534	52.997	71.4003	290.29	4.26×10^{-5}
	11	907.834	62.9458	70.7502	290.511	3.29×10^{-5}
	12	994.193	71.4289	69.9527	290.777	2.63×10^{-5}

7. Conclusion

In this study, an experimental investigation was conducted to analyze the thermal performance of pipes with transversal, helical, and cross-helical corrugation profiles, considering both average and local perspectives. Specifically, six pipes were tested, and each pipe had different pitch sizes such as 16 mm and 32 mm. In the first phase of the experiment, the average Nusselt number was used to measure the heat transfer performance along the heated length of the corrugated pipes. The resulting pressure drop penalties in all corrugated pipes were compared with the heat transfer enhancement effects. Water was utilized as the working fluid in the range of Reynolds number 4×10^3 to $Re = 16 \times 10^3$, while ethylene glycol was used in the range of 100 to 1000.

According to the average analysis results, the Nusselt number for the corrugated pipe was approximately three times higher than the smooth pipes in the Reynolds number range of 4×10^3 to 16×10^3. Transversal corrugations T16, T32, and C16 performed better than the H32, with (Nu) values that were almost 1.5 times higher. Variations in corrugation pitch resulted in significant variations observed in the performance of both helical and cross-helix corrugated pipes; smaller pitches perform better than larger pitches. On the other hand, there were no significant differences observed in the performance of both smaller and bigger pitches of transverse corrugated pipes.

At Reynolds numbers ranging from 100 to 1000, the size of the transverse corrugation pitch had a significant impact on their performance. Specifically, the smaller pitch (T16) performed better than the larger pitch (T32). However, in both cases of helical corrugation, the larger pitches (H32 and C32) enhance higher performance as compared to the smaller pitches (H16 and C16). Overall, each corrugated pipe tested showed significantly higher heat transfer compared to the smooth pipe.

The convective heat transfer coefficient on the inner wall of the pipe increases significantly by the corrugations in the range of $4 \times 10^3 < Re < 16 \times 10^3$. According to an extensive investigation of the local effects of corrugation made possible by infrared camera (IRC) analysis. This heat transfer enhancement was not continuous or uniform throughout the fluid flow along the pipe, as immediately after the corrugation it deceases and after the corrugation increases sharply. It was observed that the convective heat transfer coefficient (h) for corrugation with smaller pitches (C16, T16, and H16) gradually increases until the

subsequent corrugation reaches its maximum value until the next the corrugation. However, this trend had disappeared in the geometries with bigger pitches (C32, T32, and H32) because the fluid needs to move longer distance to reattach to the internal wall than the spacing between corrugations, as a result the distribution of (h) was more homogeneous. It was also feasible to see the local trend of Nusselt number (Nu) values as a function of z, when the radial coordinate α was fixed.

The analysis of overall performance revealed that transversal and cross-helical corrugations offer the highest enhancement in heat transfer. However, cross-helical profiles demonstrate increased pressure drops and lower overall efficiency. On the other hand, transversal and cross-helical corrugation leads to a more irregular distribution of the convective heat transfer coefficient compared to helical corrugation profiles. Transversally corrugated or cross-helically corrugated ducts with small pitch are the preferred choices when the sole objective is to achieve the highest possible convective heat transfer. Helically corrugated pipes, on the other hand, are suitable for applications where heating uniformity is crucial.

The experimental results obtained from the present investigation are valuable for designing innovative heat exchangers incorporating these types of tubes, especially when the local thermal behavior of the fluid process cannot be ignored, for instance, in the sterilization or pasteurization processes of food products or pharmaceutical applications. In these cases, the knowledge of the local effect of corrugation on heat transfer could represent an important tool for reducing the risk of the under treatment or overtreatment of the product, enhancing its final quality and safety. Moreover, considering the constant rise of energy costs and environmental pollution, the deepened knowledge of the promoting mechanism of the convective heat transfer enhancement allowed by local analysis can be a very useful tool also for improving the energy efficiency of many industrial processes.

Additionally, the results obtained can be utilized to validate numerical models. The accuracy as well as reliability of these models can be evaluated and enhanced by comparing the numerical predictions with the experimental data, which will result in more advanced predictive tools for thermal system design. Another significant outcome of this study is the implementation and testing of a robust experimental approach that can be successfully applied to optimize wall corrugation in critical thermal processes.

Given the interesting results obtained in this work with local IR analysis, the future step to extend this work will be the definition of optimal corrugation geometries to obtain the combined maximization of heat transfer enhancement and homogeneity of the heat flux distribution. Furthermore, to determine the best corrugation designs, advanced simulation tools, and experimental validation would be needed. The aim will be to achieve a balance between maximizing heat transfer and avoiding uneven heat flux which can result in high temperatures or decreased system performance. In applications where optimal performance is required, this kind of optimization could potentially be very helpful.

References:

[1] R. K. Shah and D. P. Sekulić, *Fundamentals of Heat Exchnager Design*. 2003. doi: 10.1002/9780470172605.ch10.

[2] Technaviia, "HEAT EXCHANGER MARKET 2023-2027," *Energy Convers. Manag.*, 2023, doi: 10.1016/j.enconman.2021.114234.

[3] J. Saari, "HEAT EXCHANGER DIMENSIONING," *Heat Exch.*, pp. 1–101, 2011.

[4] W. G. Xiaoyang Wang, Yue Zhou Wanxiang Yao, Yueqiu Xia, Tongyu Xu, Haolin Yang, Huayue Xie, "The challenge of the ground heat Exchangers: A review of heat transfer efficiency," *Energy Convers. Manag.*, vol. 302, no. 15 Feburary, 2024, doi: https://doi.org/10.1016/j.enconman.2024.118115.

[5] D. . F.P. and De Witt, *Fundamentals of Heat and Mass Transfer*, vol. 4, no. 1. 2002.

[6] S. & Heldman, *Introduction to Food engineering (4th edition)*, vol. 53, no. 9. 2009.

[7] R. Sims, A. Flammini, M. Puri, and S. Bracco, *Opportunities for agri-food chains to become energy-smart*, vol. 43, no. 2. 2016.

[8] T. Deák, "Food Technologies: Pasteurization," *Encycl. Food Saf.*, vol. 3, pp. 219–224, 2014, doi: 10.1016/B978-0-12-378612-8.00257-2.

[9] P. J. Fellows, "Pasteurisation," *Food Process. Technol.*, no. Chapter 7, pp. 381–395, 2009, doi: 10.1533/9781845696344.3.381.

[10] M. N. Ramesh, "Sterilization of Foods," *Encycl. Food Sci. Nutr.*, pp. 5593–5603, 2003, doi: 10.1016/b0-12-227055-x/01148-2.

[11] A. M. Foster, T. Brown, A. J. Gigiel, A. Alford, and J. A. Evans, "Air cycle combined heating and cooling for the food industry," *Int. J. Refrig.*, vol. 34, no. 5, pp. 1296–1304, 2011, doi: 10.1016/j.ijrefrig.2011.03.016.

[12] N. S. Terefe, *Food Fermentation*. Elsevier, 2016. doi: 10.1016/b978-0-08-100596-5.03420-x.

[13] D. S. Jayas, *Food Dehydration Basics*. Elsevier, 2016. doi: 10.1016/B978-0-08-100596-

5.02913-9.

[14] M. Operations and A. H. Feyissa, “An Integrated Model of Heat Transfer in Meat Products during,” 2023.

[15] A. Cappelli, L. Lupori, and E. Cini, “Trends in Food Science & Technology Baking technology : A systematic review of machines and plants and their effect on final products , including improvement strategies,” *Trends Food Sci. Technol.*, vol. 115, no. June, pp. 275–284, 2021, doi: 10.1016/j.tifs.2021.06.048.

[16] R. K. Shah and D. R. Sekulib, “Heat Exchangers,” vol. 3, pp. 1–69, 1998.

[17] G. Müller, H. Sugiyama, S. Stocker, and R. Schmidt, “Reducing energy consumption in pharmaceutical production processes: Framework and case study,” *J. Pharm. Innov.*, vol. 9, no. 3, pp. 212–226, 2014, doi: 10.1007/s12247-014-9188-z.

[18] G. Bruni, C. Martini, F. Martini, and M. Salvio, “On the Energy Performance and Energy Saving Potential of the Pharmaceutical Industry : A Study Based on the Italian Energy Audits,” 2023.

[19] “The Role of Heat Exchangers in Maintaining Sterility & Efficiency in Pharma.” https://www.tsaprocessequipments.com/exploring-the-applications-of-heat-exchangers-in-pharmaceutical-production/ (accessed May 28, 2024).

[20] N. T. Sakthivel PERUMAL , Dinesh SUNDARESAN , Rajkumar SIVANRAJU and S. T. Kamalakannan RAMALINGAM, *Heat Transfer Analysis in Counter Flow Shell and Tube Heat*. Thermal Science, 2021. [Online]. Available: 10.2298/TSCI200531077P

[21] B. Zohuri, *Heat Exchangers*. 2018. doi: 10.1016/B978-0-12-814519-7.00012-4.

[22] Arjun Kumar Prasad and Kaushik Anand, “Design Analysis of Shell Tube Type Heat Exchanger,” *Int. J. Eng. Res.*, vol. V9, no. 01, pp. 524–539, 2020, doi: 10.17577/ijertv9is010215.

[23] S. Asadbeigi, E. Ahmadi, M. Goodarzi, and A. Sagharichian, “Analyzing and simulating heat transfer and designing a shell and tube heat exchanger for the pasteurization process of tomato paste: A CFD study,” *Heliyon*, vol. 9, no. 11, p. e21593, 2023, doi: 10.1016/j.heliyon.2023.e21593.

[24] M. R. Daneshparvar and R. Beigzadeh, “Multi-objective optimization of helical baffles in the shell-and-tube heat exchanger by computational fluid dynamics and genetic algorithm,” *Energy Reports*, vol. 8, pp. 11064–11077, 2022, doi: 10.1016/j.egyr.2022.08.249.

[25] P. Bichkar, O. Dandgaval, P. Dalvi, R. Godase, and T. Dey, “Study of Shell and Tube Heat Exchanger with the Effect of Types of Baffles,” *Procedia Manuf.*, vol. 20, pp. 195–200, 2018, doi: 10.1016/j.promfg.2018.02.028.

[26] D. Thondiyil and S. Kizhakke Kodakkattu, “Optimization of a shell and tube heat exchanger with staggered baffles using Taguchi method,” *Mater. Today Proc.*, vol. 46, no. xxxx, pp. 9983–9988, 2019, doi: 10.1016/j.matpr.2021.04.092.

[27] A. A. Abbasian Arani and R. Moradi, “Shell and tube heat exchanger optimization using new baffle and tube configuration,” *Appl. Therm. Eng.*, vol. 157, no. January, 2019, doi: 10.1016/j.applthermaleng.2019.113736.

[28] K. Nilpueng, L. G. Asirvatham, A. S. Dalkılıç, O. Mahian, H. S. Ahn, and S. Wongwises, “Heat transfer and fluid flow characteristics in a plate heat exchanger filled with copper foam,” *Heat Mass Transf. und Stoffuebertragung*, vol. 56, no. 12, pp. 3261–3271, 2020, doi: 10.1007/s00231-020-02921-x.

[29] O. Arsenyeva, L. Tovazhnyanskyy, P. Kapustenko, J. J. Klemeš, and P. S. Varbanov, “Review of Developments in Plate Heat Exchanger Heat Transfer Enhancement for Single-Phase Applications in Process Industries,” *Energies*, vol. 16, no. 13, 2023, doi: 10.3390/en16134976.

[30] J. L. García-Castillo, J. A. Crespo-Quintanilla, and M. Picón-Núñez, “A novel design approach of plate heat exchangers considering the economic impact of chevron angles,” *Chem. Eng. Process. - Process Intensif.*, vol. 199, no. March, 2024, doi: 10.1016/j.cep.2024.109759.

[31] A. Behrozifard, H. R. Goshayeshi, I. Zahmatkesh, I. Chaer, S. Salahshour, and D. Toghraie, “Experimental optimization of the performance of a plate heat exchanger with Graphene oxide/water and Al_2O_3/water nanofluids,” *Case Stud. Therm. Eng.*, vol. 59, no. May, p. 104525, 2024, doi: 10.1016/j.csite.2024.104525.

[32] J. P. Vallejo and L. Lugo, “Heat transfer and hydrodynamic performance of ZrO2 geothermal nanofluids through tubular and plate heat exchangers,” *Appl. Therm. Eng.*, p. 123770, 2024, doi: 10.1016/j.applthermaleng.2024.123770.

[33] S. K. Singh, M. Mishra, and P. K. Jha, “Nonuniformities in compact heat exchangers — scope for better energy utilization : A review,” *Renew. Sustain. Energy Rev.*, vol. 40, pp. 583–596, 2014, doi: 10.1016/j.rser.2014.07.207.

[34] M. H. Rafsun Hossain Mridha, “Heat exchanger for solar thermal energy,” *Theory, Des. Optim.*, no. April, pp. 55–91, 2022, doi: 10.1016/j.enconman.2020.112666.

[35] A. Agarwal, O. B. Molwane, and I. Pitso, “Numerical analysis and performance enhancement of compact heat exchanger using computational fluid dynamics,” *J. Eng. Res.*, vol. 2021, pp. 1–12, 2021, doi: 10.36909/jer.ICIPPSD.15503.

[36] C. Abeykoon, “Compact heat exchangers – Design and optimization with CFD,” *Int. J. Heat Mass Transf.*, vol. 146, p. 118766, 2020, doi: 10.1016/j.ijheatmasstransfer.2019.118766.

[37] X. Shi, D. Che, B. Agnew, and J. Gao, “An investigation of the performance of compact heat exchanger for latent heat recovery from exhaust flue gases,” *Int. J. Heat Mass Transf.*, vol. 54, no. 1–3, pp. 606–615, 2011, doi: 10.1016/j.ijheatmasstransfer.2010.09.009.

[38] C. C. Wang, Y. T. Lin, and C. J. Lee, “Heat and momentum transfer for compact louvered fin-and-tube heat exchangers in wet conditions,” *Int. J. Heat Mass Transf.*, vol. 43, no. 18, pp. 3443–3452, 2000, doi: 10.1016/S0017-9310(99)00375-0.

[39] L. Xie, D. Zhuang, Z. Li, and G. Ding, “Technical Characteristics and Development Trend of Printed Circuit Heat Exchanger Applied in Floating Liquefied Natural Gas,” *Front. Energy Res.*, vol. 10, no. April, pp. 1–23, 2022, doi: 10.3389/fenrg.2022.885607.

[40] K. Nikitin, Y. Kato, and L. Ngo, “Printed circuit heat exchanger thermal-hydraulic performance in supercritical CO2 experimental loop,” *Int. J. Refrig.*, vol. 29, no. 5, pp. 807–814, 2006, doi: 10.1016/j.ijrefrig.2005.11.005.

[41] M. Chen, X. Sun, and R. N. Christensen, “Thermal-hydraulic performance of printed

circuit heat exchangers with zigzag flow channels," *Int. J. Heat Mass Transf.*, vol. 130, pp. 356–367, 2019, doi: 10.1016/j.ijheatmasstransfer.2018.10.031.

[42] S. Mylavarapu, X. Sun, J. Figley, N. Needler, and R. Christensen, "Investigation of high-temperature printed circuit heat exchangers for very high temperature reactors," *J. Eng. Gas Turbines Power*, vol. 131, no. 6, pp. 1–7, 2009, doi: 10.1115/1.3098425.

[43] "Micro Heat Exchanger Strengths of Tokyo Titanium are extra-fine tube manufacturing, precise welding technology and accumulating know-how." http://tokyo-titanium.com/technology/micro_heat_exchanger.html

[44] D. B. Tuckerman and R. F. W. Pease, "High-Performance Heat Sinking for VLSI," *IEEE Electron Device Lett.*, vol. EDL-2, no. 5, pp. 126–129, 1981, doi: 10.1109/EDL.1981.25367.

[45] S. S. Mehendafe, A. M. Jacobi, and R. K. Shah, "Fluid flow and heat transfer at micro- and meso-scales with application to heat exchanger design," *Appl. Mech. Rev.*, vol. 53, no. 7, pp. 175–193, 2000, doi: 10.1115/1.3097347.

[46] M. J. Afzal *et al.*, "A Review on Microchannel Fabrication Methods and Applications in Large-Scale and Prospective Industries," *Evergreen*, vol. 9, no. 3, pp. 764–808, 2022, doi: 10.5109/4843111.

[47] M. I. Hasan, A. A. Rageb, M. Yaghoubi, and H. Homayoni, "Influence of channel geometry on the performance of a counter flow microchannel heat exchanger," *Int. J. Therm. Sci.*, vol. 48, no. 8, pp. 1607–1618, 2009, doi: 10.1016/j.ijthermalsci.2009.01.004.

[48] A. Kandlikar, S.G., Garimella, S., Li, D., Colin, S. and M. King, "Heat Transfer and Fluid Flow in Minichannels and Microchannels," *Amsterdam: Elsevier,* 2006, doi: 10.1134/S0018151X23020074.

[49] C. Y. Yang, C. T. Yeh, W. C. Liu, and B. C. Yang, "Advanced micro-heat exchangers for high heat flux," *Heat Transf. Eng.*, vol. 28, no. 8–9, pp. 788–794, 2007, doi: 10.1080/01457630701328676.

[50] B. Huang, H. Li, S. Xia, and T. Xu, "Experimental investigation of the flow and heat

transfer performance in micro-channel heat exchangers with cavities," *Int. J. Heat Mass Transf.*, vol. 159, p. 120075, 2020, doi: 10.1016/j.ijheatmasstransfer.2020.120075.

[51] D. R. Ray, D. K. Das, and R. S. Vajjha, "Experimental and numerical investigations of nanofluids performance in a compact minichannel plate heat exchanger," *Int. J. Heat Mass Transf.*, vol. 71, pp. 732–746, 2014, doi: 10.1016/j.ijheatmasstransfer.2013.12.072.

[52] M. Bahiraei and A. Monavari, "Thermohydraulic characteristics of a micro plate heat exchanger operated with nanofluid considering different nanoparticle shapes," *Appl. Therm. Eng.*, vol. 179, p. 115621, 2020, doi: 10.1016/j.applthermaleng.2020.115621.

[53] N. Dharmakkan *et al.*, "A case study on analyzing the performance of microplate heat exchanger using nanofluids at different flow rates and temperatures," *Case Stud. Therm. Eng.*, vol. 44, no. February, p. 102805, 2023, doi: 10.1016/j.csite.2023.102805.

[54] C. Vashistha, A. K. Patil, and M. Kumar, "Experimental investigation of heat transfer and pressure drop in a circular tube with multiple inserts," *Appl. Therm. Eng.*, vol. 96, pp. 117–129, 2016, doi: 10.1016/j.applthermaleng.2015.11.077.

[55] C. Chen, S. Yang, and M. Pan, "Microchannel structure optimization and experimental verification of a plate heat exchanger," *Int. J. Heat Mass Transf.*, vol. 175, p. 121385, 2021, doi: 10.1016/j.ijheatmasstransfer.2021.121385.

[56] M. Pan, Y. Zhong, and Y. Xu, "Numerical investigation of fluid flow and heat transfer in a plate microchannel heat exchanger with isosceles trapezoid-shaped reentrant cavities in the sidewall," *Chem. Eng. Process. - Process Intensif.*, vol. 131, no. July, pp. 178–189, 2018, doi: 10.1016/j.cep.2018.07.018.

[57] K. S. Garud, S. G. Hwang, T. K. Lim, N. Kim, and M. Y. Lee, "First and second law thermodynamic analyses of hybrid nanofluid with different particle shapes in a microplate heat exchanger," *Symmetry (Basel).*, vol. 13, no. 8, 2021, doi: 10.3390/sym13081466.

[58] M. A. Arie, A. H. Shooshtari, S. V. Dessiatoun, E. Al-Hajri, and M. M. Ohadi, "Numerical modeling and thermal optimization of a single-phase flow manifold-microchannel plate heat exchanger," *Int. J. Heat Mass Transf.*, vol. 81, pp. 478–489,

2015, doi: 10.1016/j.ijheatmasstransfer.2014.10.022.

[59] S. R. Hosseini, M. Sheikholeslami, M. Ghasemian, and D. D. Ganji, “Nanofluid heat transfer analysis in a microchannel heat sink (MCHS) under the effect of magnetic field by means of KKL model,” *Powder Technol.*, vol. 324, pp. 36–47, 2018, doi: 10.1016/j.powtec.2017.10.043.

[60] S. B. Abubakar, “Numerical Prediction of Laminar Nanofluid Flow in Rectangular Microchannel Heat Sink,” *Adv. Res. Fluid Mech. Therm. Sci.*, vol. 7, pp. 29–38, 2017.

[61] S. Baek, R. Radebaugh, and P. E. Bradley, “A new method for heat transfer coefficient measurements of single-phase fluids during laminar flow in microchannels,” *Int. J. Heat Mass Transf.*, vol. 157, 2020, doi: 10.1016/j.ijheatmasstransfer.2020.119891.

[62] H. A. Mohammed, G. Bhaskaran, N. H. Shuaib, and H. I. Abu-Mulaweh, “Influence of nanofluids on parallel flow square microchannel heat exchanger performance,” *Int. Commun. Heat Mass Transf.*, vol. 38, no. 1, pp. 1–9, 2011, doi: 10.1016/j.icheatmasstransfer.2010.09.007.

[63] H. R. Seyf and S. Keshavarz Mohammadian, “Thermal and hydraulic performance of counterflow microchannel heat exchangers with and without nanofluids,” *J. Heat Transfer*, vol. 133, no. 8, pp. 1–9, 2011, doi: 10.1115/1.4003553.

[64] G. Wang *et al.*, “Experimental and numerical investigation of hydrothermal performance of a microchannel heat sink with pin fins,” *Case Stud. Therm. Eng.*, vol. 60, no. March, p. 104631, 2024, doi: 10.1016/j.csite.2024.104631.

[65] Satish G. Kandlikar and W. J. Grande, “Evolution of Microchannel Flow Passages -- Thermohydraulic Performance and Fabrication Technology,” *Mech. Eng.*, no. February 2012, pp. 37–41, 2010, doi: 10.1080/01457630390116077.

[66] R. W. Barber and D. R. Emerson, “The influence of Knudsen number on the hydrodynamic development length within parallel plate micro-channels,” *Adv. Fluid Mech.*, vol. 32, no. November, pp. 207–216, 2002.

[67] C. K. Oh, E. S. Oran, and R. S. Sinkovits, “Computations of High-Speed, High Knudsen Number Microchannel Flows,” *Thermophys. Heat Transf.*, vol. 11, no. 4, pp. 497–505,

1997, doi: 10.2514/2.6289.

[68] H. R. Seyf and B. Nikaaein, “Analysis of Brownian motion and particle size effects on the thermal behavior and cooling performance of microchannel heat sinks,” *Int. J. Therm. Sci.*, vol. 58, pp. 36–44, 2012, doi: 10.1016/j.ijthermalsci.2012.02.022.

[69] X. Wang, X. Xu, and S. U. S. Choi, “Thermal conductivity of nanoparticle-fluid mixture,” *J. Thermophys. heat Transf.*, vol. 13, no. 4, pp. 474–480, 1999, doi: 10.2514/2.6486.

[70] B. Fani, M. Kalteh, and A. Abbassi, “Investigating the effect of Brownian motion and viscous dissipation on the nanofluid heat transfer in a trapezoidal microchannel heat sink,” *Adv. Powder Technol.*, vol. 26, no. 1, pp. 83–90, 2015, doi: 10.1016/j.apt.2014.08.009.

[71] H. Zhou, J. Lee, M. Kang, H. Kim, H. Lee, and J. Bin In, “All laser-based fabrication of microchannel heat sink,” *Mater. Des.*, vol. 221, p. 110968, 2022, doi: 10.1016/j.matdes.2022.110968.

[72] Q. Heng, C. Tao, and Z. Tie-chuan, “Surface roughness analysis and improvement of micro-fluidic channel with excimer laser,” *Microfluid. Nanofluidics*, vol. 2, no. 4, pp. 357–360, 2006, doi: 10.1007/s10404-006-0078-7.

[73] T. F. Hong, W. J. Ju, M. C. Wu, C. H. Tai, C. H. Tsai, and L. M. Fu, “Rapid prototyping of PMMA microfluidic chips utilizing a CO2 laser,” *Microfluid. Nanofluidics*, vol. 9, no. 6, pp. 1125–1133, 2010, doi: 10.1007/s10404-010-0633-0.

[74] J. Cui *et al.*, “High-quality fabrication of diamond straight microchannels heat sink with large aspect ratio microchannels using UV nanosecond laser based on multi-feed method,” *Opt. Laser Technol.*, vol. 171, no. May 2023, p. 110429, 2024, doi: 10.1016/j.optlastec.2023.110429.

[75] L. Chen, D. Deng, G. Pi, X. Huang, and W. Zhou, “Burr formation and surface roughness characteristics in micro-milling of microchannels,” *Int. J. Adv. Manuf. Technol.*, vol. 111, no. 5–6, pp. 1277–1290, 2020, doi: 10.1007/s00170-020-06170-4.

[76] E. Vázquez, C. A. Rodríguez, A. Elías-Zúñiga, and J. Ciurana, “An experimental

analysis of process parameters to manufacture metallic micro-channels by micro-milling," *Int. J. Adv. Manuf. Technol.*, vol. 51, no. 9–12, pp. 945–955, 2010, doi: 10.1007/s00170-010-2685-4.

[77] H. U. Lee, D. W. Cho, and K. F. Ehmann, "A mechanistic model of cutting forces in micro-end-milling with cutting-condition-independent cutting force coefficients," *J. Manuf. Sci. Eng.*, vol. 130, no. 3, pp. 0311021–0311029, 2008, doi: 10.1115/1.2917300.

[78] H. J. Kang and S. H. Ahn, "Fabrication and characterization of microparts by mechanical micromachining: Precision and cost estimation," *Proc. Inst. Mech. Eng. Part B J. Eng. Manuf.*, vol. 221, no. 2, pp. 231–240, 2007, doi: 10.1243/09544054JEM609.

[79] J. Zhao *et al.*, "A study on the forming of microchannels by micro rolling of copper foils," *Mater. Charact.*, vol. 200, no. April, 2023, doi: 10.1016/j.matchar.2023.112900.

[80] J. Chae, S. S. Park, and T. Freiheit, "Investigation of micro-cutting operations," *Int. J. Mach. Tools Manuf.*, vol. 46, no. 3–4, pp. 313–332, 2006, doi: 10.1016/j.ijmachtools.2005.05.015.

[81] J. Pu, R. Sochol, Y. Jiang, and L. Lin, "MICROFLUIDIC CHANNELS FABRICATED USING A LITHOGRAPHY-FREE METHOD," *Microfluid. CHANNELS Fabr. USING A Lithogr. METHOD Univ. Electron. Sci. Technol. China , Chengdu , Sichuan , China Univ. Calif. Berkeley , Berkeley , Calif. , United StatesScience Technol.*, pp. 2374–2377, 2011.

[82] S. Choi and J. K. Park, "Two-step photolithography to fabricate multilevel microchannels," *Biomicrofluidics*, vol. 4, no. 4, 2010, doi: 10.1063/1.3517230.

[83] C. Chen, D. Hirdes, and A. Folch, "Gray-scale photolithography using microfluidic photomasks," *Proc. Natl. Acad. Sci. U. S. A.*, vol. 100, no. 4, pp. 1499–1504, 2003, doi: 10.1073/pnas.0435755100.

[84] S. G. Kandlikar and W. J. Grande, "Evolution of microchannel flow passages-thermohydraulic performance and fabrication technology," *Heat Transf. Eng.*, vol. 24, no. 1, pp. 3–17, 2003, doi: 10.1080/01457630304040.

[85] H. Matsumoto, T. Okabe, and J. Taniguchi, "Microchannel fabrication via ultraviolet-

nanoimprint lithography and electron-beam lithography using an ultraviolet-curable positive-tone electron-beam resist," *Microelectron. Eng.*, vol. 226, no. March, p. 111278, 2020, doi: 10.1016/j.mee.2020.111278.

[86] A. A. Bakar *et al.*, "Micro-sorting device by a micro-channel with multiple-size pores," *2013 Int. Symp. Micro-NanoMechatronics Hum. Sci. MHS 2013*, pp. 2–5, 2013, doi: 10.1109/MHS.2013.6710429.

[87] P. Nageswara Rao and D. Kunzru, "Fabrication of microchannels on stainless steel by wet chemical etching," *J. Micromechanics Microengineering*, vol. 17, no. 12, 2007, doi: 10.1088/0960-1317/17/12/N01.

[88] R. Fiorin, L. N. Da Costa, I. Abe, I. Chiamenti, C. C. De Moura, and H. J. Kalinowski, "Manufacturing of microchannels in soda-lime glass by femtosecond laser and chemical etching," *SBMO/IEEE MTT-S Int. Microw. Optoelectron. Conf. Proc.*, no. Cornnig 2947, pp. 8–10, 2013, doi: 10.1109/IMOC.2013.6646520.

[89] M. C. Lin, J. P. Yeh, S. C. Chen, R. Der Chien, and C. L. Hsu, "Study on the replication accuracy of polymer hot embossed microchannels," *Int. Commun. Heat Mass Transf.*, vol. 42, pp. 55–61, 2013, doi: 10.1016/j.icheatmasstransfer.2012.12.008.

[90] S. S. Deshmukh, T. Kar, S. Som, and A. Goswami, "Investigation of replication accuracy of embossed micro-channel through hot embossing using laser patterned copper mold," *Mater. Today Proc.*, vol. 60, no. March, pp. 2222–2229, 2022, doi: 10.1016/j.matpr.2022.03.128.

[91] U. Masood, M. Haggag, A. Hassan, and M. Laghari, "A Review of Phase Change Materials as a Heat Storage Medium for Cooling Applications in the Built Environment," *Buildings*, vol. 13, no. 7, 2023, doi: 10.3390/buildings13071595.

[92] V. Jagadeeswara Reddy, M. Fairusham Ghazali, and S. Kumarasamy, "Innovations in phase change materials for diverse industrial applications: A comprehensive review," *Results Chem.*, vol. 8, no. May, p. 101552, 2024, doi: 10.1016/j.rechem.2024.101552.

[93] C. J. Ho, Y. C. Liu, M. Ghalambaz, and W. M. Yan, "Forced convection heat transfer of Nano-Encapsulated Phase Change Material (NEPCM) suspension in a mini-channel heatsink," *Int. J. Heat Mass Transf.*, vol. 155, 2020, doi:

10.1016/j.ijheatmasstransfer.2020.119858.

[94] W. Zhou *et al.*, “Numerical simulation and optimization of compact latent heat exchanger with micro-channel plate in shape-stabilized composite phase change material,” *Appl. Therm. Eng.*, vol. 245, no. January, p. 122740, 2024, doi: 10.1016/j.applthermaleng.2024.122740.

[95] P. Angelopoulou, E. Giaouris, and K. Gardikis, “Applications and Prospects of Nanotechnology in Food and Cosmetics Preservation,” *Nanomaterials*, vol. 12, no. 7, pp. 1–28, 2022, doi: 10.3390/nano12071196.

[96] A. Painuly, N. K. Mishra, and P. Zainith, “Thermo-hydraulic performance evaluation and comparison of SiC-MWCNT and Al2O3-MWCNT Non-Newtonian hybrid nanofluids using a heat exchanger equipped with helically corrugated tubes: an experimental study,” *J. Therm. Anal. Calorim.*, vol. 149, no. 9, pp. 3965–3980, 2024, doi: 10.1007/s10973-024-12960-9.

[97] S. Yun, J. Kwon, D. Lee, H. H. Shin, and Y. Kim, “Heat transfer and stress characteristics of additive manufactured FCCZ lattice channel using thermal fluid-structure interaction model,” *Int. J. Heat Mass Transf.*, vol. 149, p. 119187, 2020, doi: 10.1016/j.ijheatmasstransfer.2019.119187.

[98] S. Kumar, J. Ubaid, R. Abishera, A. Schi, and V. S. Deshpande, “Tunable Energy Absorption Characteristics of Architected Honeycombs Enabled via Additive Manufacturing,” 2019, doi: 10.1021/acsami.9b12880.

[99] H. J. O. Connor, A. N. Dickson, and D. P. Dowling, “Evaluation of the mechanical performance of polymer parts fabricated using a production scale multi jet fusion printing process,” *Addit. Manuf.*, vol. 22, no. May, pp. 381–387, 2018, doi: 10.1016/j.addma.2018.05.035.

[100] J. J. Andrew, J. Ubaid, F. Hafeez, A. Schiffer, and S. Kumar, “Impact Engineering Impact performance enhancement of honeycombs through additive manufacturing-enabled geometrical tailoring,” *Int. J. Impact Eng.*, vol. 134, no. July, p. 103360, 2019, doi: 10.1016/j.ijimpeng.2019.103360.

[101] Z. Ma, D. Z. Zhang, F. Liu, J. Jiang, M. Zhao, and T. Zhang, “Lattice structures of Cu-

Cr-Zr copper alloy by selective laser melting : Microstructures , mechanical properties and energy absorption," *Mater. Des.*, vol. 187, p. 108406, 2020, doi: 10.1016/j.matdes.2019.108406.

[102] P. Wang, J. Song, M. Ling, S. Nai, and J. Wei, "Experimental analysis of additively manufactured component and design guidelines for lightweight structures : A case study using electron beam melting," *Addit. Manuf.*, vol. 33, no. November 2019, p. 101088, 2020, doi: 10.1016/j.addma.2020.101088.

[103] T. Dixit, E. Al-hajri, M. C. Paul, P. Nithiarasu, and S. Kumar, "High performance , microarchitected , compact heat exchanger enabled by 3D printing," *Appl. Therm. Eng.*, vol. 210, no. March, p. 118339, 2022, doi: 10.1016/j.applthermaleng.2022.118339.

[104] B. MENG, M. WAN, R. ZHAO, Z. ZOU, and H. LIU, "Micromanufacturing technologies of compact heat exchangers for hypersonic precooled airbreathing propulsion: A review," *Chinese J. Aeronaut.*, vol. 34, no. 2, pp. 79–103, 2021, doi: 10.1016/j.cja.2020.03.028.

[105] S. N., "Fouling and Fouling Mitigation on Heat Exchanger Surfaces," *Heat Exch. - Basics Des. Appl.*, no. March 2012, 2012, doi: 10.5772/32990.

[106] S. A. Abdollahi *et al.*, "Combining artificial intelligence and computational fluid dynamics for optimal design of laterally perforated finned heat sinks," *Results Eng.*, vol. 21, no. March, p. 102002, 2024, doi: 10.1016/j.rineng.2024.102002.

[107] E. Science, P. E. Ohenhen, and J. Gidiagba, "ADVANCED SENSING TECHNIQUES IN ELECTRO- MECHANICAL SYSTEMS : SURVEYING THE RISE OF SMART SENSORS AND THEIR IMPLICATIONS FOR ADVANCED SENSING TECHNIQUES IN ELECTRO- MECHANICAL SYSTEMS : SURVEYING THE RISE OF SMART SENSORS AND THEIR IMPLICATIONS FOR," no. December, 2023, doi: 10.51594/estj.v4i6.628.

[108] N. R. Mavani, J. M. Ali, S. Othman, M. A. Hussain, H. Hashim, and N. A. Rahman, "Application of Artificial Intelligence in Food Industry—a Guideline," *Food Eng. Rev.*, vol. 14, no. 1, pp. 134–175, 2022, doi: 10.1007/s12393-021-09290-z.

[109] X. Chu, X. Tang, H. You, M. Pang, X. Li, and W. Zhou, "Smart microchannel heat

exchangers with Built-In graded SMA vortex generators that responds to random hotspots," *Appl. Therm. Eng.*, vol. 226, no. September 2022, p. 120261, 2023, doi: 10.1016/j.applthermaleng.2023.120261.

[110] K. Jaroslaw, "A General Approach in Optimization of Heat Exchangers by Bio-Inspired Artificial Intelligence Methods," *Energies*, vol. 12, p. 4441, 2019.

[111] A. Ikram, H. Mehmood, M. T. Arshad, A. Rasheed, S. Noreen, and K. T. Gnedeka, "Applications of artificial intelligence (AI) in managing food quality and ensuring global food security," *CyTA - J. Food*, vol. 22, no. 1, 2024, doi: 10.1080/19476337.2024.2393287.

[112] S. K. Lodhi, H. K. Hussain, and I. Hussain, "Using AI to Increase Heat Exchanger Efficiency: An Extensive Analysis of Innovations and Uses," *Int. J. Multidiscip. Sci. Arts*, vol. 3, no. 4, pp. 1–14, 2024, doi: 10.47709/ijmdsa.v3i4.4617.

[113] H. Jouhara *et al.*, "Applications and thermal management of rechargeable batteries for industrial applications," *Energy*, vol. 170, pp. 849–861, 2019, doi: 10.1016/j.energy.2018.12.218.

[114] M. A. Hannan, M. M. Hoque, A. Hussain, Y. Yusof, and P. J. Ker, "State-of-the-Art and Energy Management System of Lithium-Ion Batteries in Electric Vehicle Applications: Issues and Recommendations," *IEEE Access*, vol. 6, no. c, pp. 19362–19378, 2018, doi: 10.1109/ACCESS.2018.2817655.

[115] K. Chen, S. Wang, M. Song, and L. Chen, "Structure optimization of parallel air-cooled battery thermal management system," *Int. J. Heat Mass Transf.*, vol. 111, pp. 943–952, 2017, doi: 10.1016/j.ijheatmasstransfer.2017.04.026.

[116] W. Li, S. Kadam, and Z. Yu, "Heat transfer enhancement of tubes in various shapes potentially applied to CO2 heat exchangers in refrigeration systems: Review and assessment," *Int. J. Thermofluids*, vol. 20, no. November, p. 100511, 2023, doi: 10.1016/j.ijft.2023.100511.

[117] F. Bozzoli, L. Cattani, and S. Rainieri, "Cross-helix corrugation: The optimal geometry for effective food thermal processing," *Int. J. Heat Mass Transf.*, vol. 147, p. 118874, 2020, doi: 10.1016/j.ijheatmasstransfer.2019.118874.

[118] X. Liu, M. Wang, H. Liu, W. Chen, and S. Qian, “Numerical analysis on heat transfer enhancement of wavy fin-tube heat exchangers for air-conditioning applications,” *Appl. Therm. Eng.*, vol. 199, no. September, p. 117597, 2021, doi: 10.1016/j.applthermaleng.2021.117597.

[119] Z. F. Zhou *et al.*, “Enhancement of heat transfer on micro- and macro- structural surfaces in close-loop R410A flashing spray cooling system for heat dissipation of high-power electronics,” *Appl. Therm. Eng.*, vol. 223, no. December 2022, p. 119978, 2023, doi: 10.1016/j.applthermaleng.2023.119978.

[120] R. A. Nicholls, M. A. Moghimi, and A. L. Griffiths, “Influence of latent heat based passive cooling on the performance of EV battery under automotive drive cycles,” *J. Energy Storage*, vol. 77, no. December 2023, p. 109924, 2024, doi: 10.1016/j.est.2023.109924.

[121] F. Careri, R. H. U. Khan, C. Todd, and M. M. Attallah, “Additive manufacturing of heat exchangers in aerospace applications: a review,” *Appl. Therm. Eng.*, vol. 235, no. July, p. 121387, 2023, doi: 10.1016/j.applthermaleng.2023.121387.

[122] M. Habibi and L. Cui, “Modelling and performance analysis of a novel thermophotovoltaic system with enhanced radiative heat transfer for combined heat and power generation,” *Appl. Energy*, vol. 343, no. April, p. 121221, 2023, doi: 10.1016/j.apenergy.2023.121221.

[123] J. Han *et al.*, “Advances in polyphenol-based carbon dots for biomedical engineering applications,” *Eur. Polym. J.*, vol. 197, no. July, p. 112354, 2023, doi: 10.1016/j.eurpolymj.2023.112354.

[124] S. Kalita, D. Sen, P. Sen, S. Das, and B. B. Saha, “Pool boiling heat transfer enhancement and bubble visualization on a microporous copper over CuO filmed surface through combination of chemical etching and electrochemical deposition,” *Int. Commun. Heat Mass Transf.*, vol. 144, no. March, p. 106740, 2023, doi: 10.1016/j.icheatmasstransfer.2023.106740.

[125] Z. Song, X. Zhang, B. Liu, J. Liu, and L. Wang, “Efficient degradation of tetracycline residues in pharmaceutical wastewater by Ni/Fe bimetallic atomic cluster composite

catalysts with enhanced electron transfer pathway," *Chemosphere*, vol. 335, no. June, p. 139181, 2023, doi: 10.1016/j.chemosphere.2023.139181.

[126] J. Mahesh, A. R., B. Diksha, B. Amol, and M. Mayura, "Review on Enhancement of Heat Transfer by Active Method," *Int. J. Curr. Eng. Technol.*, vol. 6, no. Special Issue-6 (Oct 2016), pp. 221–225, 2016.

[127] S. S. M. Ajarostaghi, M. Zaboli, H. Javadi, B. Badenes, and J. F. Urchueguia, "A Review of Recent Passive Heat Transfer Enhancement Methods," *Energies*, vol. 15, no. 3, 2022, doi: 10.3390/en15030986.

[128] L. Léal *et al.*, "An overview of heat transfer enhancement methods and new perspectives: Focus on active methods using electroactive materials," *Int. J. Heat Mass Transf.*, vol. 61, no. 1, pp. 505–524, 2013, doi: 10.1016/j.ijheatmasstransfer.2013.01.083.

[129] S. Thapa, S. Samir, K. Kumar, and S. Singh, "A review study on the active methods of heat transfer enhancement in heat exchangers using electroactive and magnetic materials," *Mater. Today Proc.*, vol. 45, pp. 4942–4947, 2021, doi: 10.1016/j.matpr.2021.01.382.

[130] P. Błasiak and S. Pietrowicz, "A numerical study on heat transfer enhancement via mechanical aids," *Int. J. Heat Mass Transf.*, vol. 140, pp. 203–215, 2019, doi: 10.1016/j.ijheatmasstransfer.2019.05.116.

[131] S. Rainieri, F. Bozzoli, L. Cattani, and P. Vocale, "Parameter estimation applied to the heat transfer characterisation of Scraped Surface Heat Exchangers for food applications," *J. Food Eng.*, vol. 125, no. 1, pp. 147–156, 2014, doi: 10.1016/j.jfoodeng.2013.10.031.

[132] S. Liu and M. Sakr, "A comprehensive review on passive heat transfer enhancements in pipe exchangers," *Renew. Sustain. Energy Rev.*, vol. 19, pp. 64–81, 2013, doi: 10.1016/j.rser.2012.11.021.

[133] E. Tavousi, N. Perera, D. Flynn, and R. Hasan, "Heat transfer and fluid flow characteristics of the passive method in double tube heat exchangers: A critical review," *Int. J. Thermofluids*, vol. 17, no. January, p. 100282, 2023, doi:

10.1016/j.ijft.2023.100282.

[134] K. Katoh, K. S. Choi, and T. Azuma, “Heat-transfer enhancement and pressure loss by surface roughness in turbulent channel flows,” *Int. J. Heat Mass Transf.*, vol. 43, no. 21, pp. 4009–4017, 2000, doi: 10.1016/S0017-9310(00)00033-8.

[135] H. Huang, T. Sun, G. Zhang, M. Liu, and B. Zhou, “The effects of rough surfaces on heat transfer and flow structures for turbulent round jet impingement,” *Int. J. Therm. Sci.*, vol. 166, no. March, p. 106982, 2021, doi: 10.1016/j.ijthermalsci.2021.106982.

[136] G. G. Cruz, M. A. A. Mendes, J. M. C. Pereira, H. Santos, A. Nikulin, and A. S. Moita, “Experimental and numerical characterization of single-phase pressure drop and heat transfer enhancement in helical corrugated tubes,” *Int. J. Heat Mass Transf.*, vol. 179, 2021, doi: 10.1016/j.ijheatmasstransfer.2021.121632.

[137] S. Nayak, S. Jena, A. S. S. Khan, M. K. Paswan, and V. K. Sharma, “Use of Corrugated Pipe Heat Exchangers in Waste Heat Recovery Steam Generators,” *IOP Conf. Ser. Mater. Sci. Eng.*, vol. 1123, no. 1, p. 012037, 2021, doi: 10.1088/1757-899x/1123/1/012037.

[138] T. Thangamuthu *et al.*, “Experimental investigation on the influence of carbon-based nanoparticle coating on the heat transfer characteristics of the microprocessor,” *J. Compos. Mater.*, vol. 54, no. 1, pp. 61–70, 2020, doi: 10.1177/0021998319859926.

[139] S. Pungaiya and C. Kailasanathan, “A review of surface coating technology to increase the heat transfer,” *Int. J. Mech. Eng. Robot. Res.*, vol. 7, no. 5, pp. 458–465, 2018, doi: 10.18178/ijmerr.7.5.458-465.

[140] S. Rainieri, F. Bozzoli, and G. Pagliarini, “Effect of a hydrophobic coating on the local heat transfer coefficient in forced convection under wet conditions,” *Exp. Heat Transf.*, vol. 22, no. 3, pp. 163–177, 2009, doi: 10.1080/08916150902950004.

[141] X. Ma, G. Ding, Y. Zhang, and K. Wang, “Effects of hydrophilic coating on air side heat transfer and friction characteristics of wavy fin and tube heat exchangers under dehumidifying conditions,” *Energy Convers. Manag.*, vol. 48, no. 9, pp. 2525–2532, 2007, doi: 10.1016/j.enconman.2007.03.017.

[142] M. F. Hasan, M. Danışmaz, and B. M. Majel, “Thermal performance investigation of double pipe heat exchanger embedded with extended surfaces using nanofluid technique as enhancement,” *Case Stud. Therm. Eng.*, vol. 43, no. February, 2023, doi: 10.1016/j.csite.2023.102774.

[143] D. Kim and D. K. Kim, “Experimental study of free convection from vertical tubes with curved extended surfaces,” *Int. Commun. Heat Mass Transf.*, vol. 152, p. 107246, 2024, doi: 10.1016/j.icheatmasstransfer.2024.107246.

[144] E. M. A. Mokheimer, “Performance of annular fins with different profiles subject to variable heat transfer coefficient,” *Int. J. Heat Mass Transf.*, vol. 45, no. 17, pp. 3631–3642, 2002, doi: 10.1016/S0017-9310(02)00078-9.

[145] Rajendra Karwa, *Heat and Mass Transfer Second Edition*. 2020. [Online]. Available: https://link.springer.com/book/10.1007/978-981-15-3988-6

[146] L. Wang, P. Ni, and G. Xi, “The effect of off-center placement of twisted tape on flow and heat transfer characteristics in a circular tube,” *Sci. Rep.*, vol. 11, no. 1, pp. 1–11, 2021, doi: 10.1038/s41598-021-86285-0.

[147] R. Khargotra *et al.*, “A review of different twisted tape configurations used in heat exchanger and their impact on thermal performance of the system,” *Heliyon*, vol. 9, no. 6, 2023, doi: 10.1016/j.heliyon.2023.e16390.

[148] A. Vaisi, R. Moosavi, M. Lashkari, and M. Mohsen Soltani, “Experimental investigation of perforated twisted tapes turbulator on thermal performance in double pipe heat exchangers,” *Chem. Eng. Process. - Process Intensif.*, vol. 154, no. July, p. 108028, 2020, doi: 10.1016/j.cep.2020.108028.

[149] J. Xiao, S. He, G. Xie, S. Wang, and Z. Zhang, “Visualization experiment and thermal-hydraulic behaviour of assembled self-rotating twisted tape in double-pipe heat exchangers,” *Int. Commun. Heat Mass Transf.*, vol. 155, p. 107456, 2024, doi: 10.1016/j.icheatmasstransfer.2024.107456.

[150] R. B. C., P. Kumar, S. Roy, and R. Ganesan, “A comprehensive review on compound heat transfer enhancement using passive techniques in a heat exchanger,” *Mater. Today Proc.*, vol. 54, pp. 428–436, 2022, doi: 10.1016/j.matpr.2021.09.541.

[151] P. Promvonge, “Heat transfer behaviors in round tube with conical ring inserts,” *Energy Convers. Manag.*, vol. 49, no. 1, pp. 8–15, 2008, doi: 10.1016/j.enconman.2007.06.009.

[152] F. Bozzoli, L. Cattani, A. Mocerino, S. Rainieri, I. Tougri, and M. J. Colaço, “Characterisation of the heat transfer in displaced enhancement devices by means of inverse problem approach applied to IR images,” *Quant. Infrared Thermogr. J.*, vol. 18, no. 2, pp. 108–126, 2021, doi: 10.1080/17686733.2019.1700696.

[153] M. Sheikholeslami, M. Gorji-Bandpy, and D. D. Ganji, “Review of heat transfer enhancement methods: Focus on passive methods using swirl flow devices,” *Renew. Sustain. Energy Rev.*, vol. 49, pp. 444–469, 2015, doi: 10.1016/j.rser.2015.04.113.

[154] F. Seibold, P. Ligrani, and B. Weigand, “Flow and heat transfer in swirl tubes — A review,” *Int. J. Heat Mass Transf.*, vol. 187, 2022, doi: 10.1016/j.ijheatmasstransfer.2021.122455.

[155] A. A. Azhari, A. H. Milyani, N. H. Abu-Hamdeh, and A. M. Hussin, “Thermal improvement of heat exchanger with involve of swirl flow device utilizing nanomaterial,” *Case Stud. Therm. Eng.*, vol. 44, no. August 2022, p. 102793, 2023, doi: 10.1016/j.csite.2023.102793.

[156] S. Eiamsa-ard and P. Promvonge, “Enhancement of heat transfer in a tube with regularly-spaced helical tape swirl generators,” *Sol. Energy*, vol. 78, no. 4 SPEC. ISS., pp. 483–494, 2005, doi: 10.1016/j.solener.2004.09.021.

[157] F. Bozzoli, L. Cattani, S. Rainieri, F. S. Viloche, and L. S. Borges, “International Journal of Heat and Mass Transfer Estimation of the local heat-transfer coefficient in the laminar flow regime in coiled tubes by the Tikhonov regularisation method,” *Int. J. Heat Mass Transf.*, vol. 72, pp. 352–361, 2014, doi: 10.1016/j.ijheatmasstransfer.2014.01.019.

[158] S. Rainieri, F. Bozzoli, and G. Pagliarini, “Experimental investigation on the convective heat transfer in straight and coiled corrugated tubes for highly viscous fluids: Preliminary results,” *Int. J. Heat Mass Transf.*, vol. 55, no. 1–3, pp. 498–504, 2012, doi: 10.1016/j.ijheatmasstransfer.2011.08.030.

[159] N. Jamshidi, M. Farhadi, D. D. Ganji, and K. Sedighi, “Experimental analysis of heat transfer enhancement in shell and helical tube heat exchangers,” *Appl. Therm. Eng.*, vol.

51, no. 1–2, pp. 644–652, 2013, doi: 10.1016/j.applthermaleng.2012.10.008.

[160] F. Bozzoli, L. Cattani, and S. Rainieri, “Effect of wall corrugation on local convective heat transfer in coiled tubes,” *Int. J. Heat Mass Transf.*, vol. 101, pp. 76–90, 2016, doi: 10.1016/j.ijheatmasstransfer.2016.04.106.

[161] S. Kulankara and K. E. Herold, “Surface tension of aqueous lithium bromide with heat / mass transfer enhancement additives : the effect of additive vapor transport Tension superficielle du bromure de lithium en pre d ’ additifs augmentant le transfert de chaleur et de masse : ´ mentaire,” vol. 25, pp. 383–389, 2002.

[162] Y. Jun, K. J. Kim, and J. M. Kennedy, “Dynamic surface tension of heat transfer additives suitable for use in steam condensers and absorbers Tension superficielle dynamique des additifs favorisant ´ s a ` l ’ utilisation dans les le transfert de chaleur adapte condenseurs de vapeur et les abso,” *Int. J. Refrig.*, vol. 33, no. 2, pp. 428–434, 2010, doi: 10.1016/j.ijrefrig.2009.11.006.

[163] C. Thianpong, P. Eiamsa-ard, K. Wongcharee, and S. Eiamsa-ard, “Compound heat transfer enhancement of a dimpled tube with a twisted tape swirl generator,” *Int. Commun. Heat Mass Transf.*, vol. 36, no. 7, pp. 698–704, 2009, doi: 10.1016/j.icheatmasstransfer.2009.03.026.

[164] H. H. Hamed, A. E. Mohammed, R. A. Khalefa, O. A. Habeeb, and M. A. Abdulqader, “The effect of using compound techniques (passive and active) on the double pipe heat exchanger performance,” *Egypt. J. Chem.*, vol. 64, no. 6, pp. 2797–2802, 2021, doi: 10.21608/ejchem.2021.54450.3134.

[165] M. N. O. and H. R. B. Orlande, “Inverse Heat Transfer: Fundamentals and Applications,” *Taylor Fr. New York*, 2000.

[166] B. Blackwell and J. V. Beck, “A technique for uncertainty analysis for inverse heat conduction problems,” *Int. J. Heat Mass Transf.*, vol. 53, no. 4, pp. 753–759, 2010, doi: 10.1016/j.ijheatmasstransfer.2009.10.014.

[167] O. . Alifanov, “Inverse Heat Transfer Problems,” *Springer-Verlag, New York.*, 1994.

[168] A. K. . James V. Beck, “Parameter Estimation in Engineering and Science,” vol. 73, no.

363, 1978.

[169] F. S. Viloche Bazán and J. B. Francisco, “An improved fixed-point algorithm for determining a Tikhonov regularization parameter,” *Inverse Probl.*, vol. 25, no. 4, 2009, doi: 10.1088/0266-5611/25/4/045007.

[170] J. C. Bokar and M. N. Özisik, “An inverse analysis for estimating the time-varying inlet temperature in laminar flow inside a parallel plate duct,” *Int. J. Heat Mass Transf.*, vol. 38, no. 1, pp. 39–45, 1995, doi: 10.1016/0017-9310(94)00146-M.

[171] A. K. Parwani, P. Talukdar, and P. M. V. Subbarao, “Estimation of boundary heat flux using experimental temperature data in turbulent forced convection flow,” *Heat Mass Transf. und Stoffuebertragung*, vol. 51, no. 3, pp. 411–421, 2015, doi: 10.1007/s00231-014-1421-2.

[172] C. H. Huang and S. P. Wang, “A three-dimensional inverse heat conduction problem in estimating surface heat flux by conjugate gradient method,” *Int. J. Heat Mass Transf.*, vol. 42, no. 18, pp. 3387–3403, 1999, doi: 10.1016/S0017-9310(99)00020-4.

[173] R. Das, “Application of genetic algorithm for unknown parameter estimations in cylindrical fin,” *Appl. Soft Comput. J.*, vol. 12, no. 11, pp. 3369–3378, 2012, doi: 10.1016/j.asoc.2012.07.005.

[174] A. K. Parwani, P. Talukdar, and P. M. V. Subbarao, “Estimation of transient boundary flux for a developing flow in a parallel plate channel,” *Int. J. Numer. Methods Heat Fluid Flow*, vol. 24, no. 3, pp. 522–544, 2014, doi: 10.1108/HFF-01-2012-0020.

[175] H. T. Chen, S. Y. Lin, H. R. Wang, and L. C. Fang, “Estimation of two-sided boundary conditions for two-dimensional inverse heat conduction problems,” *Int. J. Heat Mass Transf.*, vol. 45, no. 1, pp. 15–23, 2002, doi: 10.1016/S0017-9310(01)00138-7.

[176] P. C. Parth Sathavara, Ajit Kumar Parwani, “Functional estimation of space and time varying thermal properties using modified conjugate gradient method,” *Int. J. Therm. Sci.*, vol. 145, pp. 373–395, 2023, doi: 10.1080/10407782.2013.733179.

[177] I. Felde and W. Shi, “Hybrid approach for solution of inverse heat conduction problems,” *Conf. Proc. - IEEE Int. Conf. Syst. Man Cybern.*, vol. 2014-Janua, no.

January, pp. 3896–3899, 2014, doi: 10.1109/SMC.2014.6974539.

[178] H. T. Chen and X. Y. Wu, “Estimation of surface conditions for nonlinear inverse heat conduction problems using the hybrid inverse scheme,” *Numer. Heat Transf. Part B Fundam.*, vol. 51, no. 2, pp. 159–178, 2007, doi: 10.1080/10407790600878734.

[179] C. R. Beck, J. V., Blackwell, B. and St. Clair, “Inverse Heat Conduction: Ill-Posed Problems,” *Wiley Interscience, New York*, 1985.

[180] Y. Bard, “Nonlinear Parameter Estimation,” 1974.

[181] B. H. Dennis, “Simultaneous Determination of Temperatures , Heat Fluxes , Deformations , and Tractions on Inaccessible Boundaries,” no. 2, 2016.

[182] S. Rainieri, F. Bozzoli, and G. Pagliarini, “Wiener filtering technique applied to thermographic data reduction intended for the estimation of plate fins performance,” vol. 28, pp. 179–183, 2004, doi: 10.1016/S0894-1777(03)00037-2.

[183] K. Hong, D. Kim, J. Kwark, J. Nam, and H. Ryou, “Numerical Study on the Effect of the Pipe Groove Height and,” 2021.

[184] R. L. Webb, “Principles of enhanced heat transfer,” *Routledge:London,UK*, 1994.

[185] C. Chen, Y. T. Wu, S. T. Wang, and C. F. Ma, “Experimental investigation on enhanced heat transfer in transversally corrugated tube with molten salt,” *Exp. Therm. Fluid Sci.*, vol. 47, pp. 108–116, 2013, doi: 10.1016/j.expthermflusci.2013.01.006.

[186] and S. R. G. Pagliarini, P. Vocale, A. Mocerino, “Second principle approach to the analysis of unsteady flow and heat transfer in a tube with arc- shaped corrugation,” *J. Phys. Conf. Ser.*, vol. 755, no. 1, 2016, doi: 10.1088/1742-6596/755/1/011001.

[187] F. Ahmad, S. Mahmud, M. M. Ehsan, and M. Salehin, “Thermo-hydrodynamic performance evaluation of double-dimpled corrugated tube using single and hybrid nanofluids,” *Int. J. Thermofluids*, vol. 17, no. October 2022, p. 100283, 2023, doi: 10.1016/j.ijft.2023.100283.

[188] S. Qin *et al.*, “International Journal of Heat and Fluid Flow Experimental investigation of the coherent structures in a spirally corrugated pipe,” *Int. J. Heat Fluid Flow*, vol. 84,

no. March, p. 108601, 2020, doi: 10.1016/j.ijheatfluidflow.2020.108601.

[189] K. Bilen, M. Cetin, H. Gul, and T. Balta, “The investigation of groove geometry effect on heat transfer for internally grooved tubes,” *Appl. Therm. Eng.*, vol. 29, no. 4, pp. 753–761, 2009, doi: 10.1016/j.applthermaleng.2008.04.008.

[190] L. Y. Zhang *et al.*, “A numerical analysis of fluid flow and heat transfer in wavy and curved wavy channels,” *Int. J. Therm. Sci.*, vol. 171, no. March 2021, 2022, doi: 10.1016/j.ijthermalsci.2021.107248.

[191] A. R. Al-obaidi and J. Alhamid, “Investigation of flow pattern , thermohydraulic performance and heat transfer improvement in 3D corrugated circular pipe under varying structure configuration parameters with development different correlations,” *Int. Commun. Heat Mass Transf.*, vol. 126, no. June, p. 105394, 2021, doi: 10.1016/j.icheatmasstransfer.2021.105394.

[192] A. R. Al-obaidi, “Investigation on effects of varying geometrical configurations on thermal hydraulics flow in a 3D corrugated pipe,” *Int. J. Therm. Sci.*, vol. 171, no. December 2020, p. 107237, 2022, doi: 10.1016/j.ijthermalsci.2021.107237.

[193] P. Duda, “Heat Transfer Coefficient Distribution—A Review of Calculation Methods,” 2023.

[194] C. Plastic, P. Market, and L. Trends, “Corrugated Plastic Pipe Market Research Report Unlocks Analysis on the Market Financial Status , Market Size , and Market Revenue upto 2031”.

[195] U. Planning, “Design of corrugated pipes under ground loads and pipe bedding,” vol. 12, pp. 1075–1092, 2022, doi: 10.17714/gumusfenbil.1062834.

[196] C. Hao, L. Liu, Z. Wang, and S. Wan, “Research on design parameters of double hole corrugated pipe culvert,” vol. 170, no. Iceep, pp. 184–189, 2018.

[197] H. Ishibashi, S. Inada, and S. Konishi, “Development of Ultra-Thin Wall Welded Metal Pipe and Its Applications,” no. 32, pp. 44–48, 2007.

[198] S. Rainieri, A. Farina, G. Pagliarini, U. Parma, I. Industriale, and V. Scienze, “EXPERIMENTAL INVESTIGATION OF HEAT TRANSFER AND PRESSURE

DROP AUGMENTATION FOR LAMINAR FLOW IN SPIRALLY ENHANCED TUBES," in *Proc. 2nd Eur. Therm. 14th UIT Natl. Heat Transf. Conf.*, 1996, pp. 1–8.

[199] M. Khoshvaght-Aliabadi and A. Feizabadi, "Compound heat transfer enhancement of helical channel with corrugated wall structure," *Int. J. Heat Mass Transf.*, vol. 146, p. 118858, 2020, doi: 10.1016/j.ijheatmasstransfer.2019.118858.

[200] Z. Zheng, X. Huang, and Z. Jiang, "Thermal performance and heat transfer reliability analysis in helically corrugated helical tube," *Int. J. Therm. Sci.*, vol. 183, no. July 2022, p. 107849, 2022, doi: 10.1016/j.ijthermalsci.2022.107849.

[201] Y. Duan, X. Zhang, Z. Han, Q. Liu, X. Li, and L. Li, "Numerical simulation of flow and heat transfer performance of tube-shell coupled helically coiled corrugated tube heat exchanger," *Int. Commun. Heat Mass Transf.*, vol. 153, no. March, p. 107325, 2024, doi: 10.1016/j.icheatmasstransfer.2024.107325.

[202] S. M. Kirkar, A. Gönül, and A. Selim Dalkilic, "Enhancement of thermal and flow characteristics in helically coiled tubes with corrugated surfaces by Genetic Algorithm based optimization," *Int. J. Heat Fluid Flow*, vol. 106, no. November 2023, 2024, doi: 10.1016/j.ijheatfluidflow.2024.109305.

[203] W. Wang, Y. Zhang, Y. Li, H. Han, and B. Li, "Multi-objective optimization of turbulent heat transfer flow in novel outward helically corrugated tubes," *Appl. Therm. Eng.*, vol. 138, pp. 795–806, 2018, doi: 10.1016/j.applthermaleng.2017.12.080.

[204] Y. Dong, L. Huixiong, and C. Tingkuan, "Pressure drop, heat transfer and performance of single-phase turbulent flow in spirally corrugated tubes," *Exp. Therm. Fluid Sci.*, vol. 24, no. 3–4, pp. 131–138, 2001, doi: 10.1016/S0894-1777(01)00047-4.

[205] H. Cui, X. Yuan, and Z. Yao, "Experimental investigation of heat transfer and pressure drop characteristics of w-type spirally fluted tubes," *Exp. Heat Transf.*, vol. 16, no. 3, pp. 159–169, 2003, doi: 10.1080/08916150390197416.

[206] S. Rainieri and G. Pagliarini, "Convective heat transfer to temperature dependent property fluids in the entry region of corrugated tubes," *Int. J. Heat Mass Transf.*, vol. 45, no. 22, pp. 4525–4536, 2002, doi: 10.1016/S0017-9310(02)00156-4.

[207] Y. Li, S. Wu, and T. Jin, “Experimental investigation on pressure drop and friction factor of slush nitrogen turbulent flow in helically corrugated pipes,” *Cryogenics (Guildf).*, vol. 94, no. July, pp. 56–61, 2018, doi: 10.1016/j.cryogenics.2018.07.007.

[208] K. Hwang *et al.*, “Heat transfer and pressure drop characteristics of enhanced titanium tubes,” *Desalination*, vol. 159, no. 1, pp. 33–41, 2003, doi: 10.1016/S0011-9164(03)90043-9.

[209] P. Poredoš, T. Šuklje, S. Medved, and C. Arkar, “An experimental heat-transfer study for a heat-recovery unit made of corrugated tubes,” *Appl. Therm. Eng.*, vol. 53, no. 1, pp. 49–56, 2013, doi: 10.1016/j.applthermaleng.2013.01.004.

[210] M. L. Djordjević, V. P. Stefanović, and M. V. Mančić, “Pressure drop and stability of flow in archimedean spiral tube with transverse corrugations,” *Therm. Sci.*, vol. 20, no. 2, pp. 579–591, 2016, doi: 10.2298/TSCI150118212D.

[211] I. Bashtani and J. A. Esfahani, “ε-NTU analysis of turbulent flow in a corrugated double pipe heat exchanger: A numerical investigation,” *Appl. Therm. Eng.*, vol. 159, no. June, pp. 1–11, 2019, doi: 10.1016/j.applthermaleng.2019.113886.

[212] Q. Gong, C. Yu, W. Wang, and Y. Wang, “Experimental and numerical exploration on improved heat transfer by continuous spiral flow in shell of spiral wound corrugated tube heat exchanger,” *Case Stud. Therm. Eng.*, vol. 51, no. June, p. 103483, 2023, doi: 10.1016/j.csite.2023.103483.

[213] A. . Murio, *The Mollification Method and the Numerical Ill-Posed Problems*. John Wiley and Sons: New York, NY, USA, 1993.

[214] C. Ibarra-Castanedo, D. González, M. Klein, M. Pilla, S. Vallerand, and X. Maldague, “Infrared image processing and data analysis,” *Infrared Phys. Technol.*, vol. 46, no. 1-2 SPEC. ISS., pp. 75–83, 2004, doi: 10.1016/j.infrared.2004.03.011.

[215] L. Cattani, D. Maillet, F. Bozzoli, and S. Rainieri, “Estimation of the local convective heat transfer coefficient in pipe flow using a 2D thermal Quadrupole model and Truncated Singular Value Decomposition,” *Int. J. Heat Mass Transf.*, vol. 91, pp. 1034–1045, 2015, doi: 10.1016/j.ijheatmasstransfer.2015.08.016.

[216] P. Xiong *et al.*, “Simultaneous estimation of fluid temperature and convective heat transfer coefficient by sequential function specification method,” *Prog. Nucl. Energy*, vol. 131, no. April, 2021, doi: 10.1016/j.pnucene.2020.103588.

[217] D. Delpueyo, X. Balandraud, and M. Grédiac, “Heat source reconstruction from noisy temperature fields using an optimised derivative Gaussian filter,” *Infrared Phys. Technol.*, vol. 60, pp. 312–322, 2013, doi: 10.1016/j.infrared.2013.06.004.

[218] M. J. Colaço, C. J. S. Alves, and F. Bozzoli, “The reciprocity function approach applied to the non-intrusive estimation of spatially varying internal heat transfer coefficients in ducts: Numerical and experimental results,” *Int. J. Heat Mass Transf.*, vol. 90, pp. 1221–1231, 2015, doi: 10.1016/j.ijheatmasstransfer.2015.07.028.

[219] D. Gerth, “A new interpretation of (Tikhonov) regularization A new interpretation of (Tikhonov) regularization,” 2021.

[220] J. P. Ngendahayo, J. Niyobuhungiro, and F. Berntsson, “Estimation of surface temperatures from interior measurements using Tikhonov regularization,” *Results Appl. Math.*, vol. 9, p. 100140, 2021, doi: 10.1016/j.rinam.2020.100140.

[221] F. Bozzoli, L. Cattani, G. Pagliarini, and S. Rainieri, “Infrared image filtering applied to the restoration of the convective heat transfer coefficient distribution in coiled tubes,” *Opto-Electronics Rev.*, vol. 23, no. 1, pp. 107–115, 2015, doi: 10.1515/oere-2015-0004.

[222] P. K. Lamm, “Approximation of ill-posed Volterra problems via predictor-corrector regularization methods,” *SIAM J. Appl. Math.*, vol. 56, no. 2, pp. 524–541, 1996, doi: 10.1137/S0036139994274496.

[223] H. Ay, J. Y. Jang, and J. N. Yeh, “Local heat transfer measurements of plate finned-tube heat exchangers by infrared thermography,” *Int. J. Heat Mass Transf.*, vol. 45, no. 20, pp. 4069–4078, 2002, doi: 10.1016/S0017-9310(02)00132-1.

[224] C. W. Booten and J. K. Eaton, “Optically based rapid heat transfer measurements in complex internal flows,” *J. Heat Transfer*, vol. 129, no. 12, pp. 1655–1665, 2007, doi: 10.1115/1.2767751.

[225] D. Bougeard, “Infrared thermography investigation of local heat transfer in a plate fin

and two-tube rows assembly," *Int. J. Heat Fluid Flow*, vol. 28, no. 5, pp. 988–1002, 2007, doi: 10.1016/j.ijheatfluidflow.2007.01.008.

[226] F. Bozzoli and S. Rainieri, "Comparative application of CGM and Wiener filtering techniques for the estimation of heat flux distribution," *Inverse Probl. Sci. Eng.*, vol. 19, no. 4, pp. 551–573, 2011, doi: 10.1080/17415977.2010.531466.

[227] S. Chantasiriwan, "Comparison of three sequential function specification algorithms for the inverse heat conduction problem," *Int. Commun. Heat Mass Transf.*, vol. 26, no. 1, pp. 115–124, 1999, doi: 10.1016/S0735-1933(98)00127-4.

[228] S. Balduaf, A. Schulz, and S. Wittig, "High-resolution measurements of local heat transfer coefficients from discrete hole film cooling," *J. Turbomach.*, vol. 123, no. 4, pp. 749–757, 2001, doi: 10.1115/1.1387245.

[229] Y. Rathor and K. R. Aharwal, "Heat transfer enhancement due to a staggered element using liquid crystal thermography in an inclined discrete rib roughened solar air heater," *Int. Commun. Heat Mass Transf.*, vol. 118, no. September, p. 104839, 2020, doi: 10.1016/j.icheatmasstransfer.2020.104839.

[230] G. M. Carlomagno and G. Cardone, *Infrared thermography for convective heat transfer measurements*, vol. 49, no. 6. 2010. doi: 10.1007/s00348-010-0912-2.

[231] A. Rogalski, "Recent progress in infrared detector technologies," *Infrared Phys. Technol.*, vol. 54, no. 3, pp. 136–154, 2011, doi: 10.1016/j.infrared.2010.12.003.

[232] F. P. INCROPERA and D. P. DEWITT, *Fundamentals of Heat and Mass Transfer*, vol. 112. JOHN WILEY & SONS, 2023. doi: 10.1007/978-3-031-28920-0_19.

[233] S. Y. Qin *et al.*, "Experimental investigation of the coherent structures in a spirally corrugated pipe," *Int. J. Heat Fluid Flow*, vol. 84, no. March, p. 108601, 2020, doi: 10.1016/j.ijheatfluidflow.2020.108601.

[234] V. Zimparov, "Extended performance evaluation criteria for enhanced heat transfer surfaces: Heat transfer through ducts with constant heat flux," *Int. J. Heat Mass Transf.*, vol. 44, no. 1, pp. 169–180, 2001, doi: 10.1016/S0017-9310(00)00074-0.

[235] F. Bozzoli, L. Cattani, and S. Rainieri, "Effect of wall corrugation on local convective

heat transfer in coiled tubes," *Int. J. Heat Mass Transf.*, vol. 101, pp. 76–90, 2016, doi: 10.1016/j.ijheatmasstransfer.2016.04.106.

[236] K. Pavelka, S. Ruzicka, and Z. Bila, "Photo-plan creation of cylindrical objects," *ISPRS Ann. Photogramm. Remote Sens. Spat. Inf. Sci.*, vol. 2, no. 5/W1, pp. 229–234, 2013, doi: 10.5194/isprsannals-II-5-W1-229-2013.

[237] B. Cyganek and J. P. Siebert, *An Introduction to 3D Computer Vision Techniques and Algorithms*. 2009. doi: 10.1002/9780470699720.

[238] T. Astarita and G. M. Carlomagno, "Infrared Thermography for Thermo-Fluid-Dynamics," *Infrared Thermogr. Thermo-Fluid-Dynamics*, no. January 2013, pp. 1–224, 2013, doi: 10.1007/978-3-642-29508-9.

[239] V. A. Morozov, *Methods for Solving Incorrectly Posed Problems*. New york. [Online]. Available: https://www.ptonline.com/articles/how-to-get-better-mfi-results

[240] P. . Bevington, "Data Reduction and Error Analysis for the Physical Sciences," *McGraw-Hill New York, NY, USA,* 1969, doi: 10.1119/1.17439.

[241] P. G. Vicente, A. García, and A. Viedma, "Experimental investigation on heat transfer and frictional characteristics of spirally corrugated tubes in turbulent flow at different Prandtl numbers," *Int. J. Heat Mass Transf.*, vol. 47, no. 4, pp. 671–681, 2004, doi: 10.1016/j.ijheatmasstransfer.2003.08.005.

[242] H. A. Mohammed, A. K. Abbas, and J. M. Sheriff, "Influence of geometrical parameters and forced convective heat transfer in transversely corrugated circular tubes," *Int. Commun. Heat Mass Transf.*, vol. 44, pp. 116–126, 2013, doi: 10.1016/j.icheatmasstransfer.2013.02.005.

Acknowledgements

First and foremost, I would like to express my sincere gratitude to my supervisor, **Prof. Fabio Bozzoli**, for his invaluable guidance, support, and encouragement throughout my Ph.D. journey. His insights and mentorship have been helpful to my progress, and I am deeply thankful for the opportunities he has provided me such as conferences, Ph.D. schools, and research experiences abroad.

I would also like to extend my profound thanks to **Prof. Luca Cattani**, **Dr. Matteo Malavasi**, and **Dr. Luca Pagliarini** for their guidance and support. Their expertise and advice have greatly enriched my research experience.

Finaly, I owe my sincere gratitude to my parents and family for their support, patience, and encouragement during my Ph.D. journey and the writing of my thesis. Thank you for being my strength through my journey.

Dedication

To my beloved wife whose unwavering love, patience, and support have been my greatest source of strength. Thank you for standing by my side, for your endless support during late nights and long days, and for believing in me even when I doubted myself. To my daughter, whose existence and smile always gave me happiness and encouragement to move further for the success in my life.

To my parents, whose values and guidance helped me to achieve this milestone. Your constant support has been the foundation of this success. This achievement would not have been possible without your love, trust, and confidence entrusted in me.

With all my heart, this work is dedicated to you all.

Publications

1. M. W. Azam, L. Cattani, M. Malavasi, and F. Bozzoli, “Experimental Study of the Corrugation Profile Effect on the Local Heat Transfer Coefficient,” *Energies*, vol. 16, no. 20, 2023, doi: 10.3390/en16207181.
2. M. W. Azam, M. Malavasi, L. Cattani, F. Bozzoli, and S. Rainieri, “Local heat-transfer coefficient estimation in cross-helix corrugated tubes under turbulent regime,” J. Phys. Conf. Ser., vol. 2685, no. 1, 2024, doi: 10.1088/1742-6596/2685/1/012042.
3. Malavasi, M., Bozzoli, F., Cattani, L., Pagliarini, L., Azam, M. W., & Rainieri, S. (2025). Infrared thermography applied to the study of the local heat transfer enhancement in a wall corrugated tubular heat exchanger for food applications. In *Journal of Physics: Conference Series* (Vol. 2940, No. 1, p. 012013). IOP Publishing.

La borsa di dottorato è stata cofinanziata con risorse del
Programma Operativo Nazionale Ricerca e Innovazione 2014-2020, risorse FSE REACT-EU
Azione IV.4 “Dottorati e contratti di ricerca su tematiche dell’innovazione”
e Azione IV.5 “Dottorati su tematiche Green”

Muhammad Waheed Azam has a PhD fellowship in the framework of PON R&I 2014/2020 (CCI 2014IT16M2OP005), Action IV.5- “PhD on green issues”, funded by the Ministry of University and Research (MUR), Italy, FSE-REACT-EU.